Sediment Connectivity in the Coupled Tidal Flat–Seagrass–Marsh System

Qingguang Zhu
Nanxiong, Guangdong

M.S. Marine Geology, Nanjing University, 2017
B.S. Marine Science, Nanjing University, 2014

A Dissertation presented to the Graduate Faculty
of the University of Virginia in Candidacy for the Degree of
Doctor of Philosophy

Department of Environmental Sciences

University of Virginia
August, 2022

Committee Members:

Patricia L. Wiberg (advisor)

Matthew A. Reidenbach

Karen J. McGlathery

Jonathan L. Goodall

Table of Contents

Abstract

Seagrass and salt marsh are important sediment and carbon sinks in the global marine carbon cycle, yet are also among the most rapidly declining marine habitats. Their ability to sequester sediment and carbon depends on flow–sediment–vegetation interactions that promote sediment trapping and deposition, as well as high rates of primary production. Understanding sediment transport and the associated drivers within these ecosystems provides insight into how sediment and carbon accumulation in these systems responds to disturbance events and climate change. However, most previous studies of sediment transport within seagrass and saltmarsh ecosystems either have been limited in small spatial scale or mainly focused on processes relevant to one specific time scale. When submerged seagrass meadows occupy shallow tidal flats, very little is known about their effects on modulating sediment connectivity between the tidal flats and fringing intertidal marshes and the response of the coupled system to short-term disturbance events and longer-term drivers.

In this dissertation, I applied a process-based and spatially resolved hydrodynamic and sediment transport model Delft3D, in the shallow coastal bays within the Virginia Coast Reserve (VCR) on Virginia's Atlantic coast, to quantify the sediment dynamics in the coupled tidal flat–seagrass–marsh system. The overarching research questions of this dissertation are: (1) what are the mechanisms that control sediment transport in the coupled tidal flat–seagrass–marsh system, and (2) how sediment accumulation rates and fluxes in this system respond to short-term events as well as seasonal wind patterns and seagrass growth cycle. I addressed the above questions in four research chapters. First, I applied the Delft3D model that couples flow–wave–vegetation–sediment interactions in South Bay, a successful seagrass restoration site with submerged seagrass meadows dominating the subtidal flats, to quantify seasonal seagrass impacts on bay

dynamics during summer and winter conditions. Second, I extended the model simulation period to a complete annual cycle to examine the effects of seasonal and episodic variations in seagrass density on rates of sediment accumulation and carbon burial in the seagrass meadows. Third, I adapted the coupled Delft3D model to the unvegetated tidal flat–marsh system in Hog Bay, and investigated the impacts of episodic storm surge events on the coupled tidal flat–marsh system and the overall contribution of storm surge on marsh sediment deposition. Finally, I focused on analyzing annual simulation results in South Bay and examined the combined effects of seasonal wind patterns and seagrass density variations on sediment delivery and wave energy flux to an adjacent back-barrier marsh bordering the meadows in the bay.

My results show that the presence of submerged seagrass meadows on shallow tidal flats plays an important role in controlling sediment resuspension on the flats as well as sediment delivery to adjacent salt marshes. Sediment accumulation rates within seagrass meadows changed non-linearly between seasons as a function of seagrass density. While seagrass meadows effectively reduced sediment resuspension and trapped sediment at meadow edges during spring-summer growth seasons, during winter senescence low-density meadows (< 160 shoots m^{-2}) were erosional with rates sensitive to density. Due to this nonlinear control of seagrass density on sediment accumulation, there was strong variability of sediment accumulation rates in the meadow in response to winter density variations and marine heatwave events. In addition, seagrass meadows also significantly altered the timing of sediment transport to the adjacent marsh platform (winter peak, density control) and reduced total annual sediment flux by 12% compared to the simulation with no seagrass (flux controlled by winds).

I also found that episodic storm surge events play an important role in transporting suspended sediment from unvegetated tidal flats to intertidal salt marshes. Although storm surge events only occurred 5% of the time at the study site, they disproportionately contributed 40% of marsh deposition during 2009–2020. While wind-driven waves control sediment resuspension on tidal flats, marsh deposition during storms was largely determined by tidal inundation associated with storm driven water levels and increased linearly with storm surge intensity, suggesting that marshes at the study site will likely be supplied with more sediment, primarily from eroding tidal flats, if storm magnitudes and/or frequencies increase in the future.

Overall, these findings highlight the strong control vegetation has in erosional and depositional processes in shallow coastal bays and the implications for the resilience of seagrass and marsh sediment accumulation under future climate change. The results of this dissertation also provide useful information for coastal managers to inform conservation and management strategies in coastal wetlands and practical guidelines for process-based modeling of flow–wave–vegetation–sediment interactions in shallow coastal environments.

Acknowledgements

The past five years at the Environmental Sciences Department at UVA have been an amazing journey in my life. I am grateful to so many people for their support, guidance, and inspiration throughout this journey. Specifically, I would like to thank my advisor, Dr. Patricia Wiberg, for her continued support and thoughtful guidance. It has been a real privilege to work with her. Her wisdom and keen insight into sediment transport processes have inspired me to think deeper and shaped my development as a young researcher. I would also like to thank my dissertation committee members, Dr. Matthew Reidenbach, Dr. Karen McGlathery, and Dr. Jonathan Goodall, for their valuable advice and constructive feedback on my work.

I am thankful to the wonderful staff at the ABCRC, especially Cora Johnston, Donna Fauber, David Lee, Jonah Morreale, and Buck Doughty, for helping coordinate my field sampling and data collection on the Eastern Shore and making my fieldwork such a pleasant experience. I would also like to acknowledge the PIs in the Coastal Lagoon Group, Dr. Max Castorani, Dr. Peter Berg, Dr. Michael Pace, and Dr. Scott Doney, and the group mates Tyler Barnes, Libby Bieri, Kinsey Tedford, Rachel Smith, Spencer Tassone, Sara Hogan, and Amy Ferguson for the productive group meetings and constructive feedback on my research. Much appreciation to Tyler Barnes for listening to my seminar practice talk and helping me throughout my dissertation.

I am grateful for my previous mentors at Nanjing University, Dr. Ya Ping Wang, Dr. Jianhua Gao, and Dr. Shu Gao, without whom I never would have entered the field of coastal oceanography and pursued a career in science.

I could not have undertaken this journey without the support of my friends and family. Many thanks to my friends Dave and Lisa for their hospitality and encouragement. I am indebted to my parents, Zhen and Heng, and my older sister, Zhu, who have always supported me in pursuing my passions. And of course, I am so grateful for Yuan, who flew all the way from China and joined the journey with me, and has given me love and company to get through this very long journey. I am also grateful for Yuan's parents, Hua and Zhong, for their trust and unwavering support.

Primary support for this work was provided by the National Science Foundation (NSF) through the VCR LTER award 1832221 and Coastal SEES award 1427282. The developers of Delft3D are acknowledged for open access to their code.

Chapter 1. Introduction to the dissertation

1.1 Background

Seagrasses and salt marshes are important ecosystems that inhabit shallow coastal zones. While seagrasses mainly occupy shallow subtidal flats, salt marshes are mostly located in intertidal areas that are alternately inundated and drained by tides. These two ecosystems offer valuable ecosystem services (e.g., primary production, nutrient cycling, water quality control, and carbon sequestration) and provide essential habitat for various coastal species (Barbier et al., 2011). However, despite their importance in coastal ecosystems, seagrasses and salt marshes are rapidly declining in large part due to human activities and climate change (Deegan et al., 2012; Gedan et al., 2009; Orth et al., 2006; Waycott et al., 2009), and approximately 20% of seagrasses and between 25% and 50% of salt marshes were lost globally over the past century (Dunic et al., 2021; Mcowen et al., 2017).

In recent decades, seagrasses and salt marshes have increasingly been recognized as important sediment and carbon sinks (also commonly referred to as "blue carbon") in the global marine carbon cycle and they contribute more than 30% of the annual sediment carbon burial in global oceans (Duarte et al., 2005; Fourqurean et al., 2012; Wang et al., 2021). The ability of seagrass and salt marsh to sequester sediment and carbon depends on flow–sediment–vegetation interactions that promote sediment trapping and deposition (de Boer, 2007; Nepf, 2012), as well as high rates of primary production (Duarte et al., 2005). For example, previous studies on seagrass interactions with physical environments have shown that the impact of seagrass on trapping fine-grained particles from the water column and reducing sediment resuspension is the most important positive feedback for seagrass growth, as it increases light penetration to the seabed and stimulates seagrass growth (de Boer, 2007; Carr et al., 2010). In contrast, the disappearance of seagrass can cause seabed erosion and the exposure of accumulated sediment carbon to oxic conditions, leading to carbon emissions (Aoki et al., 2021; Marbà et al., 2015; Pendleton et al., 2012).

Similarly, intertidal salt marshes can effectively trap fine-grained sediment carried by flood tides when they are inundated and promote net sediment and carbon accumulation on the marsh platform (Fagherazzi et al., 2012). As sea level rises, greater tidal inundation can enhance suspended sediment deposition on the marsh platform and production of belowground biomass, thereby increasing salt marsh resilience to sea level rise (Friedrichs & Perry, 2001; Kirwan & Megonigal, 2013; Morris et al., 2002). However, these positive ecogeomorphic feedbacks might not be able to keep pace with an accelerated sea level rise rate if there is a decrease in advective sediment supply to marshes or a reduction in belowground organic production once water depth exceeds the optimum range for marsh vegetation growth (Ganju et al., 2017; Kirwan & Megonigal, 2013).

Understanding sediment distribution, deposition, and transport rates within these blue carbon ecosystems is critical for predicting future change (Duarte et al., 2013; FitzGerald & Hughes, 2019; McGlathery et al., 2013). But addressing sediment transport rates and the associated drivers is difficult because sediment transport processes in these ecosystems involve complex biological and physical interactions spanning a wide range of spatial and temporal scales (Figure 1.1). Owing to this inherent complexity, most previous studies of sediment transport within seagrass and saltmarsh ecosystems have been limited in small spatial scale or mainly focused on processes relevant to one specific time scale (de Boer, 2007; Tinoco et al., 2020). For example, previous studies of vegetation effects on flow and sediment dynamics have mainly focused on flume experiments and small-scale and short-term field measurements, and have shown that aquatic vegetation can significantly reduce turbulent energy and mean flow speed, thereby creating a favorable environment for sediment deposition in vegetation beds (Hansen & Reidenbach, 2012; Leonard & Luther, 1995; Nepf, 2012). However, many findings of these studies cannot be directly applied to a larger spatial scale or used for long-term predictions because these small-scale and short-term studies did not fully capture the inherent complexity and spatial variability of natural environments, including temporal and spatial variability of waves and currents, seabed sediment distribution and availability, spatial variations of bathymetry, and spatial extent and density variations of subtidal and intertidal vegetation (Tinoco et al., 2020). On a much longer temporal scale (mega-scale; Figure 1.1), idealized long-term morphodynamic models (e.g., transect-based or point-based models) have been developed to explore the coupled evolution of tidal flat–seagrass–marsh systems over hundreds of years (Carr et al., 2010, 2018; Mariotti & Fagherazzi, 2010; Reeves et al., 2020). These coupled model simulations have significantly improved our general understanding of the complex, large-scale behavior of tidal flat–seagrass–marsh systems and the associated key drivers (e.g., climate change, sea level rise, and inherent geology) and ecomorphodynamic feedbacks that control long-term changes, but outcomes of these idealized models usually cannot be quantitatively compared with detailed hydrodynamic and sediment transport measurements at one particular site and therefore would be difficult to use for making site-specific predictions (Wiberg et al., 2020).

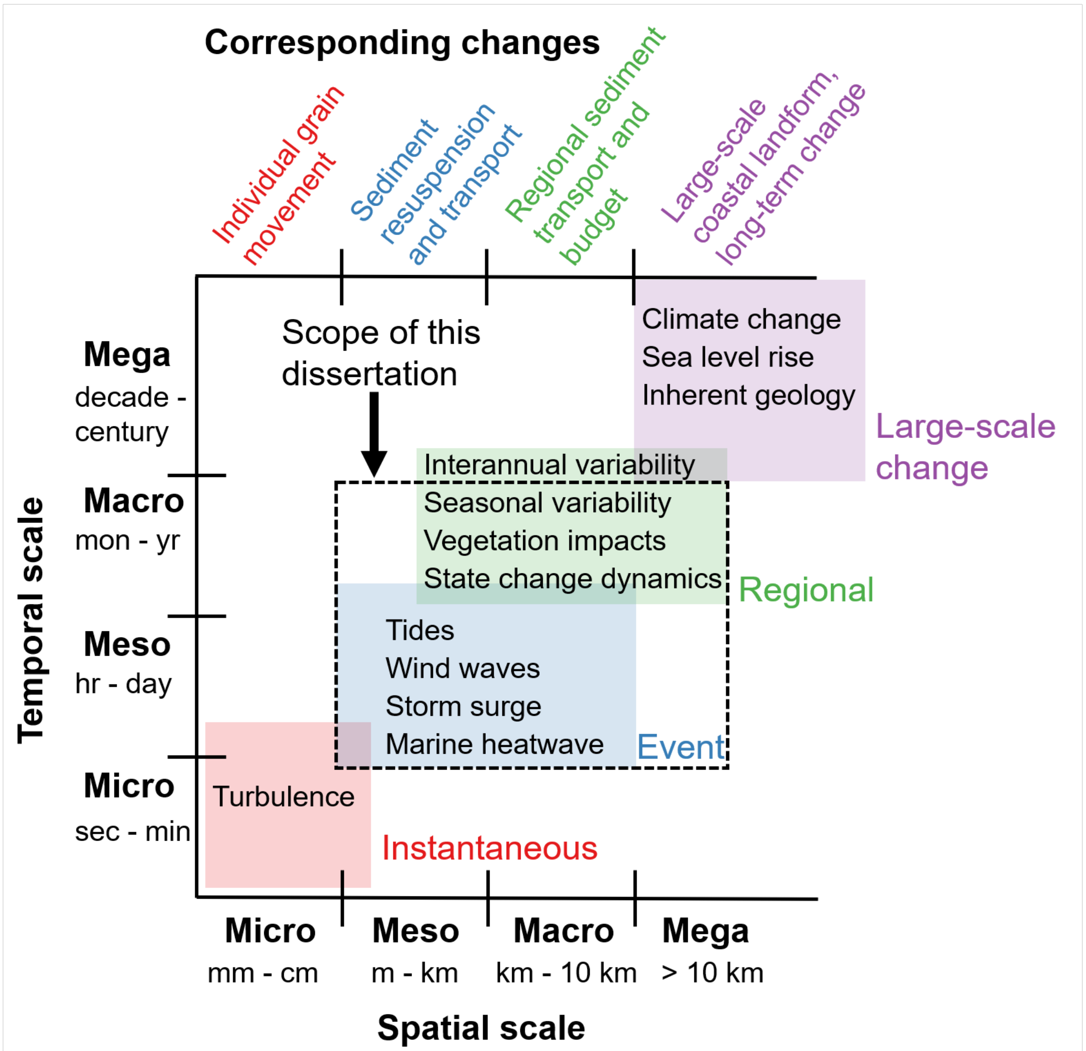

Figure 1.1 Spatial and temporal scales of physical drivers for sediment transport in coastal environments and corresponding changes (adapted from Castelle & Chaumillon 2019, and Larson & Kraus 1995). The dashed box represents the range of scales relevant to the scope of this dissertation.

Regional studies that focus on sediment dynamics on intermediate time scales (meso- to macro-scale) are most relevant to coastal planners and managers and they provide key information to inform site-specific management decisions in response to disturbance events and coastal hazards (Mogensen & Rogers, 2018; Nichols et al., 2019). On a meso-temporal time scale (from hours to days), there are many drivers controlling sediment resuspension and transport in vegetated coastal habitats such as tides, wind waves, storm surge, and marine heatwaves (Figure 1.1). While the effect of periodic tidal forcing on sediment transport has been relatively well characterized, the overall effects of episodic events (wind waves, storm surge, and marine heatwaves) within these coastal habitats have not been well quantified (Aoki et al., 2021; FitzGerald & Hughes, 2019; Wiberg et al., 2020). On a longer temporal scale (seasons to years), the overall sediment budgets and changes in sediment transport processes in these systems depend on the cumulative impact of short-term events and interannual/seasonal variability of physical drivers (e.g., variations in seasonal wind patterns) and vegetation dynamics (e.g., seasonal vegetation growth and senescence) (Castelle & Chaumillon, 2019; Coco et al., 2013; Tinoco et al., 2020). This superimposition of sediment dynamics across multiple temporal scales makes it difficult for field-based studies to identify the coastal change resulting from short-term events versus longer-term processes.

Spatially resolved numerical models (landscape models) capable of capturing the synergistic effects of flow–wave–vegetation–sediment interactions provide a tool for characterizing sediment transport in seagrass and salt marsh ecosystems on both meso- and macro-temporal scales (Beudin et al., 2017; Donatelli et al., 2018; Nardin et al., 2018). Compared with idealized long-term morphodynamic models, the outcomes of these landscape models can be directly compared with hydrodynamic and sediment transport measurements at specific sites and used for making actual predictions for the entire region once the models have been properly tested against field observations (Wiberg et al., 2020). In addition, these regional landscape models can perform long-term predictions (seasons to years) in small time increments (seconds to hours), thereby resolving the detailed sediment dynamics resulted from short-term episodic events as well as interannual/seasonal variability of physical drivers and vegetation growth dynamics. They also allow for coupling of the effects of different processes (e.g., tides, waves, and vegetation effects) on sediment transport and accumulation. Therefore, the relative contribution of these processes to the overall sediment budgets in these vegetated habitats and the resulting changes in sediment deposition patterns can be quantified by contrasting the simulation results output from model scenarios with different processes/forcing conditions.

Despite the value of landscape models in filling the knowledge gaps on intermediate time scales, some important aspects of the sediment dynamics in seagrass and salt marsh ecosystems still need to be investigated. Most of these model studies do not provide direct validation with measured flow and suspended sediment data within vegetated habitats (Mogensen & Rogers, 2018). Considering the inherent complexity of natural environments, model validation with spatially distributed data sets is necessary to obtain accurate sediment flux rates in these ecosystems. In addition, most previous studies mainly focused on sediment transport within individual ecosystem and did not resolve the coupled dynamics and sediment exchange between adjacent ecosystems in spatially resolved settings (Nardin et al., 2018). When seagrass meadows occupy shallow subtidal flats, they can significantly reduce sediment resuspension on tidal flats and sediment fluxes to the adjacent salt marsh platform (Carr et al., 2018; Donatelli et al., 2018). It is still unclear, however, how sediment fluxes to the adjacent marsh vary in response to episodic storms and seasonal growth and senescence of seagrass and what is the overall effect of seagrass meadows on reducing total sediment flux to the marsh over an annual cycle.

To better understand the sediment connectivity and associated drivers for sediment transport within seagrass and salt marsh ecosystems and the response of these ecosystems to disturbance events, this dissertation applies a process-based and spatially resolved hydrodynamic and sediment transport model Delft3D in the shallow coastal bays within the Virginia Coast Reserve (VCR) on Virginia's Atlantic coast. Both submerged (seagrass) and intertidal (salt marsh) vegetation effects on flow, waves, and sediment resuspension were included in the model, and the model was calibrated using seasonal hydrodynamic and suspended sediment field data from the study site. More details about the Delft3D model and the study site are described in the following chapters. The modeling approach presented in this dissertation resolves sediment dynamics driven by short-term events as well as seasonal wind patterns and vegetation growth cycle (Figure 1.1), and focuses on two key processes that modulate sediment connectivity between subtidal flats and intertidal salt marshes on intermediate time scales: episodic storm surge events and seasonal growth and senescence of seagrass on tidal flats. This work highlights the strong control vegetation has in erosional and depositional processes in shallow coastal bays and the implications for the resilience of seagrass and marsh sediment accumulation under future climate change. It also provides useful information for coastal managers to inform conservation and management strategies in coastal wetlands and practical guidelines for process-based modeling of flow–wave–vegetation–sediment interactions in shallow coastal environments.

1.2 Objectives and approach

The objectives of this dissertation are as follows:

(1) Establish a process-based and spatially resolved model to resolve flow–wave–vegetation–sediment interactions on both meso- and macro-temporal scales in the coupled tidal flat–seagrass–marsh system in the VCR;

(2) Calibrate and test the coupled model against seasonal field measurements of flow, waves, and suspended sediment concentration collected from the study site;

(3) Examine the effects of seasonal growth and senescence of seagrass on hydrodynamics and sediment transport on shallow tidal flats;

(4) Quantify the effects of storm surge on unvegetated tidal flat–marsh system;

(5) Quantify seasonal sediment fluxes between submerged seagrass meadows/unvegetated tidal flats and adjacent intertidal marshes and identify major drivers that control sediment transport fluxes in the coupled systems.

I address the above objectives in four research chapters, each written and formatted for publication in peer-reviewed journals. Chapter 2, “Quantifying seasonal seagrass effects on flow and sediment dynamics in a back-barrier bay”, describes the establishment of the Delft3D model that couples flow–wave–vegetation–sediment interactions in South Bay, VCR, and the application of the coupled model in quantifying seagrass impacts on bay dynamics during summer and winter conditions (Zhu et al., 2021). Chapter 3, “Seasonal growth and senescence of seagrass alters sediment accumulation rates and carbon burial in a coastal lagoon”, extends the simulation period in Chapter 2 to a complete annual cycle to examine the effects of seasonal growth and senescence of seagrass on rates of sediment accumulation and carbon burial in the South Bay seagrass meadows (Zhu et al., 2022). Chapter 4, "The importance of storm surge for sediment delivery to microtidal marshes", adapts the coupled model in previous chapters to the unvegetated tidal flat–marsh system in Hog Island Bay, and investigates the impacts of storm surge events on the coupled tidal flat–marsh system and the overall contribution of storm surge on marsh sediment deposition (Zhu & Wiberg, in review). Chapter 5, "Submerged seagrass meadows modulate sediment delivery and wave energy flux to back-barrier marshes", focuses on analyzing annual simulation results in South Bay from Chapter 3 in the context of the combined effects of seasonal wind patterns and seagrass density variations on sediment delivery and wave energy flux to the back-barrier marshes bordering the seagrass meadows in the bay. The final chapter summarizes the main findings of the dissertation.

References

Aoki, L. R., McGlathery, K. J., Wiberg, P. L., Oreska, M. P. J., Berger, A. C., Berg, P., & Orth, R. J. (2021). Seagrass Recovery Following Marine Heat Wave Influences Sediment Carbon Stocks. Frontiers in Marine Science, 7, 1170. https://doi.org/10.3389/fmars.2020.576784

Barbier, E. B., Hacker, S. D., Kennedy, C., Koch, E. W., Stier, A. C., & Silliman, B. R. (2011). The value of estuarine and coastal ecosystem services. Ecological Monographs, 81(2), 169–193. https://doi.org/10.1890/10-1510.1

Beudin, A., Kalra, T. S., Ganju, N. K., & Warner, J. C. (2017). Development of a coupled wave-flow-vegetation interaction model. Computers and Geosciences, 100, 76–86. https://doi.org/10.1016/j.cageo.2016.12.010

Carr, J., D'Odorico, P., McGlathery, K., & Wiberg, P. (2010). Stability and bistability of seagrass ecosystems in shallow coastal lagoons: Role of feedbacks with sediment resuspension and light attenuation. Journal of Geophysical Research: Biogeosciences, 115(3), G03011. https://doi.org/10.1029/2009JG001103

Carr, J., Mariotti, G., Fahgerazzi, S., McGlathery, K., & Wiberg, P. (2018). Exploring the Impacts of Seagrass on Coupled Marsh-Tidal Flat Morphodynamics. Frontiers in Environmental Science, 6(SEP), 92. https://doi.org/10.3389/fenvs.2018.00092

Castelle, B., & Chaumillon, E. (2019). Coastal Change in Tropical Overseas and Temperate Metropolitan France Inferred from a National Monitoring Network: A Summary from the Current Special Issue. Journal of Coastal Research, 88(sp1), 3–9. https://doi.org/10.2112/SI88-002.1

Coco, G., Zhou, Z., van Maanen, B., Olabarrieta, M., Tinoco, R., & Townend, I. (2013). Morphodynamics of tidal networks: Advances and challenges. Marine Geology, 346, 1–16. https://doi.org/10.1016/J.MARGEO.2013.08.005

Deegan, L. A., Johnson, D. S., Warren, R. S., Peterson, B. J., Fleeger, J. W., Fagherazzi, S., & Wollheim, W. M. (2012). Coastal eutrophication as a driver of salt marsh loss. Nature 2012 490:7420, 490(7420), 388–392. https://doi.org/10.1038/nature11533

de Boer, W. F. (2007). Seagrass-sediment interactions, positive feedbacks and critical thresholds for occurrence: A review. Hydrobiologia, 591(1), 5–24. https://doi.org/10.1007/s10750-007-0780-9

Donatelli, C., Ganju, N. K., Fagherazzi, S., & Leonardi, N. (2018). Seagrass Impact on Sediment Exchange Between Tidal Flats and Salt Marsh, and The Sediment Budget of Shallow Bays. Geophysical Research Letters, 45(10), 4933–4943. https://doi.org/10.1029/2018GL078056

Duarte, C. M., Middelburg, J. J., & Caraco, N. (2005). Major role of marine vegetation on the oceanic carbon cycle. Biogeosciences, 2(1), 1–8. https://doi.org/10.5194/bg-2-1-2005

Duarte, C. M., Losada, I. J., Hendriks, I. E., Mazarrasa, I., & Marbà, N. (2013). The role of coastal plant communities for climate change mitigation and adaptation. Nature Climate Change 2013 3:11, 3(11), 961–968. https://doi.org/10.1038/nclimate1970

Dunic, J. C., Brown, C. J., Connolly, R. M., Turschwell, M. P., & Côté, I. M. (2021). Long-term declines and recovery of meadow area across the world's seagrass bioregions. Global Change Biology, 27(17), 4096–4109. https://doi.org/10.1111/gcb.15684

Fagherazzi, S., Kirwan, M. L., Mudd, S. M., Guntenspergen, G. R., Temmerman, S., D'Alpaos, A., et al. (2012). Numerical models of salt marsh evolution: Ecological, geomorphic, and climatic factors. Reviews of Geophysics, 50(1). https://doi.org/10.1029/2011RG000359

FitzGerald, D. M., & Hughes, Z. (2019). Marsh Processes and Their Response to Climate Change and Sea-Level Rise. Annual Review of Earth and Planetary Sciences, 47, 481–517. https://doi.org/10.1146/ANNUREV-EARTH-082517-010255

Fourqurean, J. W., Duarte, C. M., Kennedy, H., Marbà, N., Holmer, M., Mateo, M. A., et al. (2012). Seagrass ecosystems as a globally significant carbon stock. Nature Geoscience, 5(7), 505–509. https://doi.org/10.1038/ngeo1477

Friedrichs, C. T., & Perry, J. E. (2001). Tidal Salt Marsh Morphodynamics: A Synthesis. Journal of Coastal Research, (27), 7–37. https://doi.org/10.2307/25736162

Ganju, N. K., Defne, Z., Kirwan, M. L., Fagherazzi, S., D'Alpaos, A., & Carniello, L. (2017). Spatially integrative metrics reveal hidden vulnerability of microtidal salt marshes. Nature Communications 2017 8:1, 8(1), 1–7. https://doi.org/10.1038/ncomms14156

Gedan, K. B., Silliman, B. R., & Bertness, M. D. (2009). Centuries of Human-Driven Change in Salt Marsh Ecosystems. Http://Dx.Doi.Org/10.1146/Annurev.Marine.010908.163930, 1, 117–141. https://doi.org/10.1146/ANNUREV.MARINE.010908.163930

Hansen, J., & Reidenbach, M. A. (2012). Wave and tidally driven flows in eelgrass beds and their effect on sediment suspension. Marine Ecology Progress Series, 448, 271–287. https://doi.org/10.3354/meps09225

Kirwan, M. L., & Megonigal, J. P. (2013). Tidal wetland stability in the face of human impacts and sea-level rise. Nature 2013 504:7478, 504(7478), 53–60. https://doi.org/10.1038/nature12856

Larson, M., & Kraus, N. (1995). Prediction of cross-shore sediment transport at different spatial and temporal scales. Marine Geology, 126(1–4), 111–127. https://doi.org/10.1016/0025-3227(95)00068-A

Leonard, L. A., & Luther, M. E. (1995). Flow hydrodynamics in tidal marsh canopies. Limnology and Oceanography, 40(8), 1474–1484. https://doi.org/10.4319/LO.1995.40.8.1474

Marbà, N., Arias-Ortiz, A., Masqué, P., Kendrick, G. A., Mazarrasa, I., Bastyan, G. R., et al. (2015). Impact of seagrass loss and subsequent revegetation on carbon sequestration and stocks. Journal of Ecology, 103(2), 296–302. https://doi.org/10.1111/1365-2745.12370

Mariotti, G., & Fagherazzi, S. (2010). A numerical model for the coupled long-term evolution of salt marshes and tidal flats. Journal of Geophysical Research, 115(F1), F01004. https://doi.org/10.1029/2009JF001326

McGlathery, K., Reidenbach, M., D'Odorico, P., Fagherazzi, S., Pace, M., & Porter, J. (2013). Nonlinear Dynamics and Alternative Stable States in Shallow Coastal Systems. Oceanography, 26(3), 220–231. https://doi.org/10.5670/oceanog.2013.66

Mcowen, C. J., Weatherdon, L. V., Van Bochove, J. W., Sullivan, E., Blyth, S., Zockler, C., et al. (2017). A global map of saltmarshes. Biodiversity Data Journal, 5(5), 11764. https://doi.org/10.3897/BDJ.5.E11764

Mogensen, L. A., & Rogers, K. (2018). Validation and Comparison of a Model of the Effect of Sea-Level Rise on Coastal Wetlands. Scientific Reports 2018 8:1, 8(1), 1–14. https://doi.org/10.1038/s41598-018-19695-2

Morris, J. T., Sundareshwar, P. V., Nietch, C. T., Kjerfve, B., & Cahoon, D. R. (2002). Responses of coastal wetlands to rising sea level. Ecology, 83(10), 2869–2877. https://doi.org/10.1890/0012-9658(2002)083[2869:ROCWTR]2.0.CO;2

Nardin, W., Larsen, L., Fagherazzi, S., & Wiberg, P. (2018). Tradeoffs among hydrodynamics, sediment fluxes and vegetation community in the Virginia Coast Reserve, USA. Estuarine, Coastal and Shelf Science, 210, 98–108. https://doi.org/10.1016/j.ecss.2018.06.009

Nepf, H. M. (2012). Flow and Transport in Regions with Aquatic Vegetation. Annual Review of Fluid Mechanics, 44(1), 123–142. https://doi.org/10.1146/annurev-fluid-120710-101048

Nichols, C. R., Wright, L. D., Bainbridge, S. J., Cosby, A., Hénaff, A., Loftis, J. D., et al. (2019). Collaborative science to enhance coastal resilience and adaptation. Frontiers in Marine Science, 6(JUL), 404. https://doi.org/10.3389/FMARS.2019.00404/BIBTEX

Orth, R. J., Carruthers, T. J. B., Dennison, W. C., Duarte, C. M., Fourqurean, J. W., Heck, K. L., et al. (2006). A Global Crisis for Seagrass Ecosystems. BioScience, 56(12), 987–996. https://doi.org/10.1641/0006-3568(2006)56[987:AGCFSE]2.0.CO;2

Pendleton, L., Donato, D. C., Murray, B. C., Crooks, S., Jenkins, W. A., Sifleet, S., et al. (2012). Estimating Global "Blue Carbon" Emissions from Conversion and Degradation of Vegetated Coastal Ecosystems. PLoS ONE, 7(9), e43542. https://doi.org/10.1371/journal.pone.0043542

Reeves, I. R. B., Moore, L. J., Goldstein, E. B., Murray, A. B., Carr, J. A., & Kirwan, M. L. (2020). Impacts of Seagrass Dynamics on the Coupled Long-Term Evolution of Barrier-Marsh-Bay Systems. Journal of Geophysical Research: Biogeosciences, 125(2). https://doi.org/10.1029/2019jg005416

Tinoco, R. O., San Juan, J. E., & Mullarney, J. C. (2020). Simplification bias: lessons from laboratory and field experiments on flow through aquatic vegetation. Earth Surface Processes and Landforms, 45(1), 121–143. https://doi.org/10.1002/ESP.4743

Wang, F., Sanders, C. J., Santos, I. R., Tang, J., Schuerch, M., Kirwan, M. L., et al. (2021). Global blue carbon accumulation in tidal wetlands increases with climate change. National Science Review, 8(9). https://doi.org/10.1093/NSR/NWAA296

Waycott, M., Duarte, C. M., Carruthers, T. J. B., Orth, R. J., Dennison, W. C., Olyarnik, S., et al. (2009). Accelerating loss of seagrasses across the globe threatens coastal ecosystems. Proceedings of the National Academy of Sciences of the United States of America, 106(30), 12377–12381. https://doi.org/10.1073/pnas.0905620106

Wiberg, P. L., Fagherazzi, S., & Kirwan, M. L. (2020). Improving Predictions of Salt Marsh Evolution Through Better Integration of Data and Models. Annual Review of Marine Science, 12(1), 389–413. https://doi.org/10.1146/annurev-marine-010419-010610

Zhu, Q., Wiberg, P. L., & Reidenbach, M. A. (2021). Quantifying Seasonal Seagrass Effects on Flow and Sediment Dynamics in a Back-Barrier Bay. Journal of Geophysical Research: Oceans, 126(2), e2020JC016547. https://doi.org/10.1029/2020JC016547

Zhu, Q., Wiberg, P. L., & McGlathery, K. J. (2022). Seasonal growth and senescence of seagrass alters sediment accumulation rates and carbon burial in a coastal lagoon. Limnology and Oceanography, 1–12. https://doi.org/10.1002/LNO.12178

Chapter 2. Quantifying seasonal seagrass effects on flow and sediment dynamics in a back-barrier bay

This chapter was published in *Journal of Geophysical Research: Oceans*:

Zhu, Q., Wiberg, P. L., & Reidenbach, M. A. (2021). Quantifying Seasonal Seagrass Effects on Flow and Sediment Dynamics in a Back-Barrier Bay. Journal of Geophysical Research: Oceans, 126(2), e2020JC016547. https://doi.org/10.1029/2020JC016547

Abstract

Seagrass growth and senescence exert a strong influence on flow structure and sediment transport processes in coastal environments. However, most previous studies of seasonal seagrass effects either focused on small-scale field measurements or did not fully resolve the synergistic effects of flow–wave–vegetation–sediment interaction at a meadow scale. In this study, we applied a coupled Delft3D-FLOW and SWAN model that included effects of seagrass on flow, waves, and sediment resuspension in a shallow coastal bay to quantify seasonal seagrass impacts on bay dynamics. The model was extensively validated using seasonal field hydrodynamic and suspended sediment data within a seagrass meadow and a nearby unvegetated site. Our results show that seagrass meadows significantly attenuated flow (60%) and waves (20%) and reduced suspended sediment concentration (85%) during summer when its density reached a maximum. Probability density distributions of combined wave-current bed shear stress within the seagrass meadow indicate that significant reductions in sediment resuspension during summer were mainly caused by flow retardation rather than wave attenuation. Although low-density seagrass in winter resulted in much smaller reductions in flow and waves compared with summer meadows, small changes in winter seagrass density resulted in large differences in the

magnitude of attenuation of flow and shear stress. Similarly, while high seagrass densities effectively trapped sediment during summer, small changes in winter density resulted in strong changes in net sediment flux into/out of the meadow. At our study site, low seagrass densities provided significant reductions in wintertime sediment loss compared to losses associated with completely unvegetated conditions.

2.1 Introduction

Seagrasses are important ecosystems that inhabit shallow coastal waters. They offer valuable ecosystem services (e.g., nutrient cycling, water quality control, and carbon sequestration) and provide favorable habitat for species (McGlathery et al., 2007; Nagelkerken et al., 2000; Oreska et al., 2017). They are also commonly referred to as natural eco-engineers that can effectively modify physical environments and stabilize the seabed (Jones et al., 1994). Previous studies on seagrass interactions with physical environments have shown that seagrasses can significantly modify the mean flow and turbulent structure (Fonseca & Fisher, 1986; Gambi et al., 1990; Hansen & Reidenbach, 2012; Koch & Gust, 1999; Widdows et al., 2008); and efficiently dissipate wave energy and attenuate wave height (Fonseca & Cahalan, 1992; Paul et al., 2012; Reidenbach & Thomas, 2018). Attenuation of currents and waves promotes suspended sediment deposition and increases water column clarity (Carr et al., 2010; De Boer, 2007; Gacia et al., 2003).

Despite their great importance in coastal ecosystems, seagrasses are one of the most rapidly declining marine habitats, threatened by eutrophication, temperature stress, and anthropogenic stressors (Orth et al., 2006; Waycott et al., 2009). Understanding state change dynamics and the response of seagrass ecosystems to climate change and human disturbance requires greater insights into flow–wave–vegetation–sediment interactions (McGlathery et al., 2013). Previous studies of seagrass effects on flow and sediment dynamics have mainly focused on laboratory investigations and small-scale and short-term field measurements, and have addressed many key questions in vegetated flow dynamics (e.g., De Boer, 2007; Ganthy et al., 2015; Hansen & Reidenbach, 2012; Nepf, 2012). However, these approaches cannot resolve the inherent complexity and spatial variability of natural environments, including temporal and spatial variability of waves and currents, seabed sediment distribution and availability, spatial variations of bathymetry, and spatial extent and density of subtidal and intertidal vegetation.

With the advancement of numerical model capability to include vegetation effects in flow and wave simulations, researchers have been able to better resolve the synergistic effects of flow–wave–vegetation–sediment interaction in spatially resolved settings. Chen et al. (2007) used a modified Nearshore Community model (NearCoM) that can account for seagrass effects on flow and waves to investigate the effects of seagrass on wave attenuation and suspended sediment transport, and predict the erosion and deposition pattern in an idealized seagrass bed in the nearshore ocean. Beudin et al. (2017) developed a coupled flow–wave–vegetation interaction model based on the Coupled–Ocean–Atmosphere–Wave–Sediment Transport (COAWST) modeling system to investigate the various interacting processes in an idealized shallow basin with a square seagrass patch (1 km by 1 km). Donatelli et al. (2018, 2019) applied this model in Barnegat Bay, USA, to quantify the effects of seagrass on hydrodynamics, wave energy, and sediment exchange between tidal flats covered by seagrass meadows and the adjacent salt marsh. Their results highlighted the complex dynamics between subtidal and intertidal landscapes and benefits of seagrass meadows in enhancing system resilience.

Although these coupled model simulations have significantly improved our understanding of seagrass impacts on flow and sediment dynamics, important aspects of seagrass–tidal flat systems still need to be investigated. Most studies do not provide direct validation with measured flow and suspended sediment data in seagrass meadows. Considering the inherent complexity of natural environments, model validation with spatially distributed data sets is necessary to obtain accurate flow patterns and sediment flux rates. Furthermore, seasonal seagrass growth and senescence in temperate climates exert a strong influence on reduction in flow and waves, and alter sediment resuspension and deposition on vegetated tidal flats (Gacia & Duarte, 2001; Ganthy et al., 2013; Hansen & Reidenbach, 2013; Hasegawa et al., 2008). Carr et al. (2018) found that low seagrass biomass in the fall/winter increased the amount of sediment resuspension in the bay, whereas dense seagrass during the growing season inhibited sediment resuspension and limited sediment delivery to adjacent salt marsh. These findings are based on long-term, transect-based simulations and do not resolve seasonal wind patterns or 2-D spatial patterns of vegetation, flow, waves, and suspended sediment. The combined effects of seasonal wind patterns and submerged seagrass density variation on sediment resuspension on subtidal flats need to be better quantified, particularly if we are interested in quantifying sediment budgets or predicting future change.

To better resolve spatial variations of dynamic factors and understand the effects of seasonal seagrass growth and winds on hydrodynamics and sediment transport, we apply a relatively high-resolution (~70 m) hydrodynamic and sediment transport Delft3D model that includes coupling of seagrass effects on flow, waves, and sediment resuspension in a shallow coastal bay (South Bay) on Virginia's Atlantic coast. Rather than simply increasing bed roughness to parameterize attenuation of flow and waves, we used a more physically based approach to simulate vegetation effects on the mean flow and wave dissipation based on the approaches of Baptist et al. (2007) and Suzuki et al. (2012). The coupled model was then extensively validated using seasonal field hydrodynamic and suspended sediment data within a seagrass meadow and a nearby unvegetated site. We used the model to quantify seagrass effects on bay dynamics under: (1) typical summer conditions when seagrass density reaches a maximum and winds are predominantly southwesterly, and (2) winter conditions when frequent and stronger northeasterly winds coincide with minimum seagrass density. The results were analyzed to address three questions. (1) What are the effects of seasonal variations in seagrass density on hydrodynamics and sediment transport in a shallow coastal bay? (2) What are the relative contributions of flow retardation and wave attenuation in reducing sediment resuspension in seagrass meadows during summer and winter conditions? (3) How do rates and patterns of sediment erosion/deposition within seagrass beds vary in response to seasonal variations in wind and seagrass density? Our results underscore the tight coupling of vegetation interactions with physical environments in shallow coastal bays, provide useful guidance on the selection of vegetation parameters for coupled model simulations, and highlight the large variations in flow reduction, bed shear stress and net sediment accumulation that accompany small changes in density when meadow densities are low.

2.2 Materials and methods

2.2.1 Study area

This study was conducted in South Bay, a shallow coastal lagoon within the Virginia Coast Reserve (VCR) with an area of ~31.5 km^2. The VCR is a shallow coastal barrier–bay system located on the eastern shore of Virginia along the Atlantic side of the Delmarva Peninsula (Figure 2.1a) and is one of the 28 sites of the Long-Term Ecological Research (LTER) network. This system lacks significant fluvial freshwater and sediment input and is a mostly undeveloped area with low nutrient loading. Since local human impact on this coastal bay system is relatively small, the VCR provides a unique opportunity to study coastal system evolution under climate change (McGlathery et al., 2007).

South Bay has an average water depth of 1.0 m below mean sea level (Reidenbach & Thomas, 2018); a barrier island (Wreck Island) with back-barrier marsh borders its eastern side (Figure 2.1b). Tides within the bay are semidiurnal with a mean tidal range of 1.2 m. Wind activity shows a strong seasonal pattern in this region, with typical southerly winds during the summertime and more frequent and stronger northerly winds in winter (Fagherazzi and Wiberg, 2009; Figure 2.1c). Wind-generated waves are the dominant force driving sediment resuspension and high suspended sediment concentration (SSC) in the shallow bays of the VCR (Lawson et al., 2007; Mariotti et al., 2010). South Bay is close to the southern geographical limit for eelgrass (*Zostera marina*) in the Western Atlantic (Aoki et al., 2020) and is a successful seagrass restoration site (McGlathery et al., 2013; Orth & McGlathery, 2012) with *Zostera marina* dominating the subtidal flats (Figure 2.1b). Maximum seagrass density occurs during summer with a peak density of approximately 400–550 shoots m^{-2}, while the minimum seagrass density is 50–100 shoots m^{-2} in winter due to senescence (Hansen & Reidenbach, 2013; Oreska et al., 2017; Reidenbach & Thomas, 2018; Rheuban et al., 2014). Because seagrass meadows can effectively trap fine particles, bed sediment in South Bay is dominated by very fine sand with a mean grain size of 71 μm (Lawson et al., 2007; Oreska et al., 2017).

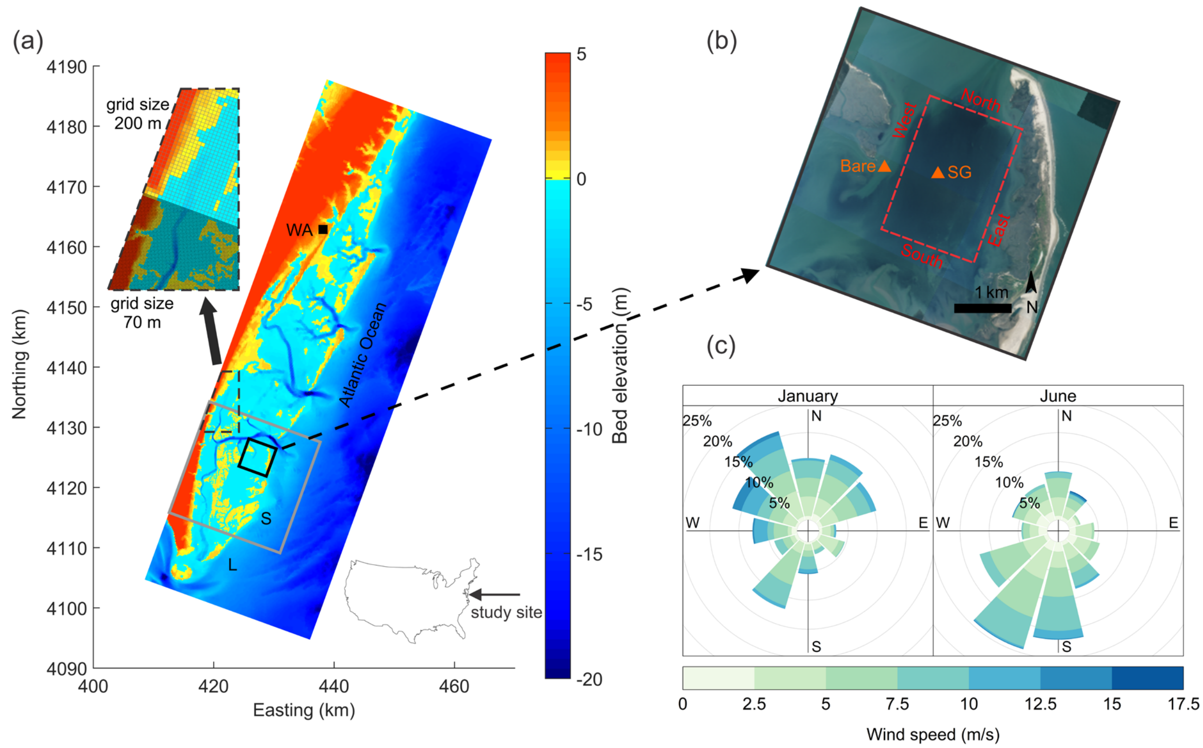

Figure 2.1 (a) Bathymetry of the model and grid interface between small and large model domains. The boundary between small and large model grids is highlighted by the gray box. S is the small model domain with a resolution of ~70 m while L represents the large model domain with a resolution of 200 m. The subpanel shows the model grid interface in a selected area highlighted by the black dashed trapezoid. WA is the NOAA tide gauge station (Wachapreague, ID: 8631044) used for water level validation (https://tidesandcurrents.noaa.gov). Coordinates of UTM zone 18N are given in km. (b) Aerial image of the study area (South Bay, VCR) and the distribution of seagrass meadow. The image is from the Virginia Institute of Marine Science Submerged Aquatic Vegetation (SAV) program (http://web.vims.edu/bio/sav). Orange triangles show the unvegetated site (Bare) and the seagrass site (SG) used for model validation. Red dashed lines show the transect location for water and sediment flux monitoring. (c) Directional distribution of winds in the study area in January and June, 2011. The wind data is from the NOAA National Data Buoy Center (Station CHLV2; https://www.ndbc.noaa.gov/station_page.php?station=chlv2). For the full record of model forcing during each time period, please refer to Figure A1.1.

2.2.2 Model descriptions

For this study, we used the process-based and spatially resolved hydrodynamic and sediment transport model Delft3D to simulate flow, waves, and sediment resuspension in the VCR. Delft3D is widely used and has been validated for various coastal environments (Apotsos et al., 2011; Dastgheib et al., 2008; Edmonds & Slingerland, 2010; Lesser et al., 2004). It solves the Navier–Stokes equations for an incompressible flow and advection–diffusion equation for multiple sediment fractions. The Delft3D model uses the Partheniades–Krone formulation to calculate cohesive sediment erosion and deposition fluxes (Lesser et al., 2004) and the Van Rijn et al. (2001) approach to estimate non-cohesive sediment transport. The Delft3D flow model can be coupled with the nearshore phase-averaged wave model SWAN to simulate flow–wave interaction. The SWAN model solves the wave action balance equation, which includes effects of wave generation, propagation, refraction, diffraction, dissipation and nonlinear wave–wave interactions (Booij et al., 1999), and passes wave parameters to the flow model to calculate combined wave–current bed shear stress.

To better resolve flow, sediment fluxes and vegetation effects in the core study area and to improve computational efficiency, we used the domain decomposition technique (Deltares, 2014) to locally refine the model grid size in South Bay and divided the overall model into two domains (Figure 2.1a). Parallel computations can be carried out on the large domain (resolution of 200 m) and small domain (resolution of ~70 m), and these two domains communicate and exchange information along their shared boundaries at each time step. Compared with previous hydrodynamic models applied in the VCR system (resolution of 250 m; Castagno et al., 2018; Nardin et al., 2018; Wiberg et al., 2015), the finer grid size (~70 m) of the small model domain is able to better resolve seagrass meadows (2×4 km) in South Bay and the bordering barrier island (0.7×5 km).

2.2.3 Coupling seagrass effects in Delft3D

In order to establish a process-based model to resolve flow–wave–vegetation–sediment interactions, vegetation effects on reduction in flow and waves were incorporated in Delft3D. Seagrass effects on flow were represented as submerged vegetation using the Baptist vegetation module in Delft3D (Baptist et al., 2007). The Baptist vegetation equation has been widely tested and validated by laboratory experiments and field measurements, and produced a good fit with those datasets (e.g., Arboleda et al., 2010; Crosato & Saleh, 2011). This method considers vegetation as cylindrical structures characterized by vegetation height (h_v), stem diameter (b_v), shoot density (N), and vegetation flow drag coefficient (C_D) and calculates the corresponding vegetation drag (τ_v). The skin bed shear stress for sediment transport (τ_b) then can be obtained by subtracting the vegetation drag from total shear stress (τ_t). The Baptist vegetation module has been successfully applied in several depth-averaged Delft3D model studies to investigate vegetation effects on coastal environments, and was able to produce reasonable simulation results (Nardin et al., 2016, 2018; Nardin & Edmonds, 2014). In order to account for vegetation bending effects under mean flow conditions, we followed the approach of Dijkstra (2009) and used a deflected vegetation height that is reduced by approximately 20% of its typical value and a calibrated seagrass flow drag coefficient (C_D). Numerous previous studies have shown that the Baptist vegetation model can generate a very similar flow condition to flexible vegetation when using an appropriate deflected height and equivalent drag coefficient values (Hu et al., 2015; Lera et al., 2019; Nardin et al., 2018). More detailed descriptions of the vegetation module in the depth-averaged Delft3D model can be obtained from Nardin et al. (2018). Numerous wave models have been developed recently to quantify wave attenuation induced by coastal vegetation (e.g., Ma et al., 2013; Phan et al., 2019; van Rooijen et al., 2016; Wu et al., 2016). In this study, the vegetation wave energy dissipation model developed by Suzuki et al. (2012) was implemented in the SWAN model to simulate seagrass effects on waves. This approach adds a vegetation dissipation term which depends on vegetation height (h_v), stem diameter (b_v), shoot density (N), and vegetation wave drag coefficient ($\widetilde{C_D}$) into the wave action density spectrum balance equation. Recent studies (e.g., Baron-Hyppolite et al., 2018; Wu et al., 2016) have shown that this explicit vegetation representation in the SWAN model can produce reasonable simulation results that were in good agreement with field data and flume experiments.

2.2.4 Model settings and validation datasets

The model used a rectangular grid of 148 by 444 nodes for the large domain and 305 by 302 nodes for the small domain. The northern, southern and eastern boundaries of the large domain are open ocean boundaries that are forced with water levels extracted from the NOAA tide gauge record at Wachapreague (WA, ID: 8631044; Figure A1.1a, c). Adjustments of tidal amplitude and tidal phase are applied at the boundaries (dampened by a factor of 0.9 and delayed 66 min; similar approach as Castagno et al., 2018) to generate the best tidal simulation results for the shallow bays. The flow model was coupled with the SWAN model every 60 minutes. Hourly wind conditions from the nearby NOAA station CHLV2 (Figure A1.1b, d) were used to drive the wave simulation and a uniform Collins bottom friction coefficient of 0.1 was used in SWAN.

Model bathymetry and high-resolution maps of bottom sediment size distributions (two mud components and one sand fraction) were extracted from Wiberg et al. (2015). The mud components comprise a 32–64 μm coarse silt fraction with a settling velocity of 3.6 mm s^{-1} and a < 32 μm size fraction with a representative floc settling velocity of 0.75 mm s^{-1} (Wiberg et al., 2015). The critical shear stress for cohesive sediment erosion was set to 0.03 N m^{-2} (Lawson et al., 2007; Reidenbach & Thomas, 2018; Reidenbach & Timmerman, 2019). For the sand fraction, a representative median grain size of 125 μm was used. Since seagrass meadows can effectively trap fine sediment and modify bottom sediment size, sediment size distributions in South Bay seagrass meadows were initialized based on local measurements from Oreska et al. (2017). A spatially and temporally constant Chézy bed roughness of 50 $m^{1/2}s^{-1}$ was used in both model domains. The active sediment layer thickness that can affect sediment availability during each individual time step was set to 5 cm.

The model was initially run for two time periods, January 1–31 and June 1–30, 2011, with typical seasonal seagrass characteristics based on previous observations in South Bay (Table 2.1; Hansen & Reidenbach, 2013; Oreska et al., 2017; Reidenbach & Thomas, 2018; Rheuban et al., 2014). An initial smoothing time of 60 h was used to improve flow stability when the model started. Four transects (North, East, South, and West) were designed in the small domain to monitor water and sediment fluxes into and out of the seagrass meadows (Figure 2.1b). Because our study site is relatively shallow with a mean depth of ~1 m and well mixed, with little evidence of stratification or strong shear within the water column (Figure A1.2), we assume that the vertical structure of velocity has a relatively small impact on the general flow and sediment transport patterns. Therefore, the coupled model was implemented in depth-averaged mode with a time step of 0.25 min to reduce computational time. Six model scenarios were considered in our simulations (Table 2.2) to differentiate the effects of seagrass on flow and waves during different seasons. These model runs were forced with the same hourly measurements of tide, wind, and waves but had different vegetation settings. Model runs W1 and S1 were run without seagrass effects in winter and summer, respectively. Seagrass effects on flow were included in model runs W2 and S2. Model runs W3 and S3 were run with seagrass effects on flow and waves using winter and summer seagrass characteristics, respectively.

Time series of water depth, velocity, significant wave height (Hs), and SSC collected at a reference bare site and a seagrass site (see locations in Figure 2.1b) during each simulation period in 2011 were compared with simulation results output from model runs W3 and S3 for model validation. More detailed descriptions of the data collection and instrument configuration can be found from Hansen & Reidenbach (2018). The model simulated depth-averaged velocity at the bare site was converted to the velocity at 0.5 m above seabed using a logarithmic velocity profile distribution (Deltares, 2014) and compared with velocity measurements at the same height. Since the mean depth of the validation sites is small (< 1 m) and the SSC in the water column does not show a strong vertical gradient (less than 5 mg L^{-1} between 0.1 m and 0.5 m above seabed based on measurement results), we assumed that the SSC measured at 0.5 m above seabed was roughly equal to depth-averaged SSC in model validation. Time series of measured SSC collected at both sites in June 2011 showed persistently high values (~30 mg L^{-1}) that were unrelated to current and wave strength. This high background turbidity is likely caused by episodically high chlorophyll concentrations in the water column during summer. A recent study by Reidenbach & Timmerman (2019) found that water column chlorophyll levels at the study site reached a maximum in June when seagrass density was high. Considering that the focus of this study is vegetation interaction with physical processes, we did not attempt to model biologically induced background turbidity levels in our model validation.

Table 2.1 Seagrass parameters input for the model.

Model period	h_v (m)	b_v (cm)	N (shoots m^{-2})	C_D	$\widetilde{C_D}$
January 1–31, 2011	0.2	0.2	50	0.2	3.0
June 1–30, 2011	0.4	0.4	400	0.4	3.0

Table 2.2 Model runs and vegetation module setup.

Model runs	Period	Seagrass effects on flow	Seagrass effects on waves
W1	January	No	No
W2	January	Yes	No
W3	January	Yes	Yes
S1	June	No	No
S2	June	Yes	No
S3	June	Yes	Yes

2.3 Results

2.3.1 Model sensitivity tests and validation

A series of model runs were carried out to test the sensitivity of flow–wave–vegetation interactions to variations in vegetation height, shoot density, and vegetation drag coefficients (Figure A1.3). Typical summer vegetation characteristics (h_v= 0.4 m, b_v = 0.4 cm, N = 400 shoots m^{-2}; Table 2.1) were set as our reference case in the calibration. In each set of calibration runs, only one vegetation parameter was changed while other parameters remained constant. The calibration results show that vegetation interaction with flow and waves is non-linear with rapid changes as a function of shoot density at low densities but little change in flow retardation after vegetation density reaches some critical value (≥ 400 shoots m^{-2} for our study site). Sediment resuspension is sensitive to shoot density and the wave drag coefficient for vegetation. Seagrass-related drag coefficients for flow and waves were used as calibration factors to match model results with seasonal field measurements. A seagrass flow drag coefficient of 0.4 (0.2) in summer (winter) produced best agreement between model results and measurements. A constant seagrass wave-drag coefficient of 3.0 was applied in both simulation periods.

The model simulated water levels in each period were checked against measured water levels at our tidal reference site at Wachapreague (WA, Figure A1.4). R-squared (R^2) and Root Mean Square Error (RMSE) were calculated for each simulation. Good agreement was obtained in January (R^2= 0.98, RMSE = 0.07 m) and in June (R^2= 0.99, RMSE = 0.05 m). The model results of run W3 and run S3 were validated using seasonal field hydrodynamic and suspended sediment data during a 4-day period in 2011 from a bare site and a seagrass site in South Bay (Figure 2.2 & Figure 2.3; for detailed validation datasets, please refer to Hansen & Reidenbach, 2018). Model skill indices (bias, RMSE, and Willmott Skill Index) were calculated to quantify model ability to characterize hydrodynamic and suspended sediment characteristics in South Bay (Table 2.3). The skill index proposed by Willmott (1981) is defined as

$$Skill = 1 - \frac{\sum |X_{model} - X_{obs}|^2}{\sum (|X_{model} - \overline{X_{obs}}| + |X_{obs} - \overline{X_{obs}}|)^2} \tag{1}$$

where X_{model} and X_{obs} are the model predicted variables and observations, respectively, and $\overline{X_{obs}}$ is the time mean observation value. A skill of one indicates perfect agreement between model results and observations, while a skill of zero shows complete disagreement.

Table 2.3 A summary of statistical metrics for model validation.

Period	Site	Parameter	Statistics		
			Bias	RMSE	Skill
January, 2011	Bare	Water level	0.07 m	0.09 m	0.95
		Hs	-0.02 m	0.05 m	0.68
		Velocity	0.04 m s^{-1}	0.05 m s^{-1}	0.84
		SSC	-3.44 mg L^{-1}	8.69 mg L^{-1}	0.80
	SG	Water level	0.06 m	0.16 m	0.94
		Hs	0.00 m	0.05 m	0.87
		SSC	-4.33 mg L^{-1}	8.13 mg L^{-1}	0.82
June, 2011	Bare	Water level	0.00 m	0.07 m	0.97
		Hs	0.00 m	0.06 m	0.56
		Velocity	0.07 m s^{-1}	0.06 m s^{-1}	0.69
	SG	Water level	0.10 m	0.07 m	0.96
		Hs	-0.01 m	0.04 m	0.67
		Velocity	0.04 m s^{-1}	0.02 m s^{-1}	0.58

Model predicted water levels slightly over-estimated measured levels in South Bay, with a positive bias less than 0.10 m; RMSE was lower than 0.16 m during each period and skill scores were very high (≥ 0.94). Despite similar wave height RMSE values at both sites, wave height skill scores for the seagrass site (0.87 & 0.67) were generally higher than those of bare site (0.68 & 0.56). The model did not reproduce the wave height peaks on January 21 and June 19 at the bare site (Figure 2.2b, d). The discrepancy for the first event was due to low wind speed input for the wave model. Although wave height measurements showed Hs ≥ 0.3 m during this period (Figure 2.2b), local wind speed records of CHLV2 station were too small (< 5 m s^{-1}) to generate such a wave event. Either spatially variable wind conditions or local amplification of wave conditions during that time could be responsible for the disagreement. The model over-predicted bare site Hs on June 19 when the winds came from the south with a wind speed of ~8 m s^{-1}. Based on the results of a preliminary model sensitivity test of wind direction impacts on Hs, southerly winds had a relatively large wind fetch for our study site, but the observation records only showed a small wave height peak during the same period. We speculate that this disagreement may have been caused by high density seagrass surrounding the bare site in summer that altered the wave pattern in the bay. The best skill score for modeled velocity was at the bare site in January (0.84); the skill scores were lower at the bare site (0.69) and seagrass site (0.58) in June when seagrass density reached its maximum. In general, model-predicted velocity captures the stronger peak velocity during ebb tides but over-estimates peak velocity during flood tides (Figure 2.2e, g & Figure 2.3f). The total modeled SSC was calculated by summing the SSC of each sediment component output from the model. Our simulation results show that the SSC in the seagrass meadow area was dominated by the < 32 μm size fraction (contributing to > 95% of total SSC variations). Therefore, we did not attempt to further separate the contribution of each sediment fraction but only show the results of total SSC (hereafter referred to as the “SSC”) in the following text. Skill scores for SSC were high in January at the bare site (0.80) and seagrass site (0.82). The model successfully captured most sediment resuspension events (Figure 2.2f & Figure 2.3e). Although direct validation of the summer SSC was not available at both sites, the summer SSC levels predicted by the model (Figure 2.2h & Figure 2.3g) were consistent with our SSC measurements inside and outside the seagrass meadow during the summer of 2019 when background turbidity was low (Figure A1.5). Sediment resuspension was greatly reduced in the seagrass meadow compared with the nearby unvegetated site during summer when seagrass density was high. Considering the inherent complexity of natural environments and the somewhat simplified dynamics of flow–wave–vegetation–sediment interactions as represented in the model, we believe that the discrepancy between observations and our model predictions is acceptable and this coupled model is able to produce reasonable simulations of these interactions under varying forcing and vegetation densities in our study system.

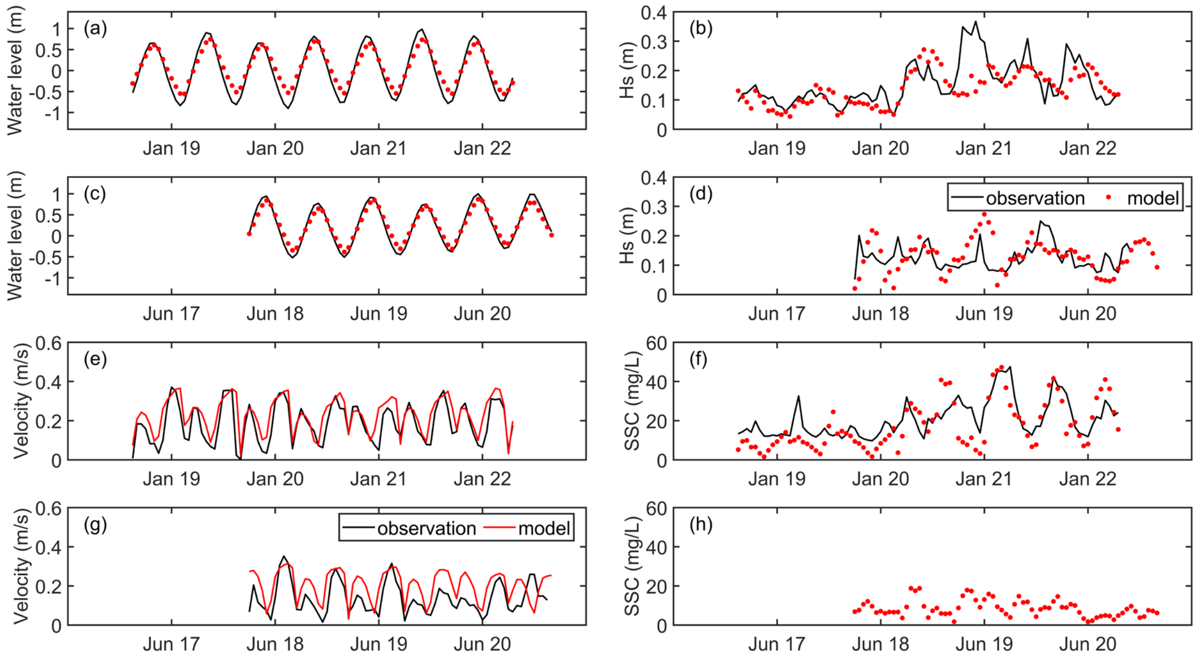

Figure 2.2 Comparison of measured and modeled hydrodynamic and suspended sediment conditions during a 4-day period at the bare site (Bare): (a) water level, (b) Hs, (e) velocity, and (f) SSC in January, 2011, and (c) water level, (d) Hs, (g) velocity, and (h) SSC in June, 2011. Black lines represent observational data, and red dots (lines) show model simulation results.

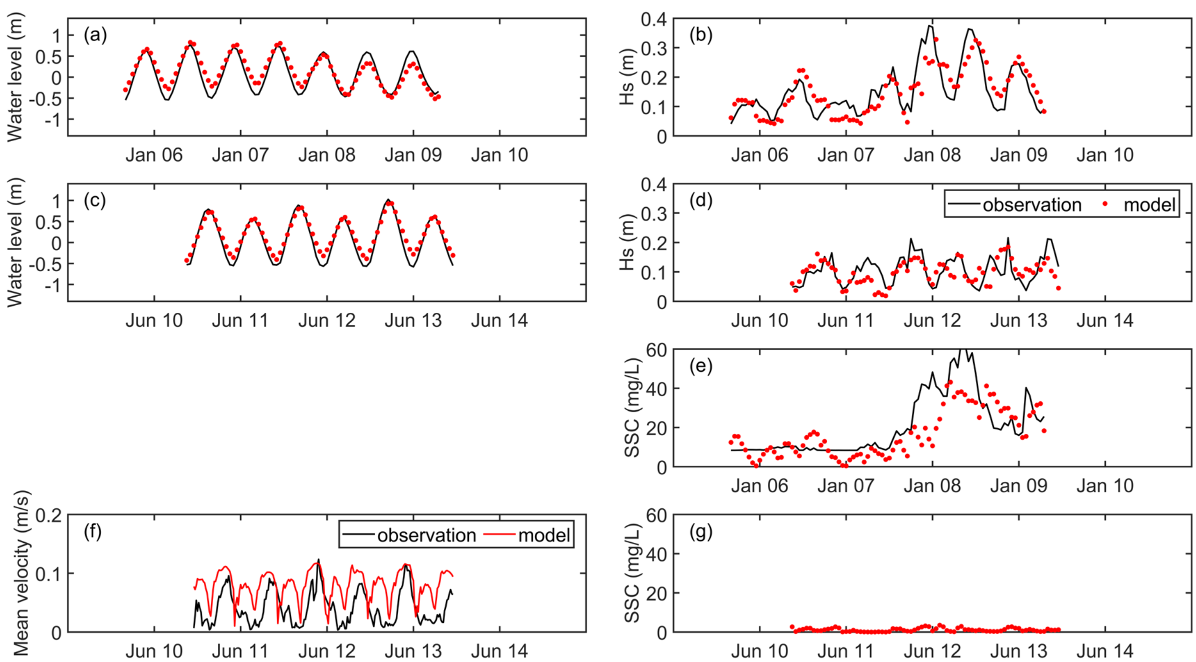

Figure 2.3 Comparison of measured and modeled hydrodynamic and suspended sediment conditions during a 4-day period at the seagrass site (SG): (a) water level, (b) Hs, and (e) SSC in January, 2011, and (c) water level, (d) Hs, (f) depth-averaged velocity, and (g) SSC in June, 2011. Black lines represent observational data, and red dots (lines) show model simulation results.

2.3.2 Seasonal seagrass effects on hydrodynamics

Numerous field measurements (e.g., Hansen & Reidenbach, 2013; Hasegawa et al., 2008; Reidenbach & Thomas, 2018) have shown that high-density seagrass in summer resulted in much larger reductions in flow and waves compared with winter meadows. This seasonal seagrass control on flow and waves was also predicted by our model. Comparison of modeled depth averaged velocity and Hs between the bare site and seagrass site output from model run W3 shows that there was < 10% reduction in flow and waves at vegetated sites during winter when seagrass density was at its minimum (Figure 2.4a, b). In contrast, seagrass meadows significantly attenuated flow (60%) and reduced wave height (20%) during late spring-early summer when its density reached a maximum (model run S3; Figure 2.4a, b). Depth averaged velocity remained low (< 0.1 m s^{-1}) in the meadows when high density seagrass occupied the seabed, even at peak flood/ebb tides (Figure 2.5a). The difference of Hs between model runs S2 and S3 reveals that Hs could be reduced by 0.1 m in a storm event (Hs $\geq$ 0.3 m) when wave attenuation effects caused by seagrass were included in the model (Figure 2.5b).

Cumulative water flux into the seagrass meadows was monitored through the model transects (Figure 2.1b) in each simulation period (January & June). There was no significant difference of water flux between model runs S2 (W2) and S3 (W3), indicating wave attenuation by seagrass had little effect on water flux into the meadows. Therefore, we only present results of model runs W1, W3, S1, and S3 here. The presence of seagrass had a strong seasonal impact on the water exchange with the seagrass meadows. During winter when seagrass density was low, flow reduction caused by seagrass was relatively weak, resulting in little change of cumulative water flux of each transect (W1 vs. W3 in Figure 2.6a). In contrast, cumulative water flux was reduced by ~70% in transects North, South, and West in model run S3 compared with model run

S1 (Figure 2.6a). Although the net water flux into the seagrass meadows (the sum of water flux through four transects) remained relatively constant with/without seagrass flow effects in cases S1 and S3, the cumulative water flux through each transect was reduced significantly in S3 due to flow reduction by seagrass. As a result of velocity retardation, seagrass meadows in summer experienced less flushing by tidal flows (decrease by ~70%) compared with the non-vegetated case, which potentially increases the vulnerability of the coastal bay to pollution and heat stress by increasing water residence time in the meadows. Cumulative water flux was also influenced by seasonal wind patterns. Prevailing southerly winds in summer caused more water to enter the system through the South transect and then discharge through the North transect to the region near the northern inlet of the bay, while northerly winds in winter kept pushing the water back into the bay, resulting in smaller water flux through the North transect than in summer (W1 and S1 in Figure 2.6a).

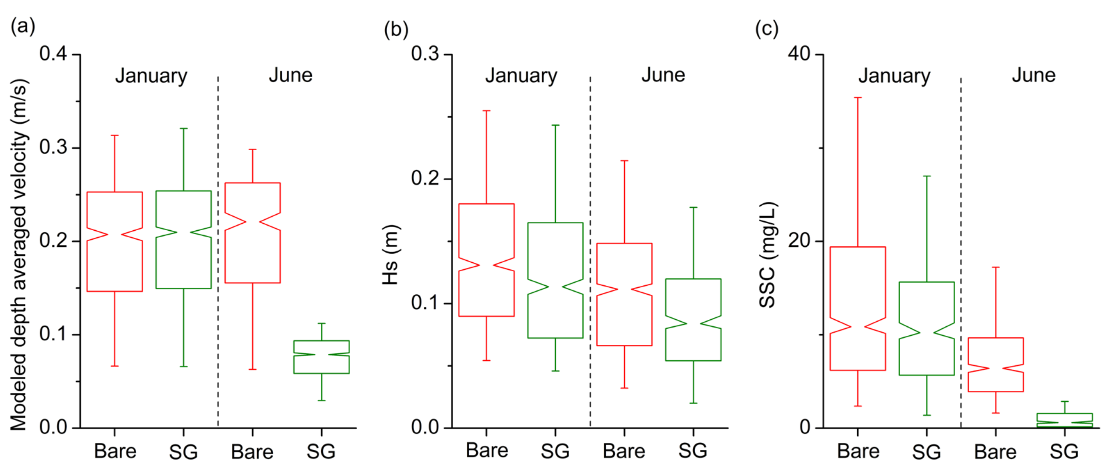

Figure 2.4 Box plots of modeled (a) depth averaged velocity, (b) Hs, and (c) total SSC at the bare site and seagrass site output from model runs W3 (January 1–31) and S3 (June 1–30) that include seagrass effects on flow and waves.

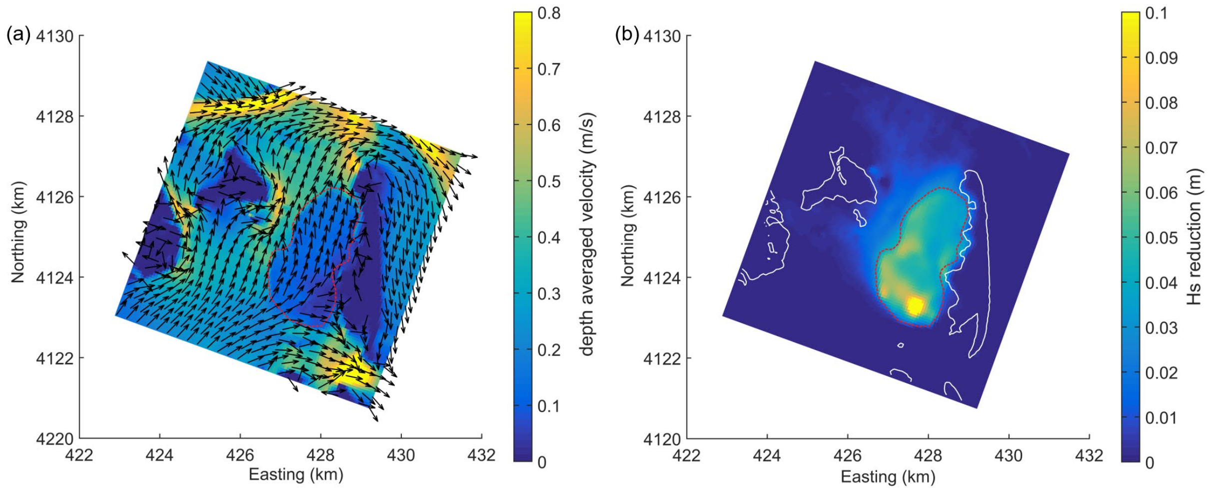

Figure 2.5 (a) Distribution of depth averaged velocity at peak ebb conditions from model run S3 (with effects of summer seagrass densities on flow and waves). The color scale indicates the magnitude of velocity, while arrows show flow direction. (b) Wave height difference between model runs S2 (without seagrass wave attenuation effects) and S3 (with seagrass wave attenuation effects) during a strong wind wave event (June 17). The red dashed line shows the meadow outline.

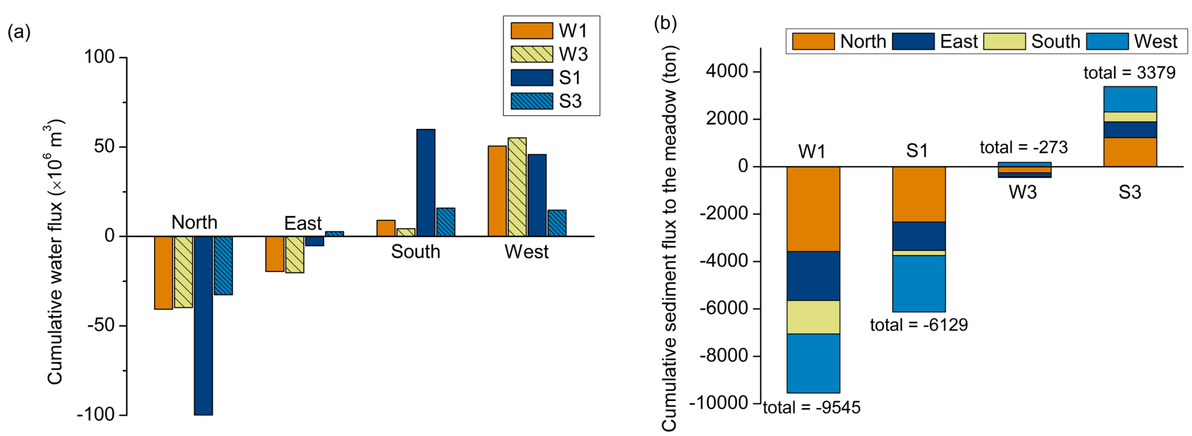

Figure 2.6 (a) Cumulative water flux and (b) cumulative sediment flux into/out of seagrass meadows through model monitoring transects during each simulation period (January 1–31 and June 1–30, 2011). Model runs W1 and S1 are without seagrass effects in winter and summer, respectively, while W3 and S3 include seagrass effects on reduction in flow and waves. Positive values denote water/sediment input while negative values indicate export of water/sediment from the meadow.

2.3.3 Seasonal seagrass effects on sediment transport

Seasonal growth and senescence of seagrass not only exerted a strong influence on attenuation of flow and waves, but also altered sediment resuspension on the flats. Model simulations show that the SSC was similar at both the bare site and seagrass site during winter when seagrass density was at its minimum (Figure 2.4c). However, SSC at the seagrass site was decreased by 85% in summer when seagrass density reached a maximum (Figure 2.4c), indicating that high density seagrass can effectively inhibit sediment resuspension. Spatial distributions of total SSC in model runs S1 and S3 during a storm event clearly demonstrate this strong seasonal control of seagrass on sediment resuspension (Figure 2.7). Without seagrass effects on flow and waves in model run S1, fine sediment in seagrass meadows was easily resuspended into the water column (Figure 2.7a). Once seagrass effects were included in model run S3, there was almost no sediment resuspension within the seagrass meadows and SSC was decreased significantly due to strong attenuation of flow and waves by high density seagrass, even during a storm event (Figure 2.7b).

Simulated sediment fluxes into and out of the seagrass meadow were calculated at each of the monitoring transects (Figure 2.6b). The results show that seagrass meadows trapped sediment in the bay during summer when seagrass density was high, with a net cumulative sediment input of 3.4×10^3 tons (S3 in Figure 2.6b). During winter when attenuation of flow and waves caused by seagrass was relatively weak, the seagrass meadows maintained a nearly balanced sediment budget (-2.7×10^2 tons; W3 in Figure 2.6b). In contrast, significant sediment output from the seagrass meadows was found in both simulation periods when seagrass effects were not included in the model (W1 and S1 in Figure 2.6b). The corresponding sediment fluxes were -9.5×10^3 tons and -6.1×10^3 tons, respectively; the flux was larger in winter as there were more frequent and stronger northerly winds during that period. Therefore, vegetation effects are critical for this system to maintain a depositional state, with low density winter seagrass providing significant reductions in sediment loss compared to completely unvegetated conditions.

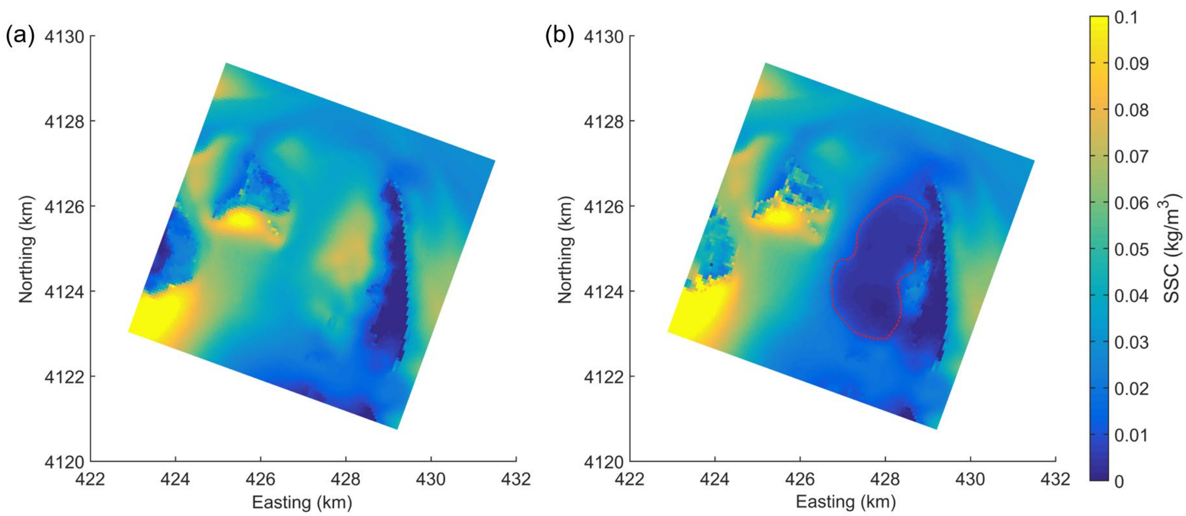

Figure 2.7 Total SSC distribution output from: (a) model run S1 (without seagrass effects) during a storm on June 17 and (b) model run S3 (with seagrass effects on flow and waves) during the same period. The red dashed line shows the meadow outline.

2.4 Discussion

2.4.1 Non-linear effects of seasonally varying seagrass density on flow

Seasonal growth and senescence of seagrass exerted a strong influence on flow patterns and water exchange at our study site (Figure 2.4a, 5a, 6a). The main factor controlling this seasonal pattern is variation in seagrass shoot density, which reached a maximum (≥ 400 shoots m^{-2}) during late spring-early summer and decreased to a minimum (50-100 shoots m^{-2}) in winter. Analysis of normalized velocity at the seagrass site (the ratio of depth averaged velocity with seagrass effects to the velocity in a completely unvegetated simulation) as a function of seagrass density (Figure 2.8a) illustrates that the most rapid changes of velocity occurred at low seagrass densities, with normalized velocity decreasing by 40% as density increases from 25 to 200 shoots m^{-2}. Once seagrass density exceeded 400 shoots m^{-2}, there was little change in flow reduction (< 7% of velocity change in the range from 400 to 800 shoots m^{-2}). Similarly, normalized bed shear stress at the seagrass site (the ratio of bed shear stress with seagrass effects to the bed shear stress in a completely unvegetated simulation) was reduced by ~90% within the low density range (0–200 shoots m^{-2}; Figure 2.8b), but by less than 5% once seagrass density ≥ 400 shoots m^{-2}. Our calibration results also show that depth averaged velocity decreased non-linearly with increasing vegetation height and vegetation drag coefficient (Figure A1.3).

The model prediction of velocity reduction at high seagrass densities agrees with previous flume studies regarding the limit of flow reduction when seagrass density is above certain thresholds (Gambi et al., 1990; Ganthy et al., 2015; Peralta et al., 2008). Higher shoot density increased the magnitude of velocity reduction when densities were moderate. However, this flow reduction effect reached a limit at the point when flow velocity was completely attenuated within the vegetation canopy due to a high shoot density above a threshold value (Peralta et al., 2008). Widdows and Brinsley (2002) reported a similar non-linear density dependent relationship between depth averaged velocity and stem density in their flume experiments with marsh vegetation (*Spartina anglica*). Their high-density threshold (~400 shoots m^{-2}) was similar to our model predicted results (Figure 2.8a), but the velocity reduction (75%) within the low-density range in their flume experiment was slightly higher than that predicted by our model (60%). Once the density threshold was reached, the velocity within the canopy decreased to almost zero, resulting in a skimming flow above the canopy.

The presence of high-density seagrass not only attenuated flow within the meadow, but also affected flow patterns outside the meadow. Velocity differences between non-vegetated case S1 and vegetated case S3 during peak ebb show that flow reduction occurred upstream and in the wake of the meadow (Figure 2.9a). Velocity reduction in these areas (~20%) was smaller than the reduction within the meadow (~60%). Due to flow obstruction by the seagrass meadow, tidal flow was deflected around the meadow and concentrated at the western edge (Figure 2.9a), resulting in flow velocity increasing by 30% at the meadow edge and water flux through the adjacent tidal channel increasing by 12% (Figure 2.9b). Flow enhancement outside the meadow, however, was not able to offset diminished water fluxes within the meadow, resulting in a 10% decrease of total water flux through the monitoring transect (Figure 2.9b). This flow acceleration and deceleration pattern caused by seagrass meadows was also reported by Beudin et al. (2017). In their rigid vegetation case, an idealized square seagrass meadow (1 km by 1 km) in the shallow basin induced an 80% reduction of depth averaged velocity in its wake and an 40% increase of depth averaged velocity at the edge. Similarly, Lera et al. (2019) found that seagrass meadows produced a lateral velocity amplification around a river mouth bar covered by dense seagrass, and this lateral velocity amplification increased with seagrass height and density. At a larger spatial scale, Nardin et al. (2018) found that salt marsh and seagrass in the VCR system could slightly increase the velocity at the tidal inlets by 2% in their most vegetated case (with double density and vegetation height).

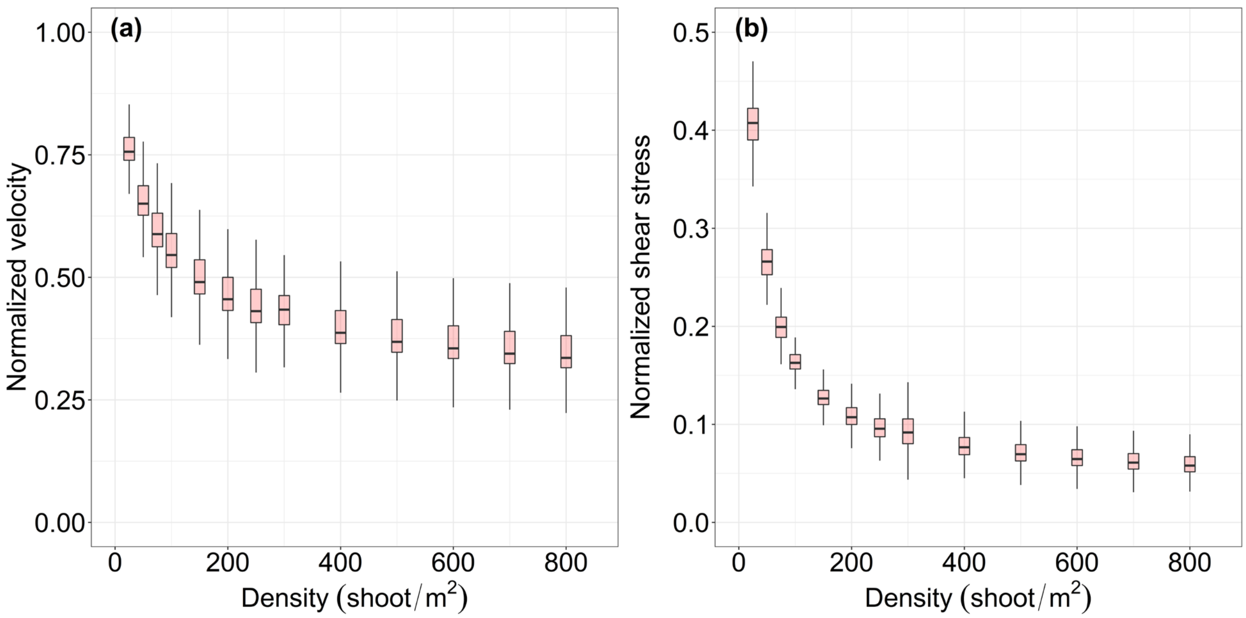

Figure 2.8 Velocity (a) and bed shear stress (b) change as a function of seagrass density at the seagrass site. The velocity and bed shear stress are normalized with respect to model run results without seagrass effects. Seagrass parameters used in these flow simulations are: h_v= 0.4 m, b_v = 0.4 cm, and C_D = 0.4.

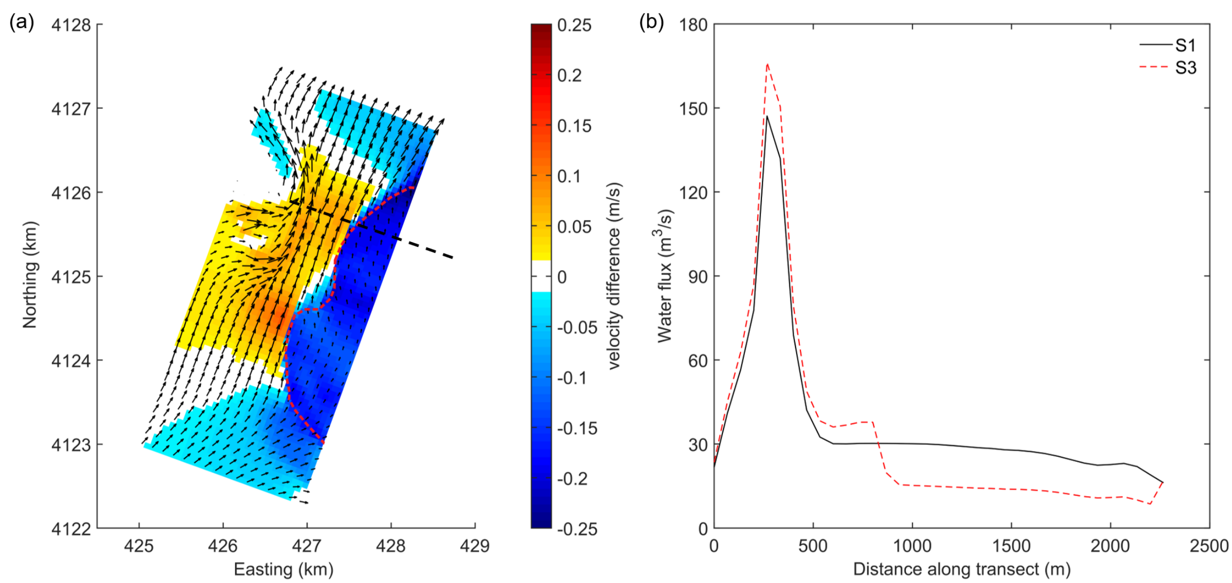

Figure 2.9 (a) Velocity difference at the western edge of seagrass meadow during peak ebb between model runs S1 (the reference summer simulation without seagrass effects) and S3 (with seagrass effects on flow and waves). Arrows show the flow direction and magnitude in S3. The color scale indicates velocity changes relative to the flow speed in model run S1 (Figure 2.5a). Positive values denote velocity acceleration while negative values denote velocity reduction. The red dashed line shows the meadow outline. (b) Water flux along the cross-meadow transect during the same time period. The transect location is shown in black dashed line in (a).

2.4.2 Contributions of attenuation of flow and waves in reducing sediment resuspension

The impact of seagrass on trapping fine-grained particles from the water column and reducing sediment resuspension is the most important positive feedback for seagrass growth, as it increases light penetration to the seabed and stimulates seagrass growth (Carr et al., 2010; De Boer, 2007). Despite significant variability in bed shear stress and SSC due to changes in flow velocity and wave conditions in response to tides and storms, seasonal seagrass growth and senescence has been shown to exert a strong control on sediment resuspension within seagrass meadows (Gacia & Duarte, 2001; Ganthy et al., 2013; Hansen & Reidenbach, 2013).

Our model simulations show that high density seagrass meadows can effectively attenuate flow (60%) and reduce wave height (20%) during late spring-early summer, resulting in a decrease in bed shear stress and SSC levels (85%), while there was no significant difference in SSC between the seagrass site and the unvegetated site in winter due to weak attenuation of flow and waves under low seagrass density conditions (Figure 2.4). This seasonal seagrass control on sediment resuspension was also captured by previous in situ hydrodynamic and SSC measurements in South Bay. These studies showed that seagrass meadows resulted in > 50% reduction in flow velocity (Hansen & Reidenbach, 2012, 2013) and approximately 30–50% attenuation in wave height (Reidenbach & Thomas, 2018; only waves that propagated in a limited range of north to south directions were included in their analysis) in summer when seagrass density was high; the resultant bed shear stresses rarely exceeded the critical shear stress to initiate sediment resuspension during the same period (Reidenbach & Timmerman, 2019). In contrast, similar dynamic conditions and SSC levels were found at both vegetated and unvegetated sites in winter (Reidenbach & Timmerman, 2019), indicating relatively weak vegetation control on sediment resuspension during the senescence period.

Both flow retardation and wave attenuation caused by seagrass contribute to reductions in sediment resuspension. However, it is difficult to quantify the relative contribution of each process in inhibiting sediment resuspension from in situ measurements because of the non-linear interaction between waves and currents (Jing & Ridd, 1996) and the lack of direct measurements of waves and currents in the wave boundary layer within a seagrass meadow (De Boer, 2007; Reidenbach & Thomas, 2018). One of the advantages of using a coupled model is it makes it possible to separate attenuation of flow and waves on sediment resuspension within seagrass meadows. Probability density distributions of combined wave–current bed shear stress at the seagrass site were calculated for each model run (Figure 2.10). When seagrass effects were not included in the model (W1 & S1), stronger wind waves in winter (Figure 2.1c) resulted in larger bed shear stresses (mean τ_b = 0.70 N m^{-2}) than in summer (mean τ_b = 0.51 N m^{-2}). Reductions in bed shear stress during summer were mainly caused by flow retardation (Figure 2.10b). Flow retardation alone reduced mean wave–current bed shear stress from 0.51 N m^{-2} to 0.08 N m^{-2} (S1 vs. S2, Figure 2.10b); including effects of wave attenuation further reduced bed shear stress to a mean value of 0.05 N m^{-2} (S3, Figure 2.10b). Low densities of seagrass in winter were sufficient to lower bed shear stresses by flow retardation (W1 vs. W2, Figure 2.10a), though the reductions were much smaller than in summer. Wave attenuation had little effect on bed shear stress at low seagrass densities (W2 vs. W3, Figure 2.10a). Although there has been little quantitative analysis on the relative contribution of flow retardation and wave attenuation in inhibiting sediment resuspension in seagrass bed, our findings based on probability density distributions of combined bed shear stress agree with the one-year observation reported by Hasegawa et al. (2008) in the Akkeshi-ko estuary, Japan. By applying sediment traps in the seagrass meadow, they found that sediment resuspension was closely related to flow reduction caused by seagrass canopy and thereby varying with seasonal seagrass growth and senescence, while sediment resuspension was not correlated with wind speed.

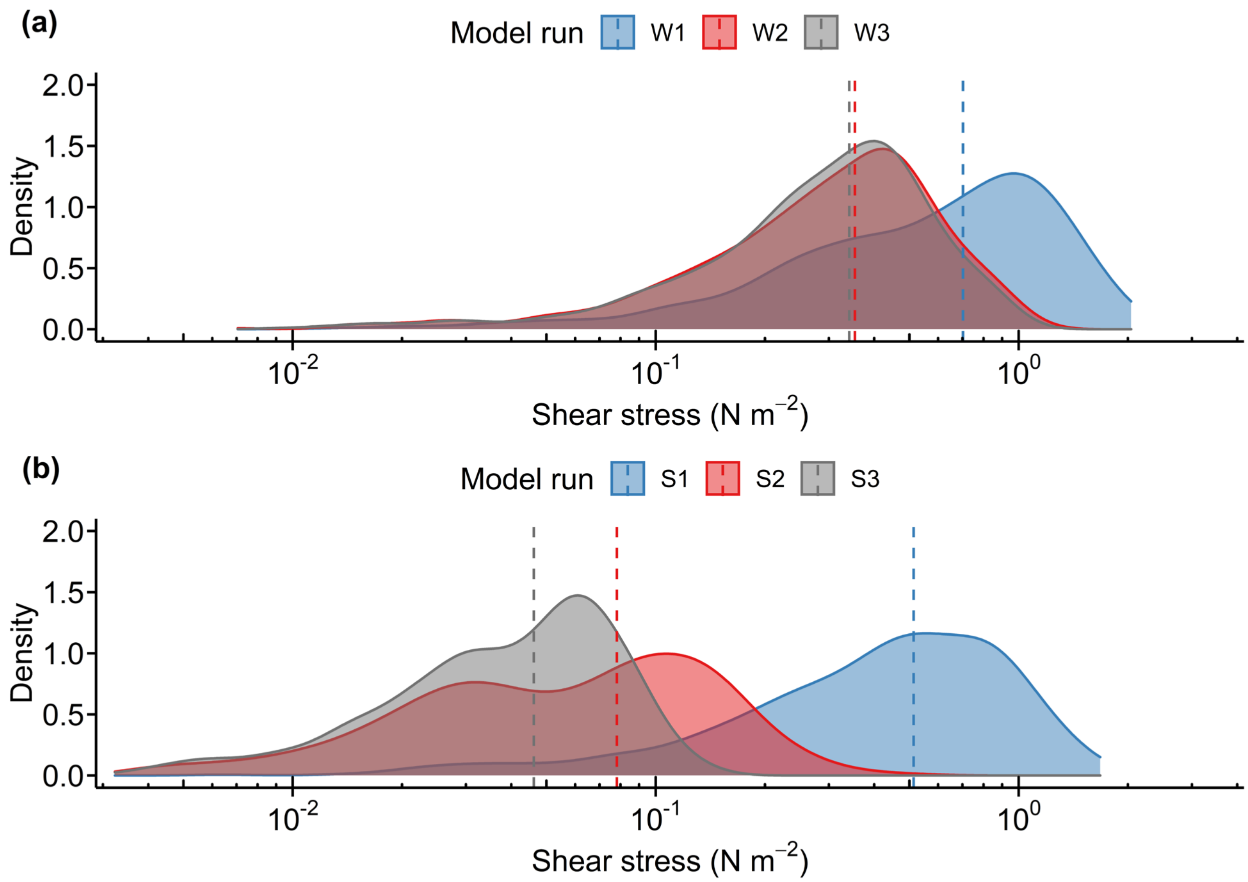

Figure 2.10 Density distributions of bed shear stress at the seagrass site in January (a) and June (b). Dashed lines denote mean shear stress of each model run. Model runs W1 and S1 are without seagrass effects; W2 and S2 include seagrass effects on flow; and W3 and S3 include seagrass effects on attenuation of flow and waves.

2.4.3 Seasonal sediment transport and deposition

Sediment accumulates within a seagrass meadow when deposition of suspended sediment is greater than local resuspension. Although previous studies have shown that seagrasses can effectively trap sediment and promote sediment deposition (Gacia et al., 1999, 2003; Gacia & Duarte, 2001; Ganthy et al., 2013, 2015), there are few direct observations of spatial erosion and deposition patterns within seagrass beds, and most of those focus on sediment grain size changes associated with seagrass (Chen et al., 2007; van Katwijk et al., 2010).

Our model results illustrate that seasonal seagrass variations had a strong impact on spatial patterns of erosion and deposition within seagrass meadows. Erosion was found just outside the western edge of the meadow in both simulation periods (Figure 2.11a, b) due to flow concentration at the edges (Beudin et al., 2017; Lera et al., 2019). During summer when seagrass density was high, slight erosion of the seagrass bed (~1 mm) was observed in some areas in the central meadow that had a shallower depth, while pronounced sediment accumulation (> 6 mm) occurred at the edges of the seagrass bed where reduced bed shear stresses allowed deposition of suspended sediment that was transported into the meadow (Figure 2.11b). The spatial erosion and deposition pattern near the meadow edges in our simulation was consistent with other model results considering seagrass meadow edge effects (Carr et al., 2016; Chen et al., 2007). These models predicted similar local scouring just outside the meadow and enhanced sediment deposition near the edges within the meadow. Our summer simulation results also show that sediment deposition was closely related to distance into the seagrass meadow. The amount of deposition decreased logarithmically with distance into the bed until the advective sediment source was depleted (Figure 2.12). When interpreting sediment deposition patterns within seagrass meadows or comparing sediment accumulation rates among different systems, it is important to consider the effects of multiple factors (e.g., different sampling location and depth, advective sediment supply, and the dependence of deposition on distance into the meadow), which may help explain the low depositional rates within the seagrass meadows during summer growth season obtained by previous studies (e.g., Gacia & Duarte, 2001).

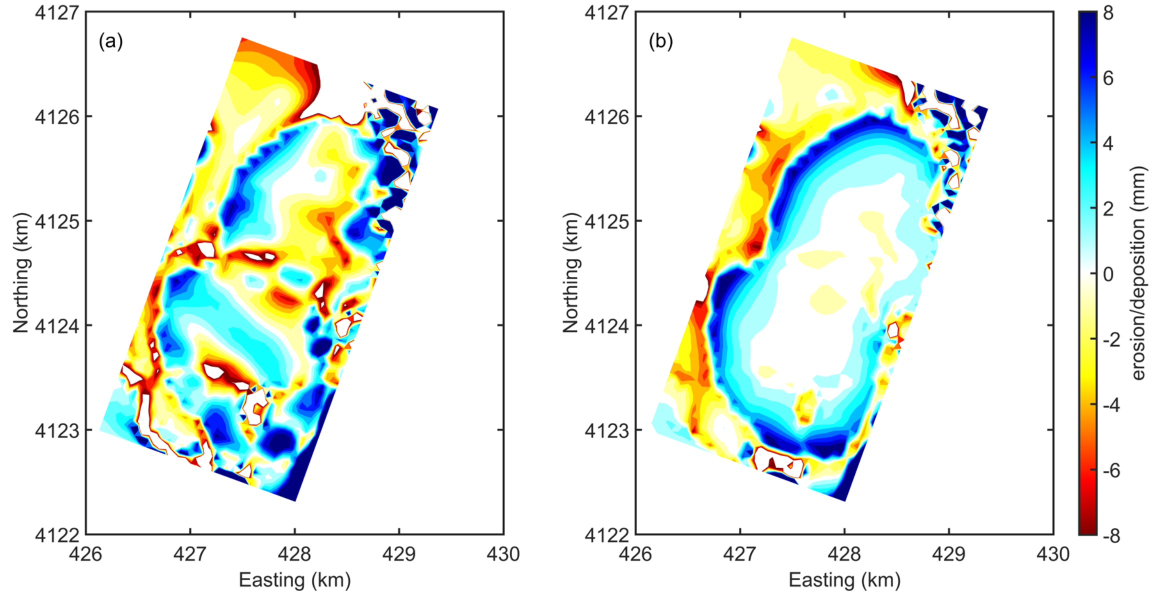

Figure 2.11 Spatial erosion/deposition patterns from simulations: (a) W3, (b) S3. Both simulations are run with seagrass effects on flow and waves for the entire month.

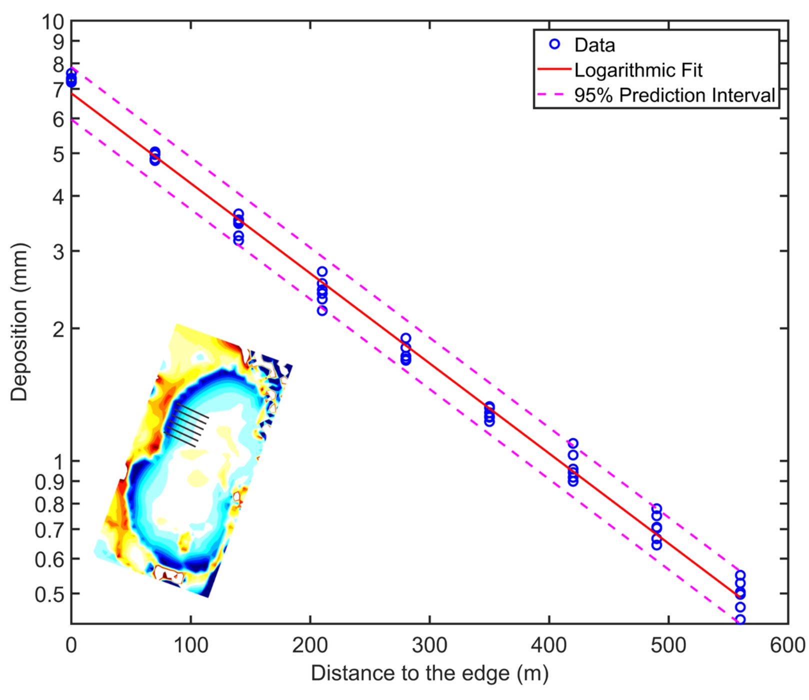

Figure 2.12 Relationship between deposition within seagrass meadows and the distance to meadow edge. Deposition data were extracted from six transects (black lines in the lower bottom map) in model run S3. The equation of the fitting curve is $log_{10}Y = -0.002X - 2.165$, with $R^2 = 0.99$.

During winter when low seagrass density coincided with stronger northerly winds, sediment resuspension was enhanced (Figure 2.4c) and a more varied pattern of erosion and deposition was found on the seagrass beds. While sediment deposition still occurred at the edges of the meadow, erosional areas expanded and severe erosion (> 5 mm) was found in the central meadow (Figure 2.11a). Low densities of seagrass allowed suspended sediment to be transported further into the meadow, resulting in regions of interior deposition in the southern portion of the meadow where larger water depths and smaller bed shear stresses promoted sediment deposition (Figure 2.11a). Unlike the relatively large and stable reduction in velocity and shear stress associated with high seagrass density in summer, flow conditions associated with low seagrass densities were more variable. Within the range of 25–200 shoots m^{-2}, the normalized bed shear stress in our flow simulations decreased from 0.4 to 0.1, a 75% reduction in bed shear stress (Figure 2.8b).

When seagrass shoot density was low in winter, small changes of density could result in strong variations in net sediment flux into/out of the meadow (Figure 2.13). The seagrass meadow maintained a nearly balanced sediment budget during winter when stem density = 50 shoots m^{-2} (-2.7×10^{2} tons; W3 in Figure 2.6b). Higher winter seagrass densities gradually increased net sediment input to the meadow (> 60 shoots m^{-2} in Figure 2.13). However, if seagrass meadows were present in much lower densities (< 50 shoots m^{-2} in Figure 2.13; W1 and S1 in Figure 2.6b) or was broadly lost from the bay as happened in the 1933 pandemic (Orth & McGlathery, 2012), the meadow area would inevitably become erosional, leading to dramatic sediment export as densities approached zero. Similarly, massive sediment loss was reported in Barnegat Bay, USA, as a result of a rapid decline in the extent of seagrass meadows within the bay system (Donatelli et al., 2018). The strong variations in flow conditions and sediment flux associated with low winter seagrass density could have a significant impact on light availability for seagrass growth, organic matter burial, and ecosystem metabolism during the senescence period (Carr et al., 2010; Lawson et al., 2012; Rheuban et al., 2014) and strongly alter annual sediment budgets and long-term dynamics of seagrass ecosystems. Considering that most previous research has focused on flow dynamics during summer when seagrass is under full-growth conditions (De Boer, 2007), more comprehensive seasonal investigations of seagrass interactions with physical environments are needed.

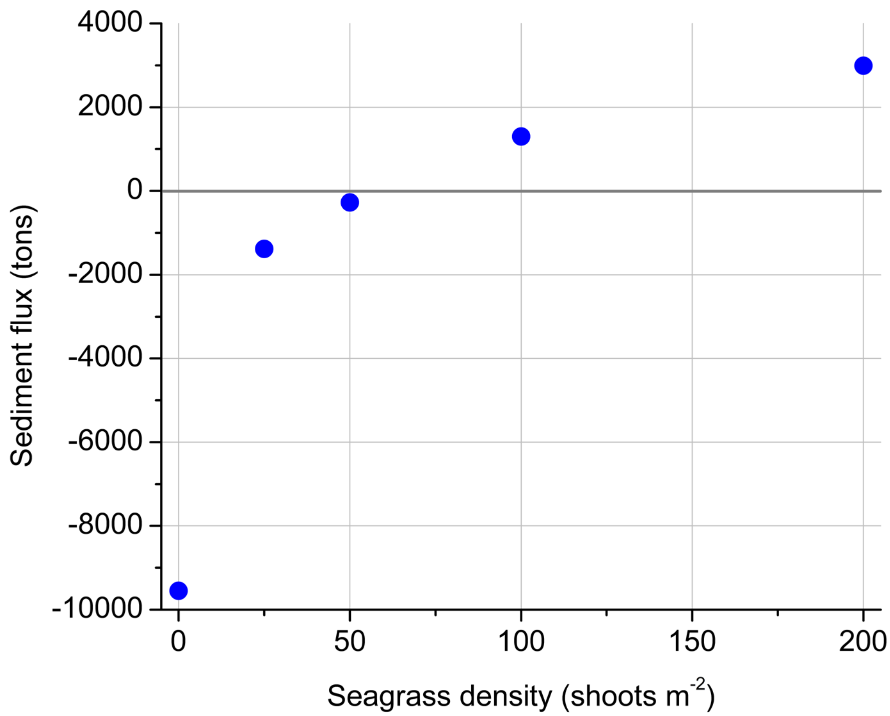

Figure 2.13 Net sediment flux into/out of seagrass meadows as a function of winter seagrass density. Positive values denote net sediment input while negative values indicate net sediment export.

2.4.4 Model limitations

Our coupled model was able to produce reasonable simulations of flow–wave–vegetation–sediment interactions under varying forcing and vegetation densities using spatially uniform seasonal vegetation inputs. However, this uniform vegetation approach may not be able to reproduce some heterogeneous patterns observed within seagrass meadows associated with spatial gradients in seagrass density, such as spatially variable accretion rates (Ganthy et al., 2013). Moreover, our model grid size (~70 m) was too coarse to resolve seagrass patchiness (usually on a scale of several meters), which has been shown to impact the distributions of bed shear stress and sediment transport rates, and consequent light environments for seagrass growth (Carr et al., 2016; Shan et al., 2020).

Another limitation of this study is the absence of vegetation dynamics in model simulations. We used representative seagrass characteristics in each period (January & June) to quantify the seasonal impacts of seagrass on flow and sediment dynamics and neglected organic matter accumulation. A more realistic approach is to simulate continuous vegetation growth and organic matter production over an annual cycle, along with vegetation interactions with the physical environment. Several studies have successfully integrated a vegetation growth module in their hydrodynamic and sediment transport simulations, either by considering vegetation growth as a function of water temperature and available photosynthetically-active radiation (Carr et al., 2010), or applying a vegetation population dynamics approach that depends on vegetation colonization, growth, mortality, and interactions with hydro-morphodynamic processes (Best et al., 2018; Brückner et al., 2019). These studies show that including vegetation growth dynamics and bio-accumulation can better characterize ecomorphodynamic processes and improve model predictive capabilities for future changes.

2.5 Conclusion

In this study, we coupled seagrass effects on flow, waves, and sediment resuspension in a spatially resolved Delft3D model and applied it in a shallow coastal bay on Virginia's Atlantic coast to better understand the effects of seasonal seagrass growth on flow and sediment dynamics. Our simulation results show that seasonal seagrass growth and senescence exerted a strong influence on bay dynamics: dense seagrass during summer significantly attenuated flow (60%) and waves (20%) and reduced SSC (85%); low-density seagrass in winter had limited effects on attenuation of flow and waves, resulting in similar SSC between the seagrass site and the unvegetated site. As a result of velocity reduction, seagrass meadows in summer experienced less flushing by tidal flows (decrease by ~70%), which potentially increases its vulnerability to pollution and heat stress by increasing water residence time in the meadows.

Model results demonstrate that the vegetation effects on flow are non-linear. Higher seagrass density increased the magnitude of flow reduction until a density threshold (400 shoots m^{-2}) was reached, which is consistent with previous flume studies regarding the limit of flow reduction by seagrass (Gambi et al., 1990; Ganthy et al., 2015; Peralta et al., 2008). Due to flow obstruction by the seagrass meadows, tidal flow was deflected around the meadow and concentrated at the western edge. Although flow velocity increased by 30% at the meadow edges, it was not able to offset the loss of water flux within the meadow and the total water flux discharged through the cross-meadow transect was reduced by 10%. While difficult to measure, the detailed hydrodynamics resolved in the model allowed us to separate the relative contributions of flow retardation and wave attenuation to reductions of bed shear stress in seagrass meadows. We found that 85% of the decrease in bed shear stress during summer was caused by flow retardation.

Seasonal seagrass variations had a strong impact on spatial patterns of erosion and deposition within seagrass meadows. Erosion was found just outside the western edge of the meadow in each season due to flow concentration at the edges. During summer when seagrass density was high, pronounced sediment accumulation (> 6 mm/month) occurred at the edges of the seagrass bed and decreased logarithmically with distance into the meadow. During winter when low seagrass densities coincided with stronger northerly winds, sediment resuspension was enhanced, and severe erosion (> 5 mm/month) was found in the central, shallower part of the meadow.

Unlike the relatively large and stable reduction in velocity and shear stress associated with high seagrass density in summer, flow conditions associated with low seagrass densities during the senescence period were more variable. When seagrass shoot density was low in winter, a small change of density could result in strong changes in net sediment flux into/out of the meadow. The strong variations in flow conditions and sediment flux associated with variations in winter seagrass densities could have a significant impact on light availability for seagrass growth, organic matter burial, and ecosystem metabolism.

References

Aoki, L. R., McGlathery, K. J., Wiberg, P. L., & Al-Haj, A. (2020). Depth Affects Seagrass Restoration Success and Resilience to Marine Heat Wave Disturbance. Estuaries and Coasts, 43(2), 316–328. https://doi.org/10.1007/s12237-019-00685-0

Apotsos, A., Jaffe, B., & Gelfenbaum, G. (2011). Wave characteristic and morphologic effects on the onshore hydrodynamic response of tsunamis. Coastal Engineering, 58(11), 1034–1048. https://doi.org/https://doi.org/10.1016/j.coastaleng.2011.06.002

Arboleda, A. M., Crosato, A., & Middelkoop, H. (2010). Reconstructing the early 19th-century Waal River by means of a 2D physics-based numerical model. Hydrological Processes, 24(25), 3661–3675. https://doi.org/10.1002/hyp.7804

Baptist, M. J., Babovic, V., Uthurburu, J. R., Keijzer, M., Uittenbogaard, R. E., Mynett, A., & Verwey, A. (2007). On inducing equations for vegetation resistance. Journal of Hydraulic Research, 45(4), 435–450. https://doi.org/10.1080/00221686.2007.9521778

Baron-Hyppolite, C., Lashley, C., Garzon, J., Miesse, T., Ferreira, C., & Bricker, J. (2018). Comparison of Implicit and Explicit Vegetation Representations in SWAN Hindcasting Wave Dissipation by Coastal Wetlands in Chesapeake Bay. Geosciences, 9(1), 8. https://doi.org/10.3390/geosciences9010008

Best, S. N., Van der Wegen, M., Dijkstra, J., Willemsen, P. W. J. M., Borsje, B. W., & Roelvink, D. J. A. (2018). Do salt marshes survive sea level rise? Modelling wave action, morphodynamics and vegetation dynamics. Environmental Modelling and Software, 109, 152–166. https://doi.org/10.1016/j.envsoft.2018.08.004

Beudin, A., Kalra, T. S., Ganju, N. K., & Warner, J. C. (2017). Development of a coupled wave-flow-vegetation interaction model. Computers and Geosciences, 100, 76–86. https://doi.org/10.1016/j.cageo.2016.12.010

Booij, N., Ris, R. C., & Holthuijsen, L. H. (1999). A third-generation wave model for coastal regions 1. Model description and validation. Journal of Geophysical Research: Oceans, 104(C4), 7649–7666. https://doi.org/10.1029/98JC02622

Brückner, M. Z. M., Schwarz, C., Dijk, W. M., Oorschot, M., Douma, H., & Kleinhans, M. G. (2019). Salt Marsh Establishment and Eco-Engineering Effects in Dynamic Estuaries Determined by Species Growth and Mortality. Journal of Geophysical Research: Earth Surface, 124(12), 2962–2986. https://doi.org/10.1029/2019JF005092

Carr, J., D'Odorico, P., McGlathery, K., & Wiberg, P. (2010). Stability and bistability of seagrass ecosystems in shallow coastal lagoons: Role of feedbacks with sediment resuspension and light attenuation. Journal of Geophysical Research: Biogeosciences, 115(3), G03011. https://doi.org/10.1029/2009JG001103

Carr, J. A., D'Odorico, P., McGlathery, K. J., & Wiberg, P. L. (2016). Spatially explicit feedbacks between seagrass meadow structure, sediment and light: Habitat suitability for seagrass growth. Advances in Water Resources, 93, 315–325. https://doi.org/10.1016/j.advwatres.2015.09.001

Carr, Joel, Mariotti, G., Fahgerazzi, S., McGlathery, K., & Wiberg, P. (2018). Exploring the Impacts of Seagrass on Coupled Marsh-Tidal Flat Morphodynamics. Frontiers in Environmental Science, 6(SEP), 92. https://doi.org/10.3389/fenvs.2018.00092

Castagno, K. A., Jiménez-Robles, A. M., Donnelly, J. P., Wiberg, P. L., Fenster, M. S., & Fagherazzi, S. (2018). Intense Storms Increase the Stability of Tidal Bays. Geophysical Research Letters, 45(11), 5491–5500. https://doi.org/10.1029/2018GL078208

Chen, S. N., Sanford, L. P., Koch, E. W., Shi, F., & North, E. W. (2007). A nearshore model to investigate the effects of seagrass bed geometry on wave attenuation and suspended sediment transport. Estuaries and Coasts, 30(2), 296–310. https://doi.org/10.1007/BF02700172

Crosato, A., & Saleh, M. S. (2011). Numerical study on the effects of floodplain vegetation on river planform style. Earth Surface Processes and Landforms, 36(6), 711–720. https://doi.org/10.1002/esp.2088

Dastgheib, A., Roelvink, J. A., & Wang, Z. B. (2008). Long-term process-based morphological modeling of the Marsdiep Tidal Basin. Marine Geology, 256(1–4), 90–100. https://doi.org/10.1016/j.margeo.2008.10.003

De Boer, W. F. (2007). Seagrass-sediment interactions, positive feedbacks and critical thresholds for occurrence: A review. Hydrobiologia, 591(1), 5–24. https://doi.org/10.1007/s10750007-0780-9

Deltares. (2014). Delft3D-FLOW User Manual (Version: 3.15.34158): Simulation of multi-dimensional hydrodynamic flows and transport phenomena, including sediments. Delft, The Netherlands: WL Delft Hydraulics

Dijkstra, J. T. (2009). How to account for flexible aquatic vegetation in large-scale morphodynamic models. In Coastal Engineering 2008 (pp. 2820–2831). World Scientific Publishing Company. https://doi.org/10.1142/9789814277426_0233

Donatelli, C., Ganju, N. K., Fagherazzi, S., & Leonardi, N. (2018). Seagrass Impact on Sediment Exchange Between Tidal Flats and Salt Marsh, and The Sediment Budget of Shallow Bays. Geophysical Research Letters, 45(10), 4933–4943. https://doi.org/10.1029/2018GL078056

Donatelli, C., Ganju, N. K., Kalra, T. S., Fagherazzi, S., & Leonardi, N. (2019). Changes in hydrodynamics and wave energy as a result of seagrass decline along the shoreline of a microtidal back-barrier estuary. Advances in Water Resources, 128, 183–192. https://doi.org/10.1016/j.advwatres.2019.04.017

Edmonds, D. A., & Slingerland, R. L. (2010). Significant effect of sediment cohesion on deltamorphology. Nature Geoscience, 3(2), 105–109. https://doi.org/10.1038/ngeo730

Fagherazzi, S., & Wiberg, P. L. (2009). Importance of wind conditions, fetch, and water levels on wave-generated shear stresses in shallow intertidal basins. Journal of Geophysical Research, 114(F3), F03022. https://doi.org/10.1029/2008JF001139

Fonseca, M., & Fisher, J. (1986). A comparison of canopy friction and sediment movement between four species of seagrass with reference to their ecology and restoration. Marine Ecology Progress Series, 29, 15–22. https://doi.org/10.3354/meps029015

Fonseca, M. S., & Cahalan, J. A. (1992). A preliminary evaluation of wave attenuation by four species of seagrass. Estuarine, Coastal and Shelf Science, 35(6), 565–576. https://doi.org/10.1016/S0272-7714(05)80039-3

Gacia, E., & Duarte, C. M. (2001). Sediment retention by a Mediterranean Posidonia oceanica meadow: The balance between deposition and resuspension. Estuarine, Coastal and Shelf Science, 52(4), 505–514. https://doi.org/10.1006/ecss.2000.0753

Gacia, E., Granata, T. C., & Duarte, C. M. (1999). An approach to measurement of particle flux and sediment retention within seagrass (Posidonia oceanica) meadows. Aquatic Botany, 65(1–4), 255–268. https://doi.org/10.1016/S0304-3770(99)00044-3

Gacia, E., Duarte, C. M., Marbà, N., Terrados, J., Kennedy, H., Fortes, M. D., & Tri, N. H. (2003). Sediment deposition and production in SE-Asia seagrass meadows. Estuarine, Coastal and Shelf Science, 56(5–6), 909–919. https://doi.org/10.1016/S0272-7714(02)00286-X

Gambi, M., Nowell, A., & Jumars, P. (1990). Flume observations on flow dynamics in Zostera marina (eelgrass) beds. Marine Ecology Progress Series, 61, 159–169. https://doi.org/10.3354/meps061159

Ganthy, F., Sottolichio, A., & Verney, R. (2013). Seasonal modification of tidal flat sediment dynamics by seagrass meadows of Zostera noltii (Bassin d'Arcachon, France). Journal of Marine Systems, 109–110(SUPPL.), S233–S240. https://doi.org/10.1016/j.jmarsys.2011.11.027

Ganthy, Florian, Soissons, L., Sauriau, P.-G., Verney, R., & Sottolichio, A. (2015). Effects of short flexible seagrass Zostera noltei on flow, erosion and deposition processes determined using flume experiments. Sedimentology, 62(4), 997–1023. https://doi.org/10.1111/sed.12170

Hansen, JCR, & Reidenbach, M. (2012). Wave and tidally driven flows in eelgrass beds and their effect on sediment suspension. Marine Ecology Progress Series, 448, 271–287. https://doi.org/10.3354/meps09225

Hansen, JCR, & Reidenbach, M. (2013). Seasonal Growth and Senescence of a Zostera marina Seagrass Meadow Alters Wave-Dominated Flow and Sediment Suspension Within a Coastal Bay. Estuaries and Coasts, 36(6), 1099–1114. https://doi.org/10.1007/s12237-013-9620-5

Hansen, Jennifer, & Reidenbach, M. (2018). Wave Dynamics and Fluid Stresses in Vegetated and Unvegetated Coastal Lagoons in Virginia, 2010-2011. Virginia Coast Reserve Long-Term Ecological Research Project Data Publication Knb-Lter-Vcr.276.2. https://doi.org/10.6073/PASTA/33682BFC1BDCDEF08C9948560177338C

Hasegawa, N., Hori, M., & Mukai, H. (2008). Seasonal changes in eelgrass functions: Current velocity reduction, prevention of sediment resuspension, and control of sediment-water column nutrient flux in relation to eelgrass dynamics. Hydrobiologia, 596(1), 387–399. https://doi.org/10.1007/s10750-007-9111-4

Hu, K., Chen, Q., & Wang, H. (2015). A numerical study of vegetation impact on reducing storm surge by wetlands in a semi-enclosed estuary. Coastal Engineering, 95, 66–76. https://doi.org/10.1016/j.coastaleng.2014.09.008

Jing, L., & Ridd, P. V. (1996). Wave-current bottom shear stresses and sediment resuspension in Cleveland Bay, Australia. Coastal Engineering, 29(1–2), 169–186. https://doi.org/10.1016/S0378-3839(96)00023-3

Jones, C. G., Lawton, J. H., & Shachak, M. (1994). Organisms as Ecosystem Engineers. Oikos, 69(3), 373. https://doi.org/10.2307/3545850

Koch, E., & Gust, G. (1999). Water flow in tide- and wave-dominated beds of the seagrass Thalassia testudinum. Marine Ecology Progress Series, 184, 63–72.

https://doi.org/10.3354/meps184063

Lawson, S., McGlathery, K., & Wiberg, P. (2012). Enhancement of sediment suspension and nutrient flux by benthic macrophytes at low biomass. Marine Ecology Progress Series, 448, 259–270. https://doi.org/10.3354/meps09579

Lawson, S. E., Wiberg, P. L., McGlathery, K. J., & Fugatf, D. C. (2007). Wind-driven sediment suspension controls light availability in a shallow coastal lagoon. Estuaries and Coasts, 30(1), 102–112. https://doi.org/10.1007/BF02782971

Lera, S., Nardin, W., Sanford, L., Palinkas, C., & Guercio, R. (2019). The impact of submersed aquatic vegetation on the development of river mouth bars. Earth Surface Processes and Landforms, 44(7), 1494–1506. https://doi.org/10.1002/esp.4585

Lesser, G. R., Roelvink, J. A., van Kester, J. A. T. M. T. M., & Stelling, G. S. (2004). Development and validation of a three-dimensional morphological model. Coastal Engineering, 51(8), 883–915. https://doi.org/https://doi.org/10.1016/j.coastaleng.2004.07.014

Ma, G., Kirby, J. T., Su, S. F., Figlus, J., & Shi, F. (2013). Numerical study of turbulence and wave damping induced by vegetation canopies. Coastal Engineering, 80, 68–78. https://doi.org/10.1016/j.coastaleng.2013.05.007

Mariotti, G., Fagherazzi, S., Wiberg, P. L., McGlathery, K. J., Carniello, L., & Defina, A. (2010). Influence of storm surges and sea level on shallow tidal basin erosive processes. Journal of Geophysical Research, 115(C11), C11012. https://doi.org/10.1029/2009JC005892

McGlathery, Karen, Reidenbach, M., D'Odorico, P., Fagherazzi, S., Pace, M., & Porter, J. (2013). Nonlinear Dynamics and Alternative Stable States in Shallow Coastal Systems. Oceanography, 26(3), 220–231. https://doi.org/10.5670/oceanog.2013.66

McGlathery, KJ, Sundbäck, K., & Anderson, I. (2007). Eutrophication in shallow coastal bays and lagoons: the role of plants in the coastal filter. Marine Ecology Progress Series, 348, 1–18. https://doi.org/10.3354/meps07132

Nagelkerken, I., Van Der Velde, G., Gorissen, M. W., Meijer, G. J., Van't Hof, T., & Den Hartog, C. (2000). Importance of mangroves, seagrass beds and the shallow coral reef as a nursery for important coral reef fishes, using a visual census technique. Estuarine, Coastal and Shelf Science, 51(1), 31–44. https://doi.org/10.1006/ecss.2000.0617

Nardin, W., & Edmonds, D. A. (2014). Optimum vegetation height and density for inorganic sedimentation in deltaic marshes. Nature Geoscience, 7(10), 722–726. https://doi.org/10.1038/NGEO2233

Nardin, W., Edmonds, D. A., & Fagherazzi, S. (2016). Influence of vegetation on spatial patterns of sediment deposition in deltaic islands during flood. Advances in Water Resources, 93, 236–248. https://doi.org/10.1016/j.advwatres.2016.01.001

Nardin, W., Larsen, L., Fagherazzi, S., & Wiberg, P. (2018). Tradeoffs among hydrodynamics, sediment fluxes and vegetation community in the Virginia Coast Reserve, USA. Estuarine, Coastal and Shelf Science, 210, 98–108. https://doi.org/10.1016/j.ecss.2018.06.009

Nepf, H. M. (2012). Flow and Transport in Regions with Aquatic Vegetation. Annual Review of Fluid Mechanics, 44(1), 123–142. https://doi.org/10.1146/annurev-fluid-120710-101048

Oreska, M. P. J., McGlathery, K. J., & Porter, J. H. (2017). Seagrass blue carbon spatial patterns at the meadow-scale. PLoS ONE, 12(4). https://doi.org/10.1371/journal.pone.0176630

Orth, R., & McGlathery, K. (2012). INTRODUCTION Eelgrass recovery in the coastal bays of the Virginia Coast Reserve, USA. Marine Ecology Progress Series, 448, 173–176. https://doi.org/10.3354/meps09596

Orth, R. J., Carruthers, T. J. B., Dennison, W. C., Duarte, C. M., Fourqurean, J. W., Heck, K. L., et al. (2006). A Global Crisis for Seagrass Ecosystems. BioScience, 56(12), 987–996. https://doi.org/10.1641/0006-3568(2006)56[987:agcfse]2.0.co;2

Paul, M., Bouma, T., & Amos, C. (2012). Wave attenuation by submerged vegetation: combining the effect of organism traits and tidal current. Marine Ecology Progress Series, 444, 31–41. https://doi.org/10.3354/meps09489

Peralta, G., van Duren, L., Morris, E., & Bouma, T. (2008). Consequences of shoot density and stiffness for ecosystem engineering by benthic macrophytes in flow dominated areas: a hydrodynamic flume study. Marine Ecology Progress Series, 368, 103–115. https://doi.org/10.3354/meps07574

Phan, K. L., Stive, M. J. F., Zijlema, M., Truong, H. S., & Aarninkhof, S. G. J. (2019). The effects of wave non-linearity on wave attenuation by vegetation. Coastal Engineering, 147, 63–74. https://doi.org/10.1016/j.coastaleng.2019.01.004

Reidenbach, M. A., & Thomas, E. L. (2018). Influence of the Seagrass, Zostera marina, on Wave Attenuation and Bed Shear Stress Within a Shallow Coastal Bay. Frontiers in Marine Science, 5(OCT), 397. https://doi.org/10.3389/fmars.2018.00397

Reidenbach, M. A., & Timmerman, R. (2019). Interactive Effects of Seagrass and the Microphytobenthos on Sediment Suspension Within Shallow Coastal Bays. Estuaries and Coasts, 42(8), 2038–2053. https://doi.org/10.1007/s12237-019-00627-w

Rheuban, J. E., Berg, P., & McGlathery, K. J. (2014). Ecosystem metabolism along a colonization gradient of eelgrass (Zostera marina) measured by eddy correlation. Limnology and Oceanography, 59(4), 1376–1387. https://doi.org/10.4319/lo.2014.59.4.1376

Shan, Y., Zhao, T., Liu, C., & Nepf, H. (2020). Turbulence and bed-load transport in channels with randomly distributed emergent patches of model vegetation. Geophysical Research Letters, e2020GL087055. https://doi.org/10.1029/2020gl087055

Suzuki, T., Zijlema, M., Burger, B., Meijer, M. C., & Narayan, S. (2012). Wave dissipation by vegetation with layer schematization in SWAN. Coastal Engineering, 59(1), 64–71. https://doi.org/10.1016/j.coastaleng.2011.07.006

van Katwijk, M. M., Bos, A. R., Hermus, D. C. R., & Suykerbuyk, W. (2010). Sediment modification by seagrass beds: Muddification and sandification induced by plant cover and environmental conditions. Estuarine, Coastal and Shelf Science, 89(2), 175–181. https://doi.org/10.1016/J.ECSS.2010.06.008

Van Rijn, L. C., Roelvink, J. A., & Horst, W. ter. (2001). Approximation formulae for sand transport by currents and waves and implementation in DELFT-MOR. Report Z3054.20, Delft Hydraulics, Delft, The Netherlands.

van Rooijen, A. A., McCall, R. T., van Thiel de Vries, J. S. M., van Dongeren, A. R., Reniers, A. J. H. M., & Roelvink, J. A. (2016). Modeling the effect of wave-vegetation interaction on wave setup. Journal of Geophysical Research: Oceans, 121(6), 4341–4359. https://doi.org/10.1002/2015JC011392

Waycott, M., Duarte, C. M., Carruthers, T. J. B., Orth, R. J., Dennison, W. C., Olyarnik, S., et al. (2009). Accelerating loss of seagrasses across the globe threatens coastal ecosystems. Proceedings of the National Academy of Sciences of the United States of America, 106(30), 12377–12381. https://doi.org/10.1073/pnas.0905620106

Wiberg, P. L., Carr, J. A., Safak, I., & Anutaliya, A. (2015). Quantifying the distribution and influence of non-uniform bed properties in shallow coastal bays. Limnology and Oceanography: Methods, 13(12), 746–762. https://doi.org/10.1002/lom3.10063

Widdows, J, Pope, N., Brinsley, M., Asmus, H., & Asmus, R. (2008). Effects of seagrass beds (Zostera noltii and Z. marina) on near-bed hydrodynamics and sediment resuspension. Marine Ecology Progress Series, 358, 125–136. https://doi.org/10.3354/meps07338

Widdows, John, & Brinsley, M. (2002). Impact of biotic and abiotic processes on sediment dynamics and the consequences to the structure and functioning of the intertidal zone. Journal of Sea Research, 48(2), 143–156. https://doi.org/10.1016/S1385-1101(02)00148-X

Willmott, C. J. (1981). On the validation of models. Physical Geography, 2(2), 184–194. https://doi.org/10.1080/02723646.1981.10642213

Wu, W. C., Ma, G., & Cox, D. T. (2016). Modeling wave attenuation induced by the vertical density variations of vegetation. Coastal Engineering, 112, 17–27. https://doi.org/10.1016/j.coastaleng.2016.02.004

Chapter 3. Seasonal growth and senescence of seagrass alters sediment accumulation rates and carbon burial in a coastal lagoon

This chapter was published in *Limnology and Oceanography*:

Zhu, Q., Wiberg, P. L., & McGlathery, K. J. (2022). Seasonal growth and senescence of seagrass alters sediment accumulation rates and carbon burial in a coastal lagoon. Limnology and Oceanography, 1–12. https://doi.org/10.1002/LNO.12178

Abstract

Seagrass meadows are important carbon sinks in the global coastal carbon cycle yet are also among the most rapidly declining marine habitats. Their ability to sequester carbon depends on flow–sediment–vegetation interactions that facilitate net deposition, as well as high rates of primary production. However, the effects of seasonal and episodic variations in seagrass density on net sediment and carbon accumulation have not been well quantified. Understanding these dynamics provides insight into how carbon accumulation in seagrass meadows responds to disturbance events and climate change. Here we apply a spatially resolved sediment transport model that includes coupling of seagrass effects on flow, waves, and sediment resuspension in a seagrass meadow to quantify seasonal rates of sediment and carbon accumulation in the meadow. Our results show that organic carbon accumulation rates were largely determined by sediment accumulation and that they both changed non-linearly as a function of seagrass shoot density. While seagrass meadows effectively trapped sediment at meadow edges during spring-summer growth seasons, during winter senescence low-density meadows (< 160 shoots m^{-2}) were erosional with rates sensitive to density. Small variations in winter densities resulted in large changes in annual sediment and carbon accumulation in the meadow; meadow-scale (hundreds

of square meters) summer seagrass dieback due to marine heatwaves can result in annual erosion and carbon loss. Our findings highlight the strong temporal and spatial variability in sediment accumulation within seagrass meadows and the implications for annual sediment carbon burial rates and the resilience of seagrass carbon stocks under future climate change.

3.1 Introduction

Seagrass meadows are essential coastal habitats that offer valuable ecosystem services including carbon sequestration, nutrient cycling and improved water quality, and sediment stabilization (de Boer, 2007; McGlathery et al., 2007). They have been recognized as important carbon sinks in the global marine carbon cycle due to high rates of net primary production and carbon burial in the sediment (Duarte et al., 2013), and contribute to more than 10% of the annual sediment carbon burial in global oceans (Fourqurean et al., 2012). Despite their importance in coastal ecosystems, seagrasses are one of the most rapidly declining marine habitats, threatened by degraded water quality, temperature stress, and sea level rise (Orth et al., 2006; Waycott et al., 2009). The disappearance of seagrass can cause seabed erosion and the exposure of accumulated sediment carbon to oxic conditions, leading to carbon emissions (Aoki et al., 2021; Pendleton et al., 2012). For seagrass meadows to be considered as effective carbon sinks, the accumulated carbon must be preserved in sediments for a long period (e.g., decades to centuries).

An accurate estimate of sediment accumulation rates within seagrass meadows is critical for quantifying sediment budgets and organic carbon burial. Various methods have been used to determine sediment accumulation rates in seagrass meadows worldwide, each focusing on different temporal scales and spatial extents (Potouroglou et al., 2017). Repeated bathymetric surveys can provide a direct measure of long-term changes in deposition at large spatial scales (Walter et al., 2020), but lack the precision to capture most short-term changes (e.g., annual or seasonal scale). Radiometric dating methods are widely used in seagrass studies to determine sedimentation rates over several decades (Duarte et al., 2013), but they have been criticized for not accounting for surface mixing effects (Johannessen and Macdonald, 2016). Sediment traps/plates are able to measure sediment deposition over a period of several days to months, but they cannot fully resolve erosion/resuspension processes on the seabed and the results are susceptible to sediment loss during retrieval (Gacia and Duarte, 2001; Nolte et al., 2013). Surface elevation tables can provide precise short-term and long-term measurements, but are limited in spatial scale and may cause local scouring of the seabed (Potouroglou et al., 2017).

Long-term sediment accumulation rates within seagrass meadows have been characterized at a number of sites using the aforementioned approaches (Duarte et al., 2013; Greiner et al., 2013; Oreska et al., 2020), but short-term dynamics of sediment accumulation in seagrass meadows remain unclear. Seagrass beds show strong temporal and spatial variability in erosion and deposition in response to seasonal seagrass growth and senescence (Hansen and Reidenbach, 2013; Zhu et al., 2021) that is difficult to interpret from long-term sedimentary records. There is also growing evidence of increasing frequency of marine heatwaves that can cause seasonal summer seagrass dieback and losses of accumulated carbon in seagrass sediments (Aoki et al., 2021; Arias-Ortiz et al., 2018). Because these short-term processes and disturbances can strongly alter annual sediment budgets and long-term dynamics of seagrass meadows, it is important to understand these seasonal sediment dynamics and the associated drivers, especially in the context of future climate change.

An alternative approach to characterizing sediment accumulation rates in seagrass meadows is through modeling. Numerical models capable of resolving the synergistic effects of flow–wave–vegetation–sediment interaction (Carr et al., 2016; Chen et al., 2007; Donatelli et al., 2018) provide a tool for understanding seasonal sediment dynamics in seagrass meadows in spatially resolved settings. However, most previous modeling studies of sediment transport within seagrass meadows have used idealized seagrass meadows or did not resolve seasonal seagrass growth and wind patterns. To better resolve spatial variations of dynamic factors and to understand the effects of seasonal growth of seagrass on sediment accumulation, we applied the process-based hydrodynamic and sediment transport Delft3D model, including coupling of seagrass effects on flow, waves, and sediment resuspension, to a seagrass meadow in a shallow coastal bay in Virginia, USA. The model has been parameterized and extensively validated using long-term data from the site (wind conditions, hydrodynamic and suspended sediment data, sediment accumulation rates, and seagrass characteristics; Zhu et al., 2021).

In this study, the coupled model was run for 12 consecutive months with seasonally varying winds and tides as well as seagrass densities. The results were analyzed to address three questions. (1) How do rates of sediment accumulation and organic carbon burial within seagrass meadows vary in response to seasonal variations in seagrass density? (2) How does short-term disturbance in seagrass density affect annual sediment accumulation rates? (3) What are the effects of seasonal variations in seagrass density on spatial sediment erosion/deposition patterns in seagrass meadows?

3.2 Study site

The study site, South Bay, is one of the back-barrier bays within the Virginia Coast Reserve Long-Term Ecological Research site (Figure 3.1a). It is bordered by a barrier island to the east and is connected to two tidal inlets that exchange water with the Atlantic Ocean (Figure 3.1b). South Bay has a mean depth of 1 m below mean sea level and an average semidiurnal tidal range of 1.2 m (Fagherazzi and Wiberg, 2009). Sea level in the study area is rising at a rate of 4–5 mm yr^{-1} (https://tidesandcurrents.noaa.gov/sltrends/sltrends_station.shtml?id=8631044). South Bay is a shallow, oligotrophic environment that provides favorable light conditions for seagrass growth and is a successful seagrass restoration site where *Zostera marina* now dominates the subtidal flats (McGlathery et al., 2012). Located at the southern geographical limit for *Zostera marina* growth in the Western Atlantic Ocean (Aoki et al., 2020), the seagrass meadows in South Bay show strong seasonal variability that significantly impacts bay dynamics (Hansen and Reidenbach, 2013; Rheuban et al., 2014). Seagrasses within the bay reach a maximum shoot density (> 500 shoots m^{-2}) in early summer and suffer from a mid-season loss due to heat stress in late summer; the density slightly increases in autumn after temperatures moderate and then declines to a minimum (50–100 shoots m^{-2}) during winter senescence. When the temperature increases in the next spring, seagrasses start to re-grow and the density gradually increases to 300 shoots m^{-2} in late spring (Figure 3.1c; Berger et al., 2020; Hansen and Reidenbach, 2013; Reidenbach and Thomas, 2018; Rheuban et al., 2014). The presence of high-density seagrass significantly reduces sediment resuspension within seagrass meadows during summer, while significant sediment resuspension occurs in winter when frequent and stronger northeasterly winds coincide with minimum seagrass density (Hansen and Reidenbach, 2013; Zhu et al., 2021).

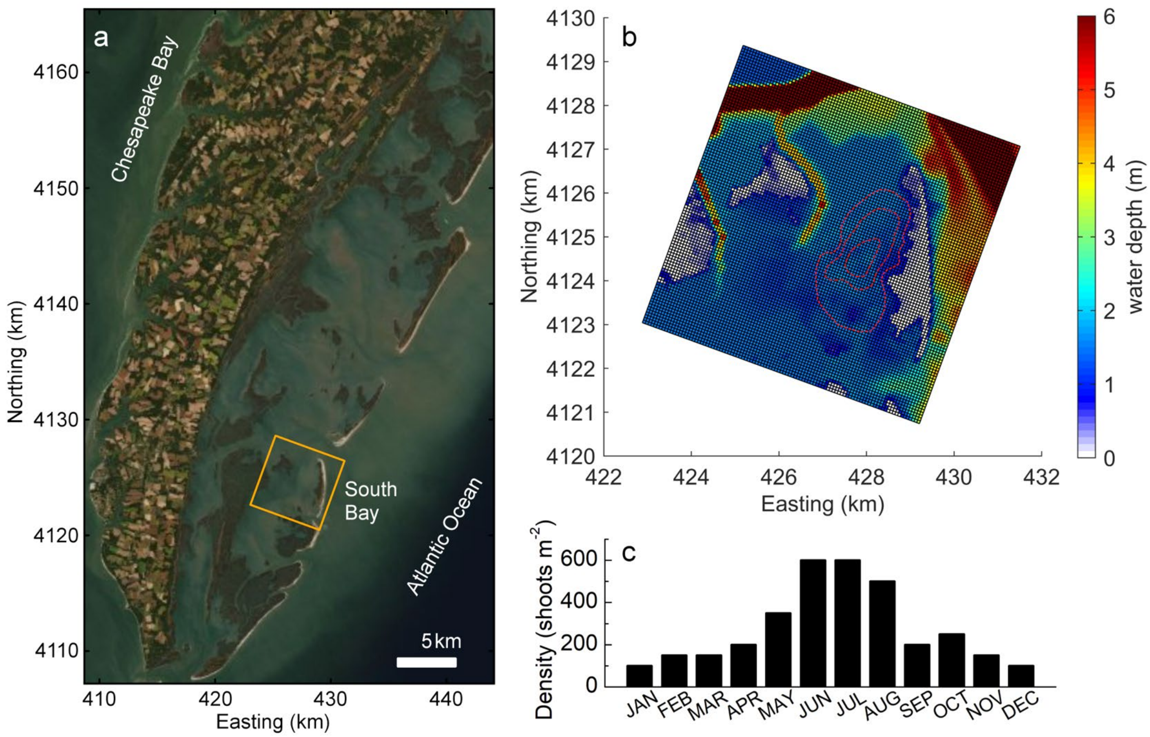

Figure 3.1 (a) Aerial image of the study area, (b) model grid and bathymetry in South Bay, and (c) typical monthly seagrass shoot density (*N*) at the central meadow throughout the year. Red dashed lines in (b) represent boundaries of three seagrass density classes (*N*, 0.8*N*, and 0.6*N*) used in the model (Table A2.1). The seagrass shoot density data shown in (c) were compiled from previous seasonal seagrass observations in South Bay (Berger et al., 2020; Hansen and Reidenbach, 2013; Reidenbach and Thomas, 2018; Rheuban et al., 2014).

Overall, seagrass meadows in South Bay effectively accumulate fine particles with an average sediment deposition rate of 6.3 mm yr^{-1} (based on radiometric dating at two representative sites; Greiner et al., 2013; Oreska et al., 2018), and resulted in a finer sediment grain size (mean = 71 μm) within the meadow than outside the meadow (mean = 124 μm; Lawson et al., 2007; McGlathery et al., 2012; Oreska et al., 2017). As a result of sediment accumulation, the seagrass meadow is able to bury organic carbon at an average rate of 42 g C m^{-2} yr^{-1} (Oreska et al., 2020).

3.3 Methods

Hydrodynamic and sediment transport simulations were conducted using the process-based and spatially resolved Delft3D FLOW/MOR model (Lesser et al., 2004), coupled with the nearshore phase-averaged wave model SWAN (Booij et al., 1999). The domain decomposition technique (Deltares, 2014) was used to locally refine the model grid in South Bay to better capture seagrass meadows in the bay and the bordering barrier island. The model grid consisted of a small model domain covering the core study area in South Bay (Fig 1b; 305 × 302 grid cells with a spatial resolution of ~70 m) and a large model domain spanning the rest of the Virginia Coast Reserve (148 × 444 grid cells with a spatial resolution of 200 m). The open ocean boundaries of the large model domain were forced with hourly water levels extracted from the NOAA tide gauge station at Wachapreague (Site ID:8631044) after adjusting tidal amplitude and phase to generate tidal simulation results in excellent agreement with measured tides at Wachapreague ($R^2 \geq 0.98$ and root mean square error ≤ 0.07 m). Wave simulations were driven by hourly wind conditions from the same NOAA station and coupled with the flow model every hour. Model bathymetry and bottom sediment size distributions and properties were extracted from Wiberg et al. (2015). Three sediment classes were used in the model: a 32–64 μm coarse silt fraction, a < 32 μm medium to fine silt fraction, and a > 64 μm sand fraction (a representative median grain size of 125 μm was defined in the model for the sand fraction). To better capture the effects of seagrass on sediment transport, sediment size distributions in the South Bay seagrass meadows were initialized based on local surveys from Oreska et al. (2017). The active sediment layer thickness, which defines the maximum erosion depth of the seabed at each model time step, was set to 5 cm to avoid unrealistically high sediment availability.

The model was implemented in depth-averaged mode with a time step of 0.25 min. Several previous studies have shown that depth-averaged Delft3D simulations are able to produce reasonable results for well-mixed shallow coastal bays, including the Virginia Coast Reserve, and to resolve the synergistic effects of flow–wave–vegetation–sediment interactions in spatially resolved settings (Nardin and Edmonds, 2014; Nardin et al., 2018; Zhu et al., 2021). In order to incorporate seagrass effects on currents and waves, the Baptist vegetation model (Baptist et al., 2007) and the Suzuki vegetation wave energy dissipation model (Suzuki et al., 2012) were implemented in the Delft3D FLOW module and the SWAN model, respectively. These two methods considered vegetation as cylindrical structures characterized by vegetation height, stem diameter, shoot density, and vegetation flow drag coefficient and wave drag coefficient (Table A2.1).

The coupled model has been parameterized and extensively validated using summer and winter hydrodynamic and suspended sediment data during a 4-day period in January and June 2011 from a seagrass site and a nearby unvegetated site in South Bay (Zhu et al., 2021). Model skill indices, including bias, root mean square error, and Willmott skill index (Willmott, 1981), were calculated for model validation parameters (water level, significant wave height, depth-averaged velocity, and total suspended sediment concentration) to quantify model ability to characterize hydrodynamic and suspended sediment characteristics in the bay. Values of the Willmont skill index are summarized in Table A2.2. Excellent agreement between modeled and measured water levels was obtained at both sites during each validation period. Wave height skill scores (0.56–0.87) for the seagrass site were generally higher than those of the unvegetated site. While generally good agreement between modeled and measured depth-averaged velocity was obtained at both sites, the model slightly over-estimated peak velocity during flood tides with an average bias of 0.05 m s^{-1} (Zhu et al., 2021). The model successfully captured most sediment resuspension events at both sites during winter (skill scores ≥ 0.80) and predicted a strong reduction of suspended sediment concentration (> 80%) in the summer seagrass meadow that is consistent with field observations. See Zhu et al. (2021) for further details of the model parameterization and validation. Overall, the coupled model is able to provide spatially resolved simulations of flow and sediment transport patterns within/outside the seagrass meadow with performance similar to that of other model studies considering seagrass effects (Chen et al., 2007; Moki et al., 2020).

In this study, we extended the simulation period considered in Zhu et al. (2021) to a complete annual cycle using winds and tidal forcing for a representative year (August 1, 2011 to July 31, 2012; Figure A2.1), with typical seasonal seagrass characteristics (shoot density ranging from 100–600 shoots m^{-2}, seagrass height ranging from 0.2–0.4 m, and stem diameter ranging from 0.2–0.4 cm) observed from the site (Table A2.1). Evaluating model sensitivity to variations in seagrass characteristics, Zhu et al. (2021) found that variations in seagrass shoot density had a larger impact on bay dynamics than did variations in seagrass height and stem diameter. Considering the wide range of annual seagrass density variation (100–600 shoots m^{-2}) and its strong impact on bay dynamics at our study site, we mainly focused on the impacts of seagrass density variations in this paper.

In order to better represent observed spatial density gradients in the meadow, three seagrass density classes were assigned in the model each month, with the highest density (N) in the central meadow, an intermediate density of $0.8N$ outside the central area, and the lowest density of $0.6N$ near meadow edges (Figure 3.1b). A reference model case without seagrass was also run for the same simulation period for comparison. The model was run for a three-month spin-up period to reach a quasi-equilibrium state prior to beginning the annual simulations, and results generated during the spin-up run were used as initial conditions for the annual simulations to avoid disturbances caused by model initialization.

The coupled model is able to simulate mineral sediment transport processes but cannot explicitly simulate organic carbon sequestration. In order to quantify organic carbon burial rates in the meadow, a negative linear relationship between sediment organic carbon concentration and sand fraction was established (Figure A2.2; $R^2 = 0.75$) based on previous measurements from Oreska et al. (2017) within the same meadow. Using this relationship, monthly distributions of sand fraction (Figure A2.3) output from model simulations were converted to maps of surface sediment organic carbon concentration (Figure A2.4). Then monthly distributions of organic carbon burial rate [mg month^{-1} cm^{-2}] in the meadow (Figure A2.5) were determined by multiplying modeled sediment accumulation rates [mm month^{-1}] by the surface sediment organic carbon concentration [mg cm^{-3}].

3.4 Results

3.4.1 Sediment and organic carbon accumulation rates vary with seagrass density

With seasonally varying seagrass densities, our simulation results show that bed shear stress and total suspended sediment concentration averaged across the seagrass meadow changed non-linearly as a function of seagrass density (Figure 3.2a, 3.2b). The most rapid changes of bed shear stress and total suspended sediment concentration occurred at low seagrass densities, while there was little change in bed shear stress and total suspended sediment concentration when seagrass densities were > 200 shoots m^{-2}. Throughout the year, sediment resuspension in the meadow was mainly controlled by seagrass density rather than wind speeds (Figure A2.6).

Similarly, seasonal growth and senescence of seagrass exerted a strong influence on sediment accumulation and carbon burial within seagrass meadows. Four low-density scenarios (seagrass shoot density N = 0, 25, 50 and 100 shoots m^{-2}) were specified during winter conditions to better resolve the effects of low seagrass density (Table A2.1). Simulation results show that rates of sediment accumulation and organic carbon burial averaged across the meadow varied strongly with seagrass density (Figure 3.2c, 3.2d). When seagrass density was lower than 160 shoots m^{-2}, typical in winter, seagrass beds were erosional with rates that were sensitive to density. When seagrass density > 200 shoots m^{-2}, rates of sediment accumulation and organic carbon burial were relatively constant due to strong flow retardation (Figure 3.2c, 3.2d, and A2.7). At the meadow scale the average organic carbon accumulation rate was largely determined by sediment accumulation (Figure 3.3; R^2 = 0.99). On the annual time scale, simulations with typical seasonal seagrass characteristics predicted a meadow-averaged sediment accumulation rate of 4.1 ± 0.5 (standard error) mm yr^{-1} and a carbon accumulation rate of 22 ± 1.6 (standard error) g C m^{-2} yr^{-1}.

Based on model results showing how monthly sediment accumulation rates vary as a function of seagrass density (Figure 3.2c), we can design density variation scenarios by changing the seagrass density in specific months and quantifying the corresponding effect (e.g., short-term winter density variations and summer seagrass dieback due to marine heatwaves) on annual sediment accumulation rates. Three density variation scenarios were constructed: lower-than-average winter density (winter seagrass density reduced by 50 shoots m^{-2}); higher-than-average winter density (winter seagrass density increased by 50 shoots m^{-2}); and a summer marine heatwave scenario with summer seagrass density reduced to 50 shoots m^{-2} (Aoki et al., 2021). For the lower-than-average winter density scenario, sediment accumulation rates in winter months were much lower than in the normal-density simulations (red symbols in Figure 3.2e) and the annual sediment accumulation rate was reduced by 44% to 2.3 mm yr^{-1}. For the higher-than-average winter density scenario, the seagrass meadow accumulated sediment during the entire winter (gray symbols in Figure 3.2e), resulting in an annual sediment accumulation rate of 6.6 mm yr^{-1}, a 61% increase compared with the rate under typical densities. For the summer marine heatwave scenario, the meadow became erosional, with an annual sediment accumulation rate of -1.0 mm yr^{-1} (Figure 3.2f), thereby leading to the release of stored carbon in seagrass sediments (-4.6 g C m^{-2} yr^{-1}). This modeling result of seabed erosion and sediment carbon loss is in general agreement with a previous study in the same meadow documenting a net loss of 20% of sediment carbon in the upper 5 cm of the bed (not including the effects of bed level changes) caused by a summer marine heatwave in 2015 (Aoki et al., 2021).

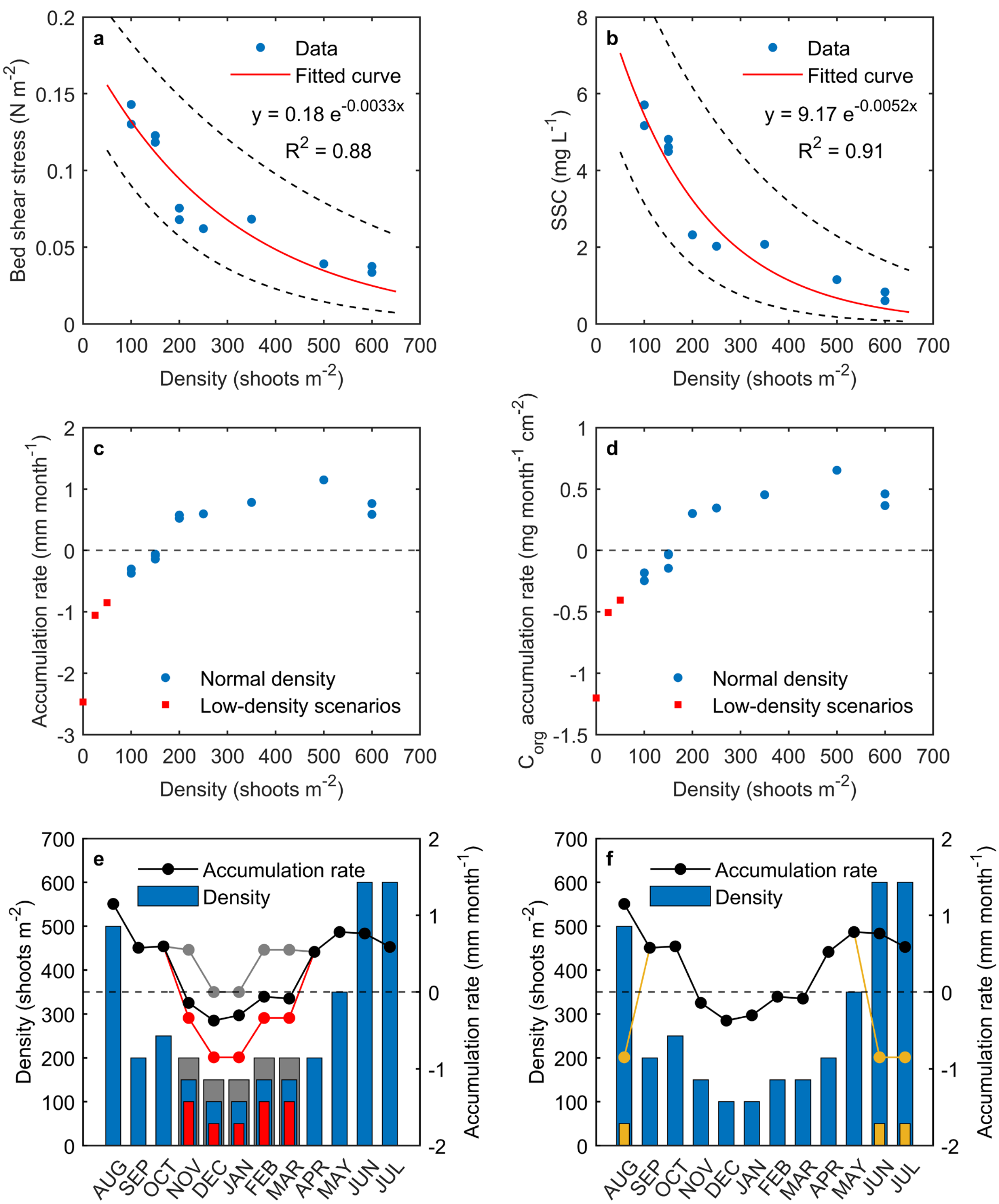

Figure 3.2 (a) Bed shear stress, (b) total suspended sediment concentration (SSC), (c) sediment accumulation rates, and (d) organic carbon accumulation rates as a function of seagrass density, (e) bar plots of seagrass density and changes of sediment accumulation rate in seagrass meadows under normal-density conditions (blue), lower-than-average winter density scenario (red), and higher-than-average winter density scenario (gray), and (f) bar plots of seagrass density and changes of sediment accumulation rate in seagrass meadows under normal-density conditions

and summer marine heatwave scenario (yellow). Red symbols in (c) and (d) are model results output from low-density scenarios using a seagrass shoot density of 0, 25, and 50 shoots m^{-2}, respectively. Details about model settings and seagrass characteristics used in model simulations are provided in Table A2.1.

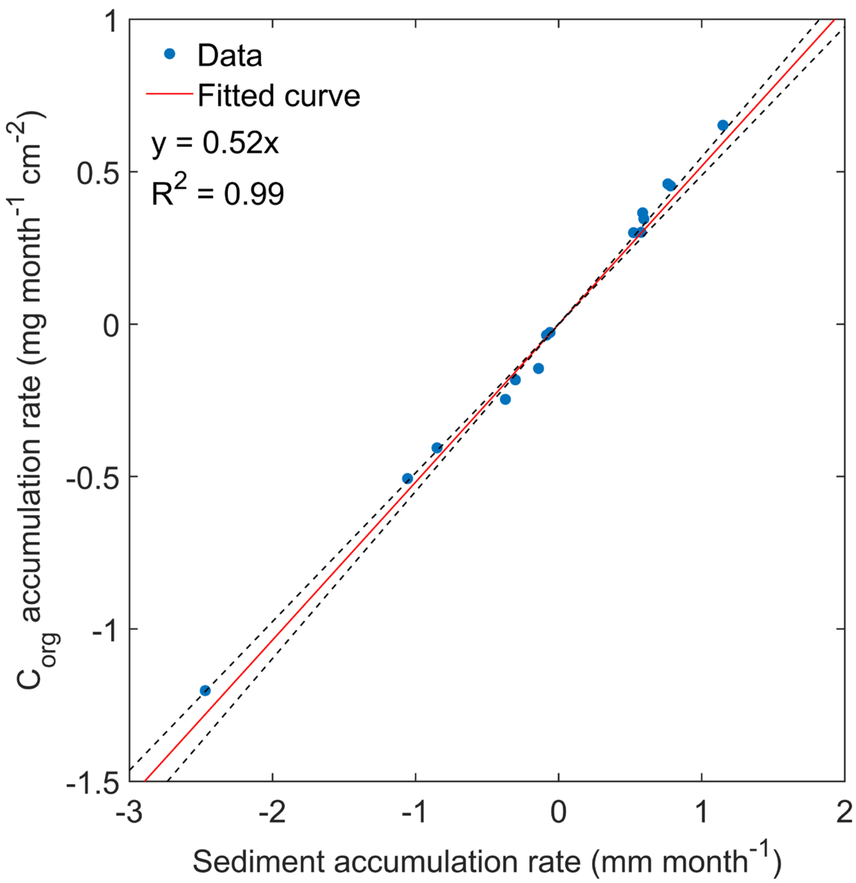

Figure 3.3 Relationship between modeled surface sediment organic carbon (C_{org}) accumulation rate and modeled sediment accumulation rate averaged across the meadow.

3.4.2 Spatial erosion and deposition pattern within meadows

To better understand the spatial variability of seasonal sediment accumulation at the meadow scale, we divided our annual simulation results into four groups according to the seagrass growth cycle at our study site: summer growth and mid-season loss from June to August, autumn regrowth from September to October, winter senescence from November to March, and early growth from April to May. Our simulation results show that there were strong spatial gradients of bed shear stress from the meadow edge toward the interior (Figure A2.8), and these spatial gradients had a significant impact on seasonal erosion/deposition patterns. Sediment accumulation mainly occurred at meadow edges during summer when seagrass density was high (Figure 3.4a) and decreased rapidly with distance into the meadow interior (Figure 3.4e). When seagrass density decreased in autumn, the meadow still accumulated sediment with a lower deposition rate, and this sediment could be transported further into the meadow interior due to weaker flow attenuation by the seagrass (Figure 3.4b, A2.8b). During the minimum densities in winter, most of the meadow experienced erosion (Figure 3.4c). The most severe erosion occurred near meadow edges during the winter senescence period (~9 mm), an amount roughly equal to the mass of sediment deposited at the edges in summer (Figure 3.4e). When seagrass started regrowing in spring, the meadow once again became depositional, with sediment accumulating at meadow edges, but at lower rates compared to the summer growing season (Figure 3.4d). Seasonal organic carbon accumulation patterns were similar to those for sediment accumulation (Figure A2.5).

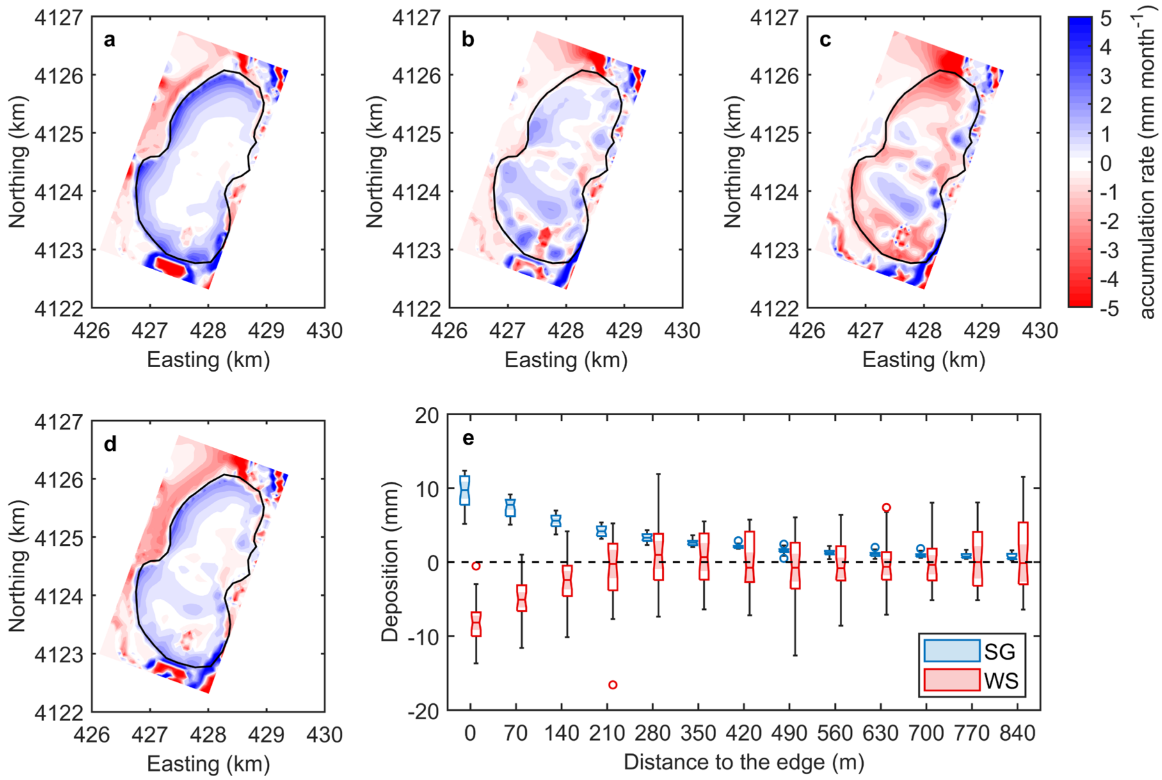

Figure 3.4 Average seasonal sediment accumulation rates output from model simulations with typical seasonal seagrass characteristics: (a) summer growth and mid-season loss, (b) autumn regrowth, (c) winter senescence, and (d) early growth. (e) Box plots of cumulative sediment accumulation during summer growth and mid-season loss (SG) and winter senescence (WS) as a function of distance to the meadow edge. The black line in (a)–(d) shows the meadow outline. The data shown in (e) were extracted from 28 interior transects perpendicular to the northern, western, and southern edges of the meadow.

On the annual time scale, the meadow-averaged sediment accumulation rate was low (0.4 ± 0.2 mm yr^{-1}) in the simulation with no seagrass, whereas the presence of a seagrass meadow maintained a higher average sediment accumulation rate of 4.1 ± 0.5 mm yr^{-1} (Figure 3.5a, 3.5b). Despite the large spatial variability of sediment accumulation rates across the meadow (Figure 3.5d), the modeled sediment accumulation rates agreed reasonably well with rates estimated from ^{210}Pb dating in previous studies at two sites of the meadow (see locations in Figure 3.5b); the modeled sediment accumulation rates at the central and northern sites were 5.0 and 4.3 mm yr^{-1}, respectively, while the rates estimated from ^{210}Pb dating were 6.6 and 6.0 mm yr^{-1} at these two sites (Greiner et al., 2013; Oreska et al., 2018). Pronounced sediment accumulation (> 4.0 mm yr^{-1}) occurred at meadow edges and in the northwestern and southern portion of the meadow interior (Figure 3.5b), in good agreement with previous observations from Oreska et al. (2017) within the same meadow. Because the amount of sediment accumulation at meadow edges in summer was largely offset by winter erosion (Figure 3.4e), the annual sediment accumulation rate near the edge was mainly dependent on deposition during autumn regrowth and spring early growth seasons. During autumn regrowth, winter senescence, and early growth seasons, sediment could be transported further into the northwestern and southern portion of the meadow (Figure 3.4) where larger water depths resulted in lower bed shear stress and promoted sediment accumulation (Figure 3.5b, 3.5c). At the meadow scale, while there was no depth preference for sediment erosion/deposition in simulations without seagrass effects (Figure 3.6a), deeper locations within the meadow tended to receive more sediment deposition than shallow ones when seagrass effects were included in model simulations (Figure 3.6b).

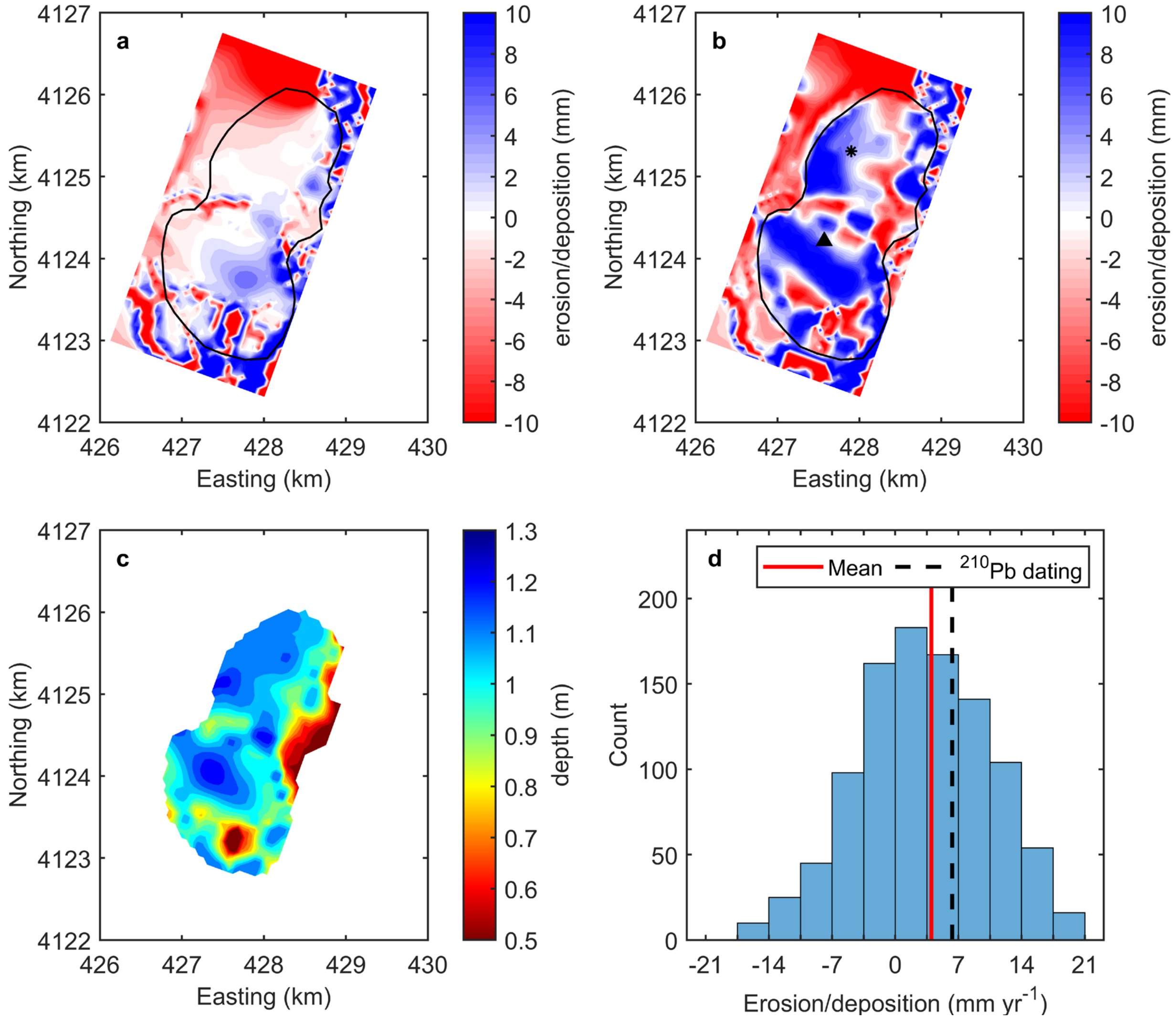

Figure 3.5 Annual sediment erosion and deposition patterns (a) without seagrass effects and (b) with seagrass effects, (c) water depth of the meadow, and (d) histogram of modeled annual sediment accumulation rates within the meadow. The asterisk and triangle in (b) show locations of sediment cores for ^{210}Pb dating collected by Oreska et al. (2018) and Greiner et al. (2013), respectively. The red line in (d) represents the mean modeled sediment accumulation rate, while the black dashed line shows the average sediment accumulation rate by ^{210}Pb dating.

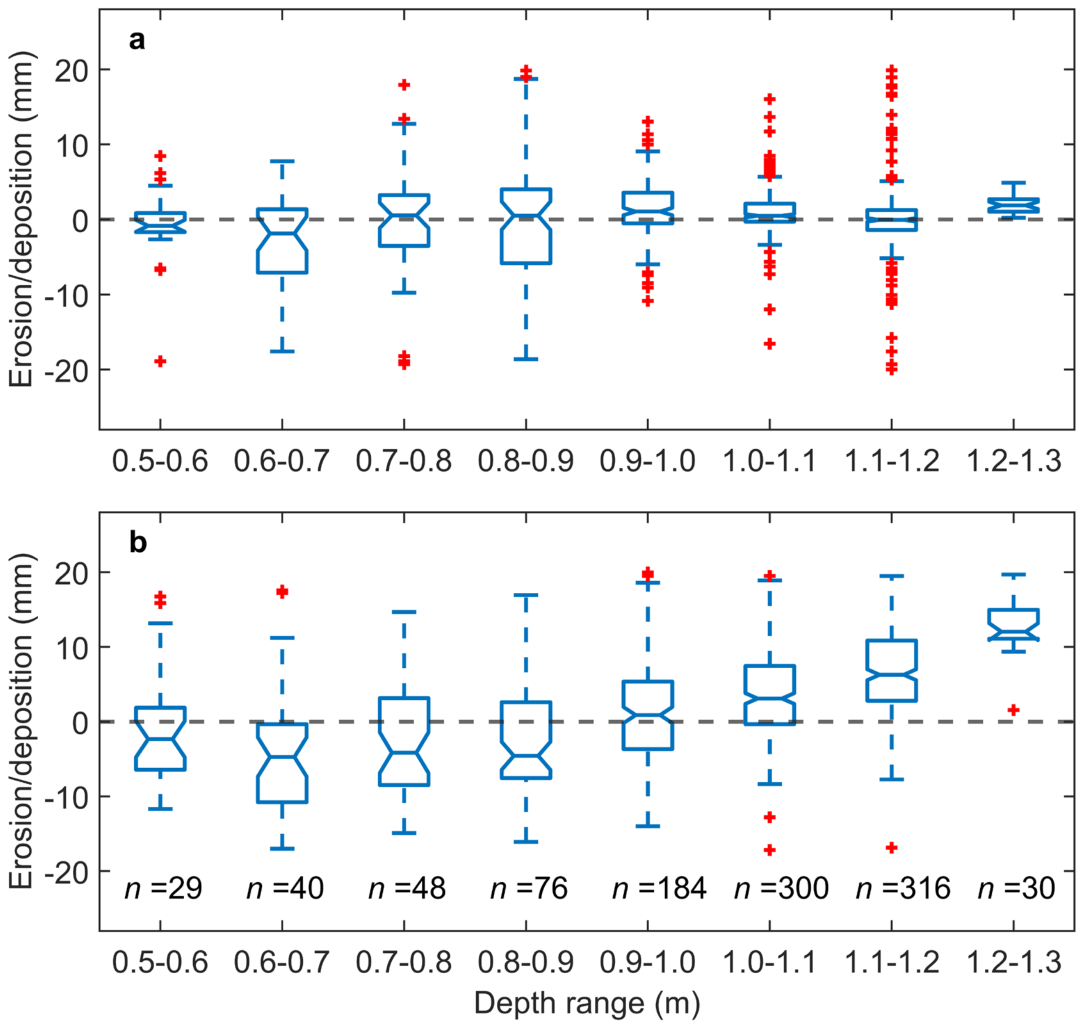

Figure 3.6 Box plots of annual sediment erosion/deposition within seagrass meadows as a function of depth without seagrass effects (a) and with seagrass effects (b).

3.5 Discussion and conclusions

A number of field studies (Hansen and Reidenbach, 2013; Hasegawa et al., 2008) have shown that high densities of seagrass in the summer growing season resulted in larger reductions in bed shear stress and sediment resuspension compared with low-density meadows in winter. However, the effects of seasonally varying seagrass densities on sediment accumulation have not been well quantified due to the lack of monthly or seasonal measurements. Our annual simulation results show that sediment accumulation rates within seagrass meadows changed non-linearly between seasons as a function of seagrass density (Figure 3.2c). The most rapid changes of sediment accumulation rates occurred at low seagrass densities in winter (Figure 3.2c), while there was little change in sediment accumulation rates when seagrass densities were > 200 shoots m^{-2} during other seasons due to effects of strong flow reduction at high shoot densities (Figure 3.2a, A2.7; Hansen and Reidenbach, 2013).

Our seagrass density variation scenarios show that small variations in winter shoot density can result in large changes (> 40%) in annual sediment accumulation rates of the meadow (Figure 3.2e). Considering that most previous research has focused on flow and sediment dynamics in high-density meadows (Donatelli et al., 2018), more comprehensive investigations of sediment accumulation during low-density seasons are needed to better resolve the effects of seagrass density variations on annual sediment accumulation. We also found that summer seagrass dieback events, for example due to marine heatwaves, can change seagrass beds from depositional (4.1 mm yr^{-1}) to erosional (-1.0 mm yr^{-1}; Figure 3.2f) on annual timescales. This strong sensitivity of sediment accumulation rates to seagrass density variations has significant implications for future scenarios of change. If seagrasses were present in much lower densities due to degradation, physical disturbance, or increasing frequency of marine heatwaves, meadows would inevitably become erosional and release accumulated carbon (Arias-Ortiz et al., 2018; Walter et al., 2020), like the observed sediment carbon loss associated with the 2015 summer marine heatwave in South Bay seagrass meadows (Aoki et al., 2021). Moreover, if seagrasses were exposed to multiple years of degraded environmental conditions, including temperature stress, the continuous erosion of seagrass beds associated with reduced seagrass growth would increase water depth of the bay and promote sediment resuspension, thereby creating a less favorable light condition for seagrass growth and potentially triggering irreversible collapse of meadows (Carr et al., 2012).

Although previous studies have shown that seagrasses can effectively trap sediment and promote sediment deposition (Gacia and Duarte, 2001), there have been few direct meadow-scale observations of spatial erosion/deposition patterns within seagrass meadows. Very little is known about the spatial sediment deposition pattern in response to seasonal seagrass density variations. Our simulation results show that edge effects play an important role in seasonal patterns of sediment accumulation and carbon burial at a meadow scale (Figure 3.4, A2.5). This is supported by spatial autoregressive analyses in the same meadow that found that edge proximity was more important than shoot density and meadow age in determining sediment organic carbon content (Oreska et al., 2017). Sediment accumulation mainly occurred at meadow edges in spring and summer growth seasons when seagrass density was relatively high (Figure 3.4a, 3.4d). The modeled sediment accumulation at meadow edges in the present study was in good agreement with other model results considering seagrass edge effects at high shoot densities (Carr et al., 2016; Chen et al., 2007). During the winter senescence period, severe erosion (~9 mm) was observed near meadow edges, an amount roughly equal to 40%–50% of the mass of sediment deposited at the edges in other seasons (Figure 3.4).

During autumn regrowth, winter senescence, and early growth seasons, lower densities of seagrass allow sediment to be advected further into the meadow (Figure 3.4b, 3.4c, and 3.4d), providing the primary mechanism for sediment deposition in the interior of the meadow. Our simulation results show that water depth exerted a strong influence on the spatial pattern of sediment accumulation in the meadow interior (Figure 3.6b). Together with edge effects, depth variations can produce strong spatial variability in sediment accumulation and carbon burial across the meadow (Figure 3.5; Oreska et al., 2017; Samper-Villarreal et al., 2016). This has implications for site selection and timing of sediment sampling to characterize sediment accumulation and carbon burial in seagrass meadows. Ideally, sampling sites should include the meadow edge and interior, as well as deeper and shallower sites. Sampling during the autumn regrowth period may provide the best representation of the annual spatial pattern of deposition (Figure 3.4b, 3.5b).

Organic carbon burial rates within the meadow were obtained by multiplying sediment accumulation rate by surface sediment organic carbon concentration at each model grid location. At the meadow scale, although there were spatial gradients of sediment organic carbon concentration from meadow edges to the interior (varying from 2 to 6 mg cm^{-3}; Figure A2.4), the spatial pattern of organic carbon burial was largely determined by sediment accumulation (Figure 3.3, Figure 3.4 vs. Figure A2.5) because of its strong spatial variability across the meadow (Figure 3.5d). This is in agreement with a recent study indicating the strong impacts of sediment accumulation rates on organic carbon burial at a basin scale (Johannessen and Macdonald, 2016). In some other systems where spatial distributions of sediment accumulation rate are relatively uniform, like those in lacustrine environments (Lin et al., 2022), the spatial pattern of organic carbon burial will more likely be controlled by spatial distributions of sediment organic carbon concentration.

On an annual time scale, our simulations with seasonal seagrass characteristics predicted a meadow-wide average sediment accumulation rate of 4.1 ± 0.5 mm yr^{-1}. This value is similar to the rapid rates of sea-level rise (4–5 mm yr^{-1}) at our study site, but is less than the average long-term sediment accumulation rate (6.3 mm yr^{-1}) determined by ^{210}Pb dating at two representative sites within the meadow (Greiner et al., 2013; Oreska et al., 2018). In future studies, more spatially distributed sediment accumulation rate measurements will be needed to constrain model simulation results and improve our understanding of spatial erosion/deposition patterns within seagrass meadows.

The modeled carbon accumulation rate averaged across the meadow (22 ± 1.6 g C m^{-2} yr^{-1}) was lower than the rate obtained from the meadow-scale carbon stock estimate in the same meadow based on 16 spatially distributed sampling sites (42 g C m^{-2} yr^{-1}; Oreska et al., 2020). The underestimation of sediment accumulation and carbon burial rates is likely due to the absence of primary production in model simulations. A more realistic approach would be to incorporate vegetation growth dynamics and organic matter trapping (e.g., Best et al., 2018; Brückner et al., 2019) into the coupled model. In addition, our model grid size (~70 m) was too coarse to resolve seagrass patchiness, which has been shown to play a significant role in distributions of bed shear stress and sediment accumulation (Carr et al., 2016; Ricart et al., 2015). Another limitation of this study is that we did not simulate temperature in the coupled model and therefore could not resolve the effects of biodegradation and mineralization on sediment carbon burial, which have been found to be important factors affecting carbon storage in other seagrass ecosystems (Sohma et al., 2018).

Our model was able to produce reasonable spatially-resolved simulations of sediment accumulation in seagrass meadows under seasonally varying winds and tides and seagrass densities. This is one of the first modeling attempts to examine in detail the extent and drivers of temporal and spatial variability in sediment accumulation and carbon burial within seagrass meadows. Our results have significant implications for seagrass ecosystems under future climate change. In a warming climate, seagrasses in temperate regions in the northern hemisphere will shift northward and the southernmost populations, like the meadows at our site, will likely face reduced growth and meadow loss due to temperature stress (Wilson and Lotze, 2019). Marine heatwaves have already impacted seagrass meadows in this region (Aoki et al., 2021; Berger et al., 2020), and these are predicted to increase in frequency in future warming oceans (Oliver et al., 2019). Our modeling results of sediment accumulation in seagrass meadows and field studies from the same region (Aoki et al., 2021) indicate that under these circumstances, seabed erosion and carbon emissions will increase. Conservation actions are therefore urgently needed to mitigate the effects of climate change on seagrass ecosystems.

References

Aoki, L. R., McGlathery, K. J., Wiberg, P. L., & Al-Haj, A. (2020). Depth Affects Seagrass Restoration Success and Resilience to Marine Heat Wave Disturbance. Estuaries and Coasts, 43(2), 316–328. https://doi.org/10.1007/s12237-019-00685-0

Aoki, L. R., McGlathery, K. J., Wiberg, P. L., Oreska, M. P. J., Berger, A. C., Berg, P., & Orth, R. J. (2021). Seagrass Recovery Following Marine Heat Wave Influences Sediment Carbon Stocks. Frontiers in Marine Science, 7, 1170. https://doi.org/10.3389/fmars.2020.576784

Arias-Ortiz, A., Serrano, O., Masqué, P., Lavery, P. S., Mueller, U., Kendrick, G. A., et al. (2018). A marine heatwave drives massive losses from the world's largest seagrass carbon stocks. Nature Climate Change, 8(4), 1–7. https://doi.org/10.1038/s41558-018-0096-y

Baptist, M. J., Babovic, V., Uthurburu, J. R., Keijzer, M., Uittenbogaard, R. E., Mynett, A., & Verwey, A. (2007). On inducing equations for vegetation resistance. Journal of Hydraulic

Research, 45(4), 435–450. https://doi.org/10.1080/00221686.2007.9521778

Berger, A. C., Berg, P., McGlathery, K. J., & Delgard, M. L. (2020). Long-term trends and resilience of seagrass metabolism: A decadal aquatic eddy covariance study. Limnology and Oceanography, 65(7), 1423–1438. https://doi.org/10.1002/lno.11397

Best, S. N., Van der Wegen, M., Dijkstra, J., Willemsen, P. W. J. M., Borsje, B. W., & Roelvink, D. J. A. (2018). Do salt marshes survive sea level rise? Modelling wave action, morphodynamics and vegetation dynamics. Environmental Modelling and Software, 109, 152–166. https://doi.org/10.1016/j.envsoft.2018.08.004

Booij, N., Ris, R. C., & Holthuijsen, L. H. (1999). A third-generation wave model for coastal regions 1. Model description and validation. Journal of Geophysical Research: Oceans, 104(C4), 7649–7666. https://doi.org/10.1029/98JC02622

Brückner, M. Z. M., Schwarz, C., Dijk, W. M., Oorschot, M., Douma, H., & Kleinhans, M. G. (2019). Salt Marsh Establishment and Eco-Engineering Effects in Dynamic Estuaries Determined by Species Growth and Mortality. Journal of Geophysical Research: Earth Surface, 124(12), 2962–2986. https://doi.org/10.1029/2019JF005092

Carr, J. A., D'Odorico, P., McGlathery, K. J., & Wiberg, P. L. (2012). Stability and resilience of seagrass meadows to seasonal and interannual dynamics and environmental stress. Journal of Geophysical Research: Biogeosciences, 117(G1), 1007. https://doi.org/10.1029/2011JG001744

Carr, J., D'Odorico, P., McGlathery, K. J., & Wiberg, P. L. (2016). Spatially explicit feedbacks between seagrass meadow structure, sediment and light: Habitat suitability for seagrass growth. Advances in Water Resources, 93, 315–325. https://doi.org/10.1016/j.advwatres.2015.09.001

Chen, S. N., Sanford, L. P., Koch, E. W., Shi, F., & North, E. W. (2007). A nearshore model to investigate the effects of seagrass bed geometry on wave attenuation and suspended sediment transport. Estuaries and Coasts, 30(2), 296–310. https://doi.org/10.1007/BF02700172

Deltares. (2014). Delft3D-FLOW User Manual (Version: 3.15.34158): Simulation of multi-dimensional hydrodynamic flows and transport phenomena, including sediments. Delft, The Netherlands: WL Delft Hydraulics

de Boer, W. F. (2007). Seagrass-sediment interactions, positive feedbacks and critical thresholds for occurrence: A review. Hydrobiologia, 591(1), 5–24. https://doi.org/10.1007/s10750-007-0780-9

Donatelli, C., Ganju, N. K., Fagherazzi, S., & Leonardi, N. (2018). Seagrass Impact on Sediment Exchange Between Tidal Flats and Salt Marsh, and The Sediment Budget of Shallow Bays. Geophysical Research Letters, 45(10), 4933–4943. https://doi.org/10.1029/2018GL078056

Duarte, C. M., Kennedy, H., Marbà, N., & Hendriks, I. (2013). Assessing the capacity of seagrass meadows for carbon burial: Current limitations and future strategies. Ocean and Coastal Management, 83, 32–38. https://doi.org/10.1016/j.ocecoaman.2011.09.001

Fagherazzi, S., & Wiberg, P. L. (2009). Importance of wind conditions, fetch, and water levels on wave-generated shear stresses in shallow intertidal basins. Journal of Geophysical Research, 114(F3), F03022. https://doi.org/10.1029/2008JF001139

Fourqurean, J. W., Duarte, C. M., Kennedy, H., Marbà, N., Holmer, M., Mateo, M. A., et al. (2012). Seagrass ecosystems as a globally significant carbon stock. Nature Geoscience, 5(7), 505–509. https://doi.org/10.1038/ngeo1477

Gacia, E., & Duarte, C. M. (2001). Sediment retention by a Mediterranean Posidonia oceanica meadow: The balance between deposition and resuspension. Estuarine, Coastal and Shelf Science, 52(4), 505–514. https://doi.org/10.1006/ecss.2000.0753

Greiner, J. T., McGlathery, K. J., Gunnell, J., & McKee, B. A. (2013). Seagrass Restoration Enhances "Blue Carbon" Sequestration in Coastal Waters. PLoS ONE, 8(8), e72469. https://doi.org/10.1371/journal.pone.0072469

Hansen, J., & Reidenbach, M. A. (2013). Seasonal Growth and Senescence of a Zostera marina Seagrass Meadow Alters Wave-Dominated Flow and Sediment Suspension Within a Coastal Bay. Estuaries and Coasts, 36(6), 1099–1114. https://doi.org/10.1007/s12237-013-9620-5

Hasegawa, N., Hori, M., & Mukai, H. (2008). Seasonal changes in eelgrass functions: Current velocity reduction, prevention of sediment resuspension, and control of sediment-water column nutrient flux in relation to eelgrass dynamics. Hydrobiologia, 596(1), 387–399. https://doi.org/10.1007/s10750-007-9111-4

Johannessen, S. C., & Macdonald, R. W. (2016). Geoengineering with seagrasses: Is credit due where credit is given? Environmental Research Letters, 11(11), 113001. https://doi.org/10.1088/1748-9326/11/11/113001

Lawson, S. E., Wiberg, P. L., McGlathery, K. J., & Fugate, D. C. (2007). Wind-driven sediment suspension controls light availability in a shallow coastal lagoon. Estuaries and Coasts, 30(1), 102–112. https://doi.org/10.1007/BF02782971

Lesser, G. R., Roelvink, J. A., van Kester, J. A. T. M. T. M., & Stelling, G. S. (2004). Development and validation of a three-dimensional morphological model. Coastal Engineering, 51(8), 883–915. https://doi.org/10.1016/j.coastaleng.2004.07.014

Lin, Q., Liu, E., Zhang, E., Bindler, R., Nath, B., Zhang, K., & Shen, J. (2022). Spatial variation of organic carbon sequestration in large lakes and implications for carbon stock quantification. CATENA, 208, 105768. https://doi.org/10.1016/J.CATENA.2021.105768

McGlathery, K. J., Reynolds, L. K., Cole, L. W., Orth, R. J., Marion, S. R., & Schwarzschild, A. (2012). Recovery trajectories during state change from bare sediment to eelgrass dominance. Marine Ecology Progress Series, 448, 209–221. https://doi.org/10.3354/meps09574

McGlathery, K. J., Sundbäck, K., & Anderson, I. (2007). Eutrophication in shallow coastal bays and lagoons: the role of plants in the coastal filter. Marine Ecology Progress Series, 348, 1–18. https://doi.org/10.3354/meps07132

Moki, H., Taguchi, K., Nakagawa, Y., Montani, S., & Kuwae, T. (2020). Spatial and seasonal impacts of submerged aquatic vegetation (SAV) drag force on hydrodynamics in shallow waters. Journal of Marine Systems, 209, 103373. https://doi.org/10.1016/j.jmarsys.2020.103373

Nardin, W., & Edmonds, D. A. (2014). Optimum vegetation height and density for inorganic sedimentation in deltaic marshes. Nature Geoscience, 7(10), 722–726. https://doi.org/10.1038/NGEO2233

Nardin, W., Larsen, L., Fagherazzi, S., & Wiberg, P. (2018). Tradeoffs among hydrodynamics, sediment fluxes and vegetation community in the Virginia Coast Reserve, USA. Estuarine, Coastal and Shelf Science, 210, 98–108. https://doi.org/10.1016/j.ecss.2018.06.009

Nolte, S., Koppenaal, E. C., Esselink, P., Dijkema, K. S., Schuerch, M., De Groot, A. V., et al. (2013, September 30). Measuring sedimentation in tidal marshes: A review on methods and their applicability in biogeomorphological studies. Journal of Coastal Conservation. Springer. https://doi.org/10.1007/s11852-013-0238-3

Oliver, E. C. J., Burrows, M. T., Donat, M. G., Sen Gupta, A., Alexander, L. V., Perkins-Kirkpatrick, S. E., et al. (2019). Projected Marine Heatwaves in the 21st Century and the Potential for Ecological Impact. Frontiers in Marine Science, 6, 734. https://doi.org/10.3389/fmars.2019.00734

Oreska, M. P. J., McGlathery, K. J., & Porter, J. H. (2017). Seagrass blue carbon spatial patterns at the meadow-scale. PLoS ONE, 12(4), e0176630. https://doi.org/10.1371/journal.pone.0176630

Oreska, M. P. J., Wilkinson, G. M., McGlathery, K. J., Bost, M., & McKee, B. A. (2018). Non-seagrass carbon contributions to seagrass sediment blue carbon. Limnology and Oceanography, 63(S1), S3–S18. https://doi.org/10.1002/lno.10718

Oreska, M. P. J., McGlathery, K. J., Aoki, L. R., Berger, A. C., Berg, P., & Mullins, L. (2020). The greenhouse gas offset potential from seagrass restoration. Scientific Reports, 10(1), 1–15. https://doi.org/10.1038/s41598-020-64094-1

Orth, R. J., Carruthers, T. J. B., Dennison, W. C., Duarte, C. M., Fourqurean, J. W., Heck, K. L., et al. (2006). A Global Crisis for Seagrass Ecosystems. BioScience, 56(12), 987–996. https://doi.org/10.1641/0006-3568(2006)56[987:AGCFSE]2.0.CO;2

Pendleton, L., Donato, D. C., Murray, B. C., Crooks, S., Jenkins, W. A., Sifleet, S., et al. (2012). Estimating Global "Blue Carbon" Emissions from Conversion and Degradation of Vegetated Coastal Ecosystems. PLoS ONE, 7(9), e43542. https://doi.org/10.1371/journal.pone.0043542

Potouroglou, M., Bull, J. C., Krauss, K. W., Kennedy, H. A., Fusi, M., Daffonchio, D., et al. (2017). Measuring the role of seagrasses in regulating sediment surface elevation. Scientific Reports, 7(1), 1–11. https://doi.org/10.1038/s41598-017-12354-y

Reidenbach, M. A., & Thomas, E. L. (2018). Influence of the Seagrass, Zostera marina, on Wave Attenuation and Bed Shear Stress Within a Shallow Coastal Bay. Frontiers in Marine Science, 5(OCT), 397. https://doi.org/10.3389/fmars.2018.00397

Rheuban, J. E., Berg, P., & McGlathery, K. J. (2014). Ecosystem metabolism along a colonization gradient of eelgrass (Zostera marina) measured by eddy correlation. Limnology and Oceanography, 59(4), 1376–1387. https://doi.org/10.4319/lo.2014.59.4.1376

Ricart, A. M., York, P. H., Rasheed, M. A., Pérez, M., Romero, J., Bryant, C. V., & Macreadie, P. I. (2015). Variability of sedimentary organic carbon in patchy seagrass landscapes. Marine Pollution Bulletin, 100(1), 476–482. https://doi.org/10.1016/j.marpolbul.2015.09.032

Samper-Villarreal, J., Lovelock, C. E., Saunders, M. I., Roelfsema, C., & Mumby, P. J. (2016). Organic carbon in seagrass sediments is influenced by seagrass canopy complexity, turbidity, wave height, and water depth. Limnology and Oceanography, 61(3), 938–952. https://doi.org/10.1002/LNO.10262

Sohma, A., Shibuki, H., Nakajima, F., Kubo, A., & Kuwae, T. (2018). Modeling a coastal ecosystem to estimate climate change mitigation and a model demonstration in Tokyo Bay. Ecological Modelling, 384, 261–289. https://doi.org/10.1016/J.ECOLMODEL.2018.04.019

Suzuki, T., Zijlema, M., Burger, B., Meijer, M. C., & Narayan, S. (2012). Wave dissipation by vegetation with layer schematization in SWAN. Coastal Engineering, 59(1), 64–71. https://doi.org/10.1016/j.coastaleng.2011.07.006

Walter, R. K., O'Leary, J. K., Vitousek, S., Taherkhani, M., Geraghty, C., & Kitajima, A. (2020). Large-scale erosion driven by intertidal eelgrass loss in an estuarine environment. Estuarine, Coastal and Shelf Science, 243, 106910. https://doi.org/10.1016/j.ecss.2020.106910

Waycott, M., Duarte, C. M., Carruthers, T. J. B., Orth, R. J., Dennison, W. C., Olyarnik, S., et al. (2009). Accelerating loss of seagrasses across the globe threatens coastal ecosystems. Proceedings of the National Academy of Sciences of the United States of America, 106(30), 12377–12381. https://doi.org/10.1073/pnas.0905620106

Wiberg, P. L., Carr, J. A., Safak, I., & Anutaliya, A. (2015). Quantifying the distribution and influence of non-uniform bed properties in shallow coastal bays. Limnology and Oceanography: Methods, 13(12), 746–762. https://doi.org/10.1002/lom3.10063

Willmott, C. J. (1981). On the validation of models. Physical Geography, 2(2), 184–194. https://doi.org/10.1080/02723646.1981.10642213

Wilson, K. L., & Lotze, H. K. (2019). Climate change projections reveal range shifts of eelgrass Zostera marina in the Northwest Atlantic. Marine Ecology Progress Series, 620, 47–62. https://doi.org/10.3354/meps12973

Zhu, Q., Wiberg, P. L., & Reidenbach, M. A. (2021). Quantifying Seasonal Seagrass Effects on Flow and Sediment Dynamics in a Back-Barrier Bay. Journal of Geophysical Research: Oceans, 126(2), e2020JC016547. https://doi.org/10.1029/2020JC016547

Chapter 4. The importance of storm surge for sediment delivery to microtidal marshes

This chapter is currently in review at *Journal of Geophysical Research: Earth Surface* with Patricia L. Wiberg as co-author.

Abstract

Storm surge has the potential to significantly increase suspended sediment flux to microtidal marshes. However, the overall effects of storm surge on microtidal marsh deposition have not been well quantified, with most modeling studies focusing on regular (astronomical) tidal flooding. Here we applied the Delft3D model to a microtidal bay–marsh complex in Hog Bay, Virginia to quantify the contributions of storm surge to marsh deposition. We validated the model using spatially distributed hydrodynamic and suspended sediment data collected from the site and ran model simulations under different storm surge conditions with/without storm-driven water level changes. Our results show that episodic storm surge events occurred 5% of the time at our study site, but contributed 40% of marsh deposition during 2009–2020. Our simulations illustrate that while wind-driven waves control sediment resuspension on tidal flats, marsh deposition during storms was largely determined by tidal inundation associated with storm-driven water levels. A moderate storm surge event can double sediment flux to most marshes around the bay and deliver more sediment to the marsh interior compared to simulations that include wind waves but not storm surge variations in water levels. Simulations of bay and marsh response to different storm surge events with varying magnitude of storm surge intensity reveal that total marsh deposition around the bay increased linearly with storm surge intensity, suggesting that future changes to storm magnitude and/or frequency would have significant implications for sediment supply to marshes at our study site.

4.1 Introduction

Intertidal salt marshes are ecosystems situated between the land and the sea. They provide essential food and nursery grounds for various coastal species and offer valuable ecosystem services such as water purification and carbon sequestration (Barbier et al., 2011). They also provide important coastal protection functions for coastal communities by promoting sediment deposition and attenuating storm waves (King & Lester, 1995; Möller et al., 2014). Despite their great importance in ecosystem and coastal protection, salt marshes are increasingly threatened by human activities and climate change (Fagherazzi et al., 2020; FitzGerald & Hughes, 2019; Gedan et al., 2009). One of the major threats to salt marshes is accelerated sea level rise (SLR) that is rising at a rate multiple times higher than the historical values when salt marshes initially formed and developed a few thousand years ago (FitzGerald & Hughes, 2019).

To keep pace with sea level rise, salt marshes need to maintain a vertical accretion rate at least as high as the relative SLR rate. Vertical accretion of salt marshes is mainly controlled by allochthonous sediment deposition on the marsh surface, belowground plant growth and decomposition, compaction, and subsidence (Allen, 2000; Cahoon et al., 1995; Friedrichs & Perry, 2001; Redfield, 1972). As sea level rises, greater tidal inundation can enhance suspended sediment deposition on the marsh platform and production of belowground biomass, thereby increasing salt marsh resilience to SLR (Friedrichs & Perry, 2001; Kirwan & Megonigal, 2013; Morris et al., 2002). However, these positive ecogeomorphic feedbacks might not be able to keep pace with an accelerated SLR rate if there is a decrease in advective sediment supply to marshes (Christiansen et al., 2000; Schuerch et al., 2019) or a reduction in belowground organic production once water depth exceeds the optimum range for marsh vegetation growth (Kirwan & Megonigal, 2013). Based on analyses of more than 5,000 marsh sediment samples collected from

33 marshes in the United States, Morris et al. (2016) corroborated that belowground organic production will likely reach a maximum under future climate change and contribute at most 3 mm yr^{-1} to total marsh accretion. Therefore, apart from belowground organic production, a significant supply of suspended sediment to marshes is necessary to promote sufficient sediment deposition on intertidal marshes to keep pace with SLR (Ganju et al., 2017).

Although sediment availability is critical for marsh survival, quantifying suspended sediment flux to the marsh is subject to significant uncertainties due to its strong spatial and temporal variability (Fagherazzi et al., 2020; FitzGerald & Hughes, 2019). There are many sediment transport processes and drivers controlling suspended sediment flux to a marsh, including current/wave induced sediment resuspension on tidal flats (French & Spencer, 1993; Lawson et al., 2007), flocculation (Christiansen et al., 2000), riverine/offshore sediment supply (Castagno et al., 2018; Yang et al., 2020), the presence of submerged aquatic vegetation (Donatelli et al., 2018; Nardin et al., 2018), marsh edge erosion (Hopkinson et al., 2018), human activities (Ma et al., 2014; Peteet et al., 2018), and long-term climate drivers (Schuerch et al., 2016). Compared with relatively well characterized tidal creek–marsh systems, the factors affecting sediment transport processes in coupled tidal flat–marsh systems have received less attention (Duvall et al., 2019; Fagherazzi et al., 2013). Recent studies of tidal flat–marsh systems have underscored the tight coupling between marsh deposition and sediment resuspension on tidal flats, either through high-resolution sediment transport modeling (Donatelli et al., 2020; Mariotti, 2020; Zhang et al., 2019) or synchronized hydrodynamic and sediment flux measurements in the bay–marsh complex (Duvall et al., 2019; Lacy et al., 2020; Schuerch et al., 2019). These studies have improved our understanding of sediment connectivity between tidal flats and marshes, but some important processes that can significantly influence marsh sediment supply are still not well incorporated in most studies, such as the effects of storm surge on marsh deposition.

Storm surge (defined here as the difference between total measured water level and astronomical tide during storms; also commonly referred to as the non-tidal residual) has the potential to significantly increase suspended sediment supply to marshes (Cahoon, 2006). Storm-driven high water levels result in longer and deeper inundation of the marsh platform, thereby increasing the total mass of suspended sediment in the water column even if suspended sediment concentration (SSC) on tidal flats remained constant during storms (Wiberg et al., 2020). Meanwhile, wind-driven waves during storms can increase bed shear stress and resuspend more sediment on tidal flats than tidal currents alone (Carniello et al., 2012; Lawson et al., 2007). Wave-induced sediment resuspension has been found to be the major contributor to marsh sediment input in many bay–marsh complexes (Duvall et al., 2019; Lacy et al., 2020; Schuerch et al., 2019). Despite the potential of storm surge to promote sediment delivery to marshes, the overall effects of storm surge on marsh deposition largely depend on the exact combination of water level variations and SSC levels (Wiberg et al., 2020). Based on field measurements and modeling of currents, waves and suspended sediment near a bay–marsh boundary in Virginia, Duvall et al. (2019) found that effective suspended sediment transport to marshes only occurred when high water and high SSC coincided over tidal flats. Although enhanced marsh sedimentation during storms has been characterized at a number of sites through field surveys, radiometric dating, and modeling (Liu et al., 2018; Schuerch et al., 2012; Tognin et al., 2021; Tweel & Turner, 2014), process-based studies that incorporate wind variability, storm-driven water level changes, and sediment resuspension processes in the coupled tidal flat–marsh systems are needed to better understand the effects of storm surge on marsh sediment delivery.

Compared with marshes in macro/meso-tidal environments, microtidal marshes (tidal range < 2 m) are more vulnerable to SLR due to limited elevation range for vegetation growth (Kirwan & Guntenspergen, 2010). Storm surge can result in much higher water levels than the highest astronomical tides in microtidal environments (Wiberg et al., 2020), providing longer and deeper inundation that promotes sediment deposition during storms. Although numerous previous studies have shown that episodic storm-driven high water levels can significantly increase sediment deposition on microtidal marshes (Goodbred & Hine, 1995; Reed, 1989; Turner et al., 2006; Tweel & Turner, 2014), the overall effects of storm surge on microtidal marsh deposition have not been well quantified, and most modeling studies focus solely on regular (astronomical) tidal flooding that cannot capture the additional effect of storm surge on marsh deposition (Wiberg et al., 2020). To better understand the contributions of storm surge to microtidal marsh deposition, we applied a spatially resolved and process-based hydrodynamic and sediment transport model to a microtidal bay–marsh complex in Virginia, USA. Our model included effects of marsh vegetation on flow and wave attenuation, and is calibrated using spatially distributed hydrodynamic and suspended sediment data from the site. We used the model to quantify the effects of storm surge on marsh deposition under different storm surge conditions with/without storm-driven water level changes. The results were analyzed to address four questions. (1) What are the effects of storm surge on hydrodynamics and sediment resuspension in shallow coastal bays? (2) How do storm-driven water level changes and variations in SSC over tidal flats affect suspended sediment flux to bay-fronted marshes in microtidal coastal bays? (3) How do rates and spatial patterns of marsh sediment deposition vary in response to different storm surge conditions? (4) What fraction of annual marsh deposition can be attributed to storm surge events? Our results underscore the tight coupling between marsh deposition and sediment resuspension on tidal flats and highlight the importance of storm surge for sediment delivery to microtidal marshes.

4.2 Materials and Methods

4.2.1 Study site

This study was conducted in Hog Bay, a shallow coastal lagoon within the Virginia Coast Reserve (VCR) Long-Term Ecological Research site. The VCR is a mostly undeveloped barrier–lagoon–marsh system located on the eastern shore of Virginia along the Atlantic side of the lower Delmarva Peninsula (Figure 4.1). The rate of SLR in the system has been 4–5 mm yr^{-1} during the past 40 years, among the highest on the U.S. Atlantic coast (https://tidesandcurrents.noaa.gov/sltrends/sltrends_station.shtml?id=8631044). The mainland area draining into the VCR consists of about 56 small watersheds that deliver negligible amounts of fluvial freshwater and sediment to the bays (Brinson et al., 1995; Stanhope et al., 2009).

The study site, Hog Bay, covers an area of ~100 km^2, and is fringed by intertidal salt marshes (~30% of total surface area) that occupy the mainland, islands, and back-barrier areas (Oertel, 2001; Figure 4.2a). The bay has a mean depth of 2.1 m below mean sea level and about 50% of the bay is shallower than 1 m at mean low tides (Oertel, 2001). Tides within the bay are semidiurnal with an average tidal range of 1.2 m (Fagherazzi & Wiberg, 2009). Wind activity has a distinct seasonal pattern in the bay, with typical southerly winds in summer and more frequent and stronger northerly winds during winter (Fagherazzi & Wiberg, 2009). Wind-generated waves during storms are the primary agent of short-term disturbance in the bay, driving strong sediment resuspension from the seabed and marsh edge erosion (Lawson et al., 2007; Mariotti et al., 2010; McLoughlin et al., 2015). On average, the shallow coastal bays in the VCR experience more than 20 extratropical storms each year (Hayden et al., 1995). Depending on atmospheric pressure and wind conditions, these meteorological events can result in varying magnitudes of increases or decreases in water levels. As a result of storm-driven water level variations, the highest measured water levels in the bay can far exceed the highest astronomical tides (Figure 4.2b), significantly increasing marsh deposition potential. For example, the average inundation time of a marsh at an elevation of 0.5 m above mean sea level during 2009–2018 in the VCR increased from 12% when considering astronomical tides alone to 20% when storm surge was included, and this added inundation time could increase marsh sediment deposition by a factor of 1.5 (Wiberg et al., 2020).

Bed sediment grain size in Hog Bay decreases from fine sand near the tidal inlets and barrier beaches to silt and mud in the mainland portion of the bay, with an average grain size of 74 µm (Lawson et al., 2007; Wiberg et al., 2015). Spatial variations in the sand and mud abundance in the bed sediment control the distribution of suspended sediment concentration (SSC) in the bay, resulting in higher SSC in landward, muddier regions and lower SSC near sandier inlets and barrier islands (Wiberg et al., 2015).

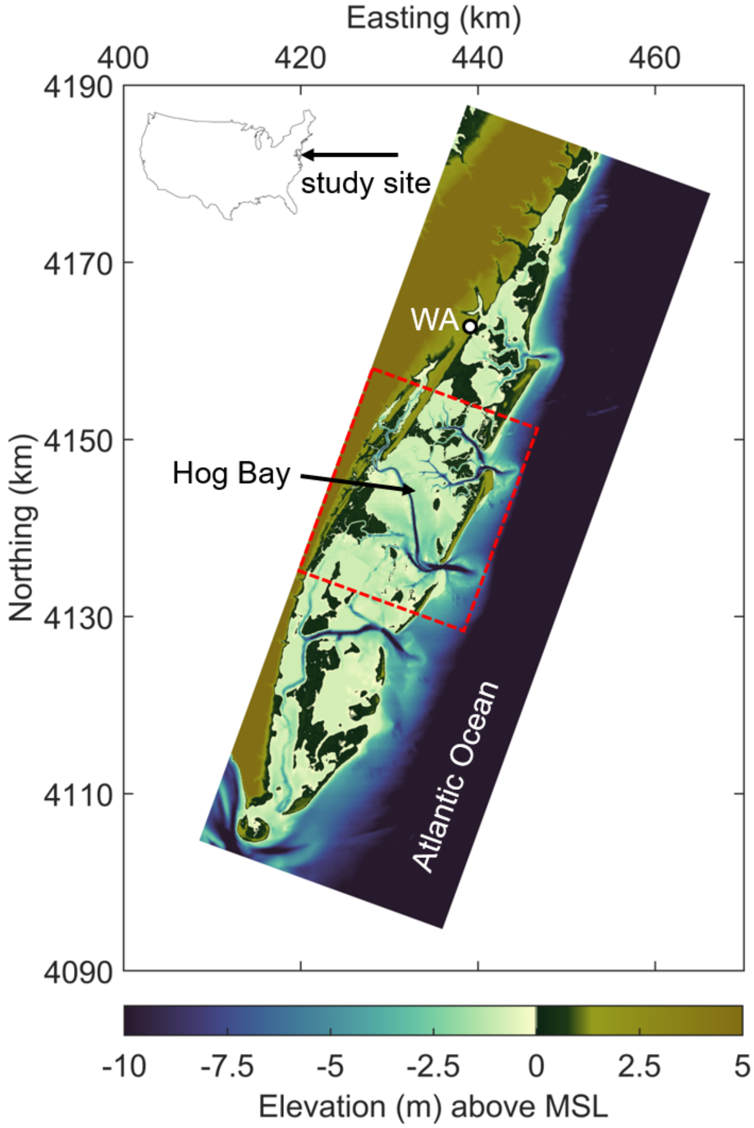

Figure 4.1 Bathymetry of the shallow coastal bays within the VCR (relative to 1983–2001 mean sea level (MSL)). Dark green areas in the map show spatial distributions of salt marshes. Red dashed lines show the shared boundaries of the refined model domain in Hog Bay and the coarse model domain covering the rest of the VCR. WA is the NOAA tide gauge and weather station (Wachapreague, ID:8631044). Coordinates of UTM zone 18N are given in km.

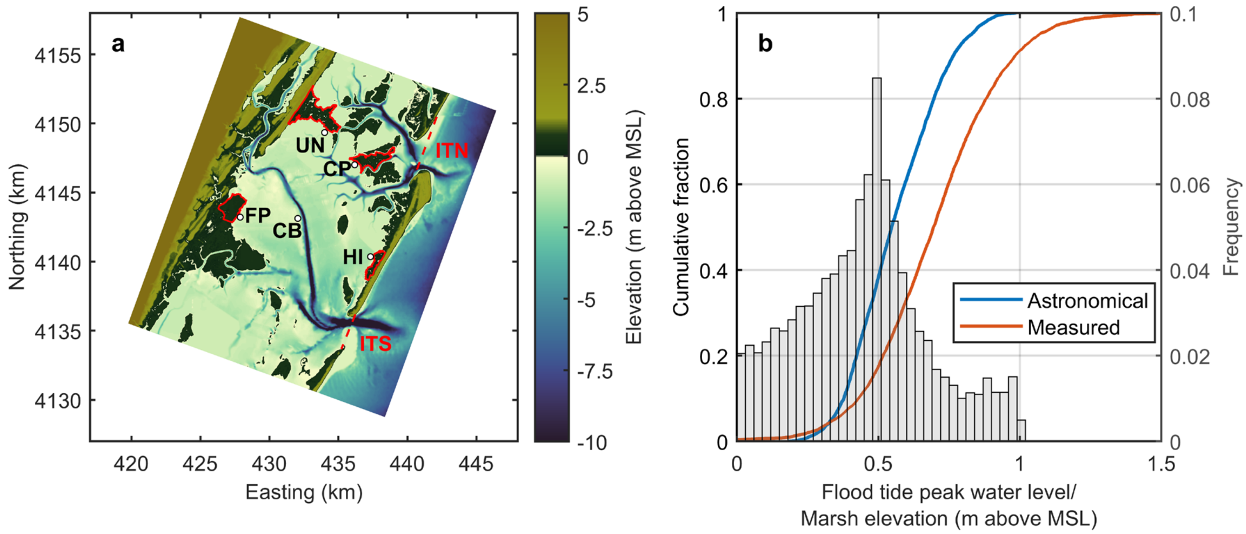

Figure 4.2 (a) Bathymetry of the refined model domain in Hog Bay (relative to 1983–2001 mean sea level (MSL)). Dark green areas in the map show spatial distributions of salt marshes. Open circles show locations of model validation sites: FP (Fowling Point), HI (Hog Island), CP (Chimney Pole), UN (Upshur Neck), and CB (Center Bay). Highlighted polygons show the areas for marsh sediment supply monitoring in model simulations. Red dashed lines show the transect location for inlet sediment flux monitoring. (b) Cumulative distribution of astronomical and measured (including storm surge) flood tide peak water level during 2010–2019 at Wachapreague (left axis) and histogram of marsh surface elevations in the model (right axis).

4.2.2 Storm surge identification

We analyzed measured water levels, astronomical tides predicted by tidal harmonic constants, and wind speeds from August 1, 2008 (the earliest data available from the site) to December 31, 2020 at the NOAA station at Wachapreague (ID:8631044; Figure 4.1) to identify major storm surge events impacting the VCR. A previous study in this region showed that using threshold values of wind speed > 11 m s^{-1} and differences between measured water levels and astronomical tides > 0.2 m was sufficient to identify major storm surge events in the VCR (Castagno et al., 2018). Therefore, we used the same thresholds and identified a total of 68 storm surge events from 2008 to 2020 (Figure A3.1).

To better characterize the impacts of these events, storm surge duration, peak storm surge, 75th percentile wind speed, mean wind direction, and cumulative storm surge intensity were determined for each individual storm surge event (Table A3.1). Storm surge duration was determined by the time during which the storm surge (measured water level − astronomical tide) was above a threshold value of 0.2 m. Cumulative storm surge intensity was calculated by integrating the storm surge over time when the surge was over the 0.2 m threshold (the total area of the region bounded by storm surge and the 0.2 m threshold line in Figure 4.3). A high value of cumulative storm surge intensity is associated with high storm-driven water levels and a long storm surge duration.

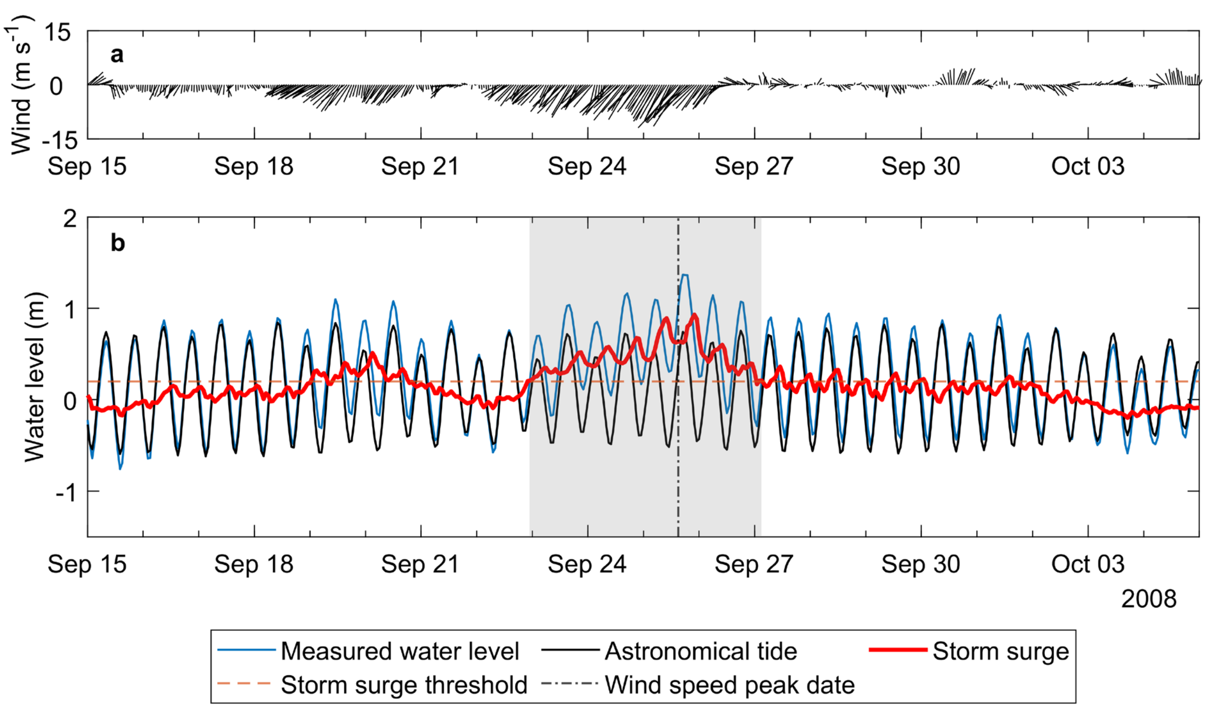

Figure 4.3 Example of identification of a storm surge event: (a) wind speed and direction and (b) measured water levels, astronomical tide, and storm surge (measured water level − astronomical tide) at Wachapreague. Lines in (a) point in the direction that the wind is blowing toward. Shaded area in (b) indicates the period of the storm surge event when storm surge is above the 0.2 m threshold. For detailed characteristics of the identified storm surge events, refer to Table A3.1.

4.2.3 Model settings and validation datasets

We used the spatially resolved and process-based Delft3D FLOW/MOR model (Lesser et al., 2004) coupled with the nearshore phase-averaged wave model SWAN (Booij et al., 1999) to simulate hydrodynamics and sediment transport in the VCR. To better resolve flow and sediment fluxes in the study area and to improve computational efficiency, the overall model was divided into two domains, a locally refined model domain in Hog Bay and a large model domain spanning the rest of the VCR, using the domain decomposition technique (Deltares, 2014). The refined model domain in Hog Bay consisted of 398 × 474 rectangular grid cells with a spatial resolution of 50 m, while the large model domain consisted of 148 × 444 rectangular grid cells with a spatial resolution of 200 m. Parallel computations can be carried out on these two domains, and they exchange information along the shared boundaries at each time step (Figure 4.1). The northern, southern and eastern open ocean boundaries of the large model domain were forced with hourly water levels extracted from the NOAA tide gauge station at Wachapreague (https://tidesandcurrents.noaa.gov/waterlevels.html?id=8631044) after adjustments of tidal amplitude and phase (dampened by a factor of 0.9 and delayed 66 min; similar approach as Castagno et al., 2018 and Zhu et al., 2021) to generate the best tidal simulation results for the shallow bays. Wave simulations were coupled with the flow model every hour using spatially uniform wind conditions from the same NOAA station and a Collins bottom friction coefficient of 0.1.

Model bathymetry and distributions of bottom sediment size were extracted from Wiberg et al. (2015). Three sediment classes were specified in the model, including a cohesive medium to fine silt fraction with a representative floc settling velocity of 0.75 mm s^{-1}, a cohesive coarse silt fraction with a settling velocity of 3.6 mm s^{-1}, and a non-cohesive sand fraction with a representative median grain size of 125 µm (Wiberg et al., 2015). The Partheniades–Krone formulation was used to calculate cohesive sediment erosion and deposition fluxes in the model (Krone, 1962; Partheniades, 1965). The critical shear stress for cohesive sediment erosion was set to 0.04 N m^{-2} based on in situ measurements in the VCR bays (Lawson et al., 2007; Reidenbach & Timmerman, 2019) and an erosion parameter of 2×10^{-5} kg m^{-2} s^{-1} was selected after model calibration to generate the best agreement between modeled and measured suspended sediment concentration in Hog Bay. For non-cohesive sediment transport, the Van Rijn et al. (2001) approach was used and the settling velocity for the specified sand fraction was internally calculated by the model. Considering that there is no significant fluvial sediment input to the shallow bays (Brinson et al., 1995) and that sediment concentrations at the open ocean boundaries are relatively low (Wiberg et al., 2015), sediment fluxes at the model boundaries of the large model domain were set to zero. Sediment was allowed to flux in and out of the coastal bays through tidal inlets in the model in light of a previous modeling study in the VCR (Castagno et al., 2018) that found that storm events can import sediment to the bays through tidal inlets.

A spatially uniform Chézy bed roughness of 65 $m^{1/2}$ s^{-1} was used in both model domains (Wiberg et al., 2015; Nardin et al., 2018). The threshold depth for drying and flooding and the minimum depth for computing sediment transport were set to 0.1 m (Wiberg et al., 2015), while the active sediment layer thickness was set to 0.05 m, with the erosion rate proportional to the availability of each sediment fraction in the active layer (Deltares, 2014). Composition of the active sediment layer was updated during each simulation time step to account for the dynamics of mixed-size sediments on the seabed; when the active layer was eroded, the underlayer (0.1 m × 10 layers) supplied sediment to the active sediment layer (Wiberg et al., 2015; Zhu et al., 2021). Sediment grain density and dry bed density were set to 2650 kg m^{-3} and 800 kg m^{-3}, respectively, for all sediment classes, which corresponds to a porosity of ~0.7 for all sediment layers regardless of grain size composition (Wiberg et al., 2015; Nardin et al., 2018). The thickness of sediment deposition on the bed was calculated from the total deposited sediment mass by dividing by the dry bed density. For a complete list of parameters used in the sediment transport module, refer to Table 4.1.

Several previous modeling studies in the VCR have shown that depth-averaged Delft3D simulations are able to produce reasonable results for the well-mixed shallow coastal bays in this system (Nardin et al., 2018; Wiberg et al., 2015; Zhu et al., 2021). In this study, the model was implemented using the same depth-averaged approach with a time step of 0.15 min. To incorporate effects of marsh vegetation on flow and wave attenuation, the Baptist vegetation model (Baptist et al., 2007) and the Suzuki vegetation wave energy dissipation model (Suzuki et al., 2012) were implemented in Delft3D flow simulation and in the SWAN model, respectively. These two methods consider vegetation as cylindrical structures and resolve vegetation effects in the momentum balance equation. See Nardin et al. (2018) and Zhu et al. (2021) for further details of the vegetation model and its parameterization in Delft3D. The dominant intertidal salt marsh vegetation in the VCR is *Spartina alterniflora* with an elevation range between mean sea level and mean high water (Sun et al., 2018). Therefore, model grid cells that are between 0–1 m above mean sea level were identified as marsh cells in both model domains and the effects of emergent marsh vegetation on flow and waves were implemented in these cells during model simulations. Spatially uniform marsh characteristics that are representative of our study site (vegetation height = 1.0 m, stem diameter = 0.5 cm, and density = 400 shoots m^{-2}) were used in the model (Christiansen et al., 2000; Nardin et al., 2018; Sun et al., 2018).

Table 4.1 Parameters used in the sediment transport module

Parameter	Value	Reference
Distributions of bottom sediment size	Maps of three sediment classes: a cohesive medium to fine silt fraction, a cohesive coarse silt fraction, and a non-cohesive sand fraction (125 μm)	Wiberg et al. (2015)
Boundary conditions for sediment input	No external sediment input for the large model domain; boundary conditions of the small model domain provided by the large model domain	Brinson et al. (1995); Wiberg et al. (2015)
Chézy bed roughness	65 $m^{1/2}$ s^{-1}	Wiberg et al. (2015); Nardin et al. (2018)
Threshold depth for drying and flooding	0.1 m	Wiberg et al. (2015)
Minimum depth for computing sediment transport	0.1 m	Wiberg et al. (2015)
Critical shear stress for cohesive sediment erosion	0.04 N m^{-2}	Lawson et al. (2007); Reidenbach & Timmerman (2019)
Erosion parameter for cohesive sediment erosion	2×10^{-5} kg m^{-2} s^{-1}	Selected for this study after model calibration
Settling velocity for cohesive sediment	0.75 mm s^{-1} (medium to fine silt fraction) and 3.6 mm s^{-1} (coarse silt fraction)	Wiberg et al. (2015)
Active sediment layer thickness	0.05 m	Wiberg et al. (2015); Zhu et al. (2021)
Sediment grain density and dry bed density	2650 kg m^{-3} and 800 kg m^{-3}	Wiberg et al. (2015); Nardin et al. (2018)
Sediment underlayers	0.1 m × 10 layers	Wiberg et al. (2015)

Multiple datasets (Fagherazzi & Mariotti, 2009a, 2009b; Lawson & Wiberg, 2006; Wiberg, 2017; Table 4.2), including time series measurements of water depth, velocity, significant wave height (Hs), and total SSC, have been collected at various locations in Hog Bay (Figure 4.2a) under different storm surge conditions. These spatially distributed hydrodynamic and suspended sediment datasets offer a unique opportunity to validate our model and quantify the effects of storm surge on the coupled tidal flat–marsh system at our study site. Therefore, we ran the model for four different time periods (January 1–21, 2003, January 28–February 06, 2009, February 26–March 05, 2009, and June 26–July 23, 2017) that coincided with the observation periods of the validation datasets (Table 4.2). During the first two simulation periods (03VAL and 09VAL), model runs were forced with hourly measured water levels and winds, and the simulation results were mainly used for flow, wave height, and SSC validation. Model runs during February 26–March 05, 2009 (09TIDE, 09MEA, 09TIDEW, and 09MEAW) were used to quantify the effects of a major storm surge event driven by northeasterly winds (Figure 4.4a, 4.4b) on marsh sediment deposition under different forcing scenarios (with/without storm surge and wind waves). During the last simulation period in June 26–July 23, 2017, the study site was dominated by strong southerly winds that did not result in significant storm surge (Figure 4.5a, 4.5b); therefore, simulation results during this period (17TIDE, 17MEA, 17TIDEW, and 17MEAW) were used for comparison with the results under strong storm surge conditions in 2009.

Table 4.2 Model run settings and validation datasets

Period	Model run	Water level forcing	Wind wave	Validation datasets
January 1–21, 2003	03VAL	Total measured water level	Yes	(Lawson & Wiberg, 2006)
January 28–February 06, 2009	09VAL	Total measured water level	Yes	(Fagherazzi & Mariotti, 2009a, 2009b)
February 26–March 05, 2009	09TIDE	Astronomical tide only	No	-
	09MEA	Total measured water level	No	-
	09TIDEW	Astronomical tide only	Yes	-
	09MEAW	Total measured water level	Yes	(Fagherazzi & Mariotti, 2009a, 2009b)
June 26–July 23, 2017	17TIDE	Astronomical tide only	No	-
	17MEA	Total measured water level	No	-
	17TIDEW	Astronomical tide only	Yes	-
	17MEAW	Total measured water level	Yes	(Wiberg, 2017)
August 1–31, 2009	09REF	Total measured water level	Yes	-

Owing to computational limitations, we did not run the spatially resolved model for a complete annual cycle to estimate annual marsh deposition rates. Instead, a reference simulation run 09REF (Table 4.2, Figure A3.2) spanning a 30-day period with minor storm surge and including wind wave coupling was carried out to estimate monthly marsh deposition in a marsh where independent measurements of marsh deposition rates were available (Table A3.2); annual deposition rates were calculated by multiplying the predicted monthly deposition by a factor of 12. The resulting estimate of annual marsh deposition associated with regular tidal flooding (no storms) was compared with measured long-term marsh accretion rates determined at the same site and with estimates of storm-surge-related marsh deposition (for detailed comparison results, refer to Section 3.2 and 4.2).

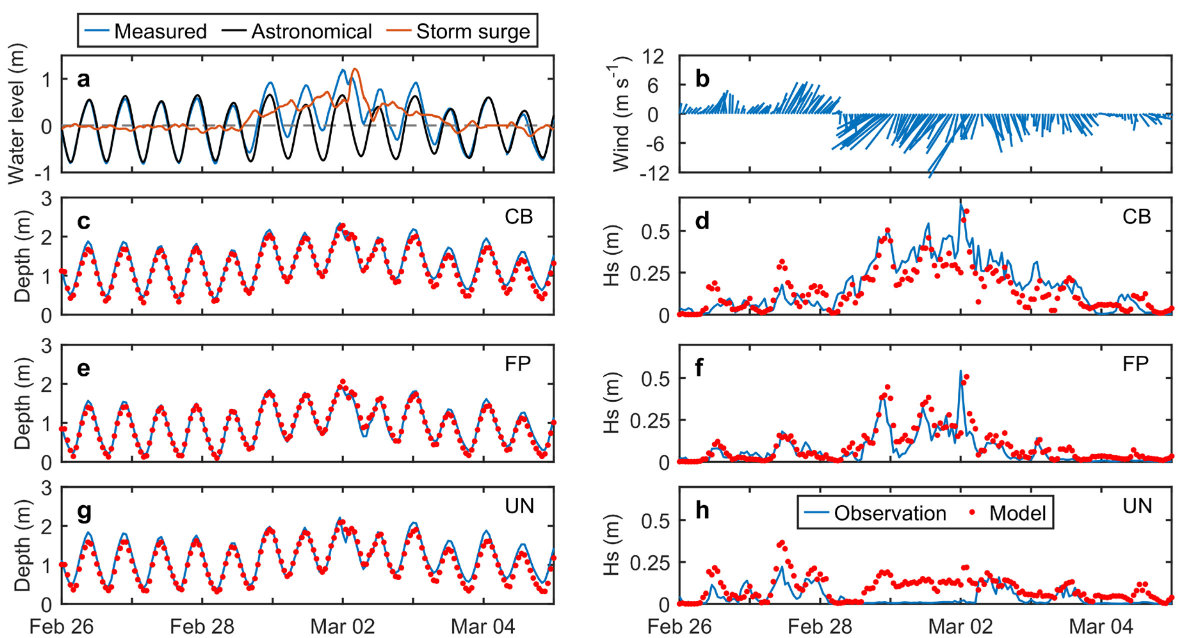

Figure 4.4 Comparison of measured and modeled hydrodynamic conditions output from 09MEAW during February 26–March 05, 2009: (a) measured water levels, astronomical tides, and calculated storm surge (non-tidal residual) at WA, (b) wind speed and direction at Wachapreague, (c) water depth at CB, (d) Hs at CB, (e) water depth at FP, (f) Hs at FP, (g) water depth at UN, and (h) Hs at UN. Lines in (b) point in the direction that the wind is blowing toward. Blue lines in (c)–(h) represent observational data, and red dots show model simulation results.

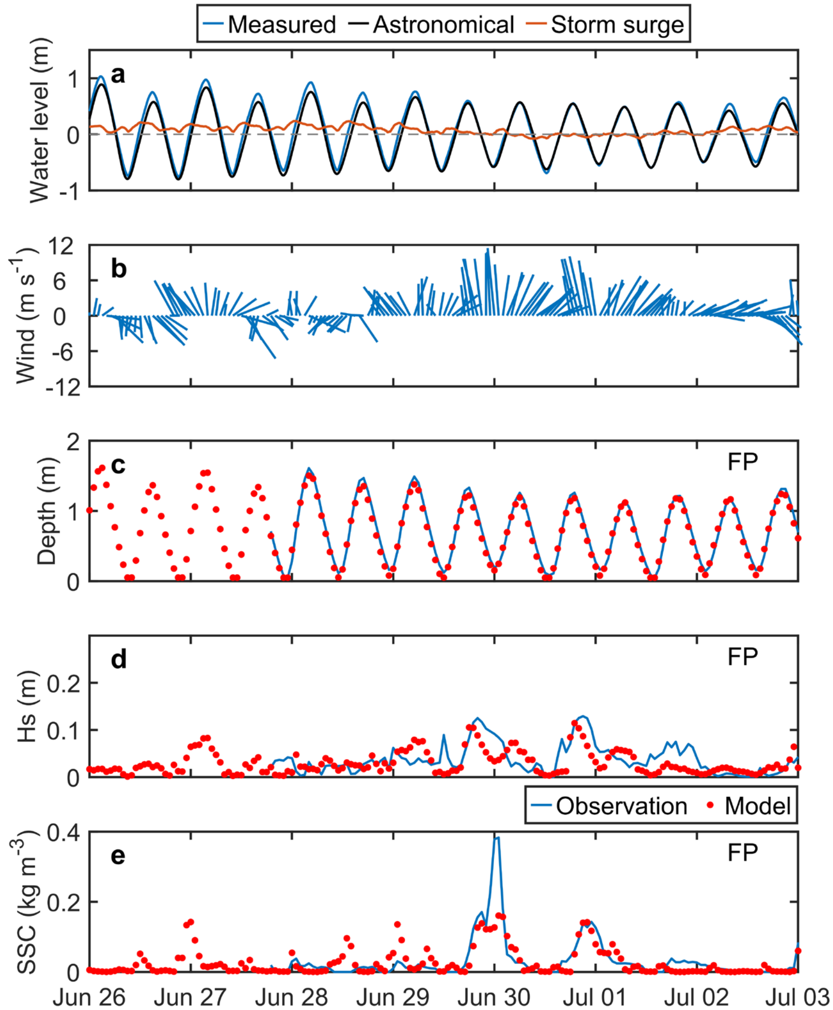

Figure 4.5 Comparison of measured and modeled hydrodynamic conditions output from 17MEAW during June 26–July 23, 2017: (a) measured water levels, astronomical tides, and calculated storm surge (non-tidal residual) at WA, (b) wind speed and direction at Wachapreague, (c) water depth, (d) Hs, and (e) total SSC at FP. Lines in (b) point in the direction that the wind is blowing toward. Blue lines in (c)–(e) represent observational data, and red dots show model simulation results.

4.2.4 Model skill indices and analysis

The output from each validation model run (03VAL, 09VAL, 09MEAW, and 17MEAW) was compared to measured water depth, velocity, significant wave height, and total SSC at validation sites. In order to quantify model ability to characterize hydrodynamic and suspended sediment characteristics in Hog Bay, model skill indices including bias, Root Mean Square Error (RMSE), and Willmott Skill Index were calculated for model validation parameters during each simulation period (Table 4.3). The skill index proposed by Willmott (1981) is defined as

$$Skill = 1 - \frac{\sum |X_{model} - X_{obs}|^2}{\sum(|X_{model} - \overline{X_{obs}}| + |X_{obs} - \overline{X_{obs}}|)^2} \tag{1}$$

where X_{model} and X_{obs} is the model simulated variables and observations, respectively, and $\overline{X_{obs}}$ is the time average of observations. A skill of one indicates perfect model predictions, while a skill of zero shows no correlation between model results and observations. In coastal hydrodynamic simulations, model skill scores for water depth and velocity are usually higher than those for wave height and SSC due to larger uncertainties in predicting the latter two variables. A skill score of 0.8 is generally good for water level and velocity predictions, while a skill score of 0.7 indicates reasonable model simulations for wave height and SSC (Liu et al., 2009; Warner et al., 2005; Zhu et al., 2021).

Model predicted variables including water depth, significant wave height, total suspended sediment concentration (summing the SSC of each sediment fraction), and total mass of marsh deposition were output from model runs under strong storm surge conditions in 2009 (09TIDE, 09MEA, 09TIDEW, and 09MEAW) and minor storm surge conditions in 2017 (17TIDE, 17MEA, 17TIDEW, and 17MEAW) for comparison. Total depositional area on the marsh around Hog Bay was determined by multiplying the number of depositional marsh grid cells in each model run by the area of the refined model grid cell (50 m × 50 m). In order to quantify the effects of varying storm surge conditions on bay erosive processes, the ratio between the time duration when the modeled maximum bed shear stress (τ_m) exceeded the critical shear stress (τ_{cr}) and the total simulation period (hereafter referred to as "seabed erosion time fraction") was calculated for each model run. In addition, four marsh polygons (FP, HI, CP, and UN) were constructed in the refined model domain to monitor total sediment fluxes into and out of the surrounding marshes (Fowling Point, Hog Island, Chimney Pole, and Upshur Neck) in Hog Bay (Figure 4.2a) and these sediment fluxes were then normalized by the area of marsh polygon for further comparison. Our simulation results show that total sediment fluxes into the marshes were dominated by suspended sediment which mainly consisted of the medium to fine silt fraction (contributing to > 80% of total sediment flux variations). Therefore, we did not attempt to further separate the contribution of each sediment fraction to marsh deposition but only show the results of total sediment flux of all sediment fractions in the following text. For the simulated events, a sediment budget of the coupled tidal flat–marsh system was constructed by calculating total sediment fluxes to marshes and into/out of the bay through tidal inlets (ITN and ITS) over the entire simulation period.

Table 4.3 A summary of statistical metrics for model validation

Model run	Site	Parameter	Statistics		
			Bias	RMSE	Skill
03VAL	HI	Depth	0.00 m	0.03 m	1.00
		East velocity	0.01 m s^{-1}	0.04 m s^{-1}	0.94
		North velocity	0.02 m s^{-1}	0.08 m s^{-1}	0.97
		SSC	0.01 kg m^{-3}	0.02 kg m^{-3}	0.69
09VAL	CB	Hs	0.04 m	0.06 m	0.83
	FP	Hs	0.04 m	0.05 m	0.43
	HI	Hs	-0.03 m	0.07 m	0.88
	CP	Hs	0.00 m	0.05 m	0.87
	UN	Hs	0.03 m	0.06 m	0.74
09MEAW	CB	Depth	-0.09 m	0.09 m	0.98
	FP	Depth	-0.02 m	0.10 m	0.99
	UN	Depth	-0.10 m	0.12 m	0.97
	CB	Hs	-0.03 m	0.07 m	0.89
	FP	Hs	0.02 m	0.06 m	0.87
	UN	Hs	0.06 m	0.06 m	0.61
17MEAW	FP	Depth	-0.05 m	0.06 m	0.99
	FP	Hs	-0.01 m	0.02 m	0.72
	FP	SSC	0.00 kg m^{-3}	0.03 kg m^{-3}	0.83

4.3 Results

4.3.1 Characteristics of storm surge events during 2008–2020

The directional distribution of winds during identified storm surge events revealed that most storm surge events (> 90%) in the VCR were associated with along-coast winds blowing from northeast (Figure A3.3; Fagherazzi et al., 2010). The total period of the identified storm surge events was 4626 hr, which roughly accounted for 5% of total time in our analysis from August 2008 to December 2020 (Table A3.1). The occurrence probability of storm surge events decreased rapidly as storm surge intensity increased (Figure 4.6a), with a median cumulative storm surge intensity of 12.5 m hr (comparable to the storm surge event recorded in 2009; model run 09MEAW). There were only two storm surge events with a cumulative storm surge intensity > 60 m hr: the Mid-Atlantic nor'easter in November 2009 (also referred to as "Nor'Ida Storm") and Hurricane Joaquin in October 2015 (Table A3.1).

Regression analysis revealed that cumulative storm surge intensity was moderately well correlated with storm surge duration (R^2 = 0.61; Figure 4.6b) and peak storm surge intensity (R^2 = 0.54; Figure 4.6c), indicating that both the duration of storm surge and storm-driven high water level play an important role in controlling cumulative storm surge intensity. Although strong winds are important drivers for storm surge events in shallow coastal bays, our analysis shows that cumulative storm surge intensity was weakly correlated with wind speed metrics (Figure 4.6d), likely owing to strong variability of wind conditions during storm surge events.

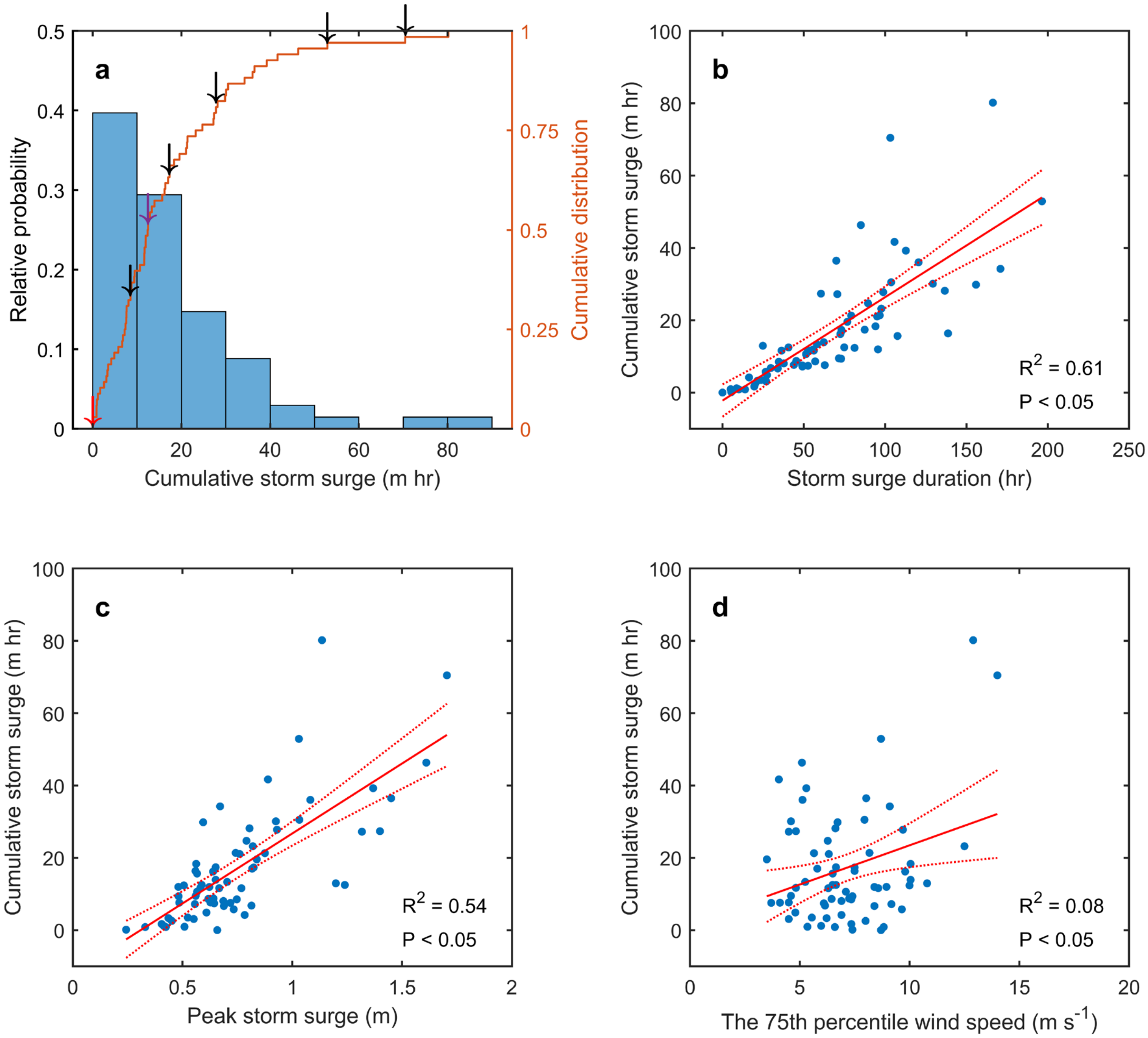

Figure 4.6 Characteristics of storm surge events in the VCR during 2008–2020: (a) probability distribution of cumulative storm surge intensity, (b) relationship between cumulative storm surge intensity and storm surge duration, (c) relationship between cumulative storm surge intensity and peak storm surge, and (d) relationship between cumulative storm surge intensity and the 75th percentile wind speed. Arrows in (a) indicate the magnitude of cumulative storm surge intensity of the simulated storm surge events in Figure 4.12, with red and purple arrows corresponding to model runs 17MEAW and 09MEAW, respectively.

4.3.2 Model validation

Generally good agreement between our model results and field measurements of water levels, currents, waves and total SSC was obtained under varying forcing and storm surge conditions in model validation runs (Table 4.3). During the first simulation period in 2003 (model run 03VAL), the modeled water depth and velocity at HI were in excellent agreement with measurements (Figure A3.4), with skill scores ≥ 0.94. The model also successfully captured most sediment resuspension events at HI (Figure A3.4e), producing a good skill score of 0.69.

Simulation results during the second model period in 2009 (model run 09VAL) were mainly used for wave height validation (Figure A3.5) and the model was able to reproduce wave patterns at 4 of the 5 validation sites with good skill scores (≥ 0.74; Table 4.3). The model overpredicted the relatively small wave height at FP during the simulation period (Figure A3.5c). Either spatially variable wind conditions near the bay–marsh boundary or local wave attenuation due to shoaling near FP could be responsible for the disagreement between model results and measurements.

During the storm surge event in 2009 (model run 09MEAW), good agreement of water depth between model results and measurements was obtained at CB, FP, and UN with high skill scores ≥ 0.97 (Figure 4.4). Wave height skill scores were generally higher at CB and FP (0.89 and 0.87) than that at UN (0.61). The overestimation of wave height at UN (Figure 4.4h) was likely caused by spatially variable wind patterns and fetch associated with marsh orientation.

Predicted water depth and wave height at FP were in good agreement with measurements (skill scores for water depth = 0.99 and wave height = 0.72) during the last simulation period in 2017 when there was no significant storm surge (model run 17MEAW; Figure 4.5). The model can reproduce most sediment resuspension events during this period with an SSC skill score of 0.83, but underestimated the SSC peak on June 30, 2017 (Figure 4.5e). This discrepancy was mainly due to very shallow water depths (< 0.15 m) at low tides at this site. Considering that the minimum water depth for computing sediment transport in the model was set to 0.1 m, the ability of the model to reproduce such a high SSC peak is limited when water depth on the tidal flats is very limited.

In addition to model validation of hydrodynamic simulations, the estimated annual marsh deposition due to regular tidal flooding (4.8 mm yr^{-1}) at a site 150 m from the marsh edge in FP marsh output from model run 09REF was in good agreement with the average long-term marsh accretion rate at the same site (4.0 mm yr^{-1}; Table A3.2) determined by surface elevation tables (SETs) and ^{137}Ce dating. Overall, given the generally good validation results at multiple validation sites obtained by our model, we believe that it is able to produce reasonable simulations of hydrodynamics and sediment transport in our study system.

4.3.3 Effects of storm surge on bay erosive processes

Comparisons of modeled significant wave height (Hs) distributions (Figure A3.6) near 4 bay–marsh boundary locations during northeasterly (09) and southerly (17) wind events, with astronomical tides only (TIDEW) and with measured tides (including storm surge; MEAW), highlight the importance of marsh boundary orientation relative to wind direction on wave patterns. The east (FP) and west (HI) facing marshes experienced high waves during the northeasterly wind event while southwestward facing marsh boundaries at CP and UN experienced low waves owing to sheltering from northeasterly winds (Figure A3.6). Wave conditions at the 4 sites were more comparable during the southerly wind event. Considering the dominant role of northeasterly winds in driving storm surge events in the VCR (Figure A3.3), northeastward facing marsh boundaries in the bay will likely receive stronger wave impacts associated with storm surge than those marsh boundaries in the northern portion of the bay.

High seabed erosion time fraction (> 0.8) was found in deep channels and near tidal inlets when the model was forced with measured tides only in model run 09MEA (no waves; Figure 4.7a), indicating strong flow velocity in these areas. In contrast, seabed erosion time fraction over the shallow tidal flats near marsh boundaries was relatively small (< 0.2). The difference between model runs 09MEA and 09TIDE (Figure 4.7b) shows that storm surge resulted in ~10% reductions in seabed erosion time fraction in most of the bay when the model was driven by tidal forcing only (no wind wave effects). This is because storm-driven high water levels in model run 09MEA resulted in a decrease in depth-averaged velocity in the bay, thereby leading to a smaller bed shear stress (proportional to the square of depth-averaged velocity in the model when driven by tidal current alone) compared with values from the model run forced with astronomical tides (09TIDE).

When wind wave effects were included in model simulations, seabed erosion time fraction significantly increased to > 0.8 in most of the bay (Figure 4.7c, 4.7e), consistent with previous modeling studies indicating the dominant role of wind-generated waves in driving high bed shear stress and sediment resuspension in the shallow bays of the VCR (Lawson et al., 2007; Mariotti et al., 2010). Despite small changes in Hs induced by storm surge (Figure A3.6), storm-driven water level variations resulted in strong spatial variability in bay erosive processes. The difference of seabed erosion time fraction between model runs 09MEAW and 09TIDEW (Figure 4.7d) demonstrates that storm-driven high water levels caused by northeasterly winds can increase the erosion time of most northeastward facing shallow tidal flats and marsh edges by

~10%, while decreasing the erosion time of southwestward facing tidal flats by about the same amount, particularly near the bay–marsh boundary at UN. Similarly, northeasterly winds together with significant storm surge in model run 09MEAW resulted in notably higher erosion time in the northeastward facing areas within the bay than the results associated with southerly winds and minor storm surge in model run 17MEAW (Figure 4.7f). For the southwestward facing bay–marsh boundaries, seabed erosion time fraction was 10% lower in model run 09MEAW than that in 17MEAW due to a smaller wind fetch of northeasterly winds in this region. Given the dominant role of northeasterly winds in driving significant storm surge in our study area, storm surge events will increase tidal flat erosion of most northeastward facing areas in the bay and potentially enhance sediment delivery to nearby marshes.

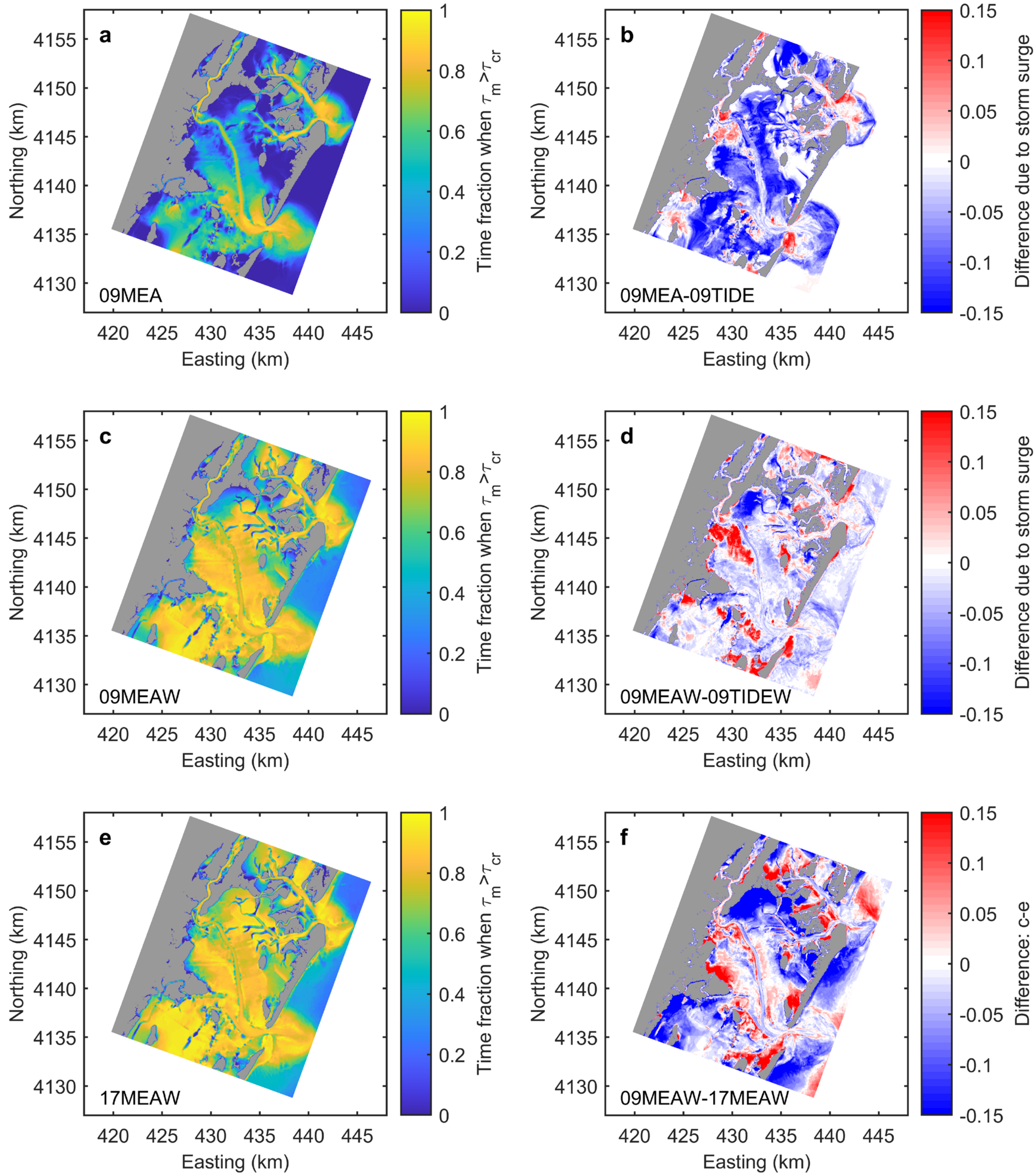

Figure 4.7 Distributions of erosion time fraction when $\tau_m > \tau_{cr}$ in the bay output from different model run: (a) 09MEA, (c) 09MEAW, and (e) 17MEAW and the difference of erosion time fraction between model runs: (b) 09MEA−09TIDE, (d) 09MEAW−09TIDEW, and (f) 09MEAW−17MEAW. Gray shading indicates the land areas.

4.3.4 Effects of storm surge on sediment delivery to marshes

Distributions of total depth-averaged SSC during peak storm conditions from model runs 09TIDEW and 09MEAW demonstrate that storm surge had a limited effect on the magnitudes and spatial patterns of SSC in the bay (Figure 4.8a, 4.8b). Maximum SSC was similar in both model runs (~0.35 kg m^{-3}), although there were more areas with high SSC over shallow tidal flats near the northeastward facing bay–marsh boundary at FP in model run 09MEAW than those in 09TIDEW. This is consistent with the increased erosion potential in this region predicted by the model (Figure 4.7d). In contrast, there was no significant difference in peak storm distributions of depth-averaged SSC between model runs 17TIDEW and 17MEAW. In both cases, high SSC was mainly found in the northern bay where the large fetch of southerly winds promoted higher waves and sediment resuspension (Figure 4.8c, 4.8d). Despite differences in SSC on the tidal flats, there was no significant difference in distributions of depth-averaged SSC at bay–marsh boundaries (FP, HI, CP, and UN) between model runs with/without storm surge effects in 2009 (Figure A3.7).

Although SSC at bay–marsh boundaries was similar in model runs with/without storm surge, sediment fluxes to marshes were notably higher when storm surge effects were included in model simulations. Comparison of marsh sediment flux between model runs 09TIDEW and 09MEAW shows that storm surge associated with northeasterly winds in 2009 was able to double sediment flux to most marshes (Figure 4.9a). In contrast, sediment flux to marshes was similar in model runs 17TIDEW and 17MEAW when there was minor storm surge associated with southerly winds in 2017, despite the occurrence of wave-generated resuspension (Figure 4.9b). Moreover, FP and HI marshes received more sediment input from the bay in model run 09MEAW than in 09TIDEW, 17TIDEW, and 17MEAW (Figure 4.9a, 4.9b), indicating that storm surge associated with northeasterly winds was able to promote sediment delivery to marshes oriented/partially oriented in the direction of surge-producing storm winds at our study site. Our simulation results illustrate that wave-induced sediment resuspension was required to significantly elevate marsh sediment input (Figure 4.9a, 4.9b) and most sediment was transported to the marsh (> 90%) during a short time period when strong wind waves coincided with storm-driven high water levels (Figure 4.9c, 4.9d). The only marsh site where wind waves were less important was CP marsh; tides contributed > 50% of sediment fluxes to this marsh (Figure 4.9a, 4.9b). This is because CP marsh is surrounded by two tidal channels (Figure 4.2a) that regulated sediment delivery to this marsh.

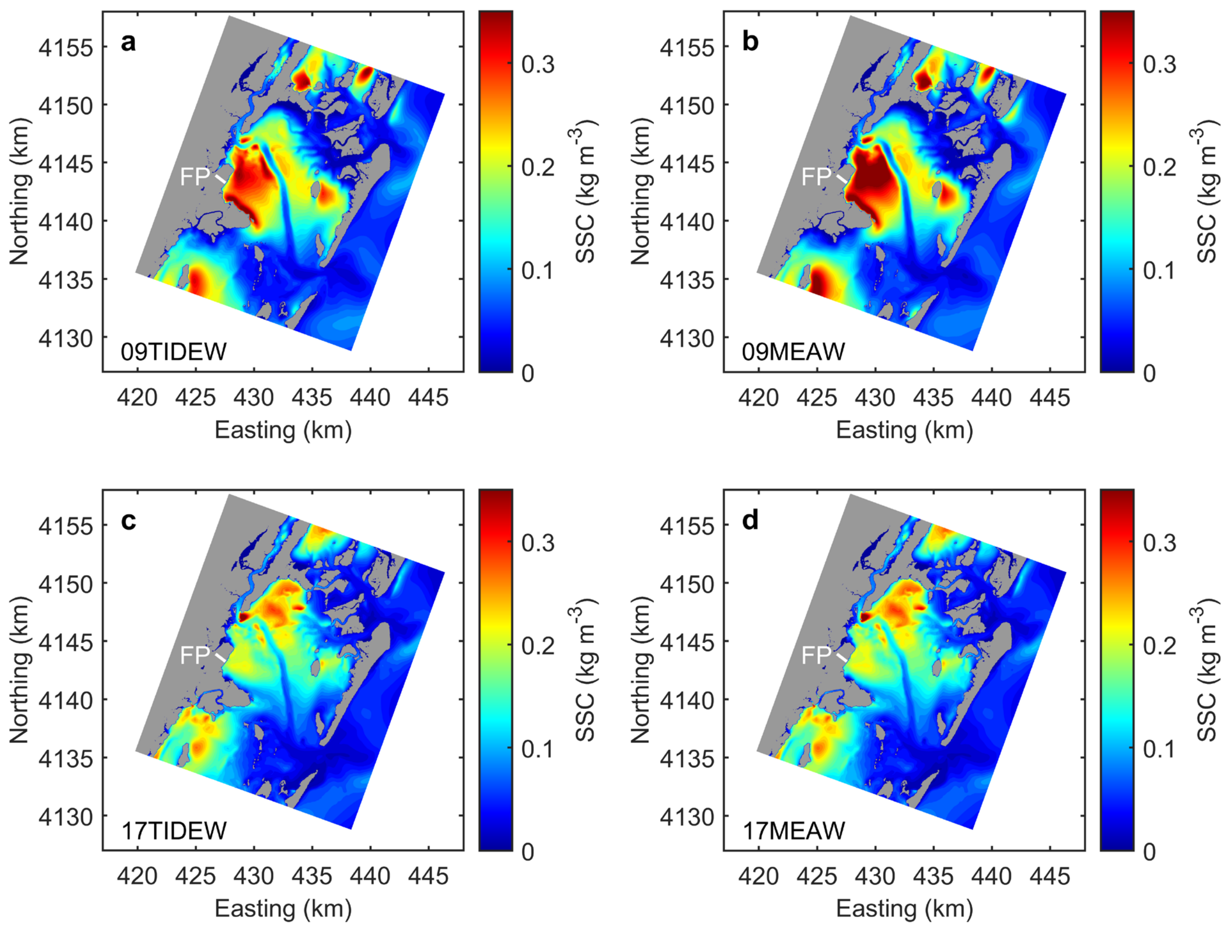

Figure 4.8 Spatial distributions of depth-averaged SSC during peak storm output from: (a) 09TIDEW, (b) 09MEAW, (c) 17TIDEW, and (d) 17MEAW. Model runs 09TIDEW/09MEAW are forced with astronomical/measured tides and northeasterly winds in 2009, while 17TIDEW/17MEAW are forced with astronomical/measured tides and southerly winds in 2017. Gray shading indicates the land areas.

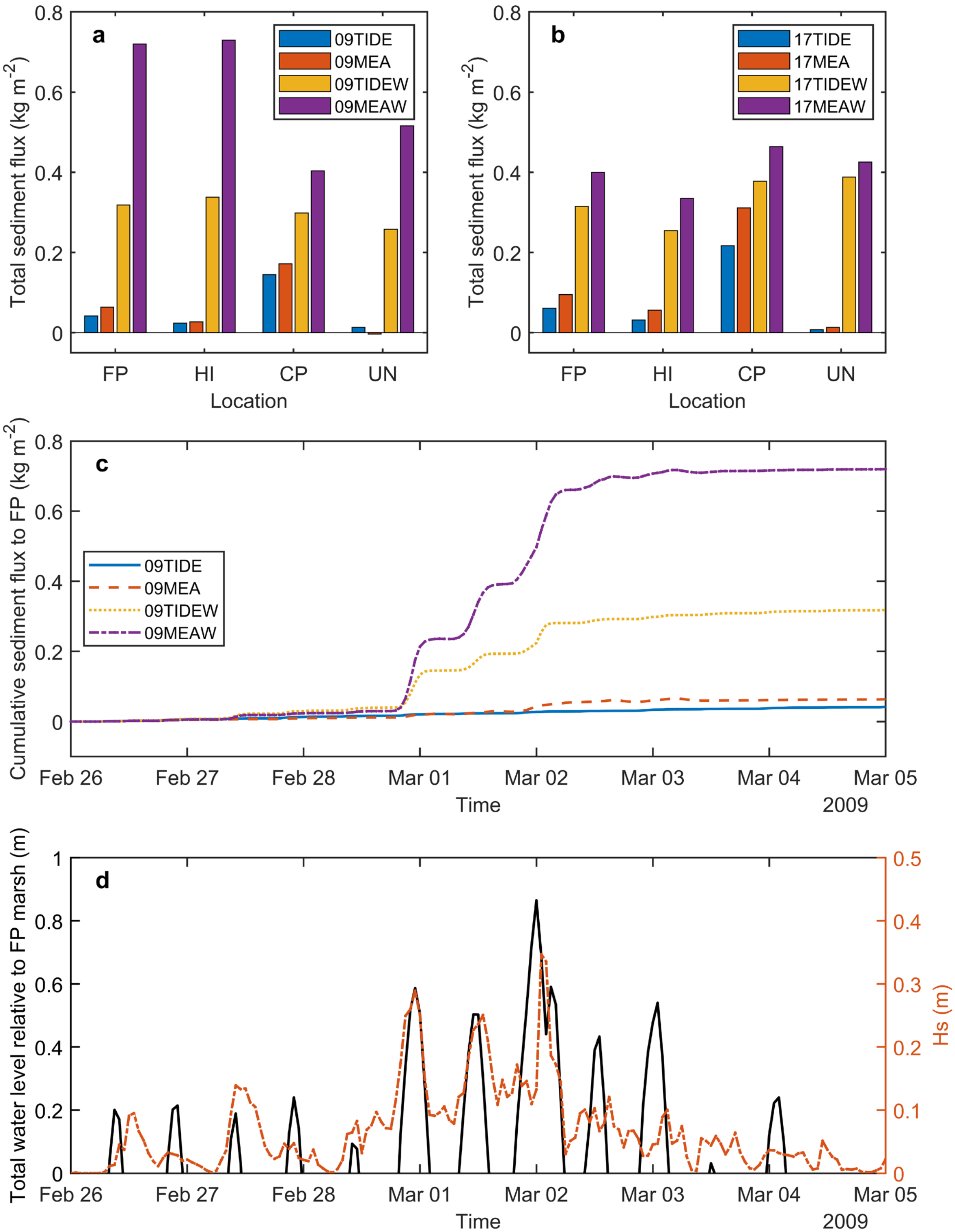

Figure 4.9 (a) Total normalized sediment flux into FP, HI, CP and UN marshes during the storm surge event driven by northeasterly winds in 2009 output from model runs 09TIDE, 09MEA, 09TIDEW, and 09MEAW. (b) Total normalized sediment flux into FP, HI, CP and UN marshes during the strong southerly wind event in 2017 (minor storm surge conditions) output from

model runs 17TIDE, 17MEA, 17TIDEW, and 17MEAW. (c) Time series of cumulative sediment flux into FP marsh during the storm surge event driven by northeasterly winds in 2009. (d) Time series of modeled water level relative to FP marsh (left axis) and significant wave height (Hs) at the model validation site near FP marsh (right axis) output from model run 09MEAW. Model runs labeled with TIDE/MEA are forced with astronomical/measured tides only, while model runs labeled with TIDEW/MEAW are forced with astronomical/measured tides and wind waves. Locations of model monitoring polygons are shown in Figure 4.2. For detailed model run settings, refer to Table 4.2.

4.3.5 Enhanced marsh deposition by storm surge

Hourly modeled water depth, depth-averaged velocity, depth-averaged SSC, and total sediment deposition along a marsh transect in FP (see transect location in Figure 4.8) were output from model runs 09TIDEW and 09MEAW to examine the effects of storm surge on marsh sediment transport during the storm surge event in 2009 (Figure 4.10). The results show that storm surge (09MEAW) increased the average marsh sediment deposition over the transect by 4 times compared with that associated with astronomical tides and wind waves (09TIDEW), mainly by increasing inundation depth and depositional area on the marsh during high tides. Storm surge increased the maximum inundation depth on the marsh from 0.2 m to 0.6 m and the water was able to further penetrate into the marsh interior (> 500 m from the marsh edge; Figure 4.10a vs. 4.10b). Due to flow attenuation caused by marsh vegetation (Figure 4.10c, 4.10d), depth-averaged SSC on the marsh decreased rapidly with distance into the marsh interior until the advective sediment source was depleted (Figure 4.10e, 4.10f). Although the maximum SSC at the marsh edge was similar in both simulations, more suspended sediment was transported onto the marsh platform during high tides with storm surge (09MEAW) than without storm surge (09TIDEW) (Figure 4.10e, 4.10f). As a result, the model run including both wind waves and storm surge predicted much higher sediment deposition on the marsh than model runs without storm surge effects or wind wave coupling (Figure 4.10g).

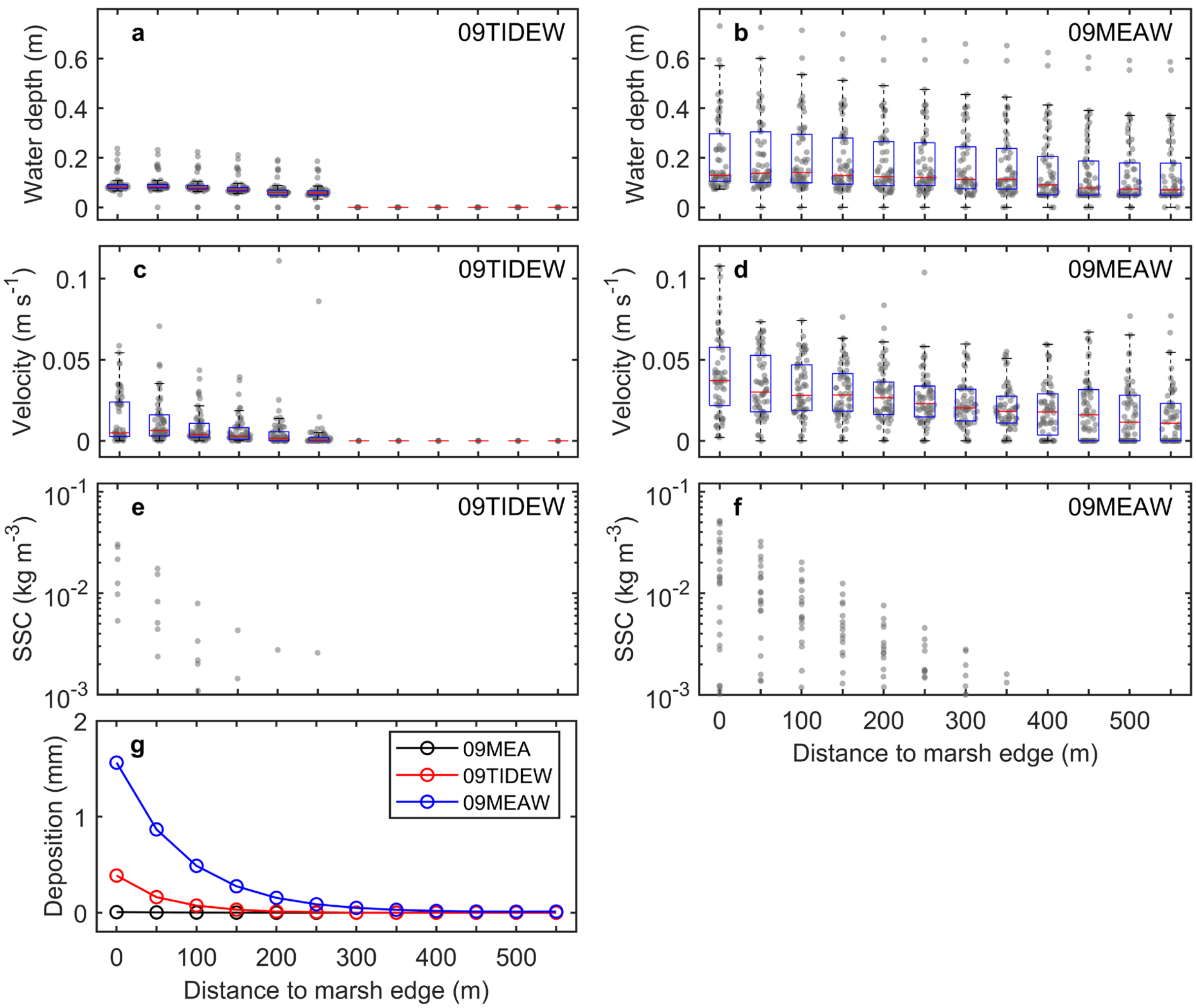

Figure 4.10 Box plots of hourly modeled hydrodynamic conditions when the marsh platform is inundated during high tides along the marsh transect at FP during the simulated storm surge event (7-day period) in 2009: (a) and (b) water depth, (c) and (d) depth-averaged velocity, (e) and (f) total depth-averaged SSC output from model runs 09TIDEW and 09MEAW, respectively. (g) Total marsh sediment deposition along the marsh transect at FP output from model runs 09MEA, 09TIDEW, and 09MEAW after the 7-day model simulation period. For better visualization, SSC in (e) and (f) is shown in logarithmic scale. Model run 09MEA is forced with measured tides only, while runs 09TIDEW/09MEAW are forced with astronomical/measured tides and wind waves. The location of marsh transect is shown in Figure 4.8.

At a larger spatial scale, marsh sediment depositional patterns output from model runs 09TIDEW and 09MEAW further confirm the importance of storm surge for enhancing marsh deposition (Figure 4.11). Pronounced sediment accumulation (> 1.0 mm) at marsh edges, which decreased rapidly with distance into the marsh interior, was found in model runs with and without storm surge, but the model simulation with storm surge had much greater vertical deposition and delivered much more sediment to the marsh interior (Figure 4.11). Accordingly, marsh depositional area and total sediment depositional mass in model run 09MEAW were 1.8 ($51\ km^2/29\ km^2$) and 1.6 times (5.7×10^4 MT/3.6×10^4 MT) as high, respectively, as those in model run 09TIDEW (Table 4.4). In contrast, these two values were similar in model runs 17TIDEW and 17MEAW when there was no significant storm surge during model simulation periods.

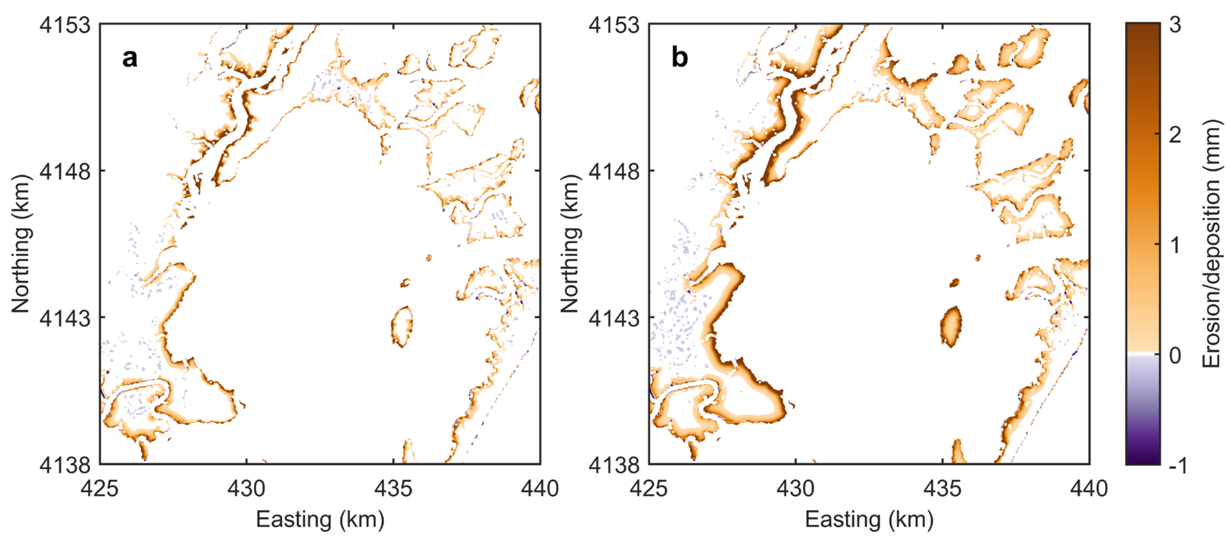

Figure 4.11 Marsh sediment depositional pattern throughout Hog Bay during the storm surge event driven by northeasterly winds in 2009 output from model runs (a) 09TIDEW (without storm surge effects) and (b) 09MEAW (with storm surge effects).

Table 4.4 Calculated depositional area and total sediment depositional mass on marshes bordering Hog Bay

Model runs	Depositional area (km^2)	Deposition ($\times 10^4$ MT)
09TIDEW	29	3.6
09MEAW	51	5.7
17TIDEW	34	3.3
17MEAW	40	3.9

MT: metric ton

4.4 Discussion

4.4.1 The role of storm surge intensity in supplying sediment to bay–marsh complexes

Our process-based model simulations show that the storm surge event in 2009 significantly increased both suspended sediment flux to marshes and marsh deposition (Figure 4.9–4.11) compared to simulations with the same winds but no storm surge. It is still unclear, however, how sediment deposition on marshes varies in response to different storm surge intensities. To better understand their relationship, we simulated bay and marsh response to five additional storm surge events with varying magnitude of cumulative storm surge intensity (Figure 4.6a, Table A3.3), selected from our storm surge event catalog. Results of these model runs together with those from model runs 09MEAW and 17MEAW reveal that total marsh deposition around the bay and depositional area on the marsh increased linearly with storm surge intensity (Figure 4.12a, A3.8), with the strongest storm surge event producing seven times the marsh deposition associated with minor storm surge conditions in model run 17MEAW. This strong correlation between marsh deposition and storm surge intensity is similar to the findings in Schuerch et al. (2013). They applied a zero-dimensional point model that included effects of mineral and organic sedimentation and autocompaction in a marsh in the southeastern North Sea and found that marsh accretion rates increased linearly with mean storm strength. It is worth noting, however, that increase in storm frequency resulted in higher marsh accretion rates at their study site than increase in storm strength (3 mm yr^{-1} vs. 1 mm yr^{-1}) and that the relative importance of storm frequency and storm strength for marsh accretion strongly depended on sediment supply from the nearby tidal flats.

Most marsh areas in our study area are fronted by tidal flats, but our model also resolves the larger tidal channels cutting through the marshes. Our simulation results show that storm surge events had a different impact on enhancing sediment deposition for marsh areas adjacent to tidal flats versus adjacent to tidal channels. Total normalized sediment fluxes into FP, HI, CP, and UN marshes all increased linearly as a function of cumulative storm surge intensity, but the increase of sediment flux into CP marsh, which is bordered by two tidal channels, was much smaller than the increase of fluxes into the other three marshes (Figure A3.9). Due to strong control of tidal channels on flow at CP marsh, tides were more important at this site and contributed > 50% of sediment fluxes to the marsh (Figure 4.9a, 4.9b). A previous study regarding the effects of waves and tidal channel hydrodynamics in a tidal channel-dominated marsh in Louisiana suggested that high ebb velocities in tidal channels during intense storm surge events can lead to net export of sediment (Fagherazzi & Priestas, 2010), which may explain the modest increase of sediment flux into CP marsh in response to increased storm surge intensity. Given that our study site is dominated by bay-fronted marshes and that the overall pattern of sediment fluxes into FP, HI, and UN marshes was similar to the integrated marsh sediment flux in the bay (Figure 4.12a, A3.9), we did not attempt to further separate the contributions of marshes adjacent to tidal channels from our integrated analysis and focus on the overall sediment budgets in the bay in the following discussion.

The linear relationship between marsh deposition and storm surge intensity has significant implications for predicting marsh deposition associated with storm surge. Cumulative storm surge intensity is a simple parameter that can be directly determined from time series of astronomical tides, measured water levels, and wind conditions (Figure 4.3). The result can be used to develop a local relationship between cumulative storm surge intensity and marsh deposition at sites where an operational hydrodynamic model has been established for predicting marsh deposition, like our modeling approach, or historical marsh deposition has been characterized for a few storm surge events, like the documented marsh deposition associated with hurricane-induced storm surge in coastal marshes in Louisiana (Tweel & Turner, 2014; Williams & Flanagan, 2009). In addition to understanding the role of historical storm surge events on marsh deposition, such a relationship allows for exploration of impacts of a change in the frequency and magnitude of storm surge events in the future. For study sites where cumulative storm surge intensity is difficult to determine due to incomplete tidal records of both astronomical and measured tides, our regression analysis of the characteristics of storm surge events indicates that the duration of storm surge events or peak storm surge would be a useful alternative indicator for storm surge intensity due to their strong linear correlation with cumulative storm surge intensity (Figure 4.6b, 4.6c).

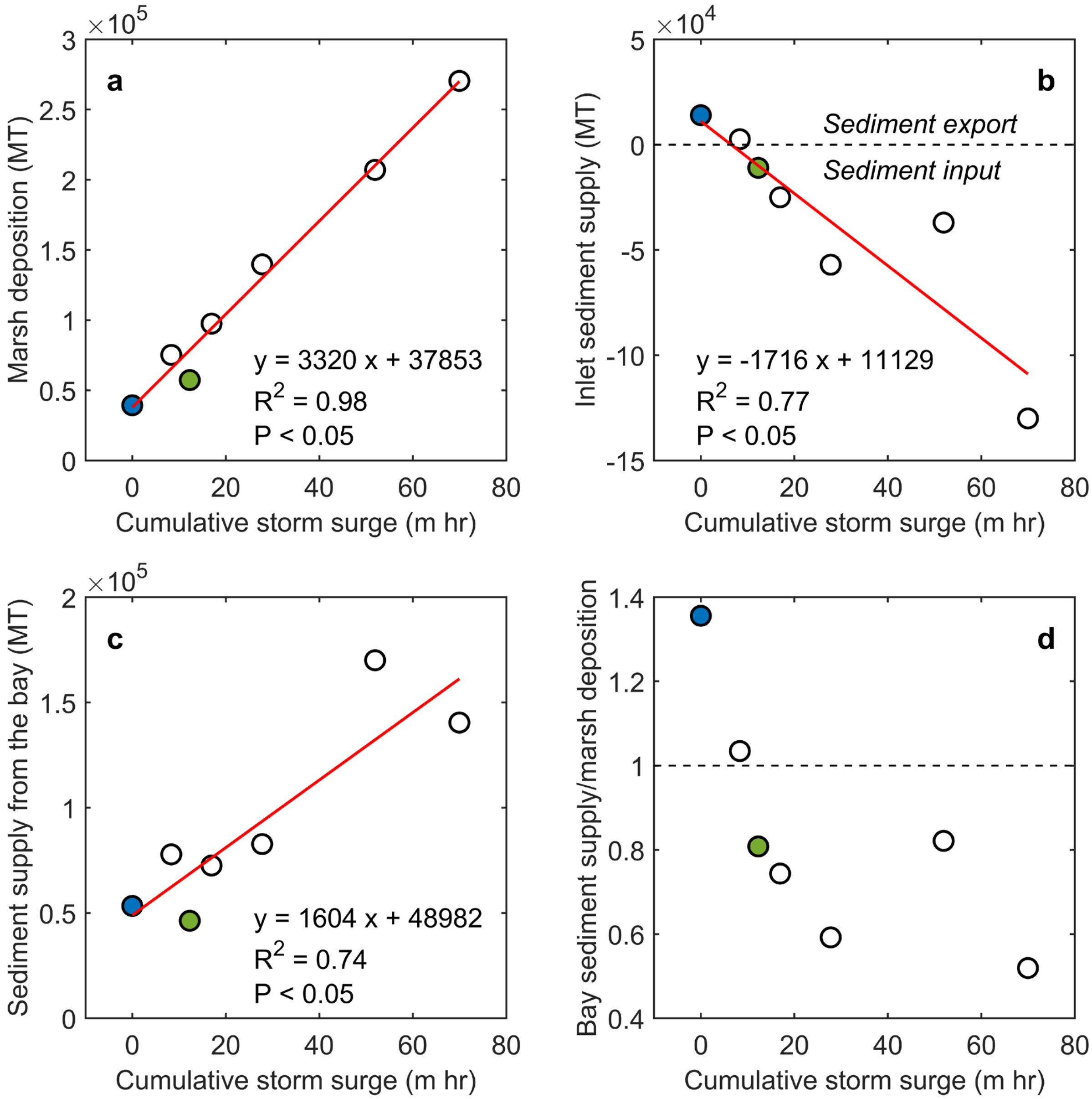

Figure 4.12 (a) Total sediment deposition on the marsh, (b) inlet sediment supply, (c) sediment supply from the bay, and (d) ratio between sediment supply from the bay and total sediment deposition on the marsh as a function of cumulative storm surge intensity. Filled blue and green symbols are model results output from model runs 17MEAW and 09MEAW, respectively.

In addition to its impact on marsh deposition, higher storm surge intensity also increased offshore sediment input to the bay and erosion of the bay bottom (tidal flats). The bay underwent net sediment export at low storm surge intensity and received increased offshore sediment import at larger values of cumulative storm surge intensity (Figure 4.12b), indicating that intense storm surge can increase the stability of the bay by enhancing sediment import to the system. This simulation result is consistent with a previous modeling study regarding the effects of storm events on supplying offshore sediment to the VCR coastal bays (Castagno et al., 2018). They used the Delft3D model to simulate a total of 52 storm events from 2009 to 2015 impacting the site and found that most of the simulated storm events resulted in net sediment import to the system and that sediment import to the bays increased with storm intensity. It is worth noting, however, that our linear regression of inlet sediment supply also shows that storm surge events with a cumulative storm surge intensity < 6.5 m hr (roughly 20% of the identified storm surge events) resulted in net sediment export (Figure 4.12b). Considering that our regression analysis of inlet sediment supply was only based on simulation results of 7 storm events, there is large uncertainty in this estimate of the threshold value of cumulative storm surge intensity for sediment export and additional simulations at low storm surge intensities are needed to better resolve this in future studies.

The increases in sediment import to the bay during storms with high storm surge intensities were not enough to offset the sediment eroded from tidal flats during these storms. Sediment budgets calculated from our simulation results show that the bay experienced increased seabed erosion in response to a larger storm surge intensity (Figure 4.12c) and that tidal flats acted as the primary sediment source for marsh deposition (> 50%) during storm surge events (Figure 4.12d). This sediment connectivity between shallow tidal flat erosion and marsh deposition during storms predicted by our model is in good agreement with recent studies on coupled tidal flat–marsh systems (Duvall et al., 2019; Lacy et al., 2020; Schuerch et al., 2019). For example, based on a seasonal transect measurement of hydrodynamic, SSC, and sediment deposition in a salt marsh in northern San Francisco Bay, Lacy et al. (2020) found that sediment supply to the marsh was closely related to sediment resuspension on the adjacent tidal flats during storms and that wave-induced sediment transport accounted for > 70% of annual marsh deposition. Collectively, both our simulation results and the recent studies on coupled tidal flat–marsh systems suggest that storms can transport significant amounts of sediment from tidal flats to the marsh surface and highlight the importance of the close coupling of sediment dynamics in bay–marsh complexes.

4.4.2 The importance of storm surge on long-term marsh deposition

Sediment transport to marshes during storm surge events contributed a significant fraction of annual marsh deposition in the VCR. The average long-term marsh accretion rate determined by surface elevation tables (SETs) and ^{137}Ce dating at a site 150 m from the marsh edge in FP marsh was ~4.0 mm yr^{-1} (Table A3.2). The model predicted sediment deposition at the same site, which included effects of sediment consolidation (using a representative porosity of 0.7), was 1.7 mm in model run 09MEAW (corresponding to the median storm surge intensity of the identified events; Figure 4.6a), indicating that a storm event with a moderate storm surge intensity can contribute 43% of the annual marsh deposition at the site. Although this estimate was based on short-term simulation results of storm surge events and did not include effects of long-term post-depositional change on the marsh (eg., erosion, subsidence, and long-term compaction), it is in general agreement with the results of a previous study regarding the effects of storm surge on marsh deposition in a nearby tidal channel marsh in the VCR (Christiansen, 1998). Based on measurements of flow rate and sediment transport flux in a marsh near Phillips Creek, this study found that there was a strong correlation of significant sediment transport events to marshes with high water levels associated with strong northeasterly winds and that 27% of the total annual marsh deposition was contributed by sediment transport during storm-driven high water levels.

Storm events with a high storm surge intensity can result in a much larger deposition than the average annual deposition on microtidal marshes. For example, the maximum cumulative storm surge intensity in our simulations was 70.5 m hr associated with the Nor'Ida Storm in November, 2009 (Figure 4.6a, Table A3.1); the modeled sediment deposition on FP marsh during this intense storm event (12.1 mm) was about three times the measured average annual deposition at the site. Similarly, Goodbred & Hine (1995) documented extensive marsh deposition in the Waccasassa Bay system in west-central Florida associated with a nearly 3 m storm surge caused by a severe extratropical storm in March 1993. The marsh deposition resulting from this single event was approximately 10 times the average annual marsh deposition. Storm surge sedimentation on the coastal marshes in southwest Louisiana caused by Hurricane Rita was characterized by Williams & Flanagan (2009). They found that marsh deposition induced by hurricane storm surge was comparable to over a century of non-storm-surge deposition. Schuerch et al. (2012) found that low marsh deposition on a barrier island in North Sea was dominated by storm tide variations and the marsh deposition rate in very stormy years could be 5 times the annual mean value.

Although the above studies have shown that episodic storm-driven high water levels can significantly increase sediment deposition on microtidal marshes, the overall effects of storm-driven increases in water levels and SSC on marsh deposition have not been well quantified. Our model results over a range of forcing conditions (with/without wind waves and storm surge) illustrate that while wind-driven waves control sediment resuspension on tidal flats, marsh deposition during storms was largely determined by tidal inundation associated with storm-driven water levels (Figure 4.13). In the absence of significant wind waves (model runs 09TIDE and 09MEA), suspended sediment flux to the marsh remained low regardless of storm surge (Figure 4.13a, 4.13b); when wind waves were large enough to cause significant resuspension (model runs 09TIDEW and 09MEAW), storm-driven high water levels increased marsh inundation (Figure A3.8) and delivered more suspended sediment to the marsh platform than regular tidal inundation alone (Figure 4.13c, 4.13d). As a result, marsh deposition in the simulation of the 2009 storm surge event using measured water levels (09MEAW) was 1.6 times higher than deposition in simulations using astronomical tides (09TIDEW; Table 4.4). Similarly, Duvall et al. (2019) combined field measurements and modeling of currents, waves and suspended sediment at the bay–marsh boundary near CP marsh and found that including storm surge effects in their marsh deposition model at least doubled marsh sediment deposition compared to that predicted by regular tidal inundation. They also found that effective suspended sediment transport to marshes only occurred when high water and high SSC coincided over tidal flats, indicating the importance of the phasing of storms with tides for marsh sediment supply. It is worth noting, however, that all of the simulated storm surge events in our study (Table A3.1) have a duration roughly longer than three complete tidal cycles (36 hr) and therefore we mainly focused on the overall impacts of storm surge events over the entire event period and did not specifically quantify the effects of different phasing of storms with tides.

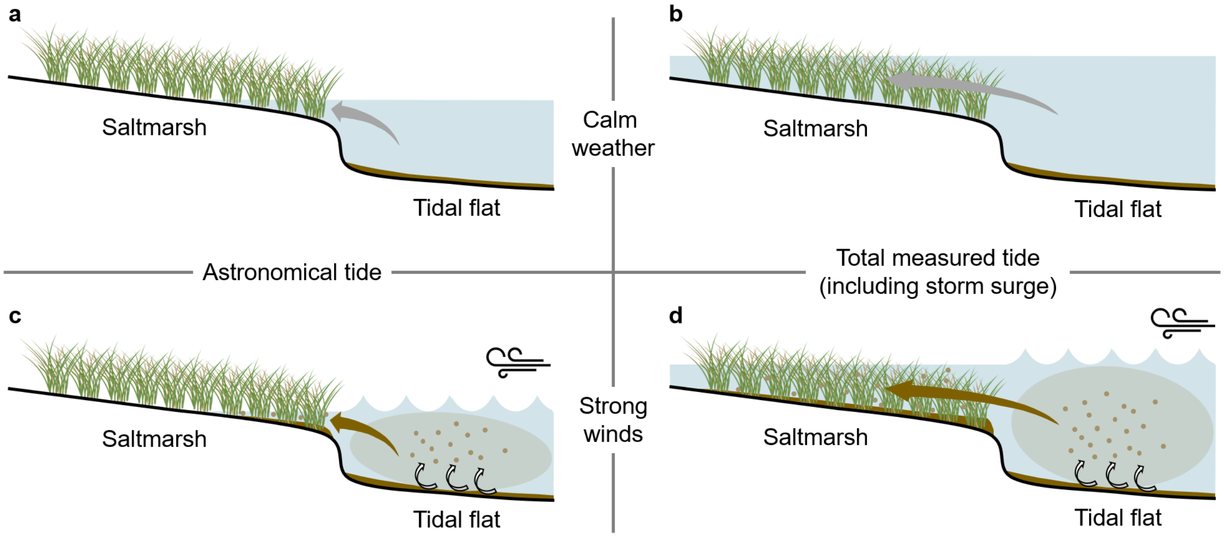

Figure 4.13 Conceptual model of sediment transport in the coupled tidal flat–microtidal marsh system under different conditions: (a) calm weather with astronomical tides (09TIDE), (b) calm weather with total measured water levels (09MEA), (c) strong winds with astronomical tides (09TIDEW), and (d) strong winds with total measured water levels (09 MEAW). The color and length of arrows indicates sediment concentration in the water column and sediment transport distance into the marsh interior, respectively.

Despite the observations that episodic storm surge events played a significant role in microtidal marsh deposition (Goodbred & Hine, 1995; Schuerch et al., 2012; Tognin et al., 2021; Tweel & Turner, 2014; Williams & Flanagan, 2009), most existing marsh deposition models focus exclusively on tidally-driven sediment transport and do not include the effects of stochastic storm surge events on marsh deposition (Fagherazzi et al., 2012; Wiberg et al., 2020). The assumption of regular tidal flooding in marsh deposition models cannot capture the enhanced inundation by storm tides and will inevitably lead to underestimation of marsh deposition rates. The additional marsh deposition associated with storm surge is particularly important for microtidal marshes where storm surge-produced high water levels can be much higher than the highest astronomical tides (Figure 4.2b). We estimated sediment mass deposited on marshes around Hog Bay during storm surge events between 2009–2020 (Table A3.1) using the linear relationship between marsh deposition and cumulative storm surge intensity shown in Figure 4.12a; the estimated storm surge-induced marsh deposition during this period was 6.3×10^6 MT. In contrast, the estimated total marsh deposition associated with regular tidal flooding was 1.6×10^7 MT (multiplying marsh depositional mass output from the 30-day reference model run 09REF by a factor of 144; Figure A3.2). Although storm surge events only occurred about 5% of the time during 2009–2020, storm surge-induced marsh deposition accounted for ~40% (6.3×10^6 MT/1.6×10^7 MT) of marsh deposition associated with regular tidal flooding. Similarly, Tognin et al. (2021) measured marsh sediment accumulation in the Venice Lagoon for a two-year period and found that storm surge-driven sediment transport contributed more than 70% of the annual total sediment accumulation on the marsh with only 25% of the observational period being storm dominated.

4.4.3 Future changes of the coupled tidal flat–marsh system and model limitations

Sea level rise and possible changes in the intensity and/or frequency of surge-producing storm events under future climate change (Colle et al., 2015; Lin et al., 2019; Nerem et al., 2018) will likely impact the stability of the coupled tidal flat-marsh system at our study site. Despite the relatively high SLR rate in the VCR (4–5 mm yr^{-1}), several previous studies have suggested that salt marshes in this system have been able to keep pace with sea level rise (Blum et al., 2020; Kirwan et al., 2010) and that marshes received a considerable amount of suspended sediment supply from the bay during storms (Christiansen, 1998; Duvall et al., 2019). This is supported by our measured long-term accretion rate at FP marsh (Table A3.2) and the sediment budgets calculated from our model simulation results (Figure 4.12c, 4.12d). Our model simulations also indicate that marsh deposition increases linearly with storm surge intensity (Figure 4.12a), suggesting that future changes to magnitude and/or frequency of extratropical cyclones impacting the VCR would have a significant impact on sediment supply to marshes. Marshes at our study site will likely be supplied with more sediment during extratropical storms than in the past if their magnitudes and/or frequencies increase in the future, while a decrease in magnitudes and/or frequencies would result in less sediment transport to marshes. Given the uncertainties of current climate model predictions on future changes of extratropical cyclone along the Mid-Atlantic coast (Colle et al., 2015; Lin et al., 2019), additional studies will be needed to better understand the impacts of future changes in storminess on marsh sediment deposition at our study site.

While marshes may keep pace with SLR under future climate change, our model simulations indicate that shallow tidal flats within the bay will experience increased erosion. Our model simulations (Figure 4.7d, 4.12c) and those from a previous modeling study of the combined effects of storm surge and SLR in the VCR (Mariotti et al., 2010) predict that erosion of the bay bottom will increase due to a higher wave-generated shear stresses associated with larger water depths. Although offshore sediment import to the VCR coastal bays is also expected to increase with storm surge intensity (Castagno et al., 2018), this increase in sediment supply to the bays is not able to offset the sediment loss from tidal flats during storms (Figure 4.12c). As a result, continuous erosion of tidal flats will increase water depth of the bay and promote larger wave conditions until depths become great enough that wave-generated shear stresses at the bed decline (Duvall et al., 2019; Fagherazzi & Wiberg, 2009).

Our model simulations suggest that there is significant spatial variability in bay-bottom erosive processes associated with surge-producing storm winds (Figure 4.7). The strongest winds in the VCR are usually from northeast (Fagherazzi & Wiberg, 2009) and they play a dominant role in driving significant storm surge in the bay (Figure A3.3). If we assume that the directional distribution of winds in the bay remains unchanged in the future, an increase in water depth and storm surge intensity will likely exacerbate this spatial variability (Figure 4.7d, 4.7f), resulting in stronger erosion in the northeastward facing shallow tidal flats than the southwestward facing tidal flats and enhanced sediment redistribution within the entire bay. Because this system lacks significant fluvial sediment input, the fate of tidal flats in the bay is likely to depend on offshore sediment input and sediment redistribution processes.

One of the limitations of this study is that our model did not resolve marsh edge retreat, which is a highly dynamic feature of microtidal marshes fringing coastal bays (Leonardi et al., 2016; Mariotti & Fagherazzi, 2013). Previous studies have shown that the eroded sediment from marsh edges can contribute a substantial amount of sediment to coastal bays and then be transported to the nearby marsh platform by flooding tides (Hopkinson et al., 2018; Mariotti & Carr, 2014). However, the contribution of marsh edge retreat to the overall sediment budget in Hog Bay has not yet been quantified. Previous analysis of shoreline changes in Hog Bay by McLoughlin et al. (2015) indicated that marsh edges in the bay have retreated at a relatively constant rate, averaging about 1.0 m yr^{-1} during the past 50 years. Volumetric erosion rates of the marsh edge in the bay can be estimated by multiplying the edge retreat rate with the average height of marsh edge scarps (~1 m; McLoughlin et al., 2015) and total perimeter of marsh edges (180 km; measured in Google Earth by tracking marsh edges around the bay). This estimate predicts a volumetric erosion rate of 1.8×10^5 m^3 per year and an annual erosional mass of marsh edge sediment released to the bay of 1.4×10^5 MT (assuming a sediment bulk density of 800 kg m^{-3}). This is ~10% of the estimated annual total mass of marsh deposition around Hog Bay due to regular tidal flooding (1.4×10^6 MT; Figure A3.2), suggesting that marsh edge retreat has made a relatively limited contribution to the sediment budget in our study site. However, if bays deepen as sea level rises, wave energy fluxes acting on marsh edges will increase and this will increase rates of edge erosion (Mariotti et al., 2010; McLoughlin et al., 2015), potentially contributing more sediment to marsh deposition than in the past. In future studies, coupling of horizontal and vertical marsh dynamics in spatially explicit models will be needed to obtain more holistic sediment budgets for coupled tidal flat–marsh systems and improve our understanding of their resilience under future climate change.

Another limitation of this study is that our estimate of total marsh deposition was based on short-term simulation results of storm surge events and did not include effects of long-term post-depositional change on the marsh (eg., erosion, subsidence, and long-term compaction). Therefore, our estimate may overpredict the contribution of storm surge to long-term microtidal marsh deposition. For example, our simulation results show that there were a few areas within the marsh interior showing slight erosion (Figure 4.11). Although total erosional mass in these areas was much smaller than sediment deposition on the marsh, a larger erosional area was present in FP marsh when storm surge effects were included in the model (Figure 4.11b). This increase in erosional area might trigger the creation of ponds and lead to rapid loss of marshes by pond expansion if inorganic sediment supply to the marsh is low (Mariotti, 2016). A more realistic approach in future studies would be to simulate continuous morphological change of the coupled tidal flat–marsh system for a longer time period and to integrate effects of long-term post-depositional change on the marsh platform. In addition, although our model estimated annual marsh deposition (4.8 mm yr^{-1}) in FP marsh is in good agreement with the average long-term marsh accretion rate at the same site (4.0 mm yr^{-1}; Table A3.2), more spatially distributed measurements of marsh sediment deposition rates, like those documenting spatial distributions of hurricane-induced marsh deposition in Louisiana (Tweel & Turner, 2014; Williams & Flanagan, 2009), will be needed to constrain model simulation results of marsh deposition associated with storm surge events and improve our understanding of spatial marsh deposition patterns in microtidal bay–marsh complexes.

4.5 Conclusion

In this study, we analyzed measured water levels, astronomical tides, and wind speeds during 2008–2020 in a microtidal bay–marsh complex in Virginia and identified major storm surge events impacting the site. Our results show that most storm surge events in the bay (> 90%) were associated with along-coast winds blowing from northeast. We then applied a spatially resolved hydrodynamic and sediment transport model to the bay–marsh complex to quantify the contributions of storm surge to marsh sediment delivery.

We validated the model using hydrodynamic and suspended sediment data collected at various locations in the bay and ran model simulations under different storm surge conditions with/without storm-driven water level changes. Model simulations of significant wave height, seabed erosion time fraction, and sediment resuspension in the bay during a northeasterly wind event in 2009 (a storm surge event with median storm surge intensity) and a southerly wind event in 2017 (with minor storm surge) were used to examine the effects of storm surge on bay erosive processes and marsh sediment delivery. The results show that storm surge can result in significant spatial variability in bay erosive processes: storm-driven high water levels caused by northeasterly winds can increase the erosion time fraction of most northeastward facing shallow tidal flats and marsh edges by ~10%, while decreasing the erosion time fraction of southwestward facing tidal flats by about the same amount. Although there was stronger seabed erosion in the model run with storm surge effects during the northeasterly wind event in 2009 than that without storm surge effects during the same period, storm surge had a limited effect on the magnitudes and spatial patterns of suspended sediment concentration in the bay.

When wind waves were large enough to cause significant sediment resuspension in the bay, storm-driven high water levels increased marsh inundation and delivered more suspended sediment onto the marsh platform than regular tidal inundation alone. A moderate storm surge event with median storm surge intensity can double sediment flux to most marshes in the study area, deliver more sediment to the marsh interior (> 500 m from the marsh edge), and result in greater vertical deposition on the marsh (× 1.6 times) compared with the simulations without storm surge variations in water levels. Comparison of total marsh deposition induced by the storm surge events during 2009–2020 with estimated deposition associated with regular tidal flooding during the same period showed that episodic storm surge events, which occurred 5% of the time, accounted for ~40% of total marsh deposition at our study site. The additional marsh deposition associated with storm surge is therefore particularly important for microtidal marshes and needs to be better resolved in marsh deposition models.

Simulations of bay and marsh response to different storm surge events with varying magnitude of storm surge intensity further revealed that total marsh deposition around the bay increased linearly with storm surge intensity and that higher storm surge intensities also increased offshore sediment input to the bay and erosion of the bay bottom. The linear relationship between marsh deposition and storm surge intensity has significant implications for predicting marsh change. Based on this relationship, it is likely that marshes at our study site will be supplied with more (less) sediment eroded from the shallow tidal flats during storms than in the past if storm magnitudes and/or frequencies increase (decrease) in the future.

References

Allen, J. R. L. (2000). Morphodynamics of Holocene salt marshes: A review sketch from the Atlantic and Southern North Sea coasts of Europe. Quaternary Science Reviews. https://doi.org/10.1016/S0277-3791(99)00034-7

Baptist, M. J., Babovic, V., Uthurburu, J. R., Keijzer, M., Uittenbogaard, R. E., Mynett, A., & Verwey, A. (2007). On inducing equations for vegetation resistance. Journal of Hydraulic Research, 45(4), 435–450. https://doi.org/10.1080/00221686.2007.9521778

Barbier, E. B., Hacker, S. D., Kennedy, C., Koch, E. W., Stier, A. C., & Silliman, B. R. (2011). The value of estuarine and coastal ecosystem services. Ecological Monographs, 81(2), 169–193. https://doi.org/10.1890/10-1510.1

Blum, L. K., Christian, R. R., Cahoon, D. R., & Wiberg, P. L. (2020). Processes Influencing Marsh Elevation Change in Low- and High-Elevation Zones of a Temperate Salt Marsh. Estuaries and Coasts 2020 44:3, 44(3), 818–833. https://doi.org/10.1007/S12237-020-00796-Z

Booij, N., Ris, R. C., & Holthuijsen, L. H. (1999). A third-generation wave model for coastal regions 1. Model description and validation. Journal of Geophysical Research: Oceans, 104(C4), 7649–7666. https://doi.org/10.1029/98JC02622

Brinson, M. M., Christian, R. R., & Blum, L. K. (1995). Multiple states in the sea-level induced transition from terrestrial forest to estuary. Estuaries, 18(4), 648–659. https://doi.org/10.2307/1352383

Cahoon, D. R. (2006). A review of major storm impacts on coastal wetland elevations. Estuaries and Coasts. Estaurine Research Federation. https://doi.org/10.1007/BF02798648

Cahoon, D. R., Reed, D. J., & Day, J. W. (1995). Estimating shallow subsidence in microtidal salt marshes of the southeastern United States: Kaye and Barghoorn revisited. Marine Geology, 128(1–2), 1–9. https://doi.org/10.1016/0025-3227(95)00087-F

Carniello, L., Defina, A., & D'Alpaos, L. (2012). Modeling sand-mud transport induced by tidal currents and wind waves in shallow microtidal basins: Application to the Venice Lagoon (Italy). Estuarine, Coastal and Shelf Science, 102–103, 105–115. https://doi.org/10.1016/j.ecss.2012.03.016

Castagno, K. A., Jiménez-Robles, A. M., Donnelly, J. P., Wiberg, P. L., Fenster, M. S., & Fagherazzi, S. (2018). Intense Storms Increase the Stability of Tidal Bays. Geophysical Research Letters, 45(11), 5491–5500. https://doi.org/10.1029/2018GL078208

Christiansen, T. (1998). Sediment deposition on a tidal salt marsh (Doctoral dissertation). University of Virginia, Charlotteville, VA.

Christiansen, T., Wiberg, P. L., & Milligan, T. G. (2000). Flow and Sediment Transport on a Tidal Salt Marsh Surface. Estuarine, Coastal and Shelf Science, 50(3), 315–331. https://doi.org/10.1006/ECSS.2000.0548

Colle, B. A., Booth, J. F., & Chang, E. K. M. (2015). A Review of Historical and Future

Changes of Extratropical Cyclones and Associated Impacts Along the US East Coast. Current Climate Change Reports, 1(3), 125-143. https://doi.org/10.1007/S40641-015-0013-7

Deltares. (2014). Delft3D-FLOW User Manual (Version: 3.15.34158): Simulation of multi-dimensional hydrodynamic flows and transport phenomena, including sediments. Delft, The Netherlands: WL Delft Hydraulics

Donatelli, C., Ganju, N. K., Fagherazzi, S., & Leonardi, N. (2018). Seagrass Impact on Sediment Exchange Between Tidal Flats and Salt Marsh, and The Sediment Budget of Shallow Bays. Geophysical Research Letters, 45(10), 4933–4943. https://doi.org/10.1029/2018GL078056

Donatelli, C., Zhang, X., Ganju, N. K., Aretxabaleta, A. L., Fagherazzi, S., & Leonardi, N. (2020). A nonlinear relationship between marsh size and sediment trapping capacity compromises salt marshes' stability. Geology, 48(10), 966–970. https://doi.org/10.1130/G47131.1

Duvall, M. S., Wiberg, P. L., & Kirwan, M. L. (2019). Controls on Sediment Suspension, Flux, and Marsh Deposition near a Bay-Marsh Boundary. Estuaries and Coasts, 42(2), 403–424. https://doi.org/10.1007/s12237-018-0478-4

Fagherazzi, S., & Mariotti, G. (2009a). ADCP wave and current data at Hog Island and Chimney Pole Marsh, VA 2009 [Dataset]. Virginia Coast Reserve Long-Term Ecological Research Project Data Publication knb-lter-vcr.165.15. https://doi.org/10.6073/pasta/a05bfce78062aa9802873efcff0144e6

Fagherazzi, S., & Mariotti, G. (2009b). Wave data for Hog Island Bay, Fowling Point and Upsur Neck, Virginia, 2009 [Dataset]. Virginia Coast Reserve Long-Term Ecological Research Project Data Publication knb-lter-vcr.164.16. https://doi.org/10.6073/pasta/4feeada0f9cc772b4a070c7dbf58ef16

Fagherazzi, S., & Priestas, A. M. (2010). Sediments and water fluxes in a muddy coastline: interplay between waves and tidal channel hydrodynamics. Earth Surface Processes and Landforms, 35(3), 284–293. https://doi.org/10.1002/ESP.1909

Fagherazzi, S., & Wiberg, P. L. (2009). Importance of wind conditions, fetch, and water levels on wave-generated shear stresses in shallow intertidal basins. Journal of Geophysical Research, 114(F3), F03022. https://doi.org/10.1029/2008JF001139

Fagherazzi, S., Mariotti, G., Porter, J., McGlathery, K., & Wiberg, P. L. (2010). Wave energy asymmetry in shallow bays. Geophysical Research Letters, 37(24). https://doi.org/10.1029/2010GL045254

Fagherazzi, S., Kirwan, M. L., Mudd, S. M., Guntenspergen, G. R., Temmerman, S., D'Alpaos, A., et al. (2012). Numerical models of salt marsh evolution: Ecological, geomorphic, and climatic factors. Reviews of Geophysics, 50(1). https://doi.org/10.1029/2011RG000359

Fagherazzi, S., Wiberg, P. L., Temmerman, S., Struyf, E., Zhao, Y., & Raymond, P. A. (2013). Fluxes of water, sediments, and biogeochemical compounds in salt marshes. Ecological Processes, 2(1), 1–16. https://doi.org/10.1186/2192-1709-2-3

Fagherazzi, S., Mariotti, G., Leonardi, N., Canestrelli, A., Nardin, W., & Kearney, W. S. (2020). Salt Marsh Dynamics in a Period of Accelerated Sea Level Rise. Journal of Geophysical Research: Earth Surface, 125(8), e2019JF005200. https://doi.org/10.1029/2019JF005200

FitzGerald, D. M., & Hughes, Z. (2019). Marsh Processes and Their Response to Climate Change and Sea-Level Rise. Annual Review of Earth and Planetary Sciences, 47, 481–517. https://doi.org/10.1146/ANNUREV-EARTH-082517-010255

French, J. R., & Spencer, T. (1993). Dynamics of sedimentation in a tide-dominated backbarrier salt marsh, Norfolk, UK. Marine Geology, 110(3–4), 315–331. https://doi.org/10.1016/0025-3227(93)90091-9

Friedrichs, C. T., & Perry, J. E. (2001). Tidal Salt Marsh Morphodynamics: A Synthesis. Journal of Coastal Research, (27), 7–37. https://doi.org/10.2307/25736162

Ganju, N. K., Defne, Z., Kirwan, M. L., Fagherazzi, S., D'Alpaos, A., & Carniello, L. (2017). Spatially integrative metrics reveal hidden vulnerability of microtidal salt marshes. Nature Communications 2017 8:1, 8(1), 1–7. https://doi.org/10.1038/ncomms14156

Gedan, K. B., Silliman, B. R., & Bertness, M. D. (2009). Centuries of Human-Driven Change in Salt Marsh Ecosystems. Http://Dx.Doi.Org/10.1146/Annurev.Marine.010908.163930, 1, 117–141. https://doi.org/10.1146/ANNUREV.MARINE.010908.163930

Goodbred, S. L., & Hine, A. C. (1995). Coastal storm deposition: Salt-marsh response to a severe extratropical storm, March 1993, west-central Florida. Geology, 23(8), 679–682. https://doi.org/10.1130/0091-7613(1995)023<0679:CSDSMR>2.3.CO;2

Hayden, B. P., Santos, M. C. F. V., Shao, G., & Kochel, R. C. (1995). Geomorphological controls on coastal vegetation at the Virginia Coast Reserve. Geomorphology, 13(1–4), 283–300. https://doi.org/10.1016/0169-555X(95)00032-Z

Hopkinson, C. S., Morris, J. T., Fagherazzi, S., Wollheim, W. M., & Raymond, P. A. (2018). Lateral Marsh Edge Erosion as a Source of Sediments for Vertical Marsh Accretion. Journal of Geophysical Research: Biogeosciences, 123(8), 2444–2465. https://doi.org/10.1029/2017JG004358

King, S. E., & Lester, J. N. (1995). The value of salt marsh as a sea defence. Marine Pollution Bulletin, 30(3), 180–189. https://doi.org/10.1016/0025-326X(94)00173-7

Kirwan, M. L., & Guntenspergen, G. R. (2010). Influence of tidal range on the stability of coastal marshland. Journal of Geophysical Research: Earth Surface, 115(F2). https://doi.org/10.1029/2009jf001400

Kirwan, M. L., & Megonigal, J. P. (2013). Tidal wetland stability in the face of human impacts and sea-level rise. Nature 2013 504:7478, 504(7478), 53–60. https://doi.org/10.1038/nature12856

Kirwan, M. L., Guntenspergen, G. R., D'Alpaos, A., Morris, J. T., Mudd, S. M., & Temmerman, S. (2010). Limits on the adaptability of coastal marshes to rising sea level. Geophysical Research Letters, 37(23), n/a-n/a. https://doi.org/10.1029/2010GL045489

Krone, R. B. (1962). Flume studies of the transport of sediment in estuarial shoaling processes: final report. Berkeley: University of California, Berkeley.

Lacy, J. R., Foster-Martinez, M. R., Allen, R. M., Ferner, M. C., & Callaway, J. C. (2020). Seasonal Variation in Sediment Delivery Across the Bay-Marsh Interface of an Estuarine Salt Marsh. Journal of Geophysical Research: Oceans, 125(1). https://doi.org/10.1029/2019jc015268

Lawson, S. E., & Wiberg, P. L. (2006). Acoustic Doppler Profiler (ADP) Time Series Measurements at Hog Island Bay at the Virginia Coast Reserve 2002-2004 [Dataset]. Virginia Coast Reserve Long-Term Ecological Research Project Data Publication knb-lter-vcr.146.21. https://doi.org/10.6073/pasta/56aa9ad800a0c4995ccdf6763b2e6fc8

Lawson, S. E., Wiberg, P. L., McGlathery, K. J., & Fugate, D. C. (2007). Wind-driven sediment suspension controls light availability in a shallow coastal lagoon. Estuaries and Coasts, 30(1), 102–112. https://doi.org/10.1007/BF02782971

Leonardi, N., Ganju, N. K., & Fagherazzi, S. (2016). A linear relationship between wave power and erosion determines salt-marsh resilience to violent storms and hurricanes. Proceedings of the National Academy of Sciences, 113(1), 64–68. https://doi.org/10.1073/PNAS.1510095112

Lesser, G. R., Roelvink, J. A., van Kester, J. A. T. M. T. M., & Stelling, G. S. (2004). Development and validation of a three-dimensional morphological model. Coastal Engineering, 51(8), 883–915. https://doi.org/10.1016/j.coastaleng.2004.07.014

Lin, N., Marsooli, R., & Colle, B. A. (2019). Storm surge return levels induced by mid-to-late-twenty-first-century extratropical cyclones in the Northeastern United States. Climatic Change, 154(1–2), 143–158. https://doi.org/10.1007/S10584-019-02431-8

Liu, K., Chen, Q., Hu, K., Xu, K., & Twilley, R. R. (2018). Modeling hurricane-induced wetland-bay and bay-shelf sediment fluxes. Coastal Engineering, 135, 77–90. https://doi.org/10.1016/j.coastaleng.2017.12.014

Liu, Y., Maccready, P., Hickey, B. M., Dever, E. P., Kosro, P. M., Banas, N. S., et al. (2009). Evaluation of a coastal ocean circulation model for the Columbia River plume in summer 2004. Journal of Geophysical Research: Oceans, 114(C2), 0–04. https://doi.org/10.1029/2008JC004929

Ma, Z., Ysebaert, T., van der Wal, D., de Jong, D. J., Li, X., & Herman, P. M. J. (2014). Long-term salt marsh vertical accretion in a tidal bay with reduced sediment supply. Estuarine, Coastal and Shelf Science, 146, 14–23. https://doi.org/10.1016/J.ECSS.2014.05.001

Mariotti, G. (2016). Revisiting salt marsh resilience to sea level rise: Are ponds responsible for permanent land loss? Journal of Geophysical Research: Earth Surface, 121(7), 1391–1407. https://doi.org/10.1002/2016JF003900

Mariotti, G. (2020). Beyond marsh drowning: The many faces of marsh loss (and gain). Advances in Water Resources, 144, 103710. https://doi.org/10.1016/J.ADVWATRES.2020.103710

Mariotti, G., & Carr, J. A. (2014). Dual role of salt marsh retreat: Long-term loss and short-term resilience. Water Resources Research, 50(4), 2963–2974. https://doi.org/10.1002/2013WR014676

Mariotti, G., & Fagherazzi, S. (2013). Critical width of tidal flats triggers marsh collapse in the absence of sea-level rise. Proceedings of the National Academy of Sciences of the United States of America, 110(14), 5353–5356. https://doi.org/10.1073/pnas.1219600110

Mariotti, G., Fagherazzi, S., Wiberg, P. L., McGlathery, K. J., Carniello, L., & Defina, A. (2010). Influence of storm surges and sea level on shallow tidal basin erosive processes. Journal of Geophysical Research, 115(C11), C11012. https://doi.org/10.1029/2009JC005892

McLoughlin, S. M., Wiberg, P. L., Safak, I., & McGlathery, K. J. (2015). Rates and Forcing of Marsh Edge Erosion in a Shallow Coastal Bay. Estuaries and Coasts, 38(2), 620–638. https://doi.org/10.1007/s12237-014-9841-2

Möller, I., Kudella, M., Rupprecht, F., Spencer, T., Paul, M., Wesenbeeck, B. K. van, et al. (2014). Wave attenuation over coastal salt marshes under storm surge conditions. Nature Geoscience 2014 7:10, 7(10), 727–731. https://doi.org/10.1038/ngeo2251

Morris, J. T., Sundareshwar, P. V., Nietch, C. T., Kjerfve, B., & Cahoon, D. R. (2002). Responses of coastal wetlands to rising sea level. Ecology, 83(10), 2869–2877. https://doi.org/10.1890/0012-9658(2002)083[2869:ROCWTR]2.0.CO;2

Morris, J. T., Barber, D. C., Callaway, J. C., Chambers, R., Hagen, S. C., Hopkinson, C. S., et al. (2016). Contributions of organic and inorganic matter to sediment volume and accretion in tidal wetlands at steady state. Earth's Future, 4(4), 110–121. https://doi.org/10.1002/2015EF000334

Nardin, W., Larsen, L., Fagherazzi, S., & Wiberg, P. (2018). Tradeoffs among hydrodynamics, sediment fluxes and vegetation community in the Virginia Coast Reserve, USA. Estuarine, Coastal and Shelf Science, 210, 98–108. https://doi.org/10.1016/j.ecss.2018.06.009

Nerem, R. S., Beckley, B. D., Fasullo, J. T., Hamlington, B. D., Masters, D., & Mitchum, G. T. (2018). Climate-change–driven accelerated sea-level rise detected in the altimeter era. Proceedings of the National Academy of Sciences, 115(9), 2022–2025. https://doi.org/10.1073/PNAS.1717312115

Oertel, G. F. (2001). Hypsographic, hydro-hypsographic and hydrological analysis of coastal bay environments, Great Machipongo Bay, Virginia. Journal of Coastal Research, 17(4), 775–783.

Partheniades, E. (1965). Erosion and Deposition of Cohesive Soils. Journal of the Hydraulics Division, 91(1), 105–139. https://doi.org/10.1061/JYCEAJ.0001165

Peteet, D. M., Nichols, J., Kenna, T., Chang, C., Browne, J., Reza, M., et al. (2018). Sediment starvation destroys New York City marshes' resistance to sea level rise. Proceedings of the National Academy of Sciences, 115(41), 10281–10286. https://doi.org/10.1073/PNAS.1715392115

Redfield, A. C. (1972). Development of a New England Salt Marsh. Ecological Monographs, 42(2), 201–237. https://doi.org/10.2307/1942263

Reed, D. J. (1989). Patterns of sediment deposition in subsiding coastal salt marshes, Terrebonne Bay, Louisiana: The role of winter storms. Estuaries, 12(4), 222–227. https://doi.org/10.2307/1351901

Reidenbach, M. A., & Timmerman, R. (2019). Interactive Effects of Seagrass and the Microphytobenthos on Sediment Suspension Within Shallow Coastal Bays. Estuaries and Coasts, 42(8), 2038–2053. https://doi.org/10.1007/s12237-019-00627-w

Schuerch, M., Rapaglia, J., Liebetrau, V., Vafeidis, A., & Reise, K. (2012). Salt Marsh Accretion and Storm Tide Variation: An Example from a Barrier Island in the North Sea. Estuaries and Coasts, 35(2), 486–500. https://doi.org/10.1007/s12237-011-9461-z

Schuerch, M., Vafeidis, A., Slawig, T., & Temmerman, S. (2013). Modeling the influence of changing storm patterns on the ability of a salt marsh to keep pace with sea level rise. Journal of Geophysical Research: Earth Surface, 118(1), 84–96. https://doi.org/10.1029/2012JF002471

Schuerch, M., Scholten, J., Carretero, S., García-Rodríguez, F., Kumbier, K., Baechtiger, M., & Liebetrau, V. (2016). The effect of long-term and decadal climate and hydrology variations on estuarine marsh dynamics: An identifying case study from the Río de la Plata. Geomorphology, 269, 122–132. https://doi.org/10.1016/J.GEOMORPH.2016.06.029

Schuerch, M., Spencer, T., & Evans, B. (2019). Coupling between tidal mudflats and salt marshes affects marsh morphology. Marine Geology, 412, 95–106. https://doi.org/10.1016/j.margeo.2019.03.008

Stanhope, J. W., Anderson, I. C., & Reay, W. G. (2009). Base Flow Nutrient Discharges from Lower Delmarva Peninsula Watersheds of Virginia, USA. Journal of Environmental Quality, 38(5), 2070–2083. https://doi.org/10.2134/JEQ2008.0358

Sun, C., Fagherazzi, S., & Liu, Y. (2018). Classification mapping of salt marsh vegetation by flexible monthly NDVI time-series using Landsat imagery. Estuarine, Coastal and Shelf Science, 213, 61–80. https://doi.org/10.1016/j.ecss.2018.08.007

Suzuki, T., Zijlema, M., Burger, B., Meijer, M. C., & Narayan, S. (2012). Wave dissipation by vegetation with layer schematization in SWAN. Coastal Engineering, 59(1), 64–71. https://doi.org/10.1016/j.coastaleng.2011.07.006

Tognin, D., D'Alpaos, A., Marani, M., & Carniello, L. (2021). Marsh resilience to sea-level rise reduced by storm-surge barriers in the Venice Lagoon. Nature Geoscience 2021 14:12, 14(12), 906–911. https://doi.org/10.1038/s41561-021-00853-7

Turner, R. E., Baustian, J. J., Swenson, E. M., & Spicer, J. S. (2006). Wetland sedimentation from hurricanes Katrina and Rita. Science, 314(5798), 449–452. https://doi.org/10.1126/SCIENCE.1129116

Tweel, A. W., & Turner, R. E. (2014). Contribution of tropical cyclones to the sediment budget for coastal wetlands in Louisiana, USA. Landscape Ecology, 29(6), 1083–1094.

https://doi.org/10.1007/s10980-014-0047-6

Van Rijn, L. C., Roelvink, J. A., & Horst, W. ter. (2001). Approximation formulae for sand transport by currents and waves and implementation in DELFT-MOR. Report Z3054.20, Delft Hydraulics, Delft, The Netherlands.

Warner, J. C., Geyer, W. R., & Lerczak, J. A. (2005). Numerical modeling of an estuary: A comprehensive skill assessment. Journal of Geophysical Research: Oceans, 110(C5), 1–13. https://doi.org/10.1029/2004JC002691

Wiberg, P. L. (2017). Wave and turbidity measurements, Fowling Point, Hog Island Bay, VA, Summer 2017 [Dataset]. Virginia Coast Reserve Long-Term Ecological Research Project Data Publication knb-lter-vcr.266.3. https://doi.org/10.6073/pasta/a24eab379c7a44f32e32b247ef4c31fe

Wiberg, P. L., Carr, J. A., Safak, I., & Anutaliya, A. (2015). Quantifying the distribution and influence of non-uniform bed properties in shallow coastal bays. Limnology and Oceanography: Methods, 13(12), 746–762. https://doi.org/10.1002/lom3.10063

Wiberg, P. L., Fagherazzi, S., & Kirwan, M. L. (2020). Improving Predictions of Salt Marsh Evolution Through Better Integration of Data and Models. Annual Review of Marine Science, 12(1), 389–413. https://doi.org/10.1146/annurev-marine-010419-010610

Williams, H. F. L., & Flanagan, W. M. (2009). Contribution of hurricane rita storm surge deposition to long-term sedimentation in Louisiana coastal woodlands and marshes. Journal of Coastal Research, 2(SI 56), 1671–1675.

Willmott, C. J. (1981). On the validation of models. Physical Geography, 2(2), 184–194. https://doi.org/10.1080/02723646.1981.10642213

Yang, S. L., Luo, X., Temmerman, S., Kirwan, M., Bouma, T., Xu, K., et al. (2020). Role of delta-front erosion in sustaining salt marshes under sea-level rise and fluvial sediment decline. Limnology and Oceanography, 65(9), 1990–2009. https://doi.org/10.1002/lno.11432

Zhang, X., Leonardi, N., Donatelli, C., & Fagherazzi, S. (2019). Fate of cohesive sediments in a marsh-dominated estuary. Advances in Water Resources, 125, 32–40. https://doi.org/10.1016/j.advwatres.2019.01.003

Zhu, Q., Wiberg, P. L., & Reidenbach, M. A. (2021). Quantifying Seasonal Seagrass Effects on Flow and Sediment Dynamics in a Back-Barrier Bay. Journal of Geophysical Research: Oceans, 126(2), e2020JC016547. https://doi.org/10.1029/2020JC016547

Chapter 5: Submerged seagrass meadows modulate sediment delivery and wave energy flux to back-barrier marshes

Abstract

Back-barrier intertidal salt marshes are important marine habitats threatened by sea level rise and wave-driven erosion. A quantitative characterization of vertical and horizontal dynamics of back-barrier marshes is critical for assessing their resilience under future climate change. Previous studies have shown that the presence of submerged seagrass meadows on tidal flats, however, can significantly reduce suspended sediment flux to the adjacent marsh platform and alter wave energy acting on the marsh edges. But it is still unclear how sediment delivery and wave energy flux to back-barrier marshes vary in response to seasonal seagrass growth and senescence and wind patterns. Here we apply a spatially resolved and extensively validated hydrodynamic and sediment transport model Delft3D in a shallow coastal bay in Virginia with seagrass meadows proximal to a back-barrier marsh (South Bay, Wreck Island). Our model includes both intertidal and submerged vegetation effects on flow, waves, and sediment resuspension, and was run for 12 consecutive months with seasonally varying tides, winds, and seagrass densities. Our simulation results show that seagrass meadows altered the timing of sediment transport to the marsh (winter peak, density control) and reduced total annual sediment flux by 12% compared to the simulation with no seagrass (flux controlled by winds). We also found that reductions in incident wave energy flux on marsh edge increased linearly with seagrass density and that seagrass meadows resulted in an overall 22% reduction of wave energy flux on marsh edge throughout the year, indicating that they can effectively reduce marsh edge erosion caused by wind waves. Our findings highlight the strong seasonal control seagrass has in back-barrier marshes and the beneficial role of seagrass in the coupled tidal flat–marsh systems.

5.1 Introduction

Barrier islands are narrow, elongated, and shore-parallel coastal landforms that account for more than 10% of the world's coastlines (Stutz & Pilkey, 2001). They are the first line of defense that protects adjacent heavily populated coastal communities and infrastructure from waves and storm surge (Arkema et al., 2013) and provides a sheltered envrionment that allows back-barrier marshes and shallow lagoons to form behind them (Davis, 1994). These unique low-energy back-barrier environments, together with barrrier islands themselves, support a variety of flora and fauna communities and offer valuable ecosystem services, including nutrient cycling, improving water quality, carbon sequestration, and shoreline stabilization (Barbier et al., 2011; Feagin et al., 2010). Despite their importance for coastal communities and ecosystems, barrier islands are one of the most rapidly migrating coastal landforms, threatened by accelerated sea level rise, reductions in sediment supply, and future changes in storminess (Ceia et al., 2010; Durán Vinent & Moore, 2014; Moore & Murray, 2018).

Recent studies have shown that back-barrier intertidal salt marshes play an important role in barrier island stability and migration (Lauzon et al., 2018; Walters et al., 2014). To keep pace with sea level rise (SLR), back-barrier marshes rely on a supply of suspended sediment from nearby tidal flats to promote vertical accretion. However, the presence of submerged seagrass meadows on tidal flats, can significantly reduce sediment resuspension on tidal flats and sediment flux to the adjacent marsh platform (Carr et al., 2018; Hansen & Reidenbach, 2012). For example, Donatelli et al. (2018) applied the Coupled–Ocean–Atmosphere–Wave–Sediment Transport (COAWST) modeling system in Barnegat Bay, USA, to quantify the effects of seagrass on sediment exchange between tidal flats covered by seagrass meadows and salt marshes fringing the bay. They found that marsh sediment deposition around the bay decreased nonlinearly with increasing seagrass coverage on tidal flats, with a maximum reduction (60%) in marsh sediment deposition when 30% of the bay was covered by seagrass meadows. On a longer temporal scale, Carr et al. (2018) used an idealized transect-based model to investigate the coupled dynamics in the tidal flat–seagrass–marsh system over a 500-year model simulation period, and they found that dense seagrass meadows during the growing season effectively trapped sediment in seagrass beds and limited sediment delivery to adjacent salt marshes, whereas low-density seagrass meadows during winter senescence increased the amount of sediment resuspension in the bay and supplied more sediment to the marsh compared with the simulation with unvegetated tidal flats.

Meanwhile, the presence of submerged seagrass meadows on tidal flats can efficiently dissipate wave energy and attenuate wave heights (Fonseca & Cahalan, 1992; Reidenbach & Thomas, 2018), thereby decreasing wave energy acting on the marsh edges and protecting them from erosion. A recent modeling study by Donatelli et al. (2019) found that up to 40% of the wave thrust (a metric of wave attack acting on marsh edge that is calculated as the vertical integral of wave-induced dynamic pressure) on marsh edges in Barnegat Bay can be reduced by submerged seagrass meadows in the bay and that both the location of the meadows and their spatial extent play an important role in the attenuation of wave thrust on marsh edges. Over the long term, model simulation results from a suite of 288 simulations of the morphodynamic exploratory model, GEOMBEST++Seagrass that couples seagrass dynamics into the evolution of barrier–marsh–bay systems showed that seagrass reduced marsh edge erosion rates in most model simulations, but it can increase marsh edge erosion rates when sediment export from the barrier–bay system was insignificant (Reeves et al., 2020).

Although these recent model simulation results have significantly improved our understanding of the complex dynamics between submerged seagrass meadows and back-barrier marshes, most of them used either transect-based simulations that generally emphasized long-term evolution or short-term spatially resolved models that did not resolve seasonal wind patterns and seagrass density variations. Seasonal seagrass growth and senescence exert a strong influence on sediment transport and accumulation within seagrass meadows (Gacia & Duarte, 2001; Hansen & Reidenbach, 2013) and therefore might significantly modulate sediment flux to the adjacent salt marsh platform. In addition, wave energy attenuation by seagrass meadows varies significantly over an annual cycle in response to seasonal variations in wind patterns and seagrass density (Reidenbach & Thomas, 2018). The combined effects of seasonal wind patterns and submerged seagrass density variations on sediment delivery and wave energy to back-barrier marshes need to be better addressed in spatially resolved settings, particularly if we are interested in quantifying the vertical and horizontal dynamics of back-barrier marshes.

In this study, we applied the spatially resolved hydrodynamic and sediment transport model Delft3D in a shallow coastal bay in Virginia, USA, with seagrass meadows proximal to a back-barrier marsh (South Bay, Wreck Island). Our model includes both intertidal (salt marsh) and submerged (seagrass) vegetation effects on flow, waves, and sediment resuspension, and has been parameterized and validated using long-term data from the site (wind conditions, hydrodynamic and suspended sediment data, sediment accumulation rates within seagrass meadows, and seasonal seagrass characteristics; see details in Chapters 2 & 3). The coupled model was run for 12 consecutive months with seasonally varying tides, winds, and seagrass characteristics, and a reference model case without seagrass effects was also run for the same simulation period for comparison. The annual simulation results were analyzed to address two questions. (1) How does seagrass modulate sediment connectivity between subtidal flats and back-barrier marshes over an annual cycle? (2) How does wave energy acting on marsh edges vary in response to seasonal variations in winds and seagrass density? Our results highlight the strong control seagrass has in back-barrier marshes and have implications for restoration and management strategies in shallow coastal bays with multiple plant communities.

5.2 Study site

This study was conducted in South Bay, a shallow back-barrier bay within the Virginia Coast Reserve (VCR) on Virginia's Atlantic coast (Figure 5.1a). This system is a mostly undeveloped area with high water quality and lacks significant fluvial freshwater and sediment input (McGlathery et al., 2007; Stanhope et al., 2009). The rate of SLR in the VCR bays is among the highest on the U.S. Atlantic coast, with an average value of 4–5 mm yr^{-1} during the past 40 years (https://tidesandcurrents.noaa.gov/sltrends/sltrends_station.shtml?id=8631044). South Bay has an area of ~31.5 km^2 and is bordered by a barrier island (Wreck Island) to the east and is connected to two tidal inlets that exchange water with the Atlantic Ocean (Figure 5.1b). The average water depth in the bay is 1.0 m below mean sea level and tides are semidiurnal with an average tidal range of 1.2 m (Reidenbach & Thomas, 2018). Wind-generated waves during storms are the primary agent driving strong sediment resuspension and erosion of marsh edges in the shallow bays of the VCR (Lawson et al., 2007; Mariotti et al., 2010; McLoughlin et al., 2015).

South Bay is a successful seagrass restoration site with *Zostera marina* now dominating the subtidal flats (McGlathery et al., 2012). The impact of seagrass meadows on bay dynamics varies throughout the year in response to seasonal variations in stem density (Figure 5.1c). Seagrass density in the bay reaches a maximum during early summer with a peak density higher than 500 shoots m^{-2} and reduces in late summer due to heat stress; the density slightly increases to approximately 250–300 shoots m^{-2} in autumn when the heat stress alleviates and then drops to a minimum of 50–100 shoots m^{-2} during winter senescence; seagrasses start to re-grow in the next spring when the temperature increases and the density gradually increases to 300 shoots m^{-2} in late spring (Berger et al., 2020; Hansen & Reidenbach, 2013; Reidenbach & Thomas, 2018; Rheuban et al., 2014). High-density seagrass meadows in the bay effectively attenuate flow and inhibit sediment resuspension on the tidal flats during summer growth seasons, while low-density meadows during winter senescence allow enhanced sediment resuspension during frequent and strong northeasterly winds (Hansen & Reidenbach, 2013; Zhu et al., 2021). Overall, seagrass meadows in the bay effectively trap fine particles within seagrass beds, resulting in a finer sediment grain size within the meadow (mean = 71 μm) than outside the meadow (mean = 124 μm) (McGlathery et al., 2012; Oreska et al., 2017). While subtidal flats are covered by submerged seagrass meadows in South Bay, the back-barrier side of Wreck Island is dominated by intertidal salt marshes (*Spartina alterniflora*), with an average marsh surface elevation of 0.3 m above mean sea level. During the past 20 years, marsh edges on Wreck Island have retreated at a relatively constant rate of about 0.6–0.8 m yr^{-1} (Figure A4.1).

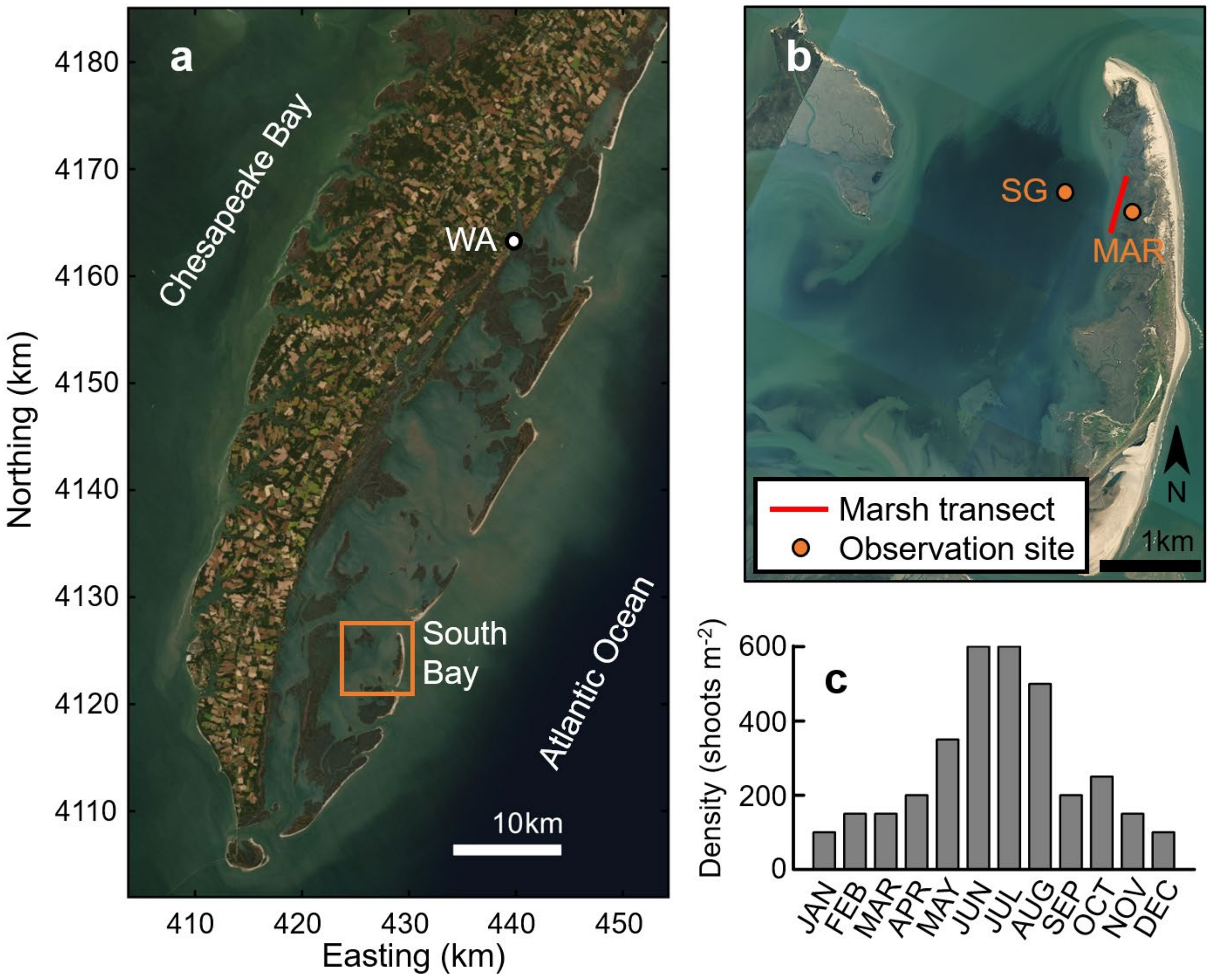

Figure 5.1 (a) Aerial image of the VCR coastal bays, (b) aerial image of South Bay and distribution of seagrass meadow, and (c) typical monthly seagrass shoot density throughout the year. WA in (a) is the NOAA tide gauge and weather station (Wachapreague, ID:8631044). The red line in (b) represents the marsh transect for sediment and wave energy flux analysis, and orange circles show locations of observation sites for hydrodynamic and suspended sediment measurements. The seagrass shoot density data shown in (c) were compiled from previous seasonal seagrass observations in South Bay (Berger et al., 2020; Hansen & Reidenbach, 2013; Reidenbach & Thomas, 2018; Rheuban et al., 2014).

5.3 Methods

We used the process-based and spatially resolved hydrodynamic and sediment transport model Delft3D (Lesser et al., 2004) coupled with the nearshore phase-averaged wave model SWAN (Booij et al., 1999) to simulate sediment transport and wave dynamics in the coupled tidal flat–seagrass–marsh system in South Bay. The model included two model domains, a locally refined model domain in South Bay with a spatial resolution of ~70 m (305 × 302 grid cells) to better resolve seagrass meadows in the bay and the bordering barrier island, and a large model domain spanning the rest of the VCR with a resolution of 200 m (148 × 444 grid cells) and providing boundary conditions for the refined model domain along the shared boundaries (Figure 2.1). The open ocean boundaries of the large model were forced with hourly water levels extracted from the NOAA tide gauge station at Wachapreague (WA, Site ID:8631044) after adjustments of tidal amplitude and phase (dampened by a factor of 0.9 and delayed 66 min) for best tidal simulation results at Wachapreague ($R^2 \geq 0.98$ and root mean square error ≤ 0.07 m). The flow model was run in depth-averaged mode and coupled hourly with the SWAN model driven by hourly wind conditions extracted from the same NOAA station at Wachapreague.

The Delft3D model uses the Partheniades–Krone formulation to calculate cohesive sediment erosion and deposition fluxes (Krone, 1962; Partheniades, 1965) and the Van Rijn et al. (2001) approach to estimate non-cohesive sediment transport. Model bathymetry and high-resolution maps of bottom sediment size distributions and properties were extracted from Wiberg et al. (2015). Three sediment classes were specified in the model, including a cohesive medium to fine silt fraction (< 32 μm), a cohesive coarse silt fraction (32–64 μm), and a non-cohesive sand fraction (125 μm). These sediment size distributions assume the bottom is unvegetated. To represent the change in bed sediment size within the meadow due to the trapping of fine sediment by seagrass, bottom sediment size distributions within the meadow in South Bay were initialized based on previous survey results from Oreska et al. (2017) in the same meadow (Figure A4.2). The Baptist vegetation model (Baptist et al., 2007) and the Suzuki vegetation wave energy dissipation model (Suzuki et al., 2012) were implemented in the Delft3D FLOW module and the SWAN model, respectively, to better resolve seagrass and marsh vegetation effects on flow, waves, and sediment resuspension. While salt marsh was considered as having constant emergent vegetation characteristics (vegetation height = 1 m, stem diameter = 0.5 cm, and shoot density = 400 shoots m^{-2}) throughout the year, seasonally varying seagrass characteristics based on previous observations in South Bay were used in the model for submerged vegetation (Figure 5.1c; Table A4.1).

After model parameterization, the coupled model was validated using summer and winter hydrodynamic and suspended sediment data during a 4-day period in January and June 2011 from a seagrass site at the center of the meadow and a nearby unvegetated site in South Bay (Figure 2.2, 2.3 in Chapter 2). Multiple model skill indices, including bias, root mean square error, and Willmott skill index (Willmott, 1981) were calculated for model validation parameters (water level, significant wave height, depth-averaged velocity, and total suspended sediment concentration) to evaluate model ability to reproduce hydrodynamic and suspended sediment characteristics within and outside the seagrass meadows in the bay. Values of these skill indices were summarized in Table 2.3 and the detailed analysis of model validation results during each period has been discussed in Chapter 2 and Zhu et al. (2021). Overall, the coupled model generated excellent skill scores for water levels (> 0.9), good skill scores for wave height and velocity (0.6–0.9), and successfully captured most sediment resuspension events at both sites with skill scores ≥ 0.8.

A follow-up study by Zhu et al. (2022; the results presented in Chapter 3) extended the simulation period of the coupled model to a complete annual cycle using winds and tidal forcing extracted from the NOAA station at WA for a representative year (August 1, 2011 to July 31, 2012; Figure A4.3), to quantify seasonal sediment accumulation rates of the seagrass meadows in the bay. A reference model case without submerged seagrass meadows and their accumulated fine-grained particles on tidal flats was also run for the same simulation period for comparison. Model simulation results show that the model case with typical seasonal seagrass characteristics predicted a meadow-averaged annual sediment accumulation rate of 4.1 mm yr^{-1}, which is 10 times greater than the rate predicted by the model case without seagrass, and that this modeled annual sediment deposition rate of the meadow is similar to long-term rates (6.3 mm yr^{-1}) estimated from in situ measurements by radiometric dating methods in the same meadow (Greiner et al., 2013; Oreska et al., 2018). Overall, the coupled model is able to provide spatially resolved simulations of hydrodynamic and sediment transport patterns within/outside the seagrass meadow with similar performance to other model studies on seagrass interactions with physical environments (Beudin et al., 2017; Chen et al., 2007; Moki et al., 2020) and to produce reasonable simulations of seasonal seagrass effects on bay dynamics in good agreements with in situ measurements in the bay (Zhu et al., 2021).

In this study, we focus on analyzing the annual simulation results from the coupled model to quantify the impacts of submerged seagrass meadows on suspended sediment delivery and wave energy flux to the adjacent back-barrier marshes. We selected a representative transect (~630 m) along the marsh edge (Figure 5.1b) for sediment flux and wave energy flux analyses. Total suspended sediment flux through the marsh transect was output from model simulations with/without seagrass in each month for comparison. Similarly, deposition at a site on the marsh behind the transect (MAR) was output from the model for each month with/without seagrass. The potential impact of wind-generated waves on marsh edge erosion was quantified using wave energy flux (also commonly referred to as wave power or wave density) output from the SWAN model every hour. A previous analysis of marsh edge erosion in the VCR coastal bays (McLoughlin et al., 2015) showed that volumetric erosion rates of marsh edges in the bays increased linearly with incident wave energy flux acting on the edges. We followed the same approach and calculated the incident wave energy flux on the monitoring marsh transect by multiplying model output wave energy flux with a refraction term $\cos(\alpha)$, where α is the angle between wave direction and the marsh edge normal direction.

Because direct observations of suspended sediment flux to the back-barrier marshes on the island were not available during the annual simulation period for model validation, additional hourly suspended sediment data were collected at a seagrass site (SG) and a marsh site (MAR) near the monitoring transect (see locations in Figure 5.1b) during a 6-day period in January 16–22, August 13–19, and September 17–23, 2020 to support our model predictions on the seasonal control of seagrass on sediment supply to back-barrier marshes. These observations were conducted during 3 storm events with similar wind conditions but in different seasons, providing an opportunity to examine seasonal impacts of seagrass on back-barrier marshes and compare with our model simulation results. At each observation site, a RBR datalogger equipped with a Seapoint optical backscatter sensor (OBS) was positioned 0.05 m above the bed to measure hourly nephelometric turbidity (NTU) and then the recorded NTU signals were converted to suspended sediment concentration (SSC) after laboratory calibration for each sensor with sediment from the site ($R^2 \geq 0.98$ for each sensor calibration).

In addition to these seasonal suspended sediment data, monthly sediment deposition rates at the marsh site MAR were measured using ceramic tiles (3 replicates with a size of 0.15 m × 0.15 m) on the marsh surface during the entire month of July 2019 and January 2020 for general comparisons with model predicted seasonal sediment deposition rates at the same site. The sediment deposited on the tiles was scraped off by a metal straight edge and dried in the oven under 60 ℃ for 48 hr and weighed.

5.4 Results

5.4.1 The impact of seagrass on marsh sediment delivery

Comparison of monthly sediment flux through the monitoring marsh transect between model simulations with/without seagrass effects shows that sediment flux to the marsh was controlled by different processes depending on whether seagrass was included in the model. When there was no seagrass in the model simulation, sediment flux to the marsh was strongly correlated with wind speed metrics (75^{th} percentile wind speed) and increased with wind speed (Figure 5.2a), with the highest sediment input to the marsh occurring in May, Aug, and September when there were strong winds impacting the system in the year of the simulation (Figure A4.3). However, when submerged seagrass meadows occupied subtidal flats, sediment flux to the marsh was controlled by seasonal variations in seagrass density. Sediment flux to the marsh decreased rapidly with seagrass density when the density was smaller than 200 shoots m^{-2}, while the flux remained low and showed little change regardless of large wind speeds during high density conditions (Figure 5.2b).

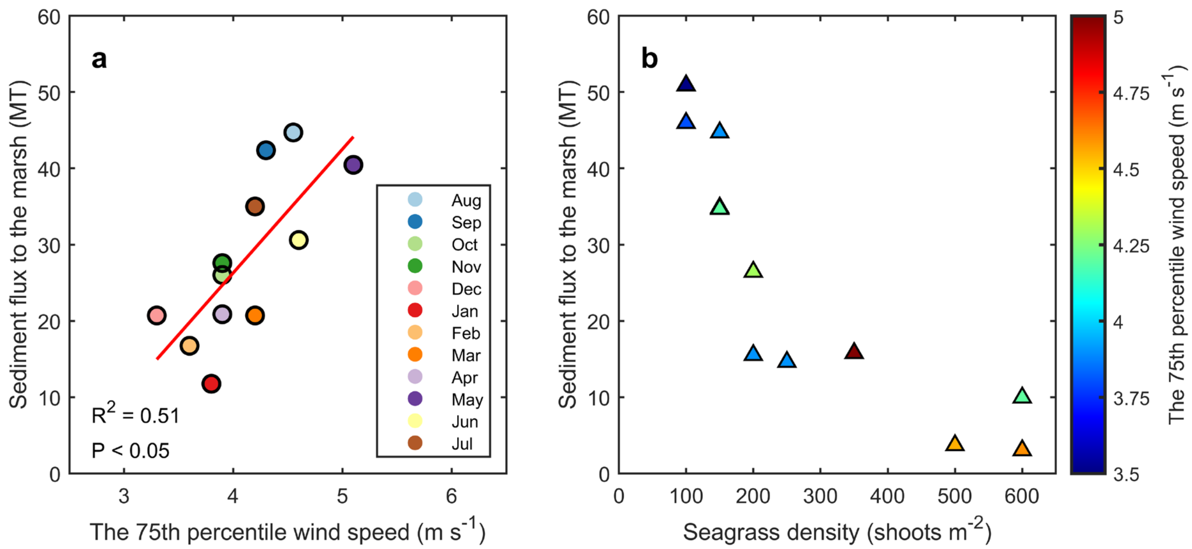

Figure 5.2 (a) Sediment flux to the marsh as a function of 75th percentile wind speeds during each month when there is no seagrass in the model, and (b) sediment flux to the marsh as a function of seagrass shoot density when seagrass effects are included in model simulations. Different colors in (a) represent the months during the annual simulation, while the color scale in (b) shows 75th percentile wind speeds of each month.

On the annual time scale, our model simulation results reveal that the presence of seagrass meadows on tidal flats altered the timing of sediment transport to the back-barrier marshes and slightly reduced total marsh sediment flux compared to unvegetated bay bottom (Figure 5.3). Total suspended sediment flux through the marsh transect output from the model run with seagrass effects (300 metric ton; hereafter referred to as MT) was slightly lower (12%) than that from the simulations without seagrass (338 MT). When there was no seagrass in the model, monthly sediment flux to the marsh was controlled by winds and remained relatively high (> 30 MT per month) from May to September (Figure 5.3b). In contrast, sediment flux to the marsh was controlled by seagrass density and reached its maximum during winter senescence (> 34 MT per month) when seagrass density reached its minimum. Because there was more fine-grained sediment accumulated in the seagrass beds in the model simulations with seagrass effects, more sediment was resuspended from the beds and transported to the marsh from November to February (seagrass density ≤ 150 shoots m^{-2}) in these simulations than those without seagrass effects (Figure 5.3b). Annual sediment deposition patterns on the marsh also varied significantly between model simulations with and without seagrass effects (Figure 5.3c); seagrass meadows altered the timing of sediment deposition on the marsh and slightly reduced total annual deposition (winter peak, density control; annual deposition of 3.0 mm yr^{-1}) compared to the simulations with no seagrass (deposition controlled by winds; annual deposition of 3.6 mm yr^{-1}).

Although direct observations of suspended sediment flux to the back-barrier marsh during the annual simulation period were not available for model validation, model predicted seasonal variations in suspended sediment flux to the marsh were generally consistent with observations of suspended sediment transported to the marsh site MAR in 2020 (Figure 5.4). Under similar storm-generated wind speed conditions (Figure 5.4a), there was stronger sediment resuspension in the seagrass meadows during winter when seagrass density was low compared with that during late summer and early fall when the density was ≥ 200 shoots m^{-2} (Figure 5.4b). Consequently, more suspended sediment was transported to the marsh during storms in winter than in high-density seasons, resulting in much higher suspended sediment concentration (SSC) at the marsh site in January (median SSC = 24.5 mg L^{-1}) than in August and September (median SSC < 5.0 mg L^{-1}; Figure 5.4b). This seasonal variation of sediment flux was also reflected in marsh deposition rate measurements by ceramic titles. Both measured and model predicted sediment deposition rates at the marsh site MAR during January (0.273 and 0.339 kg m^{-2}, respectively) were much higher than those during July (0.007 and 0.096 kg m^{-2}, respectively;

Table 5.1), indicating that high-density seagrass significantly reduced marsh sediment flux and sediment deposition on the marsh.

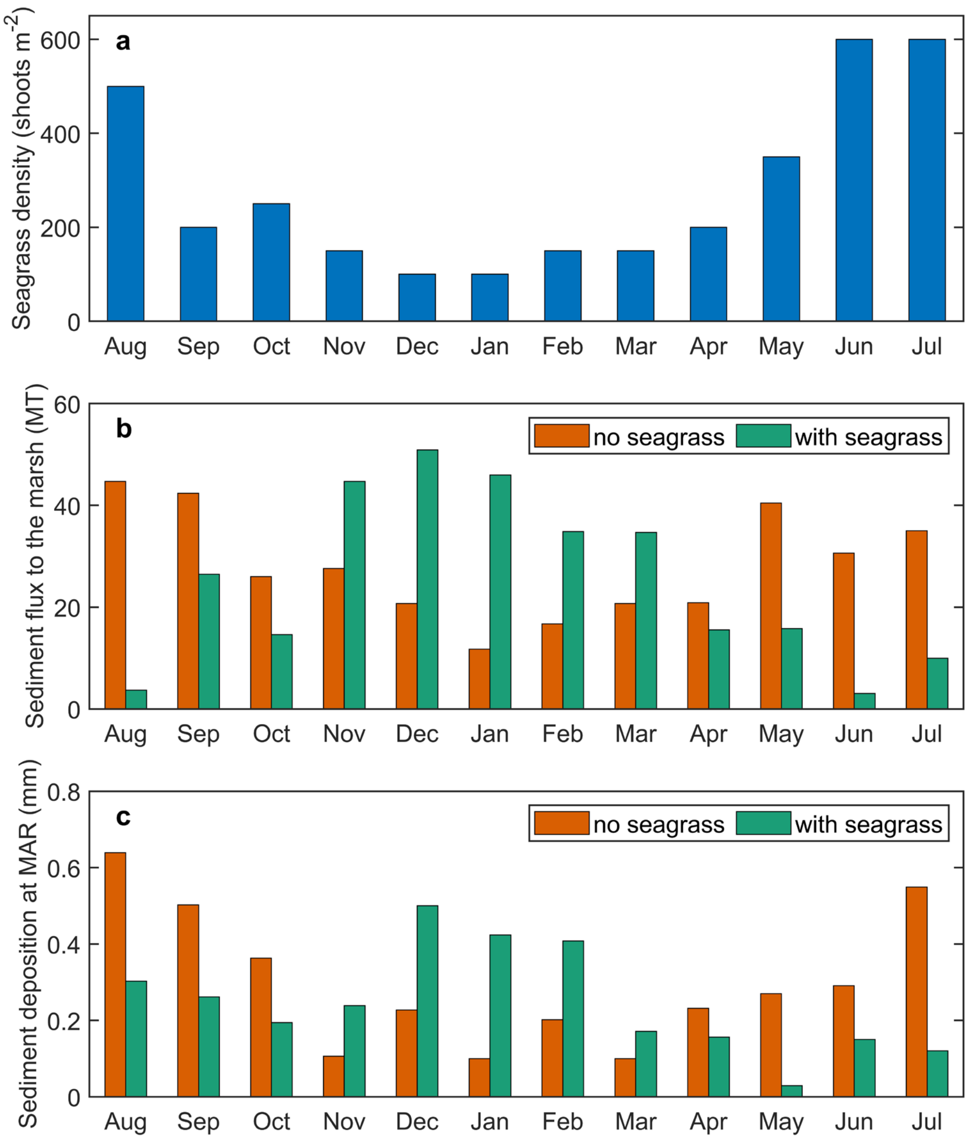

Figure 5.3 (a) Variation in seagrass shoot density during the annual simulation period, (b) changes in model predicted total suspended sediment flux to the adjacent back-barrier marshes, and (c) changes in model predicted sediment deposition at MAR with/without seagrass effects throughout the year. The model predicted an annual marsh deposition rate of 3.0 mm yr^{-1} and 3.6 mm yr^{-1} in the model simulations with and without seagrass effects, respectively.

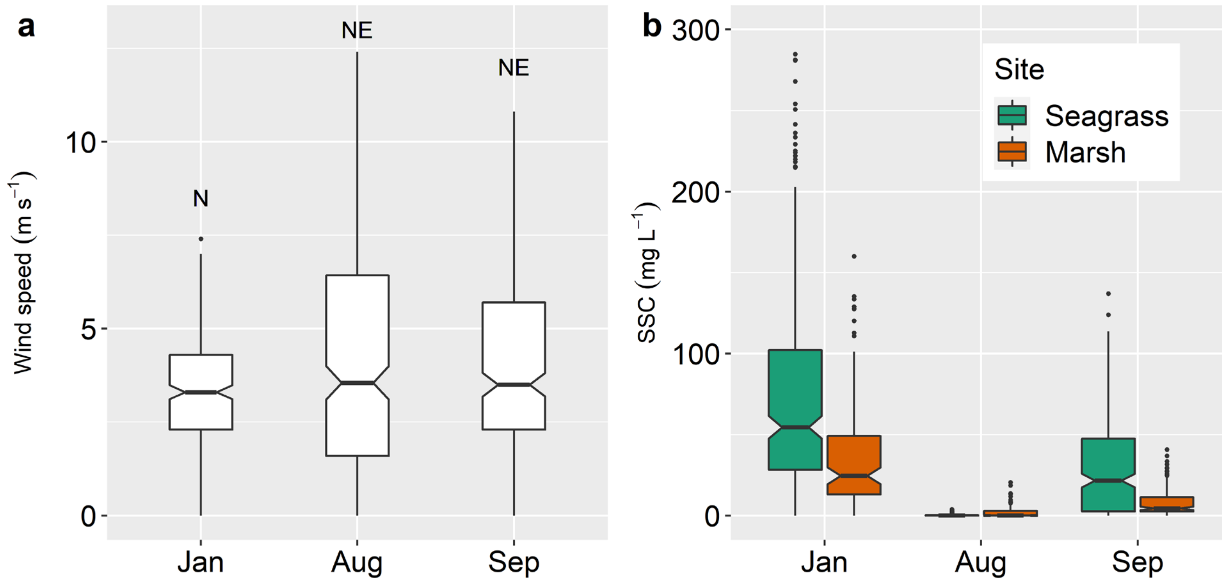

Figure 5.4 Box plots of (a) hourly wind speed and (b) suspended sediment concentration (SSC) at the seagrass site (SG) and the marsh site (MAR) during a 6-day storm period in January, August, and September 2020. Hourly wind conditions in (a) are extracted from the NOAA weather station at WA, with the dominant wind direction (blowing from) labeled on top of the whisker.

Table 5.1 Seasonal sediment deposition rates at the marsh site MAR. The measured and modeled sediment deposition rates were determined by dividing total sediment depositional mass on the ceramic tile and on the model grid cell at MAR by the corresponding area, respectively.

Season	Measured sediment deposition (kg m^{-2})	Modeled sediment deposition (kg m^{-2})
Winter (January)	0.273 ± 0.031	0.339
Summer (July)	0.007 ± 0.001	0.096

5.4.2 The impact of seagrass on wave energy attenuation on marsh edges

Seasonal growth and senescence of seagrass not only exerted a strong influence on the timing of sediment delivery to back-barrier marshes, but also altered incident wave energy flux on the marsh edges. To better understand the seasonal impact of seagrass on reducing marsh edge erosion, we divided our annual simulation results into four groups according to the seagrass growth cycle at our study site: summer growth and mid-season loss from June to August, autumn regrowth from September to October, winter senescence from November to March, and early growth from April to May. The results show that the largest overall reduction in incident wave energy flux on the marsh edge transect, 46% as indicated by the difference between the slope of the 1:1 line and the line fit to the scatter plot of incident wave energy flux output from the model simulations with/without seagrass effects, was found during summer when seagrass density was high (Figure 5.5a). When seagrass density decreased in autumn, the meadow still attenuated wave energy flux on the marsh edge but to a smaller degree (20%; Figure 5.5b). During the minimum seagrass densities in winter senescence, the reduction in incident wave energy flux induced by seagrass reached a minimum of 9% (Figure 5.5c) because of the limited effect low-density meadows had on wave attenuation. When seagrass started regrowing in the next spring, the meadow once again became more effective in attenuating wave energy flux on the marsh edges, with 25% reductions in the simulations with seagrass effects compared to the simulations with unvegetated tidal flats (Figure 5.5d).

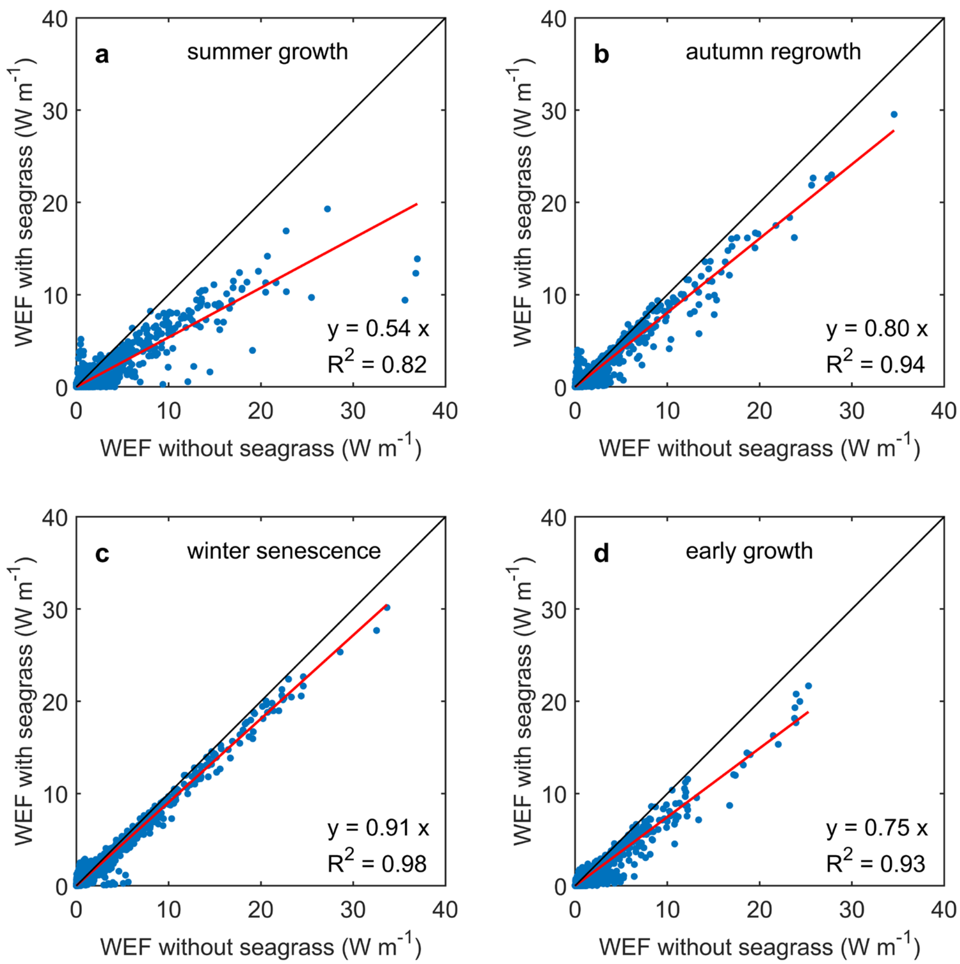

Figure 5.5 Incident wave energy flux (WEF) on the marsh transect output from model simulations with seagrass effects vs. without seagrass effects over four seasons: (a) summer growth and mid-season loss, (b) autumn regrowth, (c) winter senescence, and (d) early growth. The red line shows the linear regression line which was fit to pass through the origin, with smaller slopes indicating stronger attenuation in wave energy flux by seagrass. The black line is the 1:1 line, indicating a case with no attenuation between seagrass and no seagrass simulations.

Reductions in incident wave energy flux at the marsh edge increased linearly with seagrass density (Figure 5.6). Although there were some variations in total incident wave energy flux on the marsh edges during each month in the model simulations without seagrass effects (as indicated by the color scale in Figure 5.6), these variations in incident wave energy flux associated with seasonal wind patterns had little effect on the overall relationship between the reductions in wave energy flux on the marsh edges and seagrass density. On the annual time scale, our simulation results show that the presence of seagrass meadows on tidal flats resulted in an overall 22% reduction in incident wave energy flux on the marsh edges compared to that in the model simulations without seagrass effects (total annual wave energy flux: 1.1×10^4 vs. 1.4×10^4 W m^{-1}).

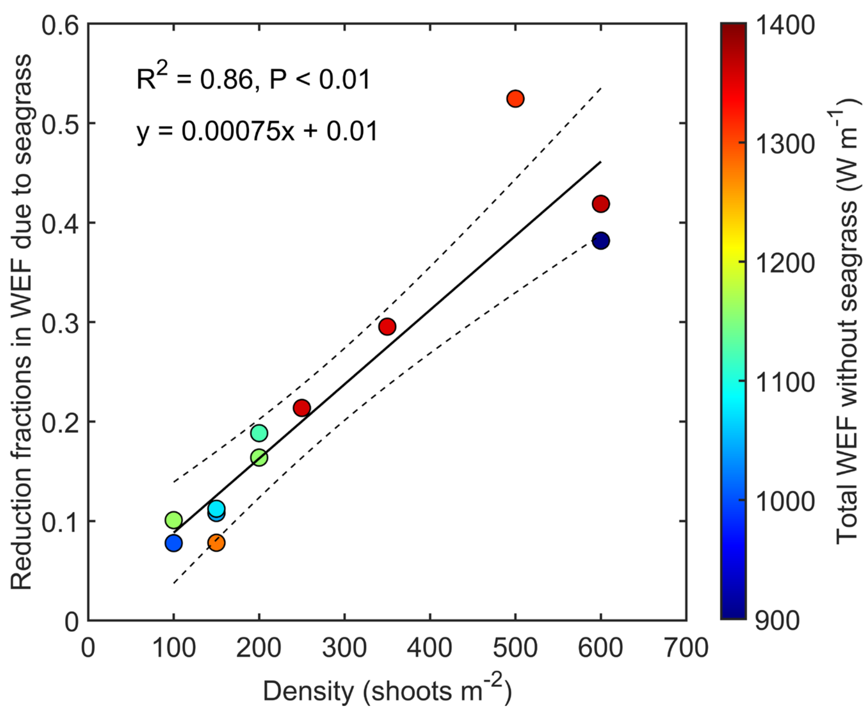

Figure 5.6 Reductions in incident wave energy flux (WEF) on the marsh edge transect due to seagrass as a function of seagrass density. The color scale shows total WEF on the marsh edge during each month in the model simulations without seagrass effects.

5.5 Discussion

The presence of submerged seagrass meadows on subtidal flats plays an important role in controlling sediment resuspension on the flats as well as sediment delivery to adjacent salt marshes (Carr et al., 2018; Hansen & Reidenbach, 2012). However, most previous research has mainly focused on sediment dynamics in high-density meadows and did not resolve the impacts of seasonal variations in seagrass density on sediment flux to the marsh in spatially resolved settings. Our annual simulation for the coupled tidal flat–seagrass–marsh system in South Bay showed that sediment fluxes to the marsh changed nonlinearly between seasons as a function of seagrass density when seagrass occupied the tidal flats. The most rapid changes in sediment flux to the marsh were found at low seagrass densities during winter senescence, while high-density meadows (> 200 shoots m^{-2}) in other seasons reduced sediment flux to the marsh to a relatively constant, low level (Figure 5.2b).

This nonlinear change of sediment flux to the marsh as a function of seagrass density is closely related to the nonlinear control of seagrass density on bed shear stress and sediment resuspension from the seabed (Ganthy et al., 2015; Peralta et al., 2008; Zhu et al., 2021). This nonlinear change of marsh sediment flux in response to seagrass density variations has implications for future scenarios of change. If seagrasses were present in lower densities due to temperature stress (Valle et al., 2014; Wilson & Lotze, 2019) or experienced meadow loss due to increasing frequency of marine heatwaves in future warming oceans (Arias-Ortiz et al., 2018; Oliver et al., 2019), meadows would become erosional and release accumulated carbon (Aoki et al., 2021; Berger et al., 2020), thereby supplying more suspended sediment to adjacent marshes. But this increase in sediment flux to the marsh associated with erosion of seagrass beds will reach a limit once the accumulated fine-grained sediment layer within the meadows has been eroded (e.g., the average thickness of the accumulated sediment layer in the restored seagrass meadows at our study site is around 12 cm; Greiner et al., 2013; Oreska et al., 2017).

Although high-density meadows significantly reduced sediment flux to the marsh during summer, our simulation results show that on an annual scale seagrasses only reduced total sediment flux to the marsh by 12% compared with the simulations without seagrass effects. This is because when seagrass effects were included in model simulations, more fine-grained sediment accumulated in the seagrass beds was resuspended into the water column and transported to the marsh platform during winter when seagrass density reached its minimum, thereby largely offsetting the low sediment input to the marsh during high-density seasons and resulting in a similar annual sediment flux to the marsh compared with the simulations with unvegetated bay bottom (Figure 5.3).

The small reduction in annual marsh sediment flux caused by seagrass predicted by our spatially resolved simulations was similar to the findings in Carr et al. (2018). They used an idealized transect-based model to quantify sediment budgets and morphodynamic changes in the coupled tidal flat–seagrass–marsh system in the VCR coastal bays over a 500-year model simulation period, and found that the normalized annual sediment flux to the marsh from tidal flats with and without seagrass was similar in magnitude but with strong seasonal variations. Our results are lower than previous estimates of the effects of submerged vegetation on reducing sediment flux to the marsh (varying from 20% to 60%; Donatelli et al., 2018; Lacy et al., 2021) which were based on field observations and model simulations during active growing seasons and therefore likely overestimate annual flux reductions. In order to obtain an accurate estimate of annual sediment flux to marshes bordering seagrass meadows, it is important to resolve sediment storage within seagrass beds and the effects of seasonal growth and senescence of seagrass.

Comparison of changes in sediment flux to the marsh with and without seagrass reveals that the presence of seagrass meadows on tidal flats significantly altered the timing of sediment transport to the marsh. When there was no seagrass in the model, or when seagrass densities were low, monthly sediment flux to the marsh was controlled by the timing of wind events. In contrast, storm events had little effect on increasing marsh sediment flux during growing seasons when there were high-density meadows on tidal flats (Figures 5.2 & 5.3). Stronger winds during low-density seasons could even generate higher sediment resuspension within a meadow compared to outside, as observed at a site with submerged aquatic vegetation in upper Chesapeake Bay in response to a major, late October storm event (Gurbisz et al., 2016). A coincidence between very strong winds and low vegetation densities could potentially supply more suspended sediment from subtidal flats to adjacent marshes and result in a higher annual marsh deposition than was captured in our annual simulations based on a year with representative wind conditions. In addition, owing to the strong seasonal control of seagrass on marsh sediment flux, marshes at our study site received much higher sediment flux during winter than other seasons (Figure 5.3b & 5.4b). The combination of low temperature and high sediment flux to the marsh during winter is beneficial to the preservation of organic-matter on the marsh (Kirwan et al., 2014) and therefore may result in a higher annual organic carbon accumulation rate on the marsh compared with the case with no seagrass on the tidal flats.

Seasonal growth and senescence of seagrass not only altered sediment delivery to the marsh, but also exerted a strong influence on attenuation of wave energy flux on marsh boundaries. Our annual simulation results show that reductions in incident wave energy flux on marsh edges caused by seagrass increased linearly with seagrass density (Figure 5.6), with the largest reduction of 46% during the summer growth period (Figure 5.5a). Although seasonal observations of wave energy flux on marsh edge were not available from the site during our annual simulation period, our predicted seasonal variations of reduction in wave energy flux by seagrass meadows are in generally good agreement with the results of a previous study in South Bay regarding the seasonal effects of seagrass on wave attenuation (Reidenbach & Thomas, 2018). Based on seasonal wave height measurements and results from an analytical wave model, this study found that attenuation of wave heights caused by seagrass in the bay was closely related with seasonal seagrass growth cycle, with the strongest attenuation during summer (30–40%) and the lowest attenuation during winter (0–15%), respectively. Our predicted attenuation of incident wave energy flux on marsh edges is also similar to the findings of Donatelli et al. (2019). Applying the COAWST modeling system in Barnegat Bay, USA, they calculated that up to 40% of the wave energy acting on fringing marsh edges can be reduced by high-density seagrass meadows in the bay and that the attenuation of wave energy on marsh edges varied with both the location and spatial extent of the meadows.

Our annual simulations with seagrass effects predicted an overall 22% reduction of the wave energy acting on marsh edges, indicating that the presence of seagrass meadows in the bay can effectively reduce marsh edge erosion caused by wind-generated waves. This finding is consistent with previous transect-based modeling studies indicating the beneficial role of seagrass in stabilizing marsh boundaries in the long-term evolution of tidal flat–seagrass–marsh systems (Carr et al., 2018; Reeves et al., 2020). It is worth noting, however, that the 22% reduction of annual incident wave energy flux on marsh edge caused by seagrass will decrease if most strong winds during the year coincide with low seagrass densities during winter (Figure

5.6). This reduction in wave energy flux could be expected to reduce the retreat rate of marsh edges by 22%, as volumetric erosion rates of marsh edges in the VCR coastal bays increased linearly with incident wave energy flux acting on the marsh edges (McLoughlin et al., 2015). Moreover, the marsh edge erosion rate at our monitoring transect can be estimated using the relationship between erosion rates and annual average wave energy flux ($y = 0.10x + 0.43$) reported by McLoughlin et al. (2015) for the VCR bays. This estimate predicts a marsh edge erosion rate of 0.56 m yr^{-1}, which is similar to rates (0.6–0.8 m yr^{-1}) determined by marsh shoreline change between 2002–2012 on Wreck Island (Figure A4.1). These estimates can be verified in future studies by a more complete analysis of marsh edge retreat rates on Wreck Island before and after the seagrass meadows occupied the subtidal flats.

Our coupled model is able to produce reasonable seasonal simulations of sediment dynamics within the coupled tidal flat–seagrass–marsh system under varying forcing and seagrass densities in spatially resolved settings (Zhu et al., 2021). Although direct observations of suspended sediment flux to the back-barrier marsh were not available during the annual simulation period, the modeled sediment fluxes to the marsh in different seagrass growing seasons are in good agreement with suspended sediment observations collected at the marsh site MAR during three seasonal storm events in 2020 (Figure 5.4b). In addition, the much higher monthly sediment deposition at MAR in January than in July predicted by the model is consistent with the sediment deposition pattern measured at the same site in a different year (Table 5.1).

On an annual timescale, our simulations with seasonal seagrass characteristics predicted an annual sediment deposition rate on the Wreck Island marsh of 3.0 mm yr^{-1} (Figure 5.3c), which is less than the rapid rates of sea-level rise (4–5 mm yr^{-1}) at our study site. Our predicted annual marsh deposition may underestimate total sediment deposition on the marsh due to the absence of organic matter trapping and contributions from overwash in model simulations, which contribute a considerable amount of sediment to total marsh deposition and may impact seasonal sediment deposition on the marsh (Kirwan & Megonigal, 2013; Walters et al., 2014). A more realistic approach would be to incorporate these processes into the coupled model. In addition, both seasonal and annual observations of marsh sediment flux and deposition that coincide with the model simulation period would help to better constrain model predictions on the sediment connectivity between seagrass meadows and the adjacent marshes in future studies. Another limitation of this study is that our model grid size (~70 m) is too coarse to resolve marsh edge retreat, which has been shown to play an important role in supplying sediment to the nearby marsh platform in some marsh systems (Hopkinson et al., 2018; Mariotti & Carr, 2014). Our model grid size also needs to be refined in future studies to better characterize the detailed sediment deposition patterns on the marsh platform, like those non-deposition/enhanced erosion zones (~10 m) near the marsh edge reported by Duvall et al. (2019).

5.6 Conclusions

Our simulation results highlight the strong seasonal control seagrass has in back-barrier marshes. The presence of seagrass meadows on tidal flats altered the timing of sediment transport to the marsh and reduced total annual flux by only 12% compared to the model case without seagrass. This has significant implications for seagrass restoration projects and coastal wetlands conservation. While high seagrass densities during growing seasons effectively reduced sediment flux to the marsh, sediment transport to the marsh was enhanced during winter as seagrass densities decreased, thereby largely offsetting the low marsh sediment input during summer. The findings present in this study, together with previous modeling studies regarding the effects of seagrass in the coupled tidal flat–marsh systems (Carr et al., 2018; Donatelli et al., 2018, 2019; Reeves et al., 2020), indicate that restoring seagrass meadows on shallow tidal flats can increase the resilience of the tidal flat–marsh system under future climate change in two ways: (1) it increases sediment deposition on tidal flats but still supplies necessary sediment for marshes to promote vertical deposition, and (2) it reduces wave energy flux on marsh edges, thereby reducing edge retreat.

References

Aoki, L. R., McGlathery, K. J., Wiberg, P. L., Oreska, M. P. J., Berger, A. C., Berg, P., & Orth, R. J. (2021). Seagrass Recovery Following Marine Heat Wave Influences Sediment Carbon Stocks. Frontiers in Marine Science, 7, 1170. https://doi.org/10.3389/fmars.2020.576784

Arias-Ortiz, A., Serrano, O., Masqué, P., Lavery, P. S., Mueller, U., Kendrick, G. A., et al. (2018). A marine heatwave drives massive losses from the world's largest seagrass carbon stocks. Nature Climate Change, 8(4), 1–7. https://doi.org/10.1038/s41558-018-0096-y

Arkema, K. K., Guannel, G., Verutes, G., Wood, S. A., Guerry, A., Ruckelshaus, M., et al. (2013). Coastal habitats shield people and property from sea-level rise and storms. Nature Climate Change 2013 3:10, 3(10), 913–918. https://doi.org/10.1038/nclimate1944

Baptist, M. J., Babovic, V., Uthurburu, J. R., Keijzer, M., Uittenbogaard, R. E., Mynett, A., & Verwey, A. (2007). On inducing equations for vegetation resistance. Journal of Hydraulic Research, 45(4), 435–450. https://doi.org/10.1080/00221686.2007.9521778

Barbier, E. B., Hacker, S. D., Kennedy, C., Koch, E. W., Stier, A. C., & Silliman, B. R. (2011). The value of estuarine and coastal ecosystem services. Ecological Monographs, 81(2), 169–193. https://doi.org/10.1890/10-1510.1

Berger, A. C., Berg, P., McGlathery, K. J., & Delgard, M. L. (2020). Long-term trends and resilience of seagrass metabolism: A decadal aquatic eddy covariance study. Limnology and Oceanography, 65(7), 1423–1438. https://doi.org/10.1002/lno.11397

Beudin, A., Kalra, T. S., Ganju, N. K., & Warner, J. C. (2017). Development of a coupled wave-flow-vegetation interaction model. Computers and Geosciences, 100, 76–86. https://doi.org/10.1016/j.cageo.2016.12.010

Booij, N., Ris, R. C., & Holthuijsen, L. H. (1999). A third-generation wave model for coastal regions 1. Model description and validation. Journal of Geophysical Research: Oceans, 104(C4), 7649–7666. https://doi.org/10.1029/98JC02622

Carr, J., Mariotti, G., Fahgerazzi, S., McGlathery, K., & Wiberg, P. (2018). Exploring the Impacts of Seagrass on Coupled Marsh-Tidal Flat Morphodynamics. Frontiers in Environmental Science, 6(SEP), 92. https://doi.org/10.3389/fenvs.2018.00092

Ceia, F. R., Patrício, J., Marques, J. C., & Dias, J. A. (2010). Coastal vulnerability in barrier islands: The high risk areas of the Ria Formosa (Portugal) system. Ocean & Coastal Management, 53(8), 478–486. https://doi.org/10.1016/J.OCECOAMAN.2010.06.004

Chen, S. N., Sanford, L. P., Koch, E. W., Shi, F., & North, E. W. (2007). A nearshore model to investigate the effects of seagrass bed geometry on wave attenuation and suspended sediment transport. Estuaries and Coasts, 30(2), 296–310. https://doi.org/10.1007/BF02700172

Davis, R. A. (1994). Barrier Island Systems — a Geologic Overview. In Geology of Holocene Barrier Island Systems (pp. 1–46). Springer, Berlin, Heidelberg. https://doi.org/10.1007/978-3-642-78360-9_1

Donatelli, C., Ganju, N. K., Fagherazzi, S., & Leonardi, N. (2018). Seagrass Impact on Sediment Exchange Between Tidal Flats and Salt Marsh, and The Sediment Budget of Shallow Bays. Geophysical Research Letters, 45(10), 4933–4943. https://doi.org/10.1029/2018GL078056

Donatelli, C., Ganju, N. K., Kalra, T. S., Fagherazzi, S., & Leonardi, N. (2019). Changes in hydrodynamics and wave energy as a result of seagrass decline along the shoreline of a microtidal back-barrier estuary. Advances in Water Resources, 128, 183–192. https://doi.org/10.1016/j.advwatres.2019.04.017

Durán Vinent, O., & Moore, L. J. (2014). Barrier island bistability induced by biophysical interactions. Nature Climate Change 2014 5:2, 5(2), 158–162. https://doi.org/10.1038/nclimate2474

Duvall, M. S., Wiberg, P. L., & Kirwan, M. L. (2019). Controls on Sediment Suspension, Flux, and Marsh Deposition near a Bay-Marsh Boundary. Estuaries and Coasts, 42(2), 403–424. https://doi.org/10.1007/s12237-018-0478-4

Feagin, R. A., Smith, W. K., Psuty, N. P., Young, D. R., Martnez, M. L., Carter, G. A., et al. (2010). Barrier Islands: Coupling Anthropogenic Stability with Ecological Sustainability. Journal of Coastal Research, 26(6), 987–992. https://doi.org/10.2112/09-1185.1

Fonseca, M. S., & Cahalan, J. A. (1992). A preliminary evaluation of wave attenuation by four species of seagrass. Estuarine, Coastal and Shelf Science, 35(6), 565–576. https://doi.org/10.1016/S0272-7714(05)80039-3

Gacia, E., & Duarte, C. M. (2001). Sediment retention by a Mediterranean Posidonia oceanica meadow: The balance between deposition and resuspension. Estuarine, Coastal and Shelf Science, 52(4), 505–514. https://doi.org/10.1006/ecss.2000.0753

Ganthy, F., Soissons, L., Sauriau, P.-G., Verney, R., & Sottolichio, A. (2015). Effects of short flexible seagrass Zostera noltei on flow, erosion and deposition processes determined using flume experiments. Sedimentology, 62(4), 997–1023. https://doi.org/10.1111/sed.12170

Greiner, J. T., McGlathery, K. J., Gunnell, J., & McKee, B. A. (2013). Seagrass Restoration Enhances “Blue Carbon” Sequestration in Coastal Waters. PLoS ONE, 8(8), e72469. https://doi.org/10.1371/journal.pone.0072469

Gurbisz, C., Kemp, W. M., Sanford, L. P., & Orth, R. J. (2016). Mechanisms of Storm-Related Loss and Resilience in a Large Submersed Plant Bed. Estuaries and Coasts, 39(4), 951–966. https://doi.org/10.1007/S12237-016-0074-4/FIGURES/10

Hansen, J., & Reidenbach, M. A. (2012). Wave and tidally driven flows in eelgrass beds and their effect on sediment suspension. Marine Ecology Progress Series, 448, 271–287. https://doi.org/10.3354/meps09225

Hansen, J., & Reidenbach, M. A. (2013). Seasonal Growth and Senescence of a Zostera marina Seagrass Meadow Alters Wave-Dominated Flow and Sediment Suspension Within a Coastal Bay. Estuaries and Coasts, 36(6), 1099–1114. https://doi.org/10.1007/s12237-013-9620-5

Hopkinson, C. S., Morris, J. T., Fagherazzi, S., Wollheim, W. M., & Raymond, P. A. (2018). Lateral Marsh Edge Erosion as a Source of Sediments for Vertical Marsh Accretion. Journal of Geophysical Research: Biogeosciences, 123(8), 2444–2465. https://doi.org/10.1029/2017JG004358

Kirwan, M. L., & Megonigal, J. P. (2013). Tidal wetland stability in the face of human impacts and sea-level rise. Nature 2013 504:7478, 504(7478), 53–60. https://doi.org/10.1038/nature12856

Kirwan, M. L., Guntenspergen, G. R., & Langley, J. A. (2014). Temperature sensitivity of organic-matter decay in tidal marshes. Biogeosciences, 11(17), 4801–4808. https://doi.org/10.5194/BG-11-4801-2014

Krone, R. B. (1962). Flume studies of the transport of sediment in estuarial shoaling processes: final report. Berkeley: University of California, Berkeley.

Lacy, J. R., Foster-Martinez, M. R., Allen, R. M., & Drexler, J. Z. (2021). Influence of Invasive Submerged Aquatic Vegetation (E. densa) on Currents and Sediment Transport in a Freshwater Tidal System. Water Resources Research, 57(8), e2020WR028789. https://doi.org/10.1029/2020WR028789

Lauzon, R., Murray, A. B., Moore, L. J., Walters, D. C., Kirwan, M. L., & Fagherazzi, S. (2018). Effects of Marsh Edge Erosion in Coupled Barrier Island-Marsh Systems and Geometric Constraints on Marsh Evolution. Journal of Geophysical Research: Earth Surface, 123(6), 1218–1234. https://doi.org/10.1029/2017JF004530

Lawson, S. E., Wiberg, P. L., McGlathery, K. J., & Fugate, D. C. (2007). Wind-driven sediment suspension controls light availability in a shallow coastal lagoon. Estuaries and Coasts, 30(1), 102–112. https://doi.org/10.1007/BF02782971

Lesser, G. R., Roelvink, J. A., van Kester, J. A. T. M. T. M., & Stelling, G. S. (2004).

Development and validation of a three-dimensional morphological model. Coastal Engineering, 51(8), 883–915. https://doi.org/10.1016/j.coastaleng.2004.07.014

Mariotti, G., Fagherazzi, S., Wiberg, P. L., McGlathery, K. J., Carniello, L., & Defina, A. (2010). Influence of storm surges and sea level on shallow tidal basin erosive processes. Journal of Geophysical Research, 115(C11), C11012. https://doi.org/10.1029/2009JC005892

Mariotti, G., & Carr, J. A. (2014). Dual role of salt marsh retreat: Long-term loss and short-term resilience. Water Resources Research, 50(4), 2963–2974. https://doi.org/10.1002/2013WR014676

McGlathery, K. J., Sundbäck, K., & Anderson, I. (2007). Eutrophication in shallow coastal bays and lagoons: the role of plants in the coastal filter. Marine Ecology Progress Series, 348, 1–18. https://doi.org/10.3354/meps07132

McGlathery, K. J., Reynolds, L. K., Cole, L. W., Orth, R. J., Marion, S. R., & Schwarzschild, A. (2012). Recovery trajectories during state change from bare sediment to eelgrass dominance. Marine Ecology Progress Series, 448, 209–221. https://doi.org/10.3354/meps09574

McLoughlin, S. M., Wiberg, P. L., Safak, I., & McGlathery, K. J. (2015). Rates and Forcing of Marsh Edge Erosion in a Shallow Coastal Bay. Estuaries and Coasts, 38(2), 620–638. https://doi.org/10.1007/s12237-014-9841-2

Moki, H., Taguchi, K., Nakagawa, Y., Montani, S., & Kuwae, T. (2020). Spatial and seasonal impacts of submerged aquatic vegetation (SAV) drag force on hydrodynamics in shallow waters. Journal of Marine Systems, 209, 103373. https://doi.org/10.1016/j.jmarsys.2020.103373

Moore, L. J., & Murray, A. B. (2018). Barrier dynamics and response to changing climate. Barrier Dynamics and Response to Changing Climate, 1–395. https://doi.org/10.1007/978-3-319-68086-6

Oliver, E. C. J., Burrows, M. T., Donat, M. G., Sen Gupta, A., Alexander, L. V., Perkins-Kirkpatrick, S. E., et al. (2019). Projected Marine Heatwaves in the 21st Century and the Potential for Ecological Impact. Frontiers in Marine Science, 6, 734. https://doi.org/10.3389/fmars.2019.00734

Oreska, M. P. J., McGlathery, K. J., & Porter, J. H. (2017). Seagrass blue carbon spatial patterns at the meadow-scale. PLoS ONE, 12(4), e0176630. https://doi.org/10.1371/journal.pone.0176630

Oreska, M. P. J., Wilkinson, G. M., McGlathery, K. J., Bost, M., & McKee, B. A. (2018). Non-seagrass carbon contributions to seagrass sediment blue carbon. Limnology and Oceanography, 63(S1), S3–S18. https://doi.org/10.1002/lno.10718

Partheniades, E. (1965). Erosion and Deposition of Cohesive Soils. Journal of the Hydraulics Division, 91(1), 105–139. https://doi.org/10.1061/JYCEAJ.0001165

Peralta, G., van Duren, L., Morris, E., & Bouma, T. (2008). Consequences of shoot density and stiffness for ecosystem engineering by benthic macrophytes in flow dominated areas: a hydrodynamic flume study. Marine Ecology Progress Series, 368, 103–115. https://doi.org/10.3354/meps07574

Reeves, I. R. B., Moore, L. J., Goldstein, E. B., Murray, A. B., Carr, J. A., & Kirwan, M. L. (2020). Impacts of Seagrass Dynamics on the Coupled Long-Term Evolution of Barrier-Marsh-Bay Systems. Journal of Geophysical Research: Biogeosciences, 125(2). https://doi.org/10.1029/2019jg005416

Reidenbach, M. A., & Thomas, E. L. (2018). Influence of the Seagrass, Zostera marina, on Wave Attenuation and Bed Shear Stress Within a Shallow Coastal Bay. Frontiers in Marine Science, 5(OCT), 397. https://doi.org/10.3389/fmars.2018.00397

Rheuban, J. E., Berg, P., & McGlathery, K. J. (2014). Ecosystem metabolism along a colonization gradient of eelgrass (Zostera marina) measured by eddy correlation. Limnology and Oceanography, 59(4), 1376–1387. https://doi.org/10.4319/lo.2014.59.4.1376

Stanhope, J. W., Anderson, I. C., & Reay, W. G. (2009). Base Flow Nutrient Discharges from Lower Delmarva Peninsula Watersheds of Virginia, USA. Journal of Environmental Quality, 38(5), 2070–2083. https://doi.org/10.2134/JEQ2008.0358

Stutz, M. L., & Pilkey, O. H. (2001). A Review of Global Barrier Island Distribution. Journal of Coastal Research, 15–22. Retrieved from http://www.jstor.org/stable/25736270

Suzuki, T., Zijlema, M., Burger, B., Meijer, M. C., & Narayan, S. (2012). Wave dissipation by vegetation with layer schematization in SWAN. Coastal Engineering, 59(1), 64–71. https://doi.org/10.1016/j.coastaleng.2011.07.006

Valle, M., Chust, G., del Campo, A., Wisz, M. S., Olsen, S. M., Garmendia, J. M., & Borja, Á. (2014). Projecting future distribution of the seagrass Zostera noltii under global warming and sea level rise. Biological Conservation, 170, 74–85. https://doi.org/10.1016/j.biocon.2013.12.017

Van Rijn, L. C., Roelvink, J. A., & Horst, W. ter. (2001). Approximation formulae for sand transport by currents and waves and implementation in DELFT-MOR. Report Z3054.20, Delft Hydraulics, Delft, The Netherlands.

Walters, D., Moore, L. J., Vinent, O. D., Fagherazzi, S., & Mariotti, G. (2014). Interactions between barrier islands and backbarrier marshes affect island system response to sea level rise: Insights from a coupled model. Journal of Geophysical Research: Earth Surface, 119(9), 2013–2031. https://doi.org/10.1002/2014JF003091

Wiberg, P. L., Carr, J. A., Safak, I., & Anutaliya, A. (2015). Quantifying the distribution and influence of non-uniform bed properties in shallow coastal bays. Limnology and Oceanography: Methods, 13(12), 746–762. https://doi.org/10.1002/lom3.10063

Willmott, C. J. (1981). On the validation of models. Physical Geography, 2(2), 184–194. https://doi.org/10.1080/02723646.1981.10642213

Wilson, K. L., & Lotze, H. K. (2019). Climate change projections reveal range shifts of eelgrass

Zostera marina in the Northwest Atlantic. Marine Ecology Progress Series, 620, 47–62. https://doi.org/10.3354/meps12973

Zhu, Q., Wiberg, P. L., & Reidenbach, M. A. (2021). Quantifying Seasonal Seagrass Effects on Flow and Sediment Dynamics in a Back‐Barrier Bay. Journal of Geophysical Research: Oceans, 126(2), e2020JC016547. https://doi.org/10.1029/2020JC016547

Zhu, Q., Wiberg, P. L., & McGlathery, K. J. (2022). Seasonal growth and senescence of seagrass alters sediment accumulation rates and carbon burial in a coastal lagoon. Limnology and Oceanography, 1–12. https://doi.org/10.1002/LNO.12178

Chapter 6. Conclusions

Understanding sediment distribution, deposition, and transport rates within seagrass and salt marsh ecosystems is critical for determining their response to disturbance events and predicting future change (Duarte et al., 2013; FitzGerald & Hughes, 2019; McGlathery et al., 2013). Based on seasonal hydrodynamic and suspended sediment field data in the VCR coastal bays and the model simulation results of the process-based and spatially resolved sediment transport model Delft3D, this dissertation provides insights into how sediment accumulation rates and transport fluxes in the coupled tidal flat–seagrass–marsh system respond to short-term disturbance events as well as seasonal variations in winds and seagrass growth cycle.

Chapters 2 and 3 show that the presence of submerged seagrass meadows on shallow tidal flats exerted a strong seasonal control in bay dynamics and sediment accumulation within the meadows. Model simulation results in South Bay show that seagrass meadows significantly attenuated flow (60%) and waves (20%) and reduced suspended sediment concentration (85%) during summer when its density reached a maximum and that significant reductions in sediment resuspension during summer were mainly caused by flow retardation rather than wave attenuation. During winter, although low densities of seagrass had relatively limited effects on attenuation of flow and waves, the meadows still provided significant reductions in wintertime sediment loss compared to losses associated with completely unvegetated conditions.

The annual simulation results in Chapter 3 reveal that organic carbon accumulation rates in the South Bay seagrass meadows were largely determined by sediment accumulation and that they both changed non-linearly as a function of seagrass shoot density. While seagrass meadows effectively trapped sediment at meadow edges during spring-summer growth seasons due to effects of strong flow reduction at high shoot densities (Hansen & Reidenbach, 2013; Peralta et al., 2008), during winter senescence low-density meadows (< 160 shoots m^{-2}) were erosional with rates sensitive to density. Based on the nonlinear relationship between sediment accumulation rates and seagrass density, density variation scenarios were designed to quantify the impacts of short-term disturbance in seagrass density on annual sediment accumulation rates of the meadows. The results show that small variations in winter seagrass densities resulted in large changes (> 40%) in annual sediment and carbon accumulation in the meadow; meadow-scale (hundreds of square meters) summer seagrass dieback due to marine heatwaves can result in annual erosion and carbon loss. This strong sensitivity of sediment accumulation rates to seagrass density variations has significant implications for future scenarios of change. If seagrasses were present in much lower densities due to degradation, physical disturbance, or increasing frequency of marine heatwaves, meadows would inevitably become erosional and release accumulated carbon (Arias-Ortiz et al., 2018; Walter et al., 2020), like the observed sediment carbon loss associated with the 2015 summer marine heatwave in South Bay seagrass meadows (Aoki et al., 2021).

The simulation results in Chapters 2 and 3 also show that edge effects play an important role in spatial patterns of sediment accumulation and carbon burial at a meadow scale. While sediment accumulation mainly occurred at meadow edges in summer growth seasons when seagrass density was relatively high, during autumn regrowth, winter senescence, and early growth seasons, lower densities of seagrass allowed sediment to be advected further into the meadow, providing the primary mechanism for sediment deposition in the interior of the meadow. This effect had not been well characterized before, and it is important to understand because it has a significant impact on spatial erosion/deposition patterns within seagrass meadows (Oreska et al., 2017).

Chapter 4 corroborates that infrequently occurring storm surge events (less than 5% of the time during a 12-year period) play a significant role in transporting suspended sediment from unvegetated tidal flats to intertidal salt marshes in Hog Bay and they disproportionately contributed ~40% of total marsh deposition around the bay. Given that most existing marsh deposition models do not include the effects of stochastic storm surge events on marsh deposition (Wiberg et al., 2020), the additional marsh deposition associated with storm surge needs to be better resolved in marsh deposition models. The detailed hydrodynamic simulations of the coupled tidal flat–marsh system in the bay during storm surge events reveal that while wind-driven waves controlled sediment resuspension on tidal flats, marsh deposition during storms was largely determined by tidal inundation associated with storm driven water levels and increased linearly with storm surge intensity. This linear relationship has significant implications for scaling marsh deposition associated with storm surge. It can be used to develop local relationships at other study sites for understanding the role of historical storm surge events on marsh deposition as well as predicting marsh elevation change in response to a change in the frequency and magnitude of storm surge events in the future.

Sediment budgets calculated from the model simulation results in Chapter 4 show that the bay experienced increased seabed erosion in response to a larger storm surge intensity and that tidal flats acted as the primary sediment source for marsh deposition (> 50%) during storm surge events. This sediment connectivity between shallow tidal flats erosion and marsh deposition during storms predicted by the model is in good agreement with recent studies on coupled tidal flat–marsh systems (Duvall et al., 2019; Lacy et al., 2020; Schuerch et al., 2019), suggesting that storms can transport significant amounts of sediment from tidal flats to the marsh surface and highlighting the importance of the close coupling of sediment dynamics in bay–marsh complexes.

Chapter 5 focuses on analyzing the annual simulation results in Chapters 2 and 3 in the context of the sediment connectivity between submerged seagrass meadows and intertidal back-barrier marshes. The results show that seagrass meadows altered the timing of sediment transport to the marsh (winter peak, density control) and reduced total annual sediment flux by 12% compared to the simulation with no seagrass (flux controlled by winds). This has implications for seagrass restoration projects and coastal wetlands conservation. While high seagrass densities during growing seasons effectively reduced sediment flux to the marsh, sediment transport to the marsh was enhanced during winter as seagrass densities decreased, thereby largely offsetting the low marsh sediment input during summer. In addition, seagrass meadows on the tidal flats also exerted a strong seasonal influence on attenuation of wave energy flux on marsh boundaries and resulted in an overall 22% reduction of wave energy acting on the marsh edge during the annual simulation period. The findings presented in this dissertation, together with previous modeling studies regarding the effects of seagrass in the coupled tidal flat–marsh systems (Carr et al., 2018; Nardin et al., 2018; Reeves et al., 2020), indicate that restoring seagrass meadows on shallow tidal flats can increase the resilience of the tidal flat–marsh system under future climate change in two ways: (1) it increases sediment deposition on tidal flats but still supplies necessary sediment for marshes to promote vertical deposition, and (2) it reduces wave energy flux on marsh edges, thereby effectively reducing edge retreat.

One of the limitations of this study is the absence of organic matter trapping and vegetation growth dynamics in model simulations, which contributes a considerable amount of sediment to total sediment deposition in coastal wetlands (Kirwan & Megonigal, 2013). Several studies have successfully integrated these processes in Delft3D simulations by applying a vegetation population dynamics approach that depends on vegetation colonization, growth, mortality, and interactions with hydro-morphodynamic processes (Best et al., 2018; Brückner et al., 2019). In future studies, including vegetation growth dynamics and bio-accumulation in model simulations would help to better characterize ecomorphodynamic processes and improve model predictive capabilities for future changes. In addition, the model grid size (≥ 50 m) in this study was too coarse to resolve marsh edge retreat, which is a highly dynamic feature in the coupled tidal flat–marsh system and plays an important role in the stability of bay–marsh boundaries and the overall sediment budgets of the system (Hopkinson et al., 2018; Leonardi et al., 2016; Mariotti & Carr, 2014). In future studies, a better coupling of horizontal and vertical marsh dynamics in spatially explicit models will be needed to obtain more holistic sediment budgets for the coupled tidal flat–marsh system and a better understanding of the effects of seagrass meadows on reducing marsh edge retreat.

Overall, the coupled model presented in this dissertation has been parameterized and extensively validated using long-term data from the VCR coastal bays (wind conditions, hydrodynamic and suspended sediment data, sediment accumulation rates, and vegetation characteristics) and was able to produce reasonable spatially-resolved simulations of flow and sediment dynamics in the coupled tidal flat–seagrass–marsh system under seasonally varying winds, tides, and seagrass densities. These spatially resolved simulations of hydrodynamic and suspended sediment variables predicted by the model can provide valuable information for habitat studies as well as seagrass and oyster restoration projects at the study site (Besterman et al., 2021; Hogan et al., 2021; Oreska et al., 2021). The model can also be used to explore the morphodynamic response of the coupled system to changes in the frequency and magnitude of episodic disturbance events (e.g., storm surge and marine heatwaves) in the future.

The results in this dissertation highlight the strong control vegetation has in erosional and depositional processes in shallow coastal bays and the complex dynamics in the coupled tidal flat–seagrass–marsh system. These findings have significant implications for the resilience of seagrass and marsh sediment accumulation under future climate change and provide practical guidelines for process-based modeling of flow–wave–vegetation–sediment interactions in shallow coastal environments.

References

Aoki, L. R., McGlathery, K. J., Wiberg, P. L., Oreska, M. P. J., Berger, A. C., Berg, P., & Orth, R. J. (2021). Seagrass Recovery Following Marine Heat Wave Influences Sediment Carbon Stocks. Frontiers in Marine Science, 7, 1170. https://doi.org/10.3389/fmars.2020.576784

Arias-Ortiz, A., Serrano, O., Masqué, P., Lavery, P. S., Mueller, U., Kendrick, G. A., et al. (2018). A marine heatwave drives massive losses from the world's largest seagrass carbon stocks. Nature Climate Change, 8(4), 1–7. https://doi.org/10.1038/s41558-018-0096-y

Best, S. N., Van der Wegen, M., Dijkstra, J., Willemsen, P. W. J. M., Borsje, B. W., & Roelvink, D. J. A. (2018). Do salt marshes survive sea level rise? Modelling wave action, morphodynamics and vegetation dynamics. Environmental Modelling and Software, 109, 152–166. https://doi.org/10.1016/j.envsoft.2018.08.004

Besterman, A. F., McGlathery, K. J., Reidenbach, M. A., Wiberg, P. L., & Pace, M. L. (2021). Predicting benthic macroalgal abundance in shallow coastal lagoons from geomorphology and hydrologic flow patterns. Limnology and Oceanography, 66(1), 123–140. https://doi.org/10.1002/LNO.11592

Brückner, M. Z. M., Schwarz, C., Dijk, W. M., Oorschot, M., Douma, H., & Kleinhans, M. G. (2019). Salt Marsh Establishment and Eco‐Engineering Effects in Dynamic Estuaries Determined by Species Growth and Mortality. Journal of Geophysical Research: Earth Surface, 124(12), 2962–2986. https://doi.org/10.1029/2019JF005092

Carr, J., Mariotti, G., Fahgerazzi, S., McGlathery, K., & Wiberg, P. (2018). Exploring the Impacts of Seagrass on Coupled Marsh-Tidal Flat Morphodynamics. Frontiers in Environmental Science, 6(SEP), 92. https://doi.org/10.3389/fenvs.2018.00092

Duarte, C. M., Losada, I. J., Hendriks, I. E., Mazarrasa, I., & Marbà, N. (2013). The role of coastal plant communities for climate change mitigation and adaptation. Nature Climate Change 2013 3:11, 3(11), 961–968. https://doi.org/10.1038/nclimate1970

Duvall, M. S., Wiberg, P. L., & Kirwan, M. L. (2019). Controls on Sediment Suspension, Flux, and Marsh Deposition near a Bay-Marsh Boundary. Estuaries and Coasts, 42(2), 403–424. https://doi.org/10.1007/s12237-018-0478-4

FitzGerald, D. M., & Hughes, Z. (2019). Marsh Processes and Their Response to Climate Change and Sea-Level Rise. Annual Review of Earth and Planetary Sciences, 47, 481–517. https://doi.org/10.1146/ANNUREV-EARTH-082517-010255

Hansen, J., & Reidenbach, M. A. (2013). Seasonal Growth and Senescence of a Zostera marina Seagrass Meadow Alters Wave-Dominated Flow and Sediment Suspension Within a Coastal Bay. Estuaries and Coasts, 36(6), 1099–1114. https://doi.org/10.1007/s12237-013-9620-5

Hogan, S., Wiberg, P. L., & Reidenbach, M. A. (2021). Utilizing airborne LiDAR data to quantify marsh edge morphology and the role of oyster reefs in mitigating marsh erosion. Marine Ecology Progress Series, 669, 17–31. https://doi.org/10.3354/MEPS13728

Hopkinson, C. S., Morris, J. T., Fagherazzi, S., Wollheim, W. M., & Raymond, P. A. (2018). Lateral Marsh Edge Erosion as a Source of Sediments for Vertical Marsh Accretion. Journal of Geophysical Research: Biogeosciences, 123(8), 2444–2465. https://doi.org/10.1029/2017JG004358

Kirwan, M. L., & Megonigal, J. P. (2013). Tidal wetland stability in the face of human impacts and sea-level rise. Nature 2013 504:7478, 504(7478), 53–60. https://doi.org/10.1038/nature12856

Lacy, J. R., Foster‐Martinez, M. R., Allen, R. M., Ferner, M. C., & Callaway, J. C. (2020). Seasonal Variation in Sediment Delivery Across the Bay‐Marsh Interface of an Estuarine Salt Marsh. Journal of Geophysical Research: Oceans, 125(1). https://doi.org/10.1029/2019jc015268

Leonardi, N., Ganju, N. K., & Fagherazzi, S. (2016). A linear relationship between wave power and erosion determines salt-marsh resilience to violent storms and hurricanes. Proceedings of the National Academy of Sciences, 113(1), 64–68. https://doi.org/10.1073/PNAS.1510095112

Mariotti, G., & Carr, J. A. (2014). Dual role of salt marsh retreat: Long-term loss and short-term resilience. Water Resources Research, 50(4), 2963–2974. https://doi.org/10.1002/2013WR014676

McGlathery, K., Reidenbach, M., D'Odorico, P., Fagherazzi, S., Pace, M., & Porter, J. (2013). Nonlinear Dynamics and Alternative Stable States in Shallow Coastal Systems. Oceanography, 26(3), 220–231. https://doi.org/10.5670/oceanog.2013.66

Nardin, W., Larsen, L., Fagherazzi, S., & Wiberg, P. (2018). Tradeoffs among hydrodynamics, sediment fluxes and vegetation community in the Virginia Coast Reserve, USA. Estuarine, Coastal and Shelf Science, 210, 98–108. https://doi.org/10.1016/j.ecss.2018.06.009

Oreska, M. P. J., McGlathery, K. J., & Porter, J. H. (2017). Seagrass blue carbon spatial patterns at the meadow-scale. PLoS ONE, 12(4), e0176630. https://doi.org/10.1371/journal.pone.0176630

Oreska, M. P. J., McGlathery, K. J., Wiberg, P. L., Orth, R. J., & Wilcox, D. J. (2021). Defining the Zostera marina (Eelgrass) Niche from Long-Term Success of Restored and Naturally Colonized Meadows: Implications for Seagrass Restoration. Estuaries and Coasts, 44(2), 396–411. https://doi.org/10.1007/S12237-020-00881-3/FIGURES/6

Peralta, G., van Duren, L., Morris, E., & Bouma, T. (2008). Consequences of shoot density and stiffness for ecosystem engineering by benthic macrophytes in flow dominated areas: a hydrodynamic flume study. Marine Ecology Progress Series, 368, 103–115. https://doi.org/10.3354/meps07574

Reeves, I. R. B., Moore, L. J., Goldstein, E. B., Murray, A. B., Carr, J. A., & Kirwan, M. L. (2020). Impacts of Seagrass Dynamics on the Coupled Long-Term Evolution of Barrier-Marsh-Bay Systems. Journal of Geophysical Research: Biogeosciences, 125(2). https://doi.org/10.1029/2019jg005416

Schuerch, M., Spencer, T., & Evans, B. (2019). Coupling between tidal mudflats and salt marshes affects marsh morphology. Marine Geology, 412, 95–106. https://doi.org/10.1016/j.margeo.2019.03.008

Walter, R. K., O'Leary, J. K., Vitousek, S., Taherkhani, M., Geraghty, C., & Kitajima, A. (2020). Large-scale erosion driven by intertidal eelgrass loss in an estuarine environment. Estuarine, Coastal and Shelf Science, 243, 106910. https://doi.org/10.1016/j.ecss.2020.106910

Wiberg, P. L., Fagherazzi, S., & Kirwan, M. L. (2020). Improving Predictions of Salt Marsh Evolution Through Better Integration of Data and Models. Annual Review of Marine Science, 12(1), 389–413. https://doi.org/10.1146/annurev-marine-010419-010610

Appendix 1: Supplemental information to Chapter 2

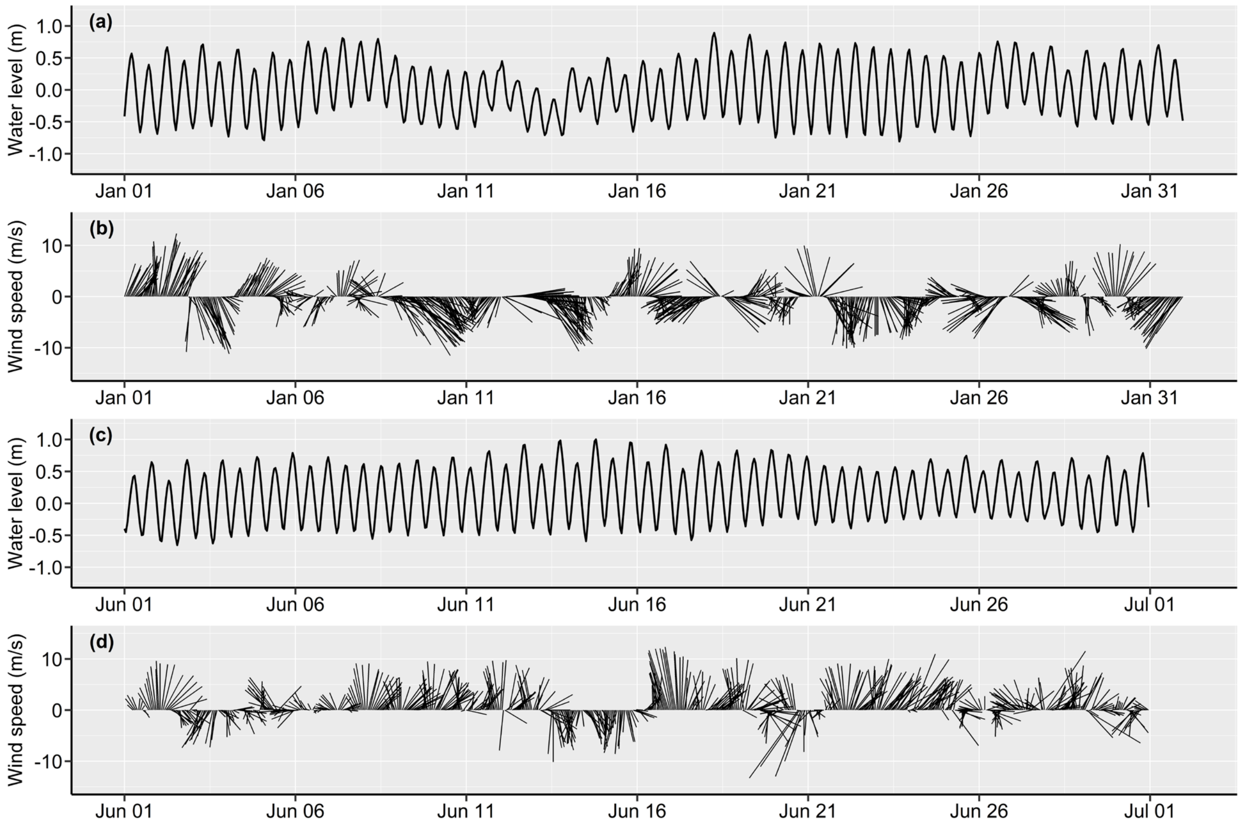

Figure A1.1 Model forcing conditions for each time period: (a) water level and (b) winds in January, and (c) water level and (d) winds in June. Water levels are extracted from NOAA tide gauge record at Wachapreague (https://tidesandcurrents.noaa.gov). The wind data is from the NOAA National Data Buoy Center (Station CHLV2; https://www.ndbc.noaa.gov/station_page.php?station=chlv2).

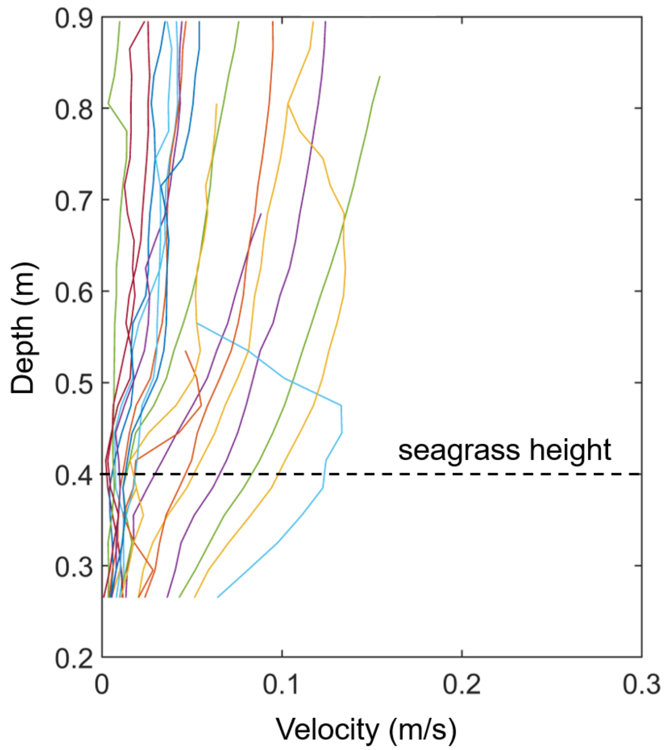

Figure A1.2 Velocity profiles measured at the seagrass site in June, 2011 (first 25-hrs of data are plotted). The dashed line shows the seagrass height.

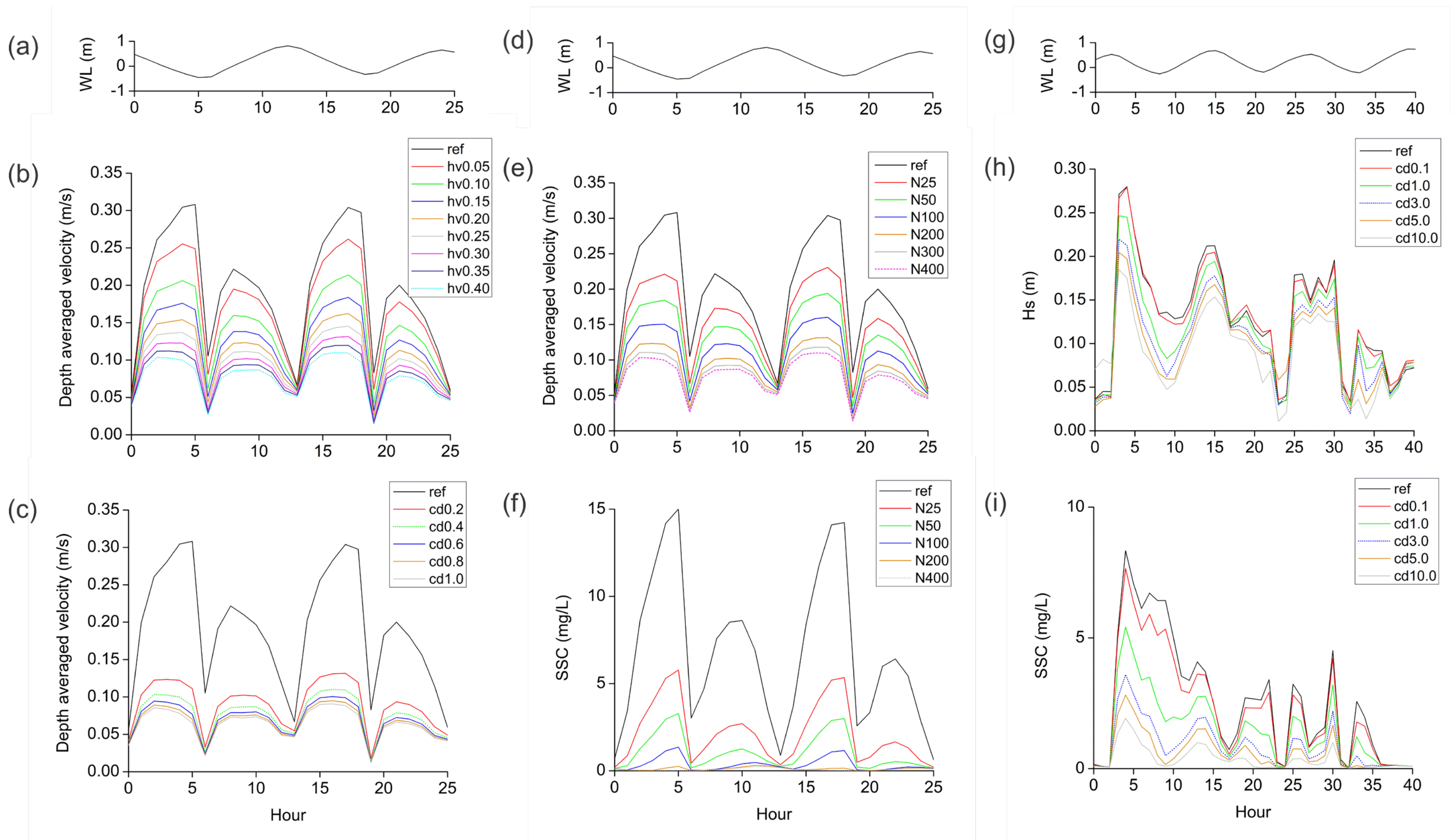

Figure A1.3 Model calibration and sensitivity test: (a) water levels under flow test, (b) effects of vegetation height on flow, (c) effects of vegetation flow drag coefficient on flow, (d) water levels under flow test, (e) effects of vegetation density on flow, (f) effects of vegetation density on SSC, (g) water levels under wave test, (h) effects of vegetation wave drag coefficient on Hs, and (i) effects of vegetation wave drag coefficient on SSC. Dashed lines show simulation results using typical summer seagrass characteristics with h_v= 0.4 m, b_v = 0.4 cm, N = 300, C_D = 0.4, and $\widetilde{C_D}$ = 3.0. ref shows simulation results at the seagrass site (SG) without vegetation effects.

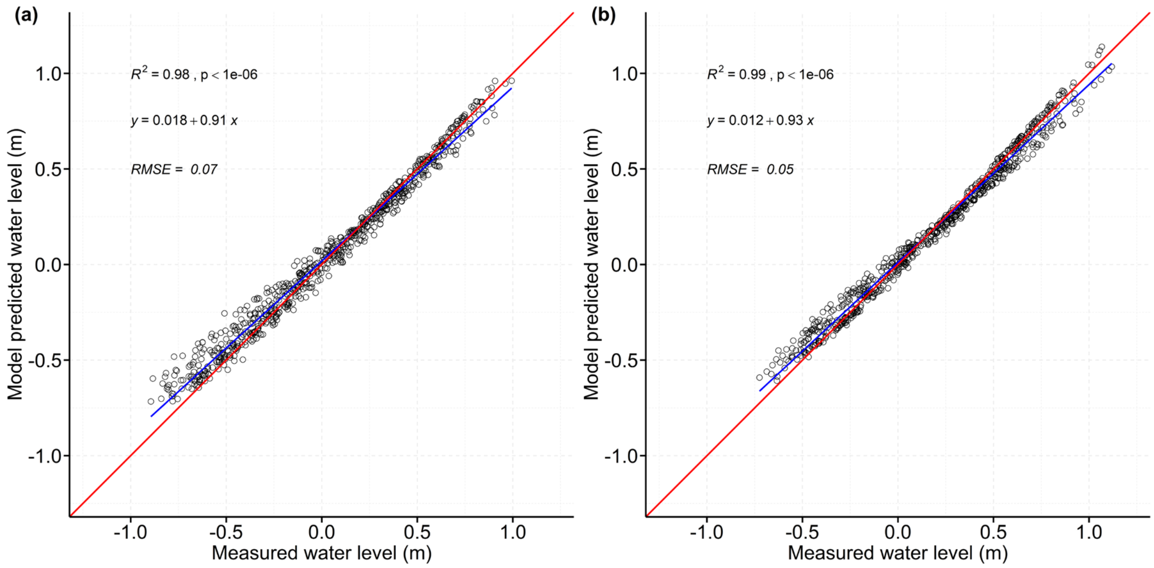

Figure A1.4 Comparison between modeled and measured water levels at Wachapreague (WA) in: (a) January and (b) June, 2011. Red lines show the 1:1 relationship, and blue lines show the linear fitting curve.

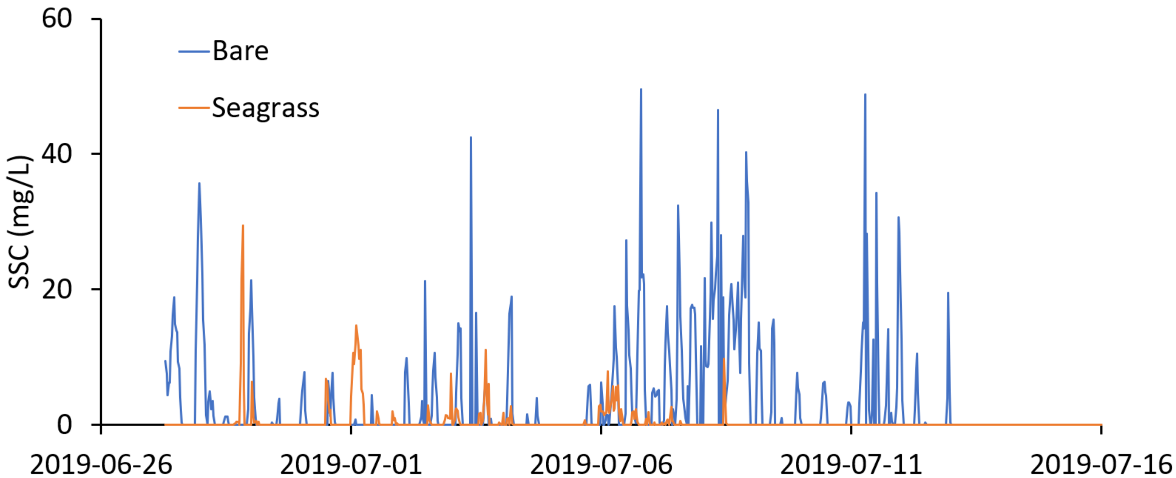

Figure A1.5 Time series of suspended sediment concentration measured at the seagrass site and the nearby bare site in 2019 summer.

Appendix 2: Supplemental information to Chapter 3

Table A2.1 Seagrass parameters input for the model. *N* is seagrass shoot density, h_v is vegetation height, b_v is stem diameter, C_D is seagrass flow drag coefficient, and $\widetilde{C_D}$ is seagrass wave drag coefficient. LD in January indicates low-density scenarios with lower shoot density than typical value of 100 shoots m^{-2}. Seagrass characteristics (density, height, and stem diameter) in the table are compiled from previous seasonal seagrass observations in South Bay (Berger et al., 2020; Hansen & Reidenbach, 2013; Reidenbach & Thomas, 2018; Rheuban et al., 2014) and have been adjusted based on seagrass growth cycle.

Simulation period	*N* (shoots m^{-2})	0.8**N* (shoots m^{-2})	0.6**N* (shoots m^{-2})	h_v (m)	b_v (cm)	C_D	$\widetilde{C_D}$
AUG, 2011	500	400	300	0.4	0.4	0.4	3.0
SEP, 2011	200	160	120	0.3	0.3	0.3	3.0
OCT, 2011	250	200	150	0.3	0.3	0.3	3.0
NOV, 2011	150	120	90	0.2	0.2	0.2	3.0
DEC, 2011	100	80	60	0.2	0.2	0.2	3.0
JAN, 2012	100	80	60	0.2	0.2	0.2	3.0
JAN, 2012 (LD)	50	40	30	0.2	0.2	0.2	3.0
JAN, 2012 (LD)	25	20	15	0.2	0.2	0.2	3.0
JAN, 2012 (LD)	0	0	0	0	0	0	0
FEB, 2012	150	120	90	0.2	0.2	0.2	3.0
MAR, 2012	150	120	90	0.2	0.2	0.2	3.0
APR, 2012	200	160	120	0.3	0.3	0.3	3.0
MAY, 2012	350	280	210	0.3	0.3	0.3	3.0
JUN, 2012	600	480	360	0.4	0.4	0.4	3.0
JUL, 2012	600	480	360	0.4	0.4	0.4	3.0

Table A2.2 Willmott skill indices for model validation parameters. A skill of 1 indicates perfect model predictions, while a skill of zero shows no correlation between model prediction and observation.

Season	Parameter	Site	
		Bare	Seagrass
January	Water level	0.95	0.94
	Wave height	0.68	0.87
	Velocity	0.84	N/A
	Suspended sediment concentration	0.80	0.82
June	Water level	0.97	0.96
	Wave height	0.56	0.67
	Velocity	0.69	0.58
	Suspended sediment concentration	N/A	N/A

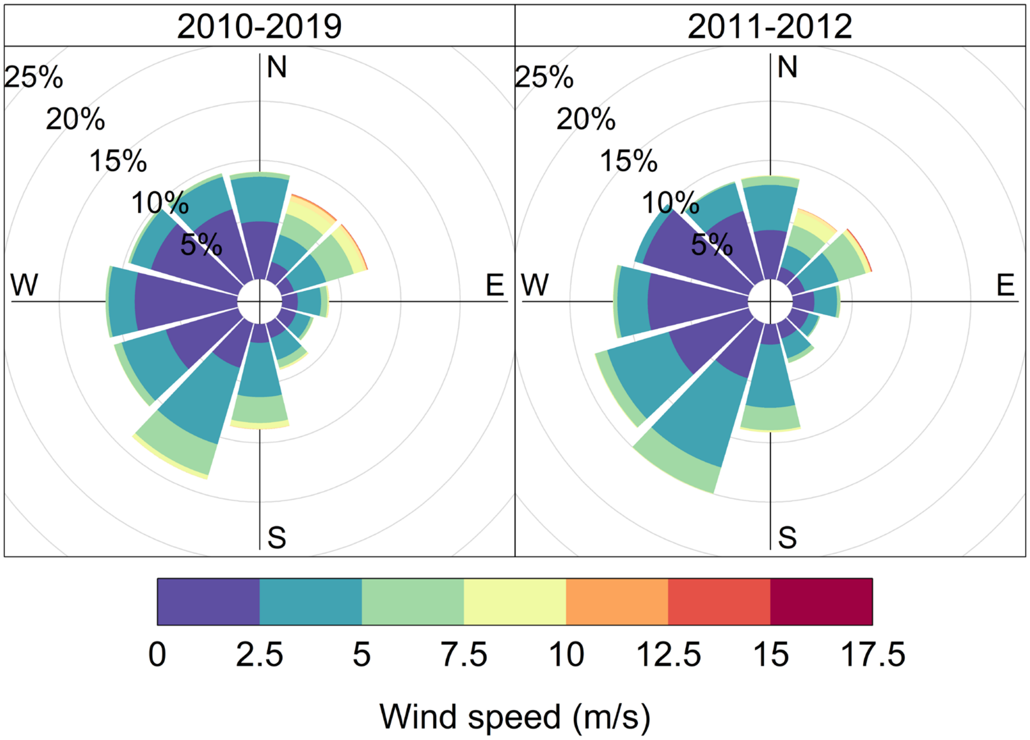

Figure A2.1 Directional distributions of winds in the study area during 2010-2019 and during the model simulation period (August 1, 2011 to July 31, 2012). The wind data are from the NOAA weather station at Wachapreague (https://tidesandcurrents.noaa.gov/stationhome.html?id=8631044).

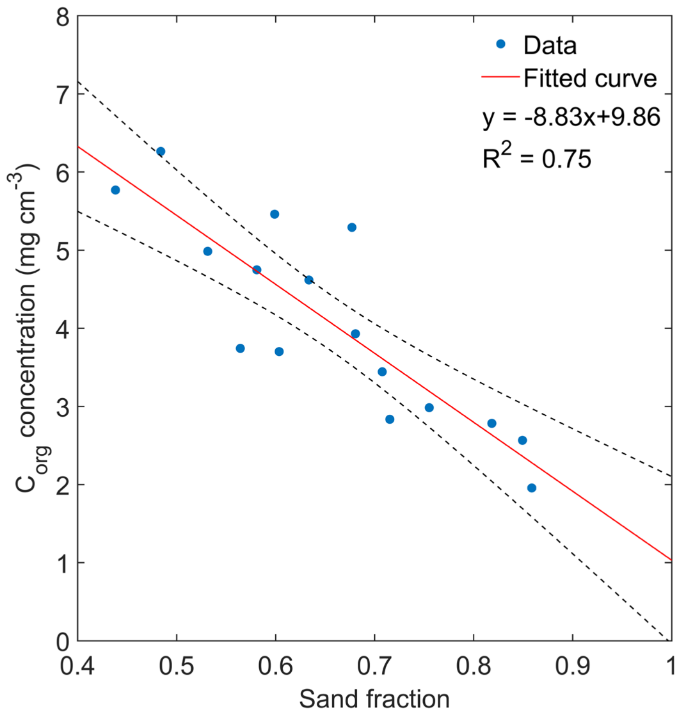

Figure A2.2 Relationship between sediment organic carbon concentration and sand fraction in South Bay seagrass meadows. Data of sediment organic carbon concentration and sand fraction were from Oreska et at. (2017).

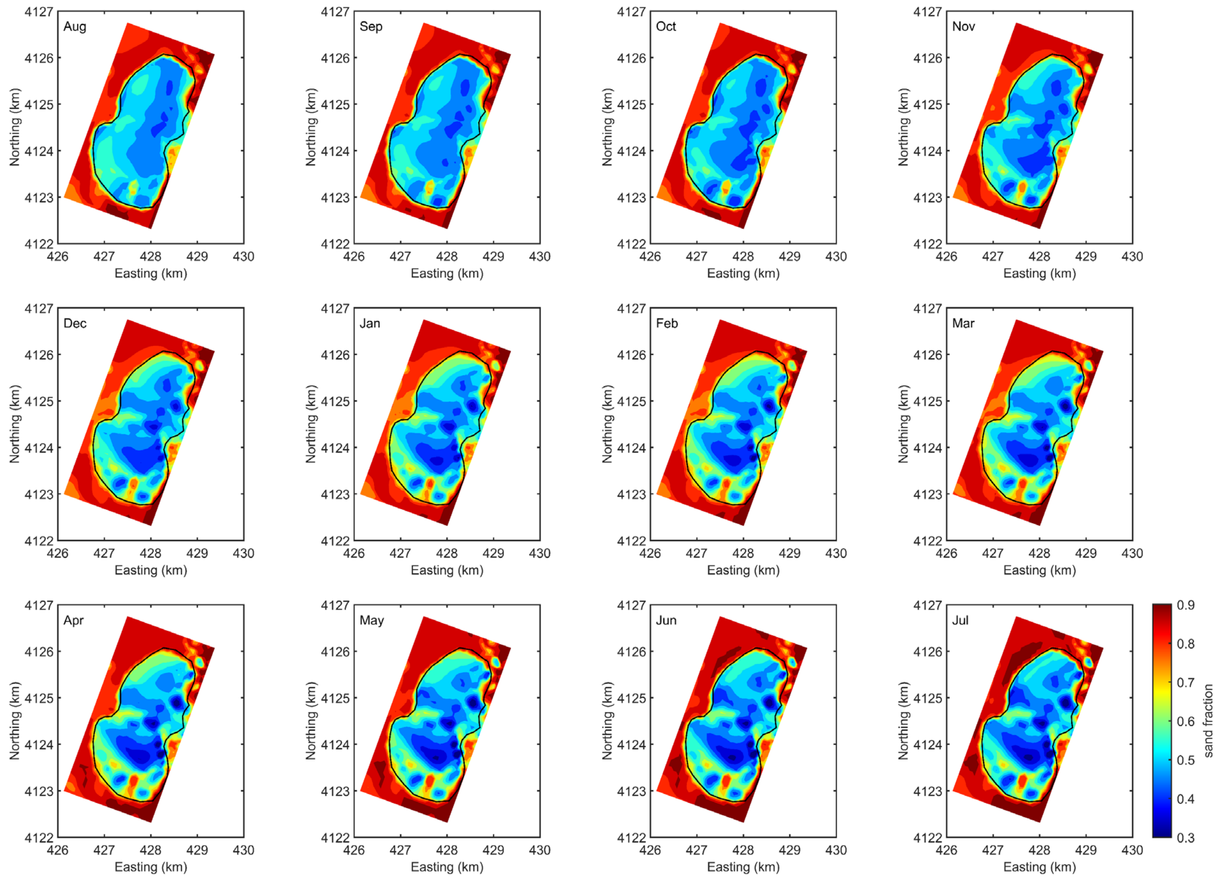

Figure A2.3 Monthly distributions of sand fraction output from simulations with seagrass effects. The black line shows the meadow outline.

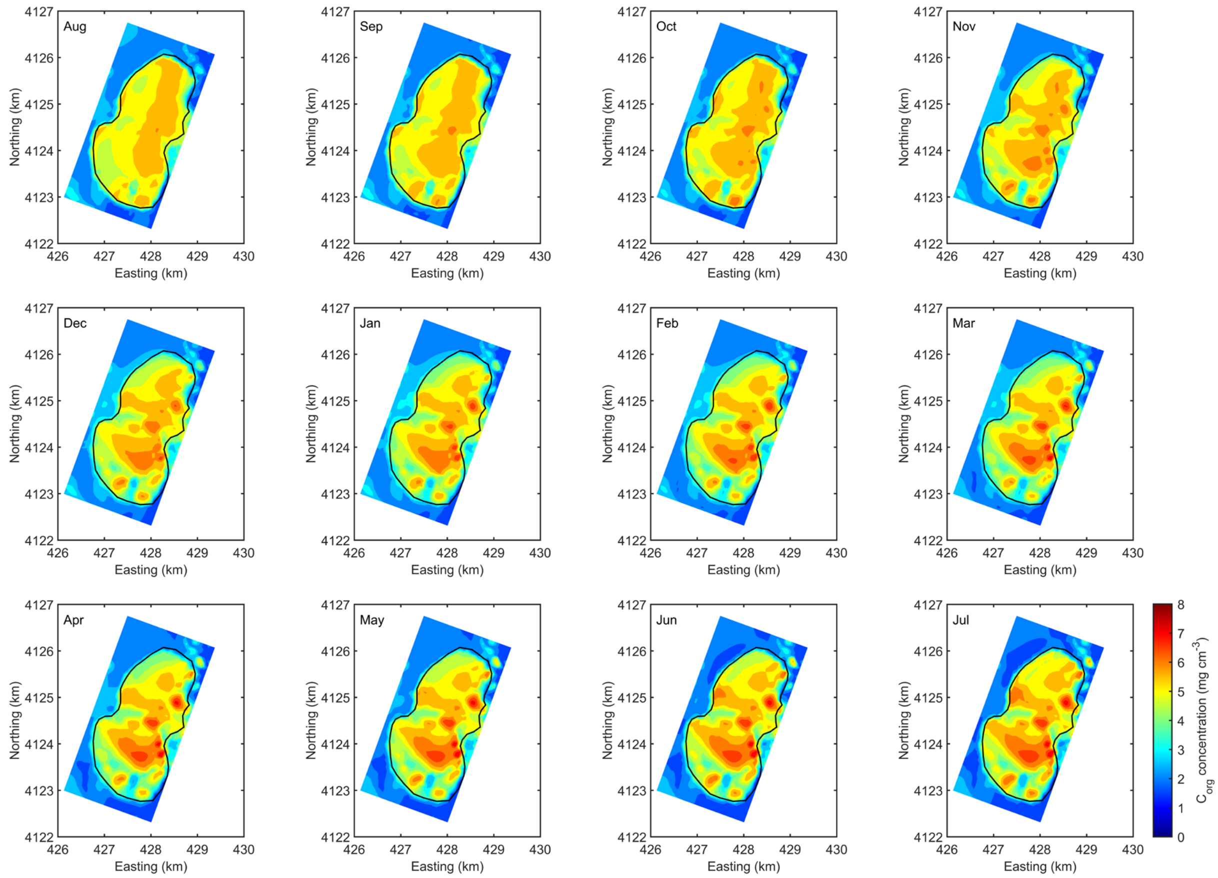

Figure A2.4 Monthly distributions of sediment organic carbon concentration converted from the sand fraction map in Figure A2.3. The black line shows the meadow outline.

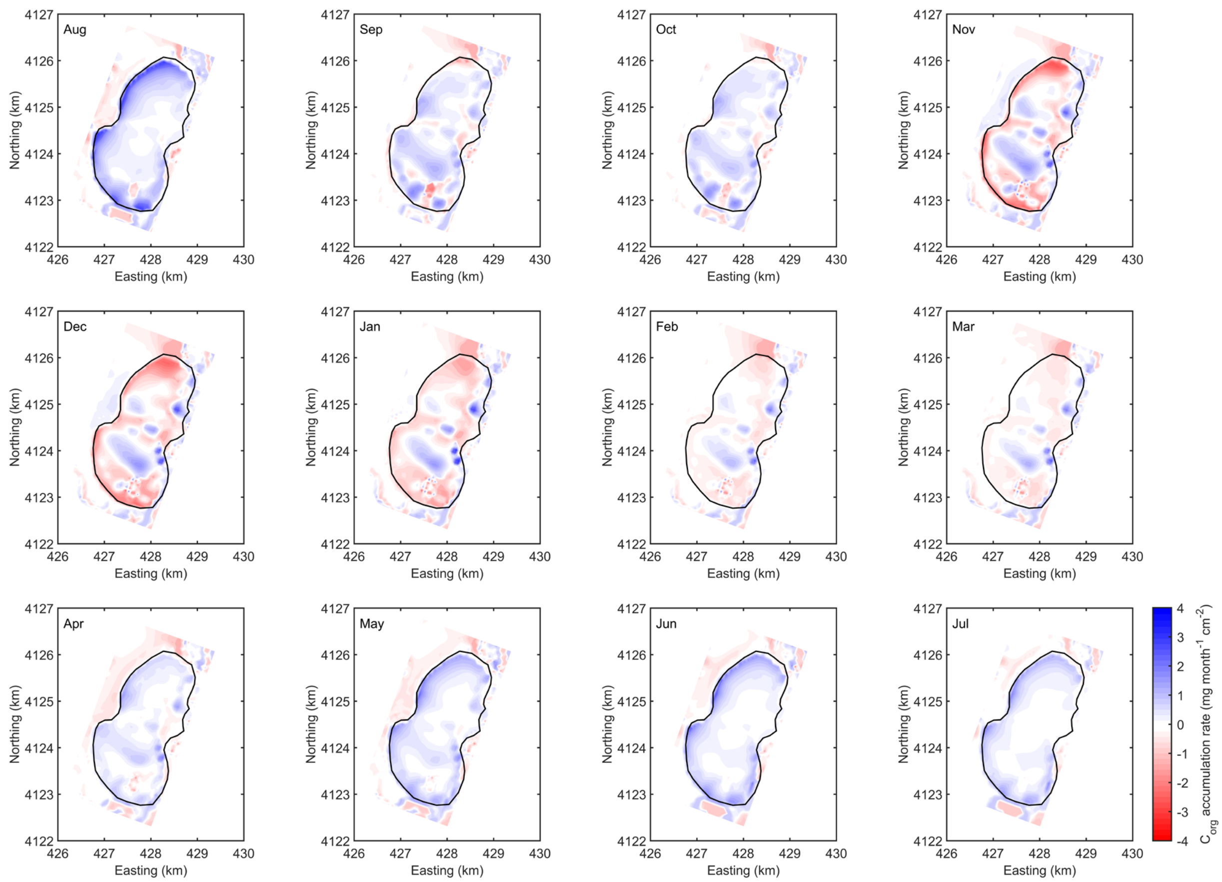

Figure A2.5 Monthly distributions of organic carbon accumulation rates in the seagrass meadow. The black line shows the meadow outline.

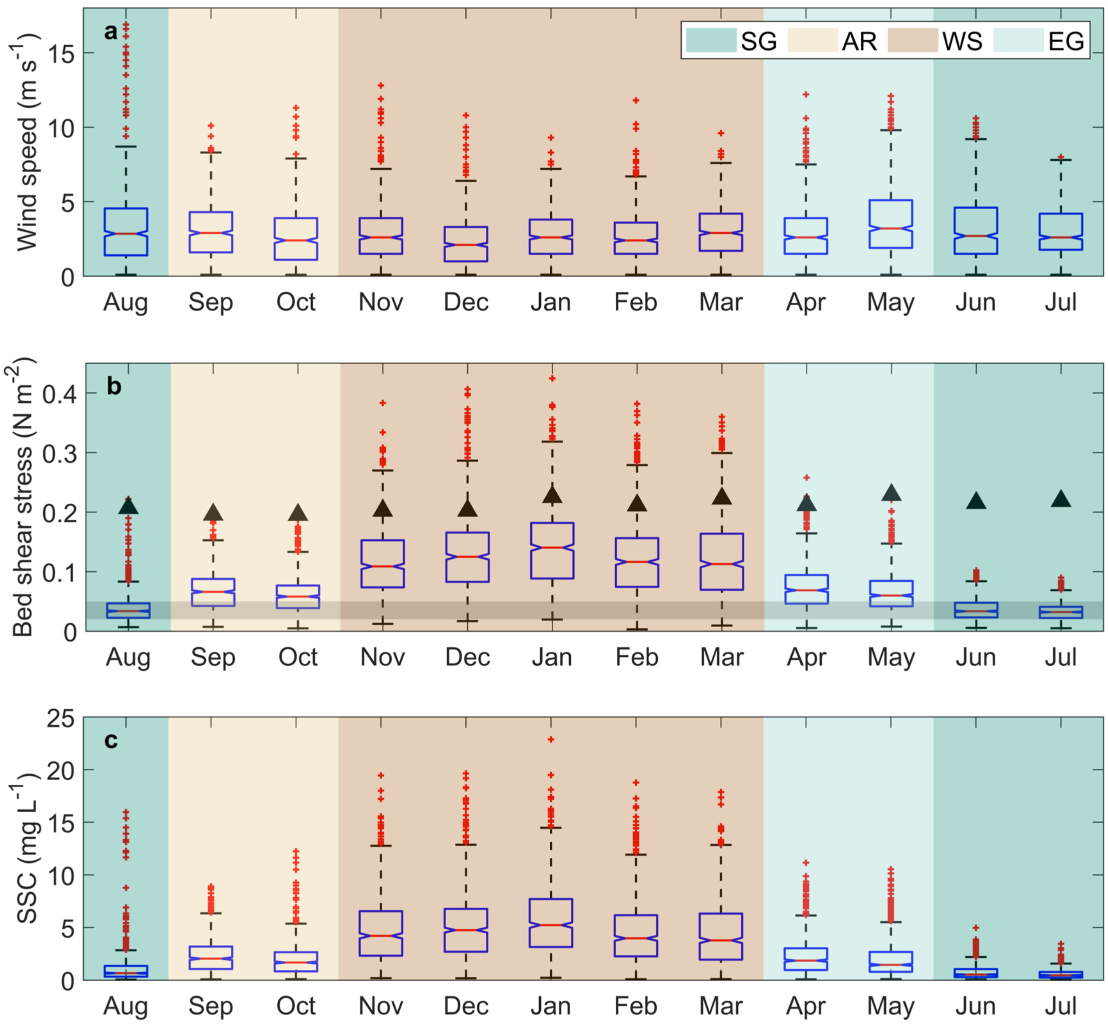

Figure A2.6 Box plots of (a) wind speeds, (b) bed shear stress averaged across the meadow, and (C) total suspended sediment concentration (SSC) averaged across the meadow when seagrass effects were included in the annual simulation. Black triangles in (b) denote the median bed shear stress output from model simulations without seagrass effects. The gray horizontal area in (b) represents the range of critical bed shear stress of 0.02 to 0.05 N m^{-2} within South Bay seagrass meadows (Reidenbach & Timmerman, 2019). The annual simulation results were divided into four groups according to the seagrass growth cycle: summer growth and mid-season loss (SG), autumn regrowth (AR), winter senescence (WS), and early growth (EG). The presence of seagrass significantly reduced bed shear stress in the meadow compared with simulation results without seagrass effects, particularly in summer when seagrass density was high. Sediment resuspension was inhibited in summer because bed shear stress within seagrass meadows rarely exceeded the critical shear stress to initiate sediment during this period except during storms; in contrast, bed shear stress and total suspended sediment concentration increased in other seasons when storm events coincided with low seagrass densities, particularly during winter senescence.

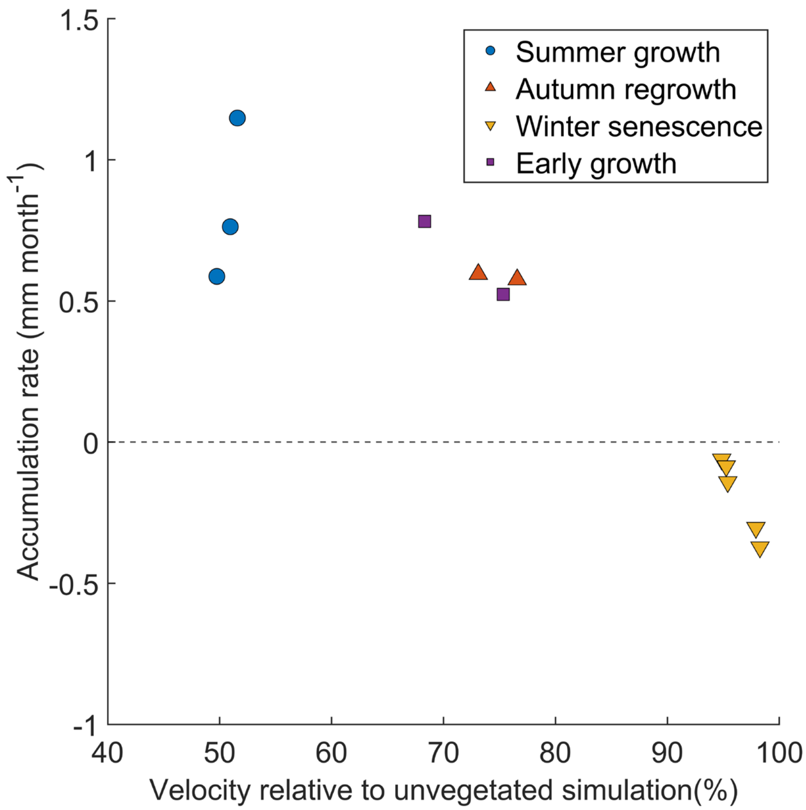

Figure A2.7 Monthly sediment accumulation rate averaged across the seagrass meadow as a function of the ratio of simulated velocities between model runs with and without seagrass effects.

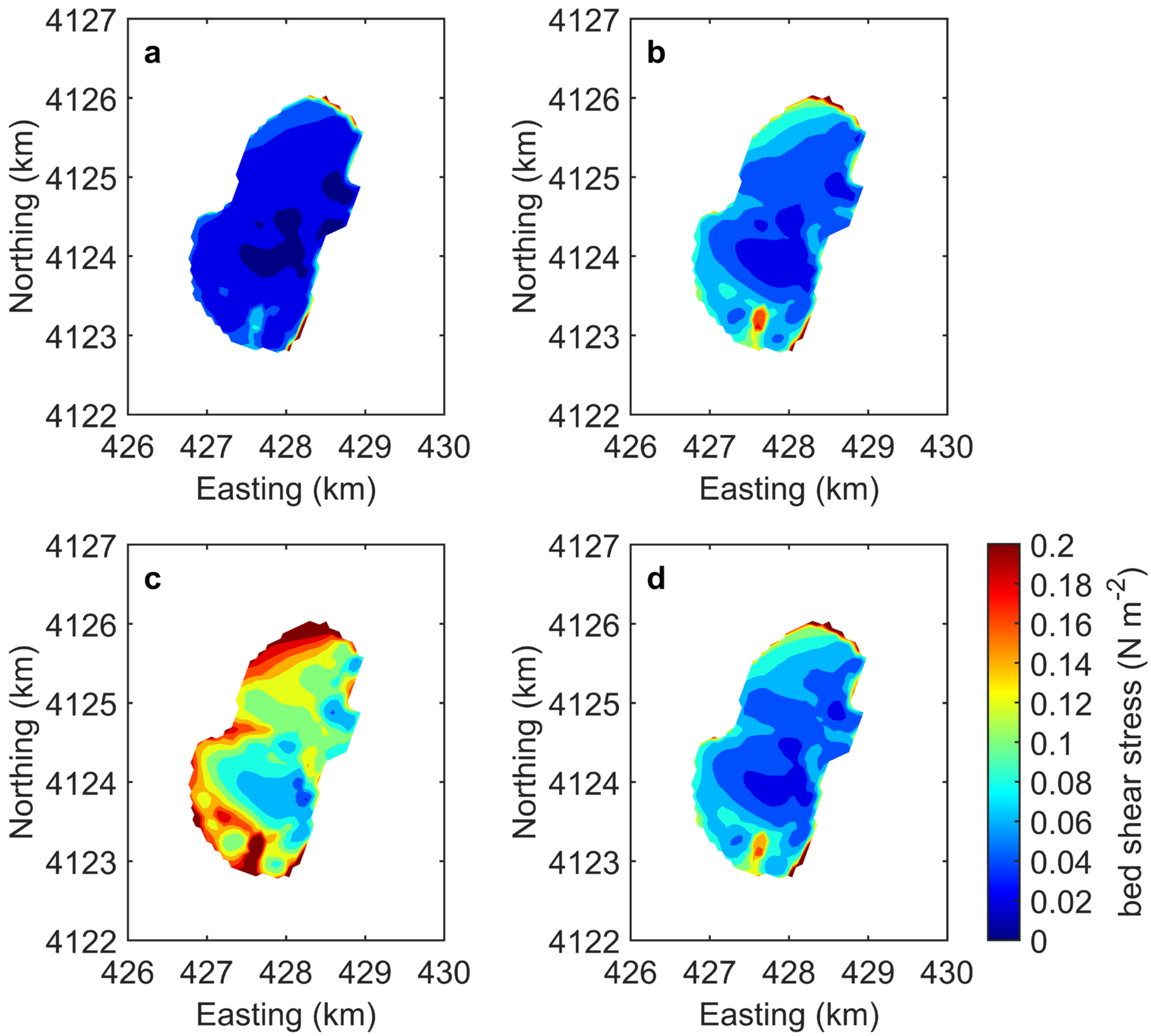

Figure A2.8 Distributions of seasonal mean bed shear stress within seagrass meadows output from simulations with seagrass effects: (a) summer growth and mid-season loss, (b) autumn regrowth, (c) winter senescence, and (d) early growth.

References

Berger, A. C., Berg, P., McGlathery, K. J., & Delgard, M. L. (2020). Long-term trends and resilience of seagrass metabolism: A decadal aquatic eddy covariance study. Limnology and Oceanography, 65(7), 1423–1438. https://doi.org/10.1002/lno.11397

Hansen, J., & Reidenbach, M. A. (2013). Seasonal Growth and Senescence of a Zostera marina Seagrass Meadow Alters Wave-Dominated Flow and Sediment Suspension Within a Coastal Bay. Estuaries and Coasts, 36(6), 1099–1114. https://doi.org/10.1007/s12237-013-9620-5

Oreska, M. P. J., McGlathery, K. J., & Porter, J. H. (2017). Seagrass blue carbon spatial patterns at the meadow-scale. PLoS ONE, 12(4), e0176630. https://doi.org/10.1371/journal.pone.0176630

Reidenbach, M. A., & Thomas, E. L. (2018). Influence of the Seagrass, Zostera marina, on Wave Attenuation and Bed Shear Stress Within a Shallow Coastal Bay. Frontiers in Marine Science, 5(OCT), 397. https://doi.org/10.3389/fmars.2018.00397

Reidenbach, M. A., & Timmerman, R. (2019). Interactive Effects of Seagrass and the Microphytobenthos on Sediment Suspension Within Shallow Coastal Bays. Estuaries and Coasts, 42(8), 2038–2053. https://doi.org/10.1007/s12237-019-00627-w

Rheuban, J. E., Berg, P., & McGlathery, K. J. (2014). Ecosystem metabolism along a colonization gradient of eelgrass (*Zostera marina*) measured by eddy correlation. Limnology and Oceanography, 59(4), 1376–1387. https://doi.org/10.4319/lo.2014.59.4.1376

Appendix 3: Supplemental information to Chapter 4

Table A3.1 Characteristics of the identified storm surge events. Storms with an asterisk indicate the additional simulated storm surge events in Figure 4.12, while the storm with a plus sign indicates model run 09MEAW.

Storm ID	Storm peak time	Duration (hr)	Peak surge (m)	75th wind speed (m s^{-1})	Mean wind direction (°)	Cumulative surge (m hr)
1	9/6/2008 13:00	9	0.4	6.0	197	1.2
2*	9/25/2008 15:00	99	0.9	9.7	37	27.8
3^{+}	3/2/2009 0:00	41	1.2	6.7	140	12.5
4	4/16/2009 14:00	44	0.6	4.5	96	7.6
5*	9/17/2009 8:00	35	0.7	7.4	50	8.5
6*	11/12/2009 20:00	103	1.7	14.0	19	70.5
7	12/19/2009 9:00	71	1.3	4.5	126	27.2
8	2/6/2010 10:00	61	1.4	4.8	161	27.4
9	9/30/2010 12:00	20	0.4	7.4	149	1.7
10	1/26/2011 11:00	49	0.7	3.7	102	7.5
11	2/22/2011 1:00	30	0.8	6.2	99	6.8
12	4/16/2011 18:00	34	0.7	8.4	184	6.7
13	8/27/2011 14:00	25	1.2	10.8	90	12.9
14	2/19/2012 19:00	24	0.5	5.6	138	3.5
15	4/22/2012 14:00	27	0.6	4.5	164	3.1
16	5/18/2012 11:00	10	0.4	8.8	78	0.9
17	10/27/2012 19:00	70	1.5	8.0	29	36.5
18	11/18/2012 12:00	156	0.6	6.7	29	29.8
19	2/8/2013 7:00	27	0.6	4.8	133	4.9
20	4/22/2013 16:00	56	0.7	8.6	47	11.6
21	5/3/2013 10:00	81	0.5	10.0	54	12.4
22*	10/13/2013 16:00	196	1.0	8.7	36	52.9
23	1/21/2014 15:00	58	0.7	5.3	99	13.3
24	2/13/2014 5:00	36	0.8	6.3	93	11.6
25	3/7/2014 10:00	62	0.7	10.1	41	13.9
26	3/16/2014 22:00	72	0.6	9.8	52	16.2
27	4/29/2014 7:00	56	0.6	8.4	74	11.9
28	5/28/2014 20:00	45	0.6	7.3	133	8.7
29	9/9/2014 7:00	75	0.6	6.5	50	12.5
30	9/24/2014 19:00	72	0.6	4.6	100	9.5
31	5/1/2015 8:00	63	0.5	4.1	65	7.6
32	6/3/2015 9:00	96	0.5	9.0	37	12.0
33	9/21/2015 14:00	171	0.7	9.1	93	34.2
34	10/2/2015 18:00	166	1.1	12.9	30	80.2
35	1/23/2016 3:00	85	1.6	5.1	101	46.3

36	2/24/2016 21:00	51	0.6	7.1	205	10.6
37	9/3/2016 11:00	121	1.1	5.1	62	36.0
38	9/29/2016 20:00	137	0.8	6.6	99	28.1
39	10/8/2016 16:00	73	0.8	5.8	28	17.0
40	1/23/2017 18:00	113	1.4	5.3	122	39.2
41	4/6/2017 12:00	53	0.6	6.1	204	7.4
42	4/24/2017 6:00	139	0.6	7.5	36	16.4
43	5/20/2017 14:00	20	0.5	8.0	67	2.5
44	8/29/2017 11:00	97	0.7	8.2	65	21.4
45	9/27/2017 13:00	108	0.6	6.5	96	15.7
46*	10/12/2017 15:00	73	0.8	7.5	48	17.3
47	10/23/2017 23:00	14	0.3	6.6	174	0.9
48	1/29/2018 7:00	0	0.7	8.7	42	0.0
49	3/12/2018 10:00	52	0.6	4.8	92	11.7
50	3/20/2018 11:00	89	0.8	6.3	38	24.7
51	4/16/2018 5:00	38	0.7	6.9	203	8.1
52	5/18/2018 21:00	22	0.4	6.2	82	3.3
53	6/11/2018 8:00	57	0.6	6.5	102	8.6
54	7/7/2018 15:00	49	0.6	9.2	33	7.2
55	9/8/2018 21:00	104	1.0	8.0	90	30.5
56	11/15/2018 16:00	16	0.8	6.9	130	4.2
57	1/13/2019 14:00	77	0.8	3.5	92	19.6
58	1/24/2019 10:00	5	0.2	7.4	243	0.1
59	6/8/2019 11:00	73	0.5	7.4	47	9.4
60	8/25/2019 15:00	95	0.8	6.3	41	21.0
61	9/6/2019 6:00	79	0.9	5.7	87	21.3
62	11/16/2019 11:00	106	0.9	4.1	28	41.7
63	3/23/2020 7:00	27	0.7	9.7	146	5.8
64	4/1/2020 1:00	129	0.9	4.6	66	30.1
65	5/19/2020 18:00	98	0.8	12.5	52	23.2
66	6/16/2020 15:00	94	0.6	10.1	50	18.3
67	8/4/2020 8:00	5	0.5	5.4	178	0.9
68	8/16/2020 8:00	87	0.7	6.7	67	17.4

Table A3.2 Long-term marsh accretion rate determined at FP (Fowling Point) marsh in the VCR.

Method	Long-term accretion rate (mm yr^{-1})
Surface elevation tables (SETs)	4.5
^{137}Ce dating	3.6
Delft3D simulation (Figure A3.2; multiplying sediment accumulation at FP output from the reference model run 09REF by a factor of 12)	4.8

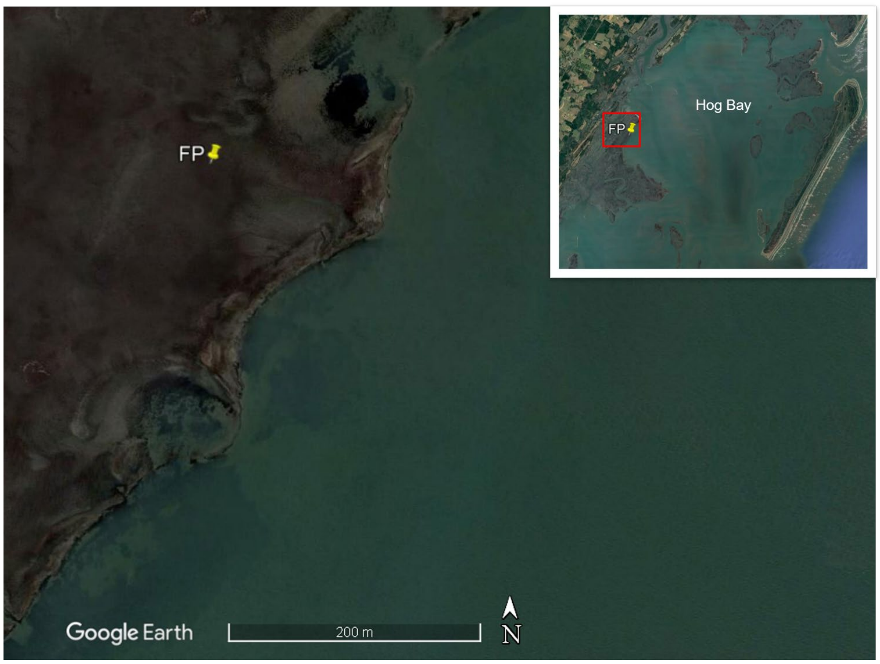

Table A3.3 Time period and model settings for the additional simulated storm surge events in Figure 4.12.

Period	Model run	Water level forcing	Wind wave	Cumulative storm surge (m hr)
September 20–28, 2008	ID2	Total measured water level	Yes	27.8
September 14–20, 2009	ID5	Total measured water level	Yes	8.5
November 8–17, 2009	ID6	Total measured water level	Yes	70.5
October 6–18, 2013	ID22	Total measured water level	Yes	52.9
October 9–16, 2017	ID46	Total measured water level	Yes	17.3

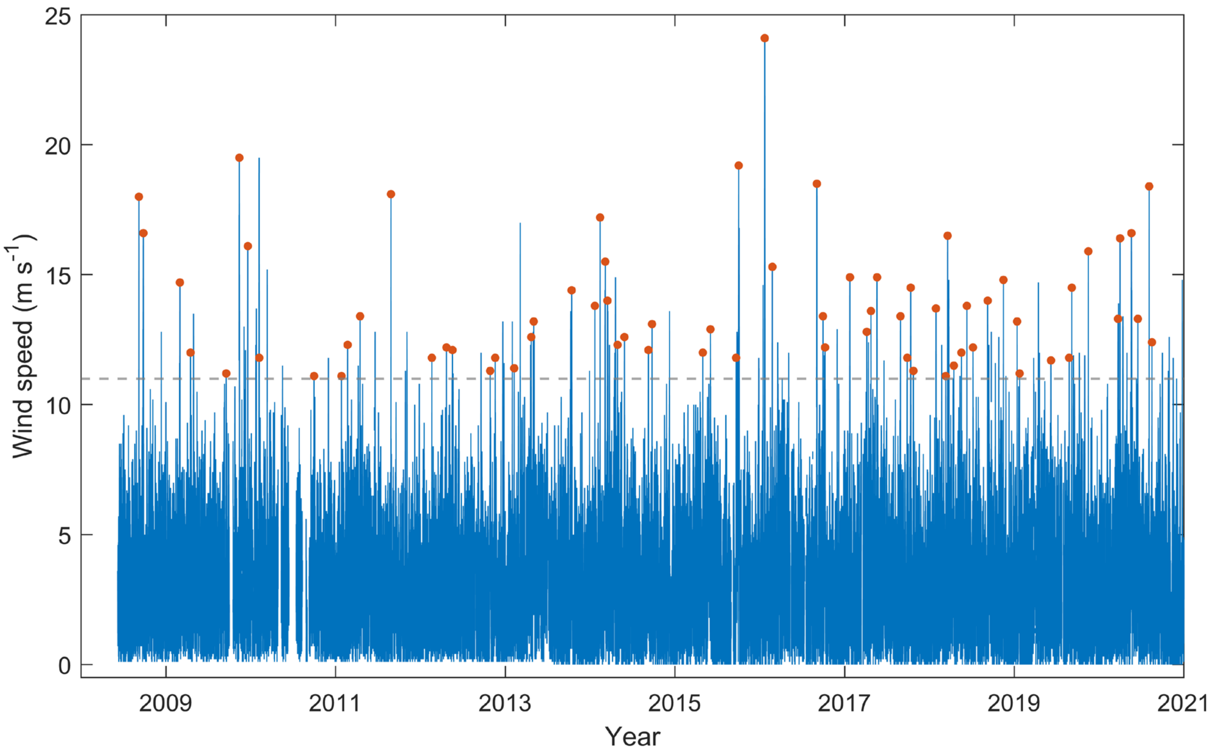

Figure A3.1 Storm surge events identified by threshold values of wind speed > 11 m s^{-1} and measured water level − astronomical tide > 0.2 m.

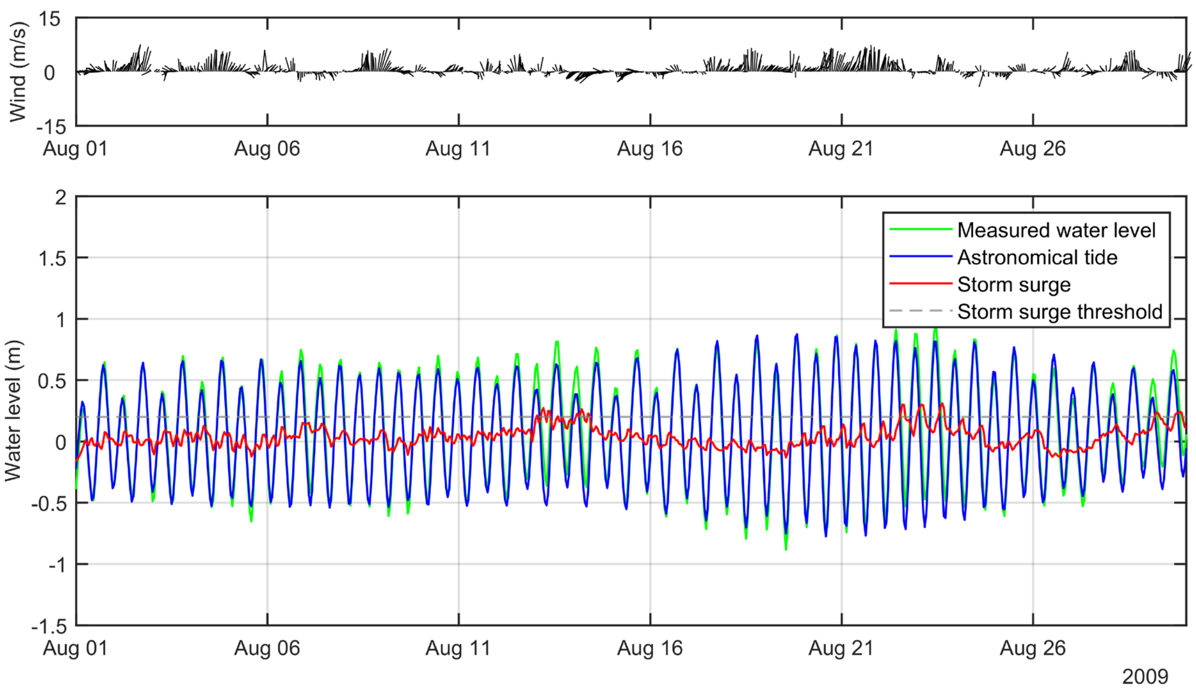

Figure A3.2 Model forcing conditions for the 30-day reference simulation run 09REF. Time series of winds (upper panel) and water levels (lower panel) are extracted from NOAA tide gauge and weather station (Wachapreague, ID:8631044). Measured water levels and wind wave coupling were used in the simulation. The 30-day simulation predicts a total sediment depositional mass on the marsh of 1.1×10^5 MT, which is used to estimate annual marsh deposition (1.4×10^6 MT) and total marsh deposition around the bay (1.6×10^7 MT) during 2009–2020 by multiplying the predicted value by a factor of 12 and 144, respectively.

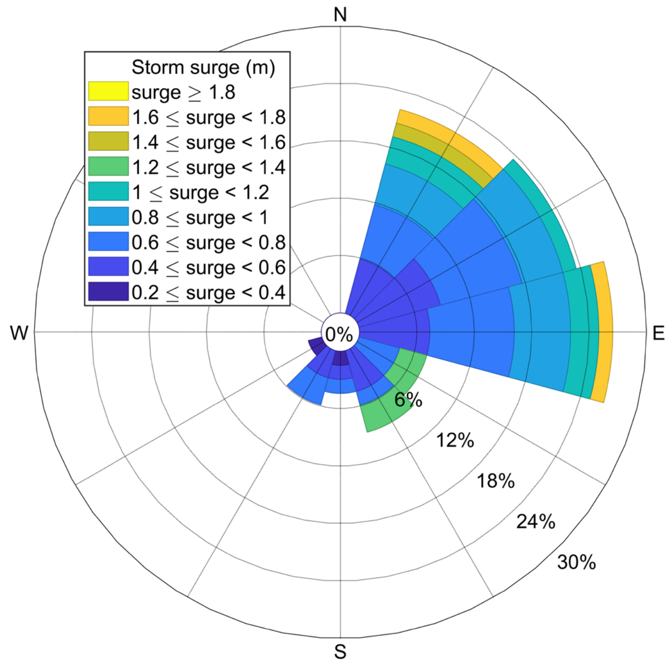

Figure A3.3 Distribution of peak storm surge of the identified storm surge events in the VCR as a function of wind direction.

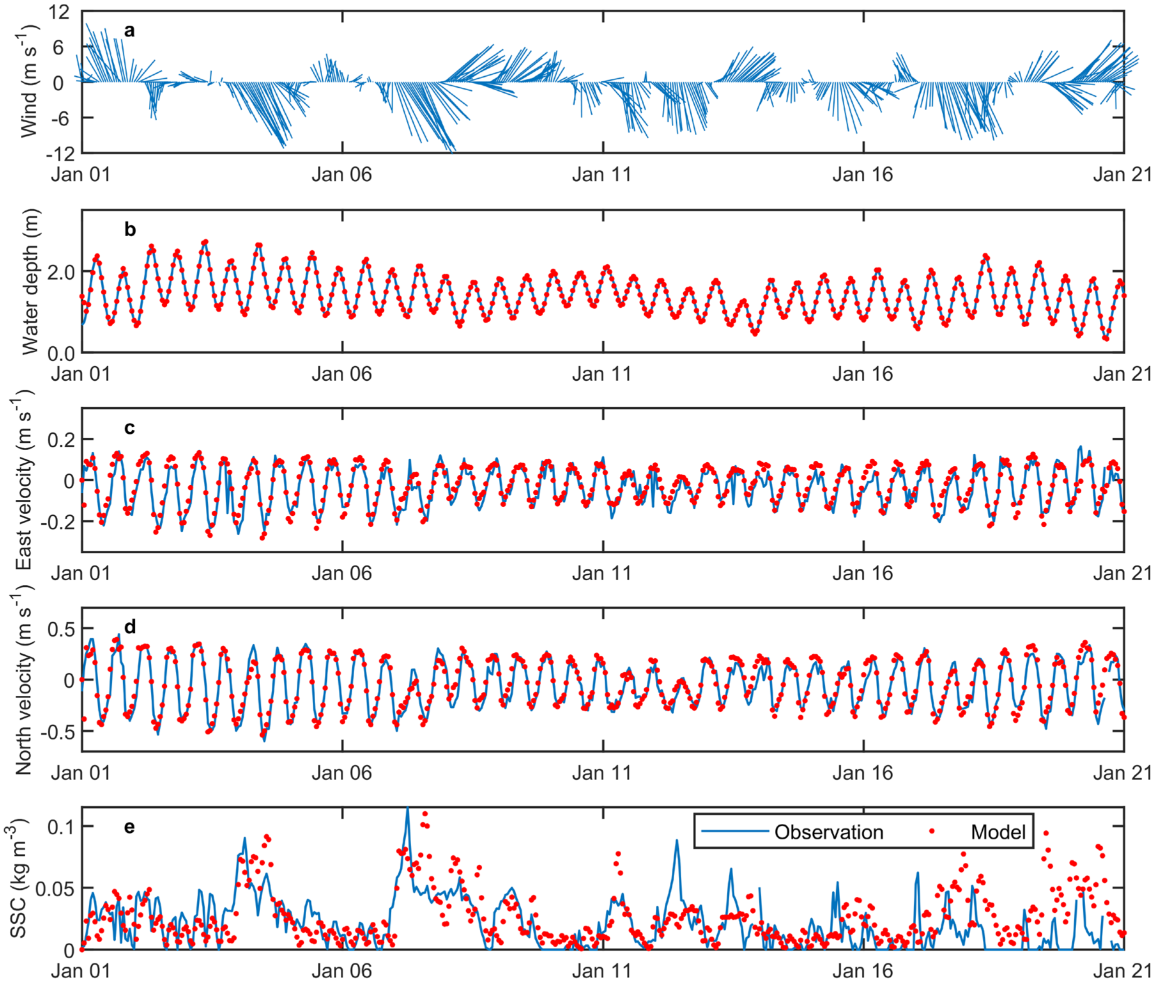

Figure A3.4 Comparison of measured and modeled hydrodynamic conditions (03VAL) during January 1–21, 2003: (a) winds, (b) water depth, (c) east velocity, (d) north velocity, and (e) total suspended sediment concentration (SSC) at HI. Lines in (a) point in the direction that the wind is blowing toward. Blue lines in (b)–(e) represent observational data, and red dots show model simulation results.

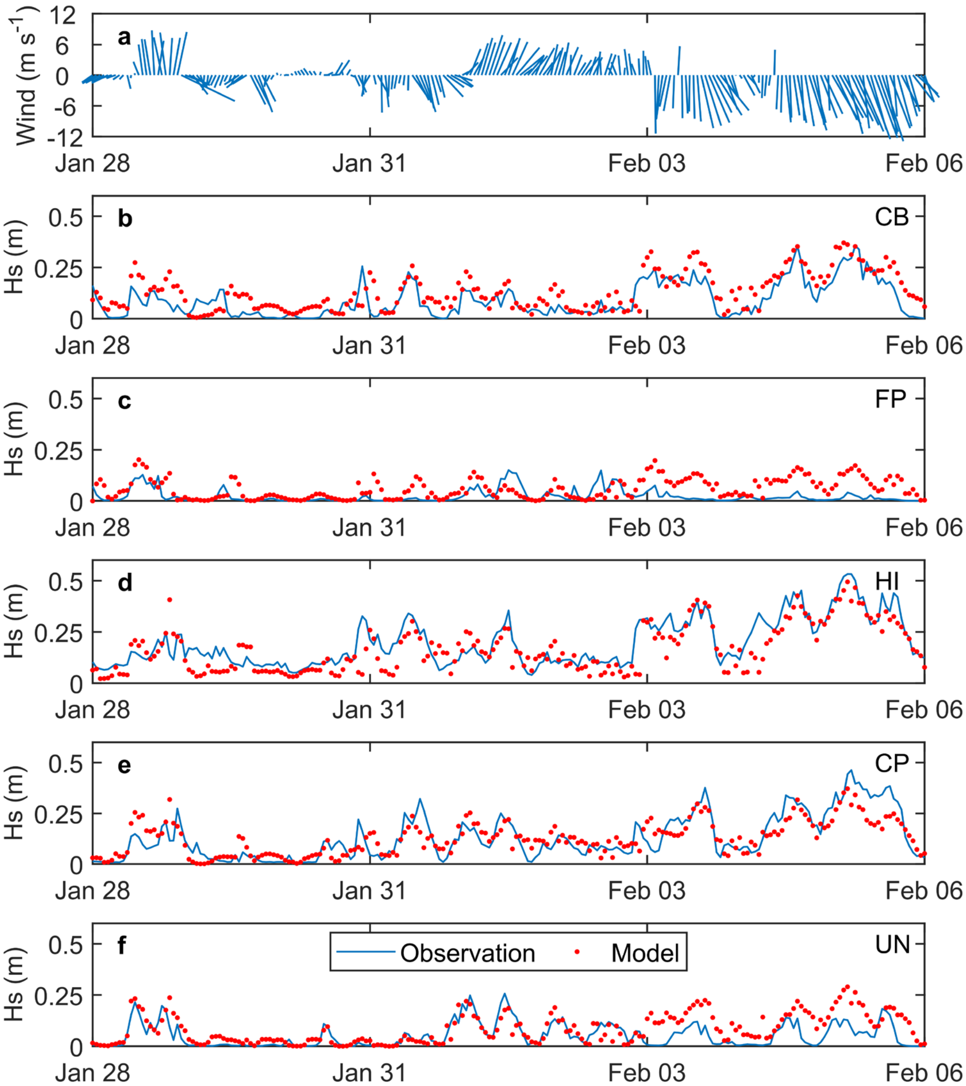

Figure A3.5 Comparison of measured and modeled wave heights (09VAL) during January 28–February 06, 2009: (a) winds, (b) wave height at CB, (c) wave height at FP, (d) wave height at HI, (e) wave height at CP, and (f) wave height at UN. Lines in (a) point in the direction that the wind is blowing toward. Blue lines in (b)–(f) represent observational data, and red dots show model simulation results.

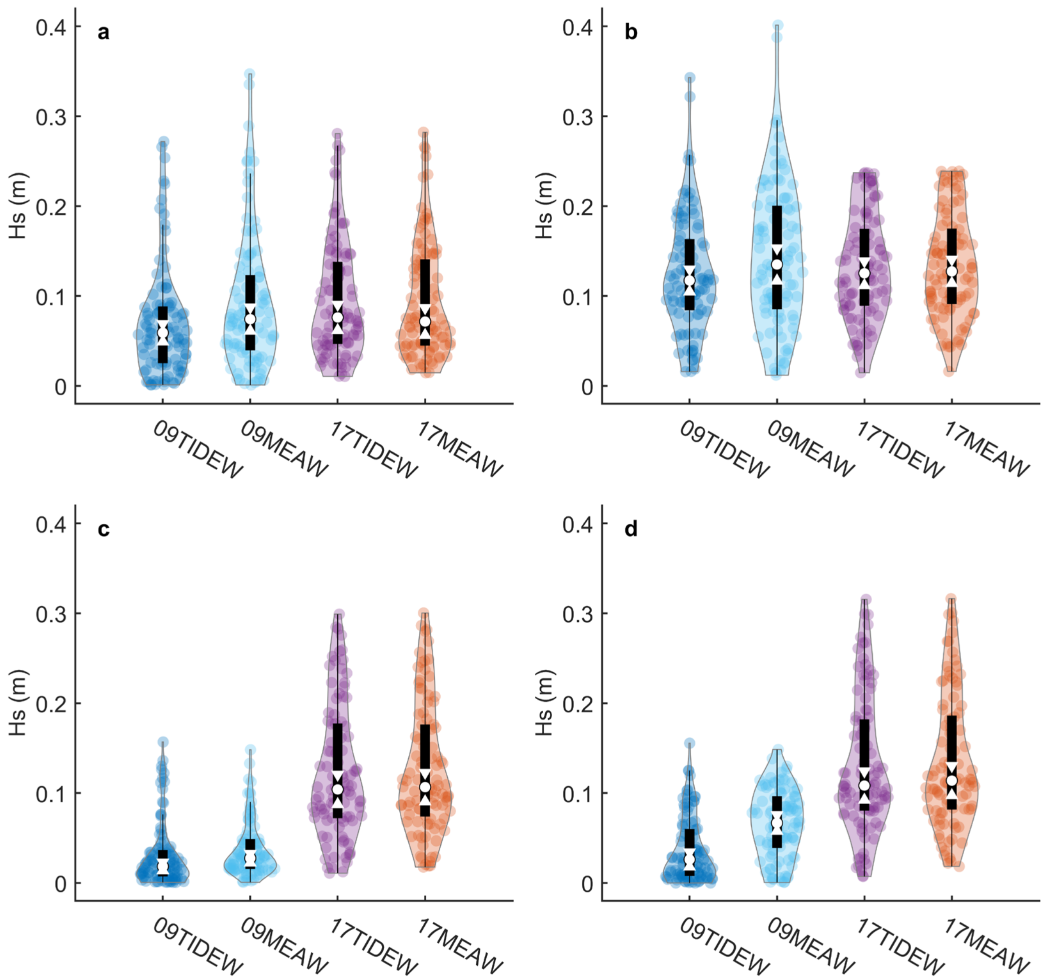

Figure A3.6 Violin plots of modeled significant wave height (Hs) at bay–marsh boundaries output from model runs in 2009 and 2017: (a) FP, (b) HI, (c) CP, and (d) UN. Model runs 09TIDEW/09MEAW are forced with astronomical/measured tides and northeasterly winds in 2009, while 17TIDEW/17MEAW are forced with astronomical/measured tides and southerly winds in 2017.

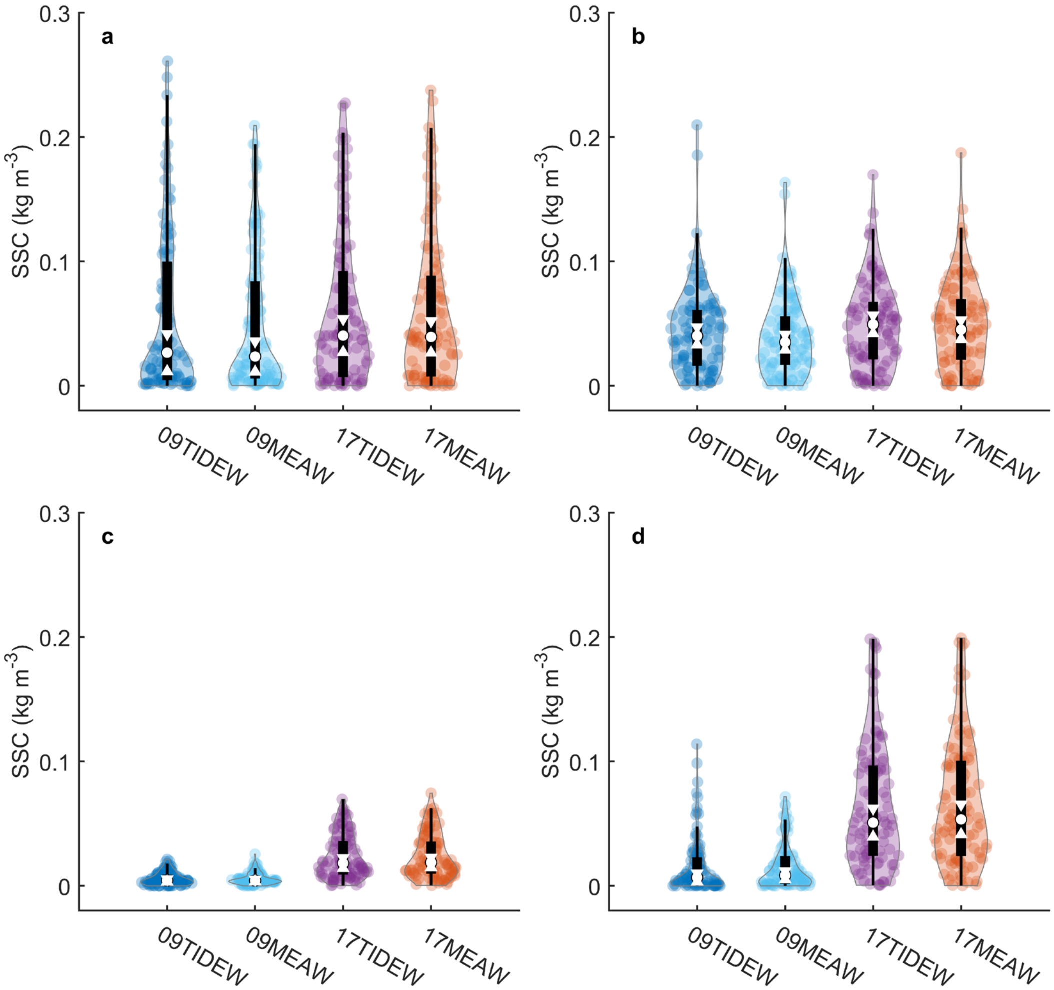

Figure A3.7 Violin plots of modeled depth averaged suspended sediment concentration (SSC) at bay–marsh boundaries output from model runs in 2009 and 2017: (a) FP, (b) HI, (c) CP, and (d) UN. Model runs 09TIDEW/09MEAW are forced with astronomical/measured tides and northeasterly winds in 2009, while 17TIDEW/17MEAW are forced with astronomical/measured tides and southerly winds in 2017.

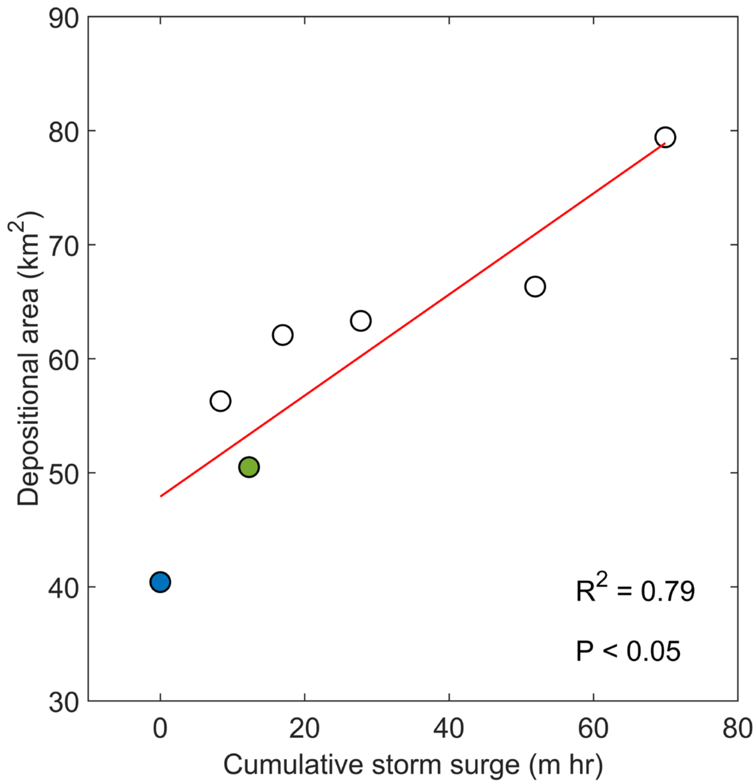

Figure A3.8 Depositional area on marshes bordering Hog Bay as a function of cumulative storm surge intensity. Filled blue and green symbols are model results output from model runs 17MEAW and 09MEAW, respectively.

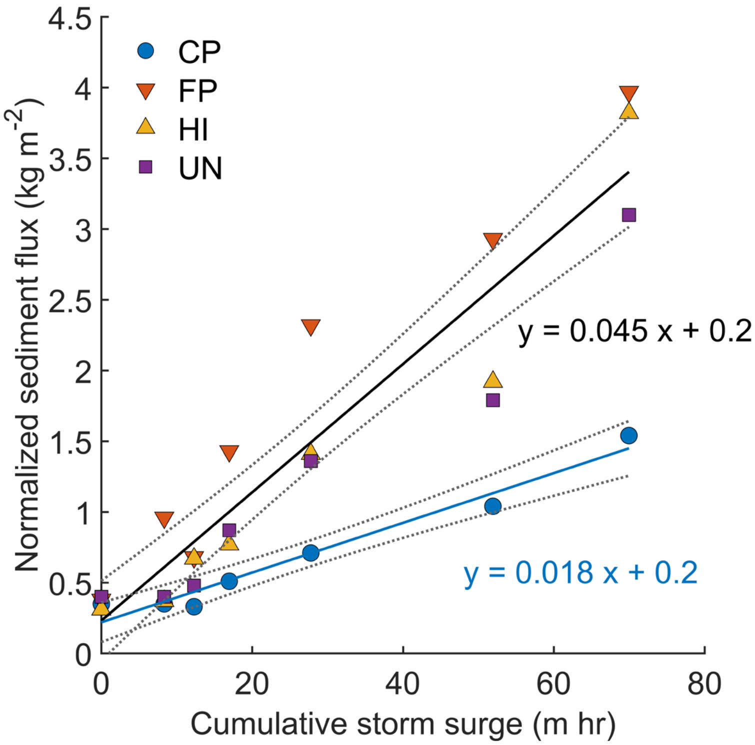

Figure A3.9 Total normalized sediment flux into CP, FP, HI and UN marshes as a function of cumulative storm surge intensity. The black solid line shows the linear regression trendline for FP, HI, and UN marshes, while the blue solid line shows the linear regression trendline for CP marsh. Dashed lines indicate 95% confidence interval.

Appendix 4: Supplemental information to Chapter 5

Table A4.1 Seagrass parameters input for the model. *N* is seagrass shoot density, h_v is vegetation height, b_v is stem diameter, C_D is seagrass flow drag coefficient, and $\widetilde{C_D}$ is seagrass wave drag coefficient. Seagrass characteristics (density, height, and stem diameter) in the table are compiled from previous seasonal seagrass observations in South Bay (Berger et al., 2020; Hansen & Reidenbach, 2013; Reidenbach & Thomas, 2018; Rheuban et al., 2014) and have been adjusted based on seagrass growth cycle. In order to better represent observed spatial density gradients in the meadow, three seagrass density classes were assigned in the model each month, with the highest density (*N*) in the central meadow, an intermediate density of 0.8*N* outside the central area, and the lowest density of 0.6*N* near meadow edges.

Simulation period	N (shoots m^{-2})	0.8*N (shoots m^{-2})	0.6*N (shoots m^{-2})	h_v (m)	b_v (cm)	C_D	$\widetilde{C_D}$
AUG, 2011	500	400	300	0.4	0.4	0.4	3.0
SEP, 2011	200	160	120	0.3	0.3	0.3	3.0
OCT, 2011	250	200	150	0.3	0.3	0.3	3.0
NOV, 2011	150	120	90	0.2	0.2	0.2	3.0
DEC, 2011	100	80	60	0.2	0.2	0.2	3.0
JAN, 2012	100	80	60	0.2	0.2	0.2	3.0
FEB, 2012	150	120	90	0.2	0.2	0.2	3.0
MAR, 2012	150	120	90	0.2	0.2	0.2	3.0
APR, 2012	200	160	120	0.3	0.3	0.3	3.0
MAY, 2012	350	280	210	0.3	0.3	0.3	3.0
JUN, 2012	600	480	360	0.4	0.4	0.4	3.0
JUL, 2012	600	480	360	0.4	0.4	0.4	3.0

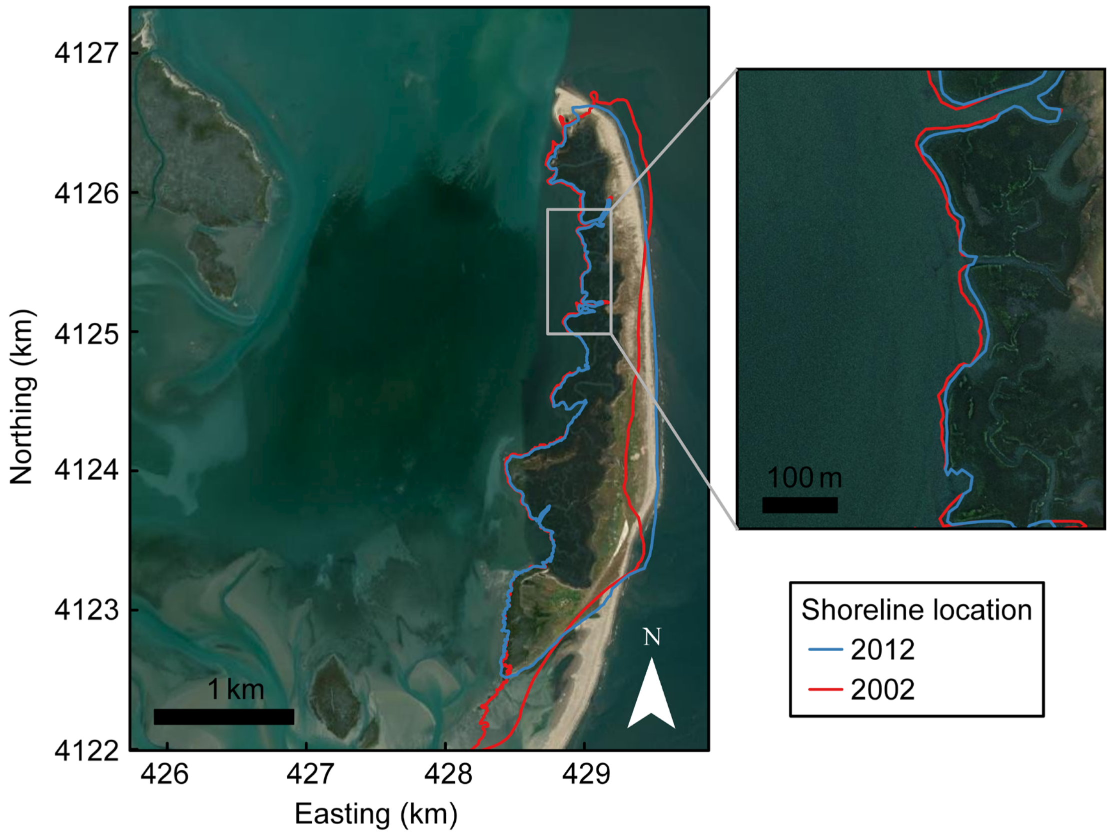

Figure A4.1 Shoreline changes of Wreck Island. Coordinates of UTM zone 18N are given in km.

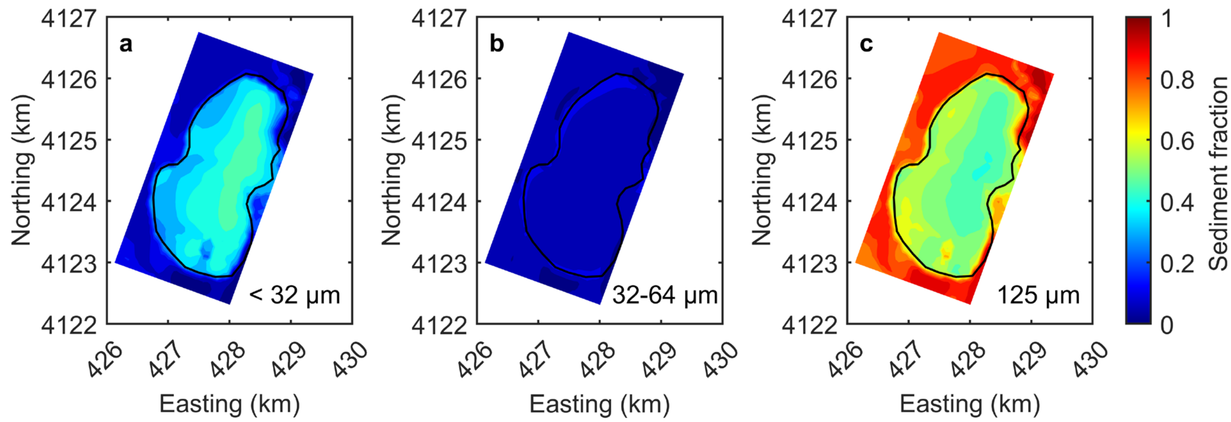

Figure A4.2 Initial distribution of different sediment fractions used in the model simulations with seagrass effects. The black line shows the meadow outline.

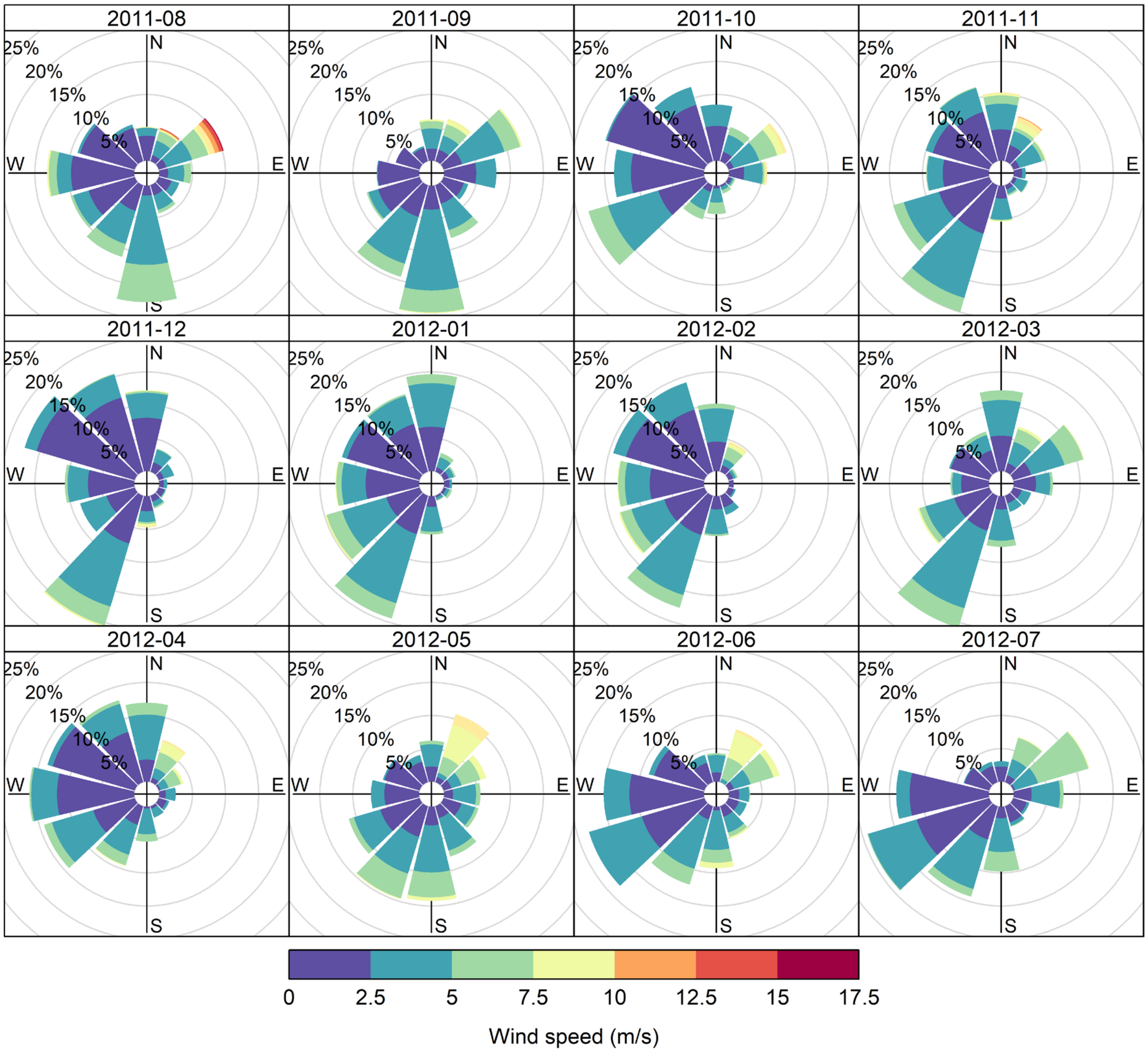

Figure A4.3 Directional distributions of monthly wind conditions in the study area during the model simulation period (August 1, 2011 to July 31, 2012). The wind data are extracted hourly from the NOAA weather station at Wachapreague (https://tidesandcurrents.noaa.gov/stationhome.html?id=8631044).

References

Berger, A. C., Berg, P., McGlathery, K. J., & Delgard, M. L. (2020). Long-term trends and resilience of seagrass metabolism: A decadal aquatic eddy covariance study. Limnology and Oceanography, 65(7), 1423–1438. https://doi.org/10.1002/lno.11397

Hansen, J., & Reidenbach, M. A. (2013). Seasonal Growth and Senescence of a Zostera marina Seagrass Meadow Alters Wave-Dominated Flow and Sediment Suspension Within a Coastal Bay. Estuaries and Coasts, 36(6), 1099–1114. https://doi.org/10.1007/s12237-013-9620-5

Reidenbach, M. A., & Thomas, E. L. (2018). Influence of the Seagrass, Zostera marina, on Wave Attenuation and Bed Shear Stress Within a Shallow Coastal Bay. Frontiers in Marine Science, 5(OCT), 397. https://doi.org/10.3389/fmars.2018.00397

Rheuban, J. E., Berg, P., & McGlathery, K. J. (2014). Ecosystem metabolism along a colonization gradient of eelgrass (*Zostera marina*) measured by eddy correlation. Limnology and Oceanography, 59(4), 1376–1387. https://doi.org/10.4319/lo.2014.59.4.1376